Site U1335[1]

Expedition 320/321 Scientists[2]

Chapter contents

[1] Expedition 320/321 Scientists, 2010. Site U1335. *In* Pälike, H., Lyle, M., Nishi, H., Raffi, I., Gamage, K., Klaus, A., and the Expedition 320/321 Scientists, *Proc. IODP,* 320/321: Tokyo (Integrated Ocean Drilling Program Management International, Inc.). doi:10.2204/iodp.proc.320321.107.2010
[2] **Expedition 320/321 Scientists' addresses.**

Background and objectives

Integrated Ocean Drilling Program (IODP) Site U1335 (5°18.735′N, 126°17.002′W; 4327.5 meters below sea level [mbsl]) (Fig. **F1**; Table **T1**) is located in the central area drilled during the Pacific Equatorial Age Transect (PEAT) program (IODP Expedition 320/321). Site U1335 (~26 Ma crust) is situated halfway between IODP Site U1336 ~340 km to the northwest and IODP Site U1337 ~390 km to the southeast, ~250 km south of the Clipperton Fracture Zone. Site U1335 is located on a broad plateau within north-northeast–trending abyssal hill topography. Thick sediment deposits cover the abyssal hills, with a thinning sediment cover on the hills. Site U1335 is draped with ~420 m of sediment cover (Fig. **F2**), estimated to be ~360 m prior to drilling. Water depth in the vicinity of Site U1335 is between 4300 and 4400 m, apart from the topography around seamounts that are 15–20 km away from the drill site (Fig. **F1B**).

Based on stage-pole reconstructions of Pacific plate motion and observations of basement age from previous drilling sites, along with magnetic anomaly maps (Cande et al., 1989), we estimated prior to drilling that Site U1335 is located on 26 Ma crust. The best control on age is information from Deep Sea Drilling Project (DSDP) Site 79, located ~600 km and 4.5° east and 3° south of Site U1335, apparently on the same fracture zone segment, with the Clipperton Fracture Zone to the north. The base of Site 79 reaches the Miocene/Oligocene boundary, or ~23 Ma on the most recent astronomically calibrated timescales.

Site U1335 was proposed for drilling to focus on the paleoceanographic events in the late Oligocene and into the early and middle Miocene, including the climatically significant Oligocene–Miocene transition and recovery from the Mi-1 glaciation event. In conjunction with Sites U1336 and U1337, it was also designed to provide a latitudinal transect for early Miocene age slices.

At the end of the Oligocene, a significant multimillion year long rise in the oxygen isotope record (Lear et al., 2004) is closely followed by a relatively short, sharp increase in oxygen isotope values that has been interpreted as a major glacial episode (Mi-1) (Zachos et al. 1997, 2001a, 2001b; Pälike et al., 2006a, 2006b) and correlated to a pronounced drop in sea level (Miller et al., 1991). This event is very close to the Oligocene/Miocene boundary and has now been astronomically age calibrated in several ocean basins (Shackleton et al., 2000; Billups et al., 2004; Pälike et al.,

doi:10.2204/iodp.proc.320321.107.2010

2006b). Although there are clear periodic isotopic signals indicating major changes in ice volume, ocean temperatures, and/or ocean structure, this biostratigraphic boundary has always been somewhat of an enigma. Unlike the major changes in isotopic stratigraphy, biostratigraphies of the planktonic microfossils show very little change at all across this boundary. In fact, it is one of the most difficult epoch boundaries to pick using only microfossil biostratigraphies.

At Ocean Drilling Program (ODP) Leg 199 Sites 1218 and 1219 this interval was well recovered; however, carbonate preservation still presented a problem for foraminifer stratigraphy. Both sites were deep and well within the lysocline, making the application of temperature proxies such as Mg/Ca ratios in foraminifer tests more difficult (Lear et al., 2008). At the time Miocene–Oligocene sediments were deposited, Site 1218 already resided on 18 m.y. old crust and was ~4100 m deep. Site 1219 was on ~34 m.y. old crust and was ~4.5 km deep (Lyle, Wilson, Janecek, et al., 2002). There was a relative increase in large diatoms near this boundary in the siliceous coarse fraction, suggesting increased productivity; however, detailed high-resolution flux rates across this interval have yet to be determined. A well-recovered section on the latest Oligocene Equator, near the late Oligocene ridge crest as targeted by Site U1335, should provide both the resolution and the preservation required to better describe the changes in the equatorial ocean taking place at this time.

We positioned Site U1335 and the other PEAT sites slightly south of the estimated paleoequatorial position at their target ages in order to maximize the time that drill sites remain within the equatorial zone (i.e., ±2° of the Equator), to allow for some southward bias of the equatorial sediment mound relative to the hotspot frame of reference (Knappenberger, 2000), and to place the interval of maximum interest above the basal hydrothermal sediments. We located the site using the digital age grid of seafloor age from Müller et al. (1997), heavily modified and improved with additional magnetic anomaly picks from Petronotis (1991), Petronotis et al. (1994), and DSDP/ODP basement ages. For this grid, each point is then backrotated in time to zero age, using the fixed-hotspot stage-poles from Koppers et al. (2001) and Engebretson et al. (1985) and the paleopole data from Sager and Pringle (1988). From the backtracked latitudes for each grid point we then obtained the paleoequator at the crustal age by contouring.

One of the common objectives of the PEAT program for all sites is to provide a limited depth transect for several Cenozoic key horizons, such as the Eocene–Oligocene transition (Coxall et al., 2005) and Oligocene–Miocene transition (Shackleton et al., 2000; Pälike et al., 2006b; Zachos et al., 2001b). For this objective, Sites U1335–U1337 will form a combined depth transect for Oligocene–Miocene time. Site U1335 had an estimated crustal paleodepth of ~3.3 km during the Oligocene–Miocene transition.

All Expedition 320/321 drill sites have in common the objective to improve and extend the extensive intercalibrated bio-, magneto-, chemo-, and astronomical stratigraphies for the Cenozoic (e.g., Shackleton et al., 2000; Pälike et al., 2006a).

The seismic reflection data (Fig. **F2**) (Pälike et al., 2008; Lyle et al., 2006) allowed us to optimize the Site U1335 position on seismic Line PEAT-6C-sl-8, which trends north–south. Site U1335 was moved south of the intersection of this line with the east-west Cross-line PEAT-6C-sl-1 to better image basement and obtain a more expanded lower sediment section. We estimated sediment thickness using interval velocities published for DSDP Site 574 by Mayer et al. (1985), which drilling determined later to underestimate the basal interval velocities and therefore total sediment thickness. The subbottom profiler sections image ~20 m of transparent surface sediment and ~100 m of layered sediments in the upper sediment column (Pälike et al., 2008). Site U1335 is located along the flank of a wide valley that trends north–northeast, on elevated seafloor above a moat around the seamounts (Fig. **F1B**). Sediment cover is thick on the plateau but is highly variable along the edges. There is variable sedimentation along the eastern edge and the thick sediment cover on the plateau ranging from 300 to 600 ms two-way traveltime (TWT) (Lyle et al., 2006; Pälike et al., 2008). Nevertheless, the seafloor is relatively flat because the sediment has filled in the basement topography at ~200 ms TWT. Based on correlation to the central equatorial Pacific seismic stratigraphy of Mayer et al. (1985), middle Miocene sediment has been exposed.

A site survey piston Core RR0603-6JC was taken east of Site U1335 (Fig. **F1B**). The cores recovered mottled brown to light brown cyclic carbonates and siliceous biogenic sediments with carbonate contents between 20 and 85 wt%. Survey piston core sediments range from foraminifer-nannofossil oozes with radiolarians and diatoms to radiolarian-diatom oozes with foraminifers and nannofossils. The age at the base of this core is ~2.4 Ma based on calcareous nannofossil stratigraphy and a tie from the physical property data to the global isotope stratigraphy.

Science summary

Two holes were cored at Site U1335 (5°18.735′N, 126°17.002′W; 4327.5 mbsl) (Fig. F1; Table T1), targeting paleoceanographic events in the late Oligocene and into the early and middle Miocene, including and focusing on the climatically significant Oligocene–Miocene transition and the recovery from the Mi-1 glaciation event (Zachos et al., 2001b; Pälike et al., 2006a) and the expansion of the East Antarctic cryosphere (Holbourn et al., 2005). Site U1335 also provides data toward a depth transect across the latest Oligocene and Miocene (see "Latest Oligocene–earliest Miocene [Site U1335; 26 Ma crust]" in the "Expedition 320/321 summary" chapter) that will allow exploitation and verification of a previous astronomical age calibration from Site 1218 (Pälike et al., 2006b).

Site U1335 (~26 Ma crust) is situated halfway between Site U1336 ~340 km toward the northwest and Site U1337 ~390 km toward the southeast, ~250 km south of the Clipperton Fracture Zone (Lyle et al., 2006). At Site U1335, seafloor basalt is overlain by ~414 m of pelagic sediment. The oldest sediment is of late Oligocene age (26 Ma).

The sedimentary sequence at Site U1335 is divided into two major lithologic units (see "Lithostratigraphy"). The topmost ~64 m thick lithologic Unit I comprises an alternating sequence of earliest late Miocene to Pleistocene calcareous nannofossil, diatom, radiolarian, and foraminifer oozes. The topmost sediment of Unit I is younger than the Pleistocene/Pliocene boundary (see "Biostratigraphy") as recognized by the top of planktonic foraminifer *Globigerinoides fistulosus* (between Samples 320-U1335A-1H-CC and 2H-2, 104–106 cm) and then follows a continuous biostratigraphic succession to the early late Miocene. Below, lithologic Unit II comprises a ~350 m thick succession of late Miocene to late Oligocene (calcareous nannofossil Zone NP25) nannofossil ooze and chalk overlying basalt (lithologic Unit III) (Figs. F3, F4). One of the prominent features of Unit II is the presence of at least 49 described beds (2–176 cm thick) of nannofossil foraminifer ooze that have sharp basal boundaries, many of which are irregular and some of which are inclined. These beds are interpreted as gravity flow deposits from the nearby seamounts and represent ~2% of the total sediment recovered.

Holes U1335A and U1335B provided high-quality advanced piston corer (APC)-cored sediments from the mudline to ~341 and 378 m core depth below seafloor (CSF), respectively (Cores 320-U1335A-36H and 320-U1335B-41H). At the time it was recovered, the APC-cored interval from Hole U1335B represented the second deepest APC-cored depth in ODP and IODP history. Below this depth we encountered stiffer and harder sediment, after which we switched to the extended core barrel (XCB) cutting shoe. XCB coring advanced to ~420 m drilling depth below seafloor (DSF) through lower Miocene and upper Oligocene sediments with high recovery. In the basal section, Core 320-U1335B-46X recovered pieces of basalt up to 10 cm in length with a glassy rim and overlain by nannofossil chalks of Unit II. For detailed coring activities, see "Operations."

The sediment column at Site U1335 represents the youngest end-member drilled during Expedition 320 and provides one of the most stratigraphically complete and expanded lower Miocene sections from the equatorial Pacific to date (~320 m cored depth from the lowermost to uppermost Miocene).

At Site U1335, carbonate content fluctuates between 12 and 87 wt% within Unit I (see "Geochemistry") (Fig. F5), presumably reflecting the close proximity of the seafloor to the lysocline. With the exception of the depth interval from 140 to 220 m CSF, the remainder of Unit II exhibits uniformly high calcium carbonate content between 80 and 90 wt%. From ~150 to 210 m CSF (approximately equivalent to Cores 320-U1335A-16H through 22H), carbonate content cycles between ~50 and 90 wt% and corresponds to a change in dominant sediment color from light greenish gray to tan, displaying higher magnetic susceptibility values up to 25×10^{-5} SI.

A series of upper Oligocene through upper middle Miocene cores (320-U1335A-8H through 40X) were recovered with distinct colors ranging from light grayish green to light blue (see "Lithostratigraphy"), similar but much thicker in total stratigraphic thickness (~70–170 and ~200–350 m) than those observed at Site U1334 (see the "Site U1334" chapter). The colored carbonate oozes have extremely low magnetic susceptibilities that complicated a confident stratigraphic correlation. These colored oozes have lost almost their entire magnetic susceptibility signal from ~70 to ~105 m CSF and below ~210 m CSF (Figs. F4, F6, F7). Similar colored cores have previously been described for DSDP Sites 78 and 79 (Hays et al., 1972).

All major microfossil groups occur in sediments from Site U1335, representing a complete biostratigraphic succession at the shipboard sample resolution level of Pleistocene to uppermost Oligocene sediments, including a thick sequence of lower Miocene nannofossil ooze and chalk (see "Biostratigraphy"). Radiolarians are present through most of the section apart from the basal 3 m of nannofossil chalk. They provide a coherent high-resolution biochronology through a complete sequence of radiolarian zones

from RN14 (Pleistocene) to RP21 (upper Oligocene). Calcareous nannofossils are present and moderately to well preserved through most of the succession, representing the complete sequence from Zone NP25 (upper Oligocene) above basaltic basement through Zone NN20 (Pleistocene). Planktonic foraminifers are present throughout the succession and are moderately to well preserved. Recognized planktonic foraminifer zones range from Zone PT1a (Pleistocene) to Zone O6 (upper Oligocene). Nannofossil, radiolarian, and planktonic foraminifer datums are in good agreement. Benthic foraminifers are present through most of the section and indicate lower bathyal to abyssal paleodepths. The Oligocene–Miocene transition at Site U1335 was encountered at ~350 m and was fully recovered in Cores 320-U1335A-37X and 320-U1335B-38H as approximated by the planktonic foraminifer datum base of *Paragloborotalia kugleri* between Samples 320-U1335A-37X-4, 136–138 cm, and 37X-CC (midpoint = 348.6 m CSF), in good agreement with the calcareous nannofossil event top of *Sphenolithus delphix* at 349.7 m CSF between Samples 320-U1335A-37X-6, 50 cm, and 37X-CC. The oldest sediment overlying seafloor basalt has been assigned to calcareous nannofossil Zone NP25 (24.4–26.8 Ma).

Sedimentation rates, as derived from the magneto- and biostratigraphic age determinations (see **"Stratigraphic correlation and composite section"**), vary throughout the section and are ~6 m/m.y. in the late to middle Miocene to recent sediment cover, ~17 m/m.y. in the middle early Miocene and as high as ~25 m/m.y. throughout the late Oligocene and early Miocene. There is no obvious hiatus at the shipboard biostratigraphic resolution, although some condensed horizons exist (e.g., near the early/middle Miocene boundary and in the early late Miocene; see **"Biostratigraphy"**). The presence of all major fossil groups as well as a detailed and partly well resolved magnetostratigraphy will allow us to achieve one of the main PEAT objectives of arriving at an integrated Cenozoic stratigraphy and age calibration for the Miocene and late Oligocene.

A full physical property program was run on cores from Site U1335. This program comprises Whole-Round Multisensor Logger (WRMSL) measurements of magnetic susceptibility, bulk density, and *P*-wave velocity; natural gamma radiation (NGR); and measurements of color reflectance, followed by discrete measurements of moisture and density (MAD) properties, sound velocities, and thermal conductivity in Hole U1335A. All track data vary throughout the section, allowing a detailed correlation among holes, with the exception of a low magnetic susceptibility signal within an interval extending slightly above and below the light greenish gray tinted cores of Unit II (see **"Lithostratigraphy"** for exact color definitions), between ~70 and 110 and ~210 and ~380 m CSF. Magnetic susceptibility varies between 5×10^{-5} and 20×10^{-5} SI in the upper parts of Unit I and then increases to ~25×10^{-5} SI toward the lower part of Unit I, coinciding with the presence of clayey radiolarian ooze within the major lithology of nannofossil ooze. Magnetic susceptibility values decrease at the top of Unit II (~64 m CSF) and then fall to values around -1×10^{-5} SI near 70 m CSF. Between ~110 and 150 m CSF, magnetic susceptibility values increase slightly and become highly variable (0 to 10×10^{-5} SI). Magnetic susceptibility values are higher in the interval from 160 to 200 m CSF, coinciding with an observed decrease in Fe reduction (see **"Lithostratigraphy"**). Below 200 m CSF, the magnetic susceptibility signature is dominantly diamagnetic, with values close to zero. Magnetic susceptibility values slightly increase again in the basal 20 m of Unit II (below ~400 m CSF). NGR is elevated at the surface sediment (~73 counts per second [cps]) but low throughout the rest of the sedimentary column. *P*-wave velocities from the WRMSL agree with discrete velocity measurements and reflect key lithologic transitions, particularly the ooze to chalk transition near ~220 m CSF. *P*-wave velocities are between 1460 and 1490 m/s in Unit I and the upper part of Unit II and then increase to >1500 m/s. Slightly below the ooze–chalk transition near 345 m CSF, velocities increase significantly, reaching 1600–1750 m/s at the bottom of Unit II. This partly explains the thicker sediment section than was expected from seismic data prior to coring (~60 m thicker). Bulk density and grain density increase with depth, with an increase in wet bulk density from 1.2 to 1.6 g/cm^3 in Unit I to ~1.7 g/cm^3 at the top of Unit II and ~1.8 g/cm^3 in the basal part of the section. Sediment porosity ranges from 70% to 90% in Unit I to 50%–60% at ~300 m CSF in Unit II. Ephemeral whole-round samples were collected at ~96, ~196, and ~305 m CSF for shore-based studies of sediment permeability.

The coring effort in Holes U1335A and U1335B was successful at covering stratigraphic gaps between cores at this site from the surface throughout most of the APC-cored section (see **"Stratigraphic correlation and composite section"**), with the exception of a gap (~1 m) at the bottom of Core 320-U1335A-16H due to flow-in (~146.40–151.46 m CSF). Features in magnetic susceptibility and gamma ray attenuation (GRA) density are well aligned down to a depth of 337 m CSF (Hole 1335A) and 344 m CSF (Hole U1335B), corresponding to ~398 m core composite depth below seafloor (CCSF-A). Between ~230 and ~398 m CCSF-A, GRA density data allowed confident alignment of cores despite very low magnetic suscep-

tibility values. The section below ~398 m CCSF-A was mostly XCB cores, lacked clearly identifiable features, and therefore had to be appended to the splice. A single spliced record was assembled for the aligned cores down to Section 320-U1335B-37H-6 (343.76 m CSF; 398.15 m CCSF-A). Stratigraphic correlation between individual holes indicates a growth factor (ratio between the CCSF-A and CSF depth scales) of ~16%. Stratigraphic correlation resulted in a complete splice through the Eocene–Oligocene transition almost to basement (~38 Ma).

A full range of paleomagnetic analyses was conducted on 78 archive halves and 257 discrete samples from Site U1335 for the APC-cored section (upper ~378 m). The most prominent feature of the records is the magnetic intensity and susceptibility low that occurs between ~70 and 110 m CSF and below ~210 m CSF. We could not obtain any reliable paleomagnetic directions from this interval because the magnetic intensity after 20 mT alternating field (AF) demagnetization is on the order of 10^{-5} A/m, which is comparable to the noise level of the superconducting rock magnetometer (see **"Paleomagnetism"**). The drilling overprint was generally weak when nonmagnetic core barrels were used (Cores 320-U1335A-1H through 16H and 320-U1335B-1H through 19H). In contrast, cores collected with the steel core barrels are highly overprinted. Except for the low magnetic intensity interval, the cleaned paleomagnetic data provide a series of distinct ~180° alternations in declination. When combined with biostratigraphic age constraints (see **"Biostratigraphy"**), the data allow a continuous magnetostratigraphy from Chrons C1n (0–0.781 Ma) to C5n.2n (9.987–11.040 Ma) from 0 to 65.95 m CSF in Hole U1335A and from Chrons C1n to C5r.1n (11.118–11.154 Ma) from 0 to 66.225 m CSF in Hole U1335B. Below the bottom of the first magnetic low zone (~70–110 m CSF), magnetostratigraphy is again interpretable downhole: from Chrons C5Br (15.160–15.974 Ma) to C6n (18.748–19.722 Ma) from 155.35 to 208.40 m CSF in Hole U1335A and from Chrons C5AAn (13.015–13.183 Ma) to C5Er (18.524–18.748 Ma) from 107.95 to 202.60 m CSF in Hole U1335B. The highlights of the magnetostratigraphy at Site U1335 are the identifications of (1) a previously observed cryptochron (C5Dr-1n) in two holes and (2) 40 potential geomagnetic excursions (10 of which are recorded in both holes).

A standard shipboard suite of geochemical analyses of pore water and organic and inorganic sediment properties was undertaken on samples from Site U1335. Site U1335 is marked by alkalinities between 2.5 and 4.3 mM throughout, sulfate concentrations between 23 and 28 mM, and dissolved phosphate concentrations of ~2 µM in the shallowest sample, decreasing to ~0.5 µM in the uppermost ~50 m. The most striking features in the interstitial water geochemistry are three dissolved manganese peaks with concentrations of up to 44, 13, and 5 µM at ~0–40, 50–80, and 150–210 m CSF, respectively. Dissolved iron also shows three peaks, with concentrations up to 6 µM at ~6 m CSF, between 90 and 170 m CSF, and between 190 and 370 m CSF. Minima in dissolved Fe correspond to elevated Mn concentrations. The alternating pattern of dissolved Mn and Fe correspond well to apparent color changes in the sediment column (see **"Lithostratigraphy"**). Lithium concentrations decrease from ~26 µM at the sediment surface to 5 µM at ~300 m CSF, below which Li concentrations increase strongly to ~32 µM. The Sr concentration profile mirrors that of Li, with concentrations ranging between 82 and 250 µM. Sr values increase from the top to 200 m CSF, followed by a decrease toward basement. Calcium carbonate, inorganic carbon (IC), and total carbon (TC) contents were determined on sediment samples from Hole U1335A (Fig. **F5**). $CaCO_3$ contents ranged between 13 and 96 wt%. In the uppermost ~67 m, carbonate contents range from 12 to 87 wt%, and concentrations are then consistently high (~72–96 wt%) between 67 and 157 m CSF and below 222 m CSF. Carbonate contents vary more widely (between 37 and 89 wt%) from 157 to 222 m CSF. Total organic carbon (TOC) concentrations were determined by acidification and are generally low.

Wireline logging was not conducted at Site U1335. Five downhole temperature measurements were conducted in Hole U1335B with the advanced piston corer temperature tool (APCT-3) and reveal a thermal gradient of 7.5°C/km. Temperature data combined with whole-round core temperature conductivity measurements indicate the heat flow is 7 mW/m² at this site. This is much lower than values obtained for any of the other Expedition 320 sites and would suggest recirculation of seawater through basement, consistent with some of the interstitial pore water results (see **"Geochemistry"**).

Highlights

Highly expanded Miocene sedimentary section

One of the highlights from Site U1335 is the recovery of a thick Miocene carbonate-dominated section from the central equatorial Pacific, one of the high-priority objectives of the PEAT program. The early Miocene (7.1 m.y. duration) is captured in ~190 m of sediment, corresponding to a sedimentation rate of 27 m/m.y. The middle Miocene (4.4 m.y. duration) is recovered in ~95 m sediment, with a sedimentation rate of ~21 m/m.y. The sedimentation rate from the

late Oligocene into the Miocene is just under 20 m/m.y. These high sedimentation rates will facilitate the study of paleoceanographic processes at unprecedented resolution for the equatorial Pacific.

Oligocene–Miocene transition and depth transects

Site U1335 was planned as the youngest and shallowest component of the PEAT Oligocene–Miocene depth transect component, which will allow the study of critical intervals (such as the Mi-1 glacial inception; see Zachos et al., 2001b; Pälike et al., 2006a) and variations of the equatorial calcium carbonate compensation depth (CCD) throughout this transition and during the latest Oligocene and early Miocene. Site U1335 is estimated to have been ~3.3 km deep during the Oligocene–Miocene transition, ~1.5 km shallower than today. The dominant lithologies are nannofossil ooze and chalk, with better preservation of calcareous microfossils than any other site drilled during Expedition 320, which will allow us to achieve the prime objective for this site. Physical property data from Site U1335 provide an important contribution toward the Cenozoic megasplice, connecting with younger sediments from ODP Leg 138 (e.g., Site 850) and older sediments from Leg 199 (Site 1218), allowing the generation of astronomically calibrated datums and isotope stratigraphies from the Miocene into the Eocene.

Geochemical front

At Site U1335 we recovered an interval of light greenish gray carbonates that show a distinct peak in dissolved Fe concentrations, characteristic of a geochemical alteration front. At Site U1335, this zone is similar to but much thicker in total stratigraphic thickness (~70–170 and ~200–350 m CSF) than that observed at Site U1334 (~50 m; see the **"Site U1334"** chapter). Although the paleomagnetic signal was lost in most parts of this section, sediments recovered will provide the opportunity to study organic matter degradation while these sites migrated from south to north through the equatorial belts of high productivity. Paleolatitudinal reconstructions show that these characteristic geochemical alteration fronts can be mapped to similar equatorial positions between Sites U1334 and U1335, roughly between the Equator and ~2°N. One feature of interest at Site U1335 is the observation that the multicolored interval of sediments is interrupted between ~170 and 200 m CSF (Cores 320-U1335A-18H through 20H), again showing higher magnetic susceptibility values. It remains to be established whether this interruption in the geochemical alteration front is related to the shape and position of the equatorial high-productivity zone or instead is the result of reduced sedimentation rates during this time (late early Miocene). Interstitial pore water profiles provide additional important information about the redox chemical processes operating in this zone (see **"Geochemistry"**), which have also been observed at Sites 78, 79, and 574 (e.g., Hays et al., 1972).

Gravity flow deposits

One of the prominent features of Unit II is the presence of at least 49 described beds (2–176 cm thick) of nannofossil foraminifer ooze that have sharp basal boundaries, many of which are irregular and some of which are inclined. These beds are interpreted as gravity flow deposits from the nearby seamounts and represent ~2% of the total sediment recovered. Their grain size fines upward from medium sand to silt, and they are often darker colored than immediately overlying deposits and instantly recognizable by their coarser texture. Angular basalt fragments (<1 mm), fish teeth, and pyritized foraminifers and radiolarians were also found within the basal parts of these beds, of which at least three show parallel or cross-laminations in their upper or middle part. These beds, interpreted as gravity flow deposits, are present with an approximate frequency of one or two beds per core. The abundance and thickness of these beds is highest within Cores 320-U1335-21H through 37X (189.4–350.1 m CSF). No gravity flow deposits were observed in Cores 320-U1335A-3H through 8H. The provenance of these deposits, as indicated by the observed basalt fragments, is inferred to be the nearby seamounts (Fig. **F1B**) situated ~15–20 km northeast and southeast of Site U1335, with present summit water depths that are 400–600 m shallower than Site U1335. Initial indications are that these gravity flow deposits, unlike those observed at Site U1331, might not be very erosive and therefore essentially add to the sediment column rather than removing large sections of geological time. The high sedimentation rates at Site U1335 will allow paleoceanographic studies to avoid the generally thin layers of gravity flows.

Age transect of seafloor basalt

At Site U1335 we recovered what appear to be fresh fragments of seafloor basalt with an age of ~26 Ma, as inferred by the oldest biostratigraphic datums from the sediment above. This material will, when combined with other PEAT basalt samples, provide important sample material for the study of seawater alteration of basalt.

Operations

Times for Site U1335 are given in local ship time, which was universal time coordinated (UTC) – 9 h.

Transit to Site U1335

The 375 nmi voyage from Site U1334 to Site U1335 took 42.3 h at an average speed of 8.9 kt. Shortly after departing Site U1334, propulsion Motor 16A on the port propeller shaft had to be taken offline because of defective field coils. This was the second propulsion motor to exhibit the same problem during Expedition 320. Propulsion Motor 15A on the starboard shaft had to be removed from the grid shortly after leaving Honolulu. It is expected that these units will be repaired during the port call in Honolulu. The rest of the voyage was made with reduced revolutions on both shafts (120 rpm instead of 140 rpm). Although capable of higher shaft revolutions, the lower shaft power was necessary to keep the ambient temperature in the propulsion room from moving into a critically high range.

Site U1335

Hole U1335A

The ship slowed and was in dynamic positioning (DP) mode over Hole U1335A at 1630 h on 15 April 2009. We assembled the drill string, lowered it to the seafloor, and started coring Hole U1335A at 0355 h on 16 April. The estimated water depth based on the recovery of the first core was 4339.0 m DRF (4327.5 mbsl) (Table **T1**).

Cores 1H through 36H were taken from 0 to 341.4 m DSF, and we recovered 354.7 m (104%) (Table **T1**). APC piston coring to this depth is an operational highlight for this site. Nonmagnetic core barrels were used for Cores 1H through 16H, and steel barrels were used for all other cores. Nine core barrels required drilling over to release them from the formation (Cores 19H through 22H, 26H, 27H, and 34H through 36H) and Cores 16H and 36H only partially stroked.

We then switched to XCB coring and took Cores 37X through 45X from 341.4 to 421.1 m DSF and recovered 67.9 m (85%). We retrieved Core 45X after taking ~1 h to advance only 3 m. When retrieving this core, it apparently became stuck in the drill string just above the bottom-hole assembly. We attempted to free the stuck core barrel with the wireline jars by alternating the tension on the coring line for ~1 h when the overshot shear pin parted. Once we recovered the sinker bars and wireline jars, we pumped another core barrel down on top of it and this succeeded in dislodging the stuck core, which dropped back down to the bit. When Core 45X was recovered, it contained hard limestone and the XCB bit was very worn down, so we decided it was best to stop coring in this hole. The basement depth is deeper than anticipated and suggests higher seismic velocities in the sediment column from Site U1335 than those from the nearest site (574). Once Hole U1335A was completed, the bit was pulled free of the seafloor at 1725 h on 18 April and the vessel offset 25 m west.

Hole U1335B

We started coring Hole U1335B at 1955 h on 18 April with the bit 5 m deeper than at Hole U1335A. The seafloor depth based on the recovery of the first core was 4339.6 m DRF (4328.1 mbsl).

APC Cores 1H through 41H were taken from 0 to 378.2 m DSF, and we recovered 392.7 m (104%). At the time, this was the second deepest APC penetration in the history of ocean drilling. Nonmagnetic core barrels were used on Cores 1H through 19H, and steel barrels were used on all remaining cores. Formation temperature measurements were made with the APCT-3 at 22.3, 41.3, 60.3, 79.3, and 98.3 m DSF (Cores 3H, 5H, 7H, 9H, and 11H, respectively). Twelve core barrels had to be drilled over to release them from the formation (Cores 19H, 20H, and 35H through 41H). Cores 37H through 41H did not achieve a full stroke and were advanced by recovery.

After switching to XCB coring, we took Cores 42X through 46X from 378.2 to 417.5 m DSF and recovered 36.0 m (92%). Coring was terminated when basement was reached.

Originally we had planned three holes at Site U1335. However, after recovering a continuous Miocene section with nearly complete recovery and overlap between the two holes, we decided to not core a third hole at Site U1335. The fact that the cores contained frequent turbidites and a very weak magnetic signal in the interval with the distinctly colored (diagenetically altered) sediment also contributed to this decision. Instead we decided to use our remaining time to core at Site U1336 to provide the second PEAT expedition more information for optimizing their operations plan.

We pulled the drill string out of the hole, and the bit cleared the seafloor at 1215 h on 21 April. Before the drill string was recovered, we spent 1 h to slip and cut 115 ft of drill line. Once drilling line maintenance was completed, the drill string was recovered, the beacon retrieved, and the drilling equipment secured for transit. The vessel departed for Site U1336 at 2145 h on 21 April.

Lithostratigraphy

Drilling at Site U1335 recovered a ~420 m thick section of pelagic sediments overlying seafloor basalt (Fig. F4). The sedimentary sequence at Site U1335 is divided into two major lithologic units (Fig. F4; Table T2). The upper part of the sedimentary sequence (0–64 m CSF; Unit I) is characterized by an alternating sequence of multicolored nannofossil, diatom, and radiolarian oozes of early late Miocene to Pleistocene age. Unit II is a ~350 m thick sequence of nannofossil ooze and chalk of late Oligocene to early late Miocene age. This unit is characterized by pronounced changes in color, both at the thick stratigraphic scale (20–190 m) (Fig. F6) and superimposed centimeter- to millimeter-scale color banding. Unit II contains many thin beds of nannofossil foraminifer ooze overlying sharp basal contacts (Fig. F4).

Lithologic units and boundaries are defined by changes in lithology, physical properties, and calcium carbonate ($CaCO_3$) content as measured by coulometry. Lithologic differences, based on both visual core description and smear slide observations, are primarily attributable to varying distributions of biogenic components (nannofossils, diatoms, radiolarians, and foraminifers). Lithologic descriptions are based primarily on sediments recovered in Hole U1335A, supplemented with observations from Hole U1335B.

Unit I

Intervals: 320-U1335A-1H-1, 0 cm, through 7H-6, 44 cm; 320-U1335B-1H-1, 0 cm, through 8H-5, 75 cm

Depths: Hole U1335A = 0–64.34 m CSF; Hole U1335B = 0–67.05 m

Age: Pleistocene to early late Miocene

Lithology: alternation of nannofossil ooze, diatom nannofossil ooze, clayey nannofossil ooze, foraminifer nannofossil ooze, nannofossil foraminifer ooze, radiolarian diatom ooze, nannofossil diatom ooze, clayey diatom ooze, clayey radiolarian ooze, and clay

The major lithologies in Unit I are white (10YR 8/1) through dark grayish brown (2.5Y 4/2) nannofossil ooze, very pale brown (10YR 8/2) foraminifer nannofossil ooze, very pale brown (10YR 7/3) through olive-brown (2.5Y 4/3) diatom nannofossil ooze, light gray (10YR 7/2) to very pale brown (10YR 7/4) radiolarian diatom ooze, very pale brown (10YR 8/4) and olive-brown (2.5Y 4/3) nannofossil diatom ooze, dark gray (10YR 4/1) clayey nannofossil ooze, very dark grayish brown (10YR 3/2) clayey radiolarian ooze, brown (10YR 4/3) clayey diatom ooze, and brown (10YR 4/3) clay.

Sediments in Unit I show cyclic alternations in lithology of 30–80 cm thickness. An exception to this is a ~9 m thick white (10YR 8/1) to very pale brown (10YR 8/2) nannofossil ooze observed between 45.5 and 54.5 m CSF (from interval 320-U1335A-5H-6, 80 cm, to 6H-6, 9 cm). Beneath this interval, the lowermost part of Unit I consists of clay-rich sediments of very dark grayish brown (10YR 3/2) clayey radiolarian ooze and brown (10YR 4/3) clay that alternate with grayish brown (2.5Y 5/2) to light brownish gray (2.5Y 6/2) nannofossil ooze with diatoms (e.g., Cores 320-U1335A-7H and 320-U1335B-7H). Clay-rich intervals are characterized by high magnetic susceptibility (up to 22×10^{-5} SI), low L* (25–30), elevated b* and L* (10–15), and low GRA bulk density (<1.2 g/cm^3) values (Fig. F4). The nannofossil ooze layer shows low magnetic susceptibility (<6.0×10^{-5} SI), high L* (>80), low b* (<10), and high bulk density (up to 1.7 g/cm^3) values. Bioturbation is generally intense in Unit I, particularly in the alternating multicolored biogenic oozes.

The Unit I/II boundary is located at interval 320-U1335A-7H-6, 44 cm (64.34 m CSF), and is defined at the base of an alternating sequence of clayey radiolarian ooze with clay and nannofossils and nannofossil ooze with diatoms (Table T2). Below the unit boundary to interval 320-U1335A-8H-2, 50 cm (67.90 m CSF), physical property data show a transition to lower magnetic susceptibility, higher L*, lower b*, and higher GRA bulk density values (Fig. F4).

Unit II

Intervals: 320-U1335A-7H-6, 44 cm, to at least 45X-CC, 15 cm; 320-U1335B-8H-5, 75 cm, to 46X-CC, 8 cm

Depths: Hole U1335A = 64.34 to at least 420.08 m CSF; Hole U1335B 67.05–418.04 m CSF

Age: early late Miocene to late Oligocene

Lithology: nannofossil ooze, radiolarian nannofossil ooze, foraminifer nannofossil ooze, nannofossil foraminifer ooze, and nannofossil chalk

Major lithologies in Unit II are white (10YR 8/1) to very pale brown (10YR 8/4) and light greenish gray (10Y 8/1 to 5GY 7/1) nannofossil ooze and white (2.5Y 8/1) and pale yellow (2.5Y 7/3) nannofossil chalk. Several 10–50 cm thick interbedded layers of yellow (10YR 7/6) to light greenish gray (5GY 7/1) nannofossil radiolarian ooze occur in the middle part of Unit II (157–176 m CSF in Hole U1335A). In

addition, two distinct thin beds (18–23 cm thick) of nannofossil diatom ooze are interbedded within the nannofossil ooze (Samples 320-U1335B-10H-3, 62–80 cm, and 24H-6, 40–63 cm) (Figs. F8, F9). In the middle part of Unit II (157–176 m CSF in Hole U1335A), some intercalations of white (N 8) to pale yellow (2.5Y 7/4) and light greenish gray (5GY 7/1) nannofossil ooze contain radiolarians or diatoms with abundances reaching between 10% and 25% (see "Site U1335 smear slides" in "Core descriptions"). These intervals of nannofossil radiolarian ooze, nannofossil diatom ooze, and nannofossil ooze with radiolarians or diatoms show darker colors relative to the immediately overlying and underlying nannofossil ooze intervals. Bioturbation is generally minor throughout Unit II.

One of the most prominent features of Unit II is the intercalation of at least 49 beds (2–162 cm thick) of white (N 8 and 10YR 8/1), light greenish gray (10Y 8/1, 10GY 8/1, and 5GY 8/1), and light gray (N 7) nannofossil foraminifer ooze (Table T3). These beds have sharp basal boundaries, many of which are irregular, some of which are inclined. Grain size fines upward from medium sand to silt within these beds. Basal sediments are often darker colored than the immediately overlying deposits. Basal sediments are dominated by nannofossil foraminifer ooze and are instantly recognizable in the split core by their coarse texture during preparation (surface scraping) for line scan imaging. Angular basalt fragments (<1 mm), fish teeth, and pyritized foraminifers and radiolarians are also found concentrated in these basal deposits (Fig. F10). At least three of these beds show parallel or cross-laminations in their middle or upper part.

In the basal part of Unit II, at least five thin (4–13 cm thick) intervals of nannofossil chalk contain sand- to pebble-sized fresh basalt clasts with a glassy rim in nannofossil chalk (see "Site U1335 smear slides" in "Core descriptions"). Boundaries between basalt-containing nannofossil ooze and adjacent nannofossil oozes are not clear because of bioturbation and XCB drilling disturbance (biscuits).

Nannofossil ooze in Unit II displays pronounced changes in color, both at the thick stratigraphic scale (20–190 m) (Fig. F6) and superimposed centimeter- to millimeter-scale color banding (Fig. F11). At the top of Unit II, sediment color shifts downhole from pale yellow (2.5Y 8/2) toward white (N 8) and light greenish gray (10Y 8/1) around 67–72 m CSF (Hole U1335A). The white and light greenish gray color persists for ~100 m downhole and then reverts back to pale yellow and very pale brown for ~20 m (Fig. F6). Below 192 m, sediments are consistently white (N 8) and light greenish gray over a 180 m thick interval to 372 m CSF (Hole U1335A). Around 372 m CSF, color shifts back from white (N 8) to pale yellow (2.5Y 7/3) toward pale brown (10YR 7/3) to the base of the sediment column (Fig. F6). Superimposed on these gross changes in sediment color within the light greenish gray intervals millimeter- to centimeter-scale light greenish gray (5GY 8/1, 10GY 8/1, 5G 8/1, 5GY 7/1, 10GY 7/1, and 5G 7/1), light gray (N 7), and gray (N 6) color bands are common (Figs. F4, F11). The color bands occur both with sharply defined boundaries and with more diffusive boundaries. Sometimes the sharply defined color bands occur in discrete beds that are distinctly more consolidated than immediately over- and underlying sediments (Fig. F11). Based on smear slide observations, the lithology of the color-banded sediments (nannofossil ooze) is identical to the immediately over- and underlying sediments (see "Site U1335 smear slides" in "Core descriptions"). Submillimeter-sized opaques, presumably sulfide minerals such as pyrite, form streaks and fill burrows.

Magnetic susceptibility is extremely low in Unit II between 68 and 118 m CSF and between 200 and 400 m CSF (Fig. F4). These two intervals broadly correspond to the light greenish gray intervals. Reflectance parameters a* and b* shift in a stepwise manner to lower values or toward green (a*) and blue (b*) with the observed color shift toward light greenish gray (Fig. F6). Within the stratigraphic interval between 118 and 199 m CSF (Hole U1335A), magnetic susceptibility data show sporadic peaks that correspond to the slightly darker, siliceous fossil-rich intervals (i.e., nannofossil radiolarian ooze, nannofossil ooze with radiolarians, and nannofossil ooze with diatoms). Higher magnetic susceptibility values in the radiolarian- and diatom-rich intervals indicate higher clay contents than the adjacent pure nannofossil oozes.

Unit III

Intervals: 320-U1335B-46X-CC, 8 cm, through at least 46X-CC, 46 cm; no basalt drilled in Hole U1335A

Depth: Hole U1335B = 418.04 to at least 418.42 m CSF

Lithology: basalt

Pieces of basalt up to 10 cm in length were recovered at the base of Hole U1335B. These basalt pieces have glassy rims and are overlain by the nannofossil chalks of Unit II.

Redox-related color changes

The homogeneous lithology of Unit II is overprinted by vivid color changes similar to those observed at Site U1334. Light greenish gray nannofossil ooze occurs in two stratigraphic intervals, between 70 and 170 m and 192 and 323 m. Magnetic susceptibility drops to near zero, and reflectance parameters a* and b* shift to lower values with the observed color shifts toward light greenish gray (Fig. F6). Pore water profiles for dissolved Fe and Mn concentrations show downhole changes that are consistent with the changes in sediment color and magnetic susceptibility data (see "Geochemistry"). A significant peak in dissolved Fe in the pore fluids occurs in the light greenish gray intervals between 80 and 165 m and 203 and 316 m CSF (Hole U1335A), with distinct minima that correspond to the return to pale brown color and higher magnetic susceptibility between the greenish layers and at the base of the section (see "Geochemistry"). The pattern of changing sediment color, physical and magnetic properties, and pore water chemistry in the two intervals suggests loss of Fe-bearing minerals during diagenesis by microbial Fe reduction. A diagenetic origin for the color bands is suggested by (1) their occurrence in the interval of the sequence that has undergone Fe reduction, (2) their lack of lithological specificity, and (3) the consolidation sometimes associated with discrete beds that show particularly prominent banding. Similar gray and light greenish gray banding is reported from sediments recovered from Ongtong Java Plateau (ODP Leg 130), where they are enriched in iron sulfides in gray layers and in iron and magnesium silicates in green layers (Lind et al., 1993).

Gravity flow deposits

Throughout the sedimentary section drilled at Site U1335, sharp irregular contacts occur between lithologies (Table T3; Figs. F10, F12). Many of these sharp contacts are directly overlain by coarser sediment (i.e., nannofossil foraminifer ooze), generally showing a normal grading. The coarse-grained sediments directly overlying the sharp contacts are clearly of erosional origin and sometimes contain angular basalt fragments (Fig. F10), pyritized foraminifers and/or radiolarians, and fish teeth at the base. There is a concentration of grayish layers in the basal intervals of the nannofossil foraminifer ooze that may reflect increased porosity in coarse sediments and intensified iron sulfide precipitation. In some cases, coarse intervals show cross or parallel laminations in the middle of the bed. These features indicate that the erosional contacts and their overlying coarse sediments are the product of mass flow events, likely turbidity currents. The thickness of the inferred turbidites is typically between 2 and 25 cm, with a maximum thickness of 176 cm in Sections 320-U1335B-36H-2 and 36H-3 (Table T3). Gravity flow deposits occur with an approximate frequency of one or two beds per core, and their total thickness occupies a minimum of 2% of the recovered sediment. The abundance and thickness of turbidites is highest within Cores 320-U1335A-21H through 37X (189.4–350.1 m CSF). In contrast, no gravity flow deposits are observed between Cores 320-U1335A-3H and 8H (18.4–75.9 m CSF). The presence of basalt fragments at the base of some turbidites suggests that the provenance of the inferred turbidites observed at Site U1335 is likely one or both of the two seamounts located 15 to 20 km northeast and southeast (present summit water depth is ~400–600 m shallower than Site U1335) (Fig. F1).

Sediments across the Oligocene–Miocene transition

The Oligocene/Miocene boundary was recovered in both holes at Site U1335 (Fig. F4). The Oligocene/Miocene boundary (23.0 Ma) is approximated by the first appearance of the planktonic foraminifer *P. kugleri,* whereas the last occurrence of nannofossil *S. delphix* falls 100 k.y. before the Oligocene/Miocene boundary (23.1 Ma). *P. kugleri* is present in Sample 320-U1335A-37X-4, 136–138 cm, and the top of *S. delphix* falls between Samples 320-U1335A-37X-6, 50 cm, and 37X-CC (see "Biostratigraphy"). Therefore, the Oligocene/Miocene boundary is estimated to fall between Samples 320-U1335A-37X-4, 136–138 cm, and 37X-CC. Magnetostratigraphic data are not available for these intervals because of XCB coring in Hole U1335A (below Core 320-U1335A-37X) and loss of signal in Hole U1335B (see "Magnetostratigraphy"). No shipboard splice is available for this interval (see "Stratigraphic correlation and composite section"). The Oligocene–Miocene transition in Holes U1335A and U1335B occurs in white to light greenish gray nannofossil ooze with frequent millimeter- to centimeter-scale color bands and a sharp boundary (interval 320-U1335A-37X-6, 44 cm) overlain by an 18 cm thick bed of nannofossil foraminifer ooze that fines upward. No prominent change in lithology, GRA bulk density, reflectance, or magnetic susceptibility is seen through the Oligocene–Miocene transition.

Summary

At Site U1335, Oligocene seafloor basalt is overlain by ~420 m of calcareous sediments that are divided into two lithologic units. The sediments are primarily composed of nannofossil oozes and nannofossil chalks. The Pleistocene through late middle

Miocene sedimentary sequence (Unit I) contains more radiolarians, diatoms, and clay relative to the Oligocene through late middle Miocene sediments (Unit II). Unit II is characterized by homogeneous nannofossil ooze and nannofossil chalk with interbedded nannofossil radiolarian ooze that corresponds to the transition from early to middle Miocene. Unit II is marked by two intervals of major color change from very pale brown to pale yellow to light greenish gray and back to pale brown nannofossil ooze. Intervals of light greenish gray nannofossil ooze are overprinted by vivid color banding ranging from millimeter- to centimeter-scale similar to that observed at Site U1334. Throughout Unit II, sharp irregular contacts are frequent and often overlain by coarser sediment (i.e., nannofossil foraminifer ooze) interpreted as mass flow events and appear to be turbidites. Fresh seafloor basalt was recovered at the base of the sedimentary section.

Biostratigraphy

At Site U1335, we recovered a 420 m thick succession of Pleistocene to upper Oligocene sediments, including an expanded sequence of lower Miocene nannofossil ooze and chalk. A Pliocene–Pleistocene succession of nannofossil and radiolarian ooze was recovered from the top 29 m of the hole. This was deposited on top of 135 m of upper and middle Miocene nannofossil ooze and an expanded succession of 185 m of lower Miocene nannofossil ooze. A 71 m thick interval of upper Oligocene nannofossil chalk was recovered above basement. Radiolarians are present through most of the section apart from the basal 3 m of nannofossil chalk. They provide a coherent, high-resolution biochronology through a complete sequence of radiolarian zones from Zone RN14 (Pleistocene) to Zone RP21 (upper Oligocene). Calcareous nannofossils are present and moderately to well preserved through most of the succession. There appears to be a complete sequence of nannofossil zones from Zone NN20-21 (Pleistocene) to Zone NP25 (upper Oligocene). Planktonic foraminifers are generally well preserved throughout the section, enabling a complete sequence of planktonic foraminifer zones from Zone PT1a (Pleistocene) to Zone O6 (upper Oligocene) to be recognized. Nannofossil, radiolarian, and planktonic foraminifer datums are in good agreement. An integrated calcareous and siliceous microfossil biozonation is shown in Figure **F13.** A detailed age-depth plot including biostratigraphic and paleomagnetic datums is shown in Figure **F14.** Benthic foraminifers are present through most of the section and indicate lower bathyal to abyssal paleodepths.

Calcareous nannofossils

Calcareous nannofossil biostratigraphy is based on analysis of core catcher samples from both holes and from samples from most core sections of Hole U1335A. Depth positions and age estimates of biostratigraphic marker events are shown in Table **T4.** Nannofossils are generally abundant and moderately to well preserved throughout but with some intervals of poor to moderate preservation in the upper Miocene (Cores 320-U1335-4H through 8H; Zones NN7–NN12).

Nannofossils are present and moderately to well preserved within the topmost sample (320-U1335A-1H-1, 40 cm) with an assemblage dominated by abundant *Gephyrocapsa* spp., *Calcidiscus leptoporus,* and *Florisphaera profunda*. This sample is assigned to an undifferentiated Zone NP20-21 because of the presence of questionable *Emiliania huxleyi*. The top of *Pseudoemiliania lacunosa* in Sample 320-U1335A-1H-3, 100 cm, marks the top of Zone NN19. A continuous succession of nannofossil datums (Table **T4**) suggests that there is near-continuous stratigraphy through the Pliocene–Pleistocene. It was not possible to reliably pick some of the additional datums within Zone NN19 that are based on size changes within the genus *Gephyrocapsa*. Because of relatively low sedimentation rates, however, several well-calibrated datums that are separated by 10–100 k.y. within the lower Pleistocene–Pliocene interval are found at the same level in the present section-resolution biostratigraphy (the top of *Calcidiscus macintyrei* at 1.61 Ma together with the top of *Discoaster brouweri* at 1.93 Ma, the top of *Discoaster pentaradiatus* at 2.39 Ma with the top of *Discoaster surculus* at 2.49 Ma, the top of *Sphenolithus* spp. at 3.54 Ma with the top of *Reticulofenestra pseudoumbilicus* at 3.70 Ma, the top of *Ceratolithus acutus* at 5.04 Ma with the top of *Ceratolithus rugosus* at 5.05 Ma, and the top of *Triquetrorhabdulus rugosus* at 5.28 Ma with the base of *C. acutus* at 5.35 Ma). Very low abundances or absence of some additional marker species also prevented the use of their associated datums, including the top of *Helicosphaera sellii,* base of common *Discoaster triradiatus,* and base of *Ceratolithus larrymayeri*. The Miocene/Pliocene boundary (5.33 Ma) is located between the datums at the top of *T. rugosus* at 5.28 Ma and base of *C. acutus* at 5.35 Ma, which both occur between Samples 320-U1335A-3H-CC and 4H-1, 66 cm.

Nannofossil datums within the 46 m sequence of upper Miocene nannofossil ooze indicate a sedimenta-

tion rate of ~7 m/m.y., similar to that within the Pliocene–Pleistocene interval (Fig. F14). Additional datums within Zone NN11, based on *Nicklithus amplificus* (top of *N. amplificus* and abundance crossover of *N. amplificus*/*T. rugosus*), were not possible to place because of the very rare occurrence of *N. amplificus,* which was only observed in Sample 320-U1335A-4H-6, 66 cm. *Catinaster calyculus* was absent. The co-occurrence of the base of *Discoaster hamatus,* base of *Catinaster coalitus,* and top of *Coccolithus miopelagicus* datums between Samples 320-U1335A-7H-4, 82 cm, and 7H-6, 79 cm, marks the Zone NN8/NN9 boundary. Sedimentation rates also remain low (~7 m/m.y.) in the lower part of the upper Miocene. The middle/late Miocene boundary (11.60 Ma) is placed close to the top common *Discoaster kugleri* (11.58 Ma), which occurs at 72.8 m CSF between Samples 320-U1335A-8H-4, 90 cm, and 8H-6, 90 cm.

Sedimentation rates are significantly higher below the middle/late Miocene boundary: ~18 m/m.y. to ~19 Ma, increasing to ~33 m/m.y. from ~19 Ma through to the base of the hole in the upper Oligocene (~25 Ma). Almost all lower and middle Miocene datums and nannofossil zones were recognized, although the Zone NN4/NN5 boundary could not be accurately determined because of the absence of *Helicosphaera ampliaperta* in these sediments. The additional datum of the base of *Discoaster petaliformis* (15.70 Ma) (*Discoaster signus* in Raffi et al., 2006) was, however, recognized between Samples 320-U1335A-16H-CC and 17H-2, 70 cm, within the upper part of Zone NN4. At Site U1335 there is a short interval at the base of Zone NN4 between the base common occurrence of *Sphenolithus heteromorphus* and the top common occurrence of *Sphenolithus belemnos,* where both of these taxa are pre.sent at low abundances (cf. Young, 1999), some of which may represent intergrading morphologies between these two morphotypes. The intra–Zone NN2 bioevents of the base of *H. ampliaperta* and the abundance crossover of *Helicosphaera euphratis*/*Helicosphaera carteri* could not be recognized in this succession because of the absence of *H. ampliaperta* and patchy distribution of other *Helicosphaera* species. The additional event of the top acme of *Triquetrorhabdulus carinatus* (Raffi et al., 2006) is, however, easily identified toward the base of Zone NN2. Although the placement of the Zone NN1/NN2 boundary, as defined by the base of *Discoaster druggii,* is usually problematic because of the rarity and poorly defined nature of this taxon (Young, 1999), *D. druggii* is conspicuously present in Samples 320-U1335A-36H-CC and 37X-2, 90 cm. These two samples also bracket the base of *Sphenolithus disbelemnos,* which has been used as a proxy for the Zone NN1/NN2 boundary (Young, 1999); this may indicate that *D. druggii* has a short interval of increased abundance at the base of its range and may still be of some use in determining the Zone NN1/NN2 boundary.

The placement of the Oligocene/Miocene boundary (23.0 Ma), based on the planktonic foraminifer event of the base of *P. kugleri* at 348.6 m CSF, is in good agreement with the topmost Oligocene nannofossil event, the top of *S. delphix* at 349.7 m CSF between Samples 320-U1335A-37X-6, 50 cm, and 37X-CC. There are three nannofossil events closely spaced around the Zone NP25/NN1 boundary: top of *Sphenolithus ciperoensis,* abundance crossover of *Triquetrorhabdulus longus*/*T. carinatus,* and top common of *Cyclicargolithus abisectus*. At Sites U1332–U1335, there is no clear "acme" event of *C. abisectus;* however, it does appear to have a clear and consistent top occurrence, at least in the eastern equatorial Pacific, close to the Zone NP25/NN1 boundary at the same level as the top acme calibration on the ODP Leg 199 timescale (Lyle, Wilson, Janecek, et al., 2002).

Radiolarians

The radiolarian stratigraphy at Site U1335 (Fig. F13; Table T5) spans the interval from Zone RN14 (lower Pleistocene) in Core 320-U1335-1H to the uppermost part of Zone RP21 (upper Oligocene) in the upper part of Core 320-U1335-44X (Samples 320-U1335-44X-2, 105–107 cm, and 44X-4, 105–107 cm) (Tables T6, T7). The assemblages are generally well preserved throughout the recovered section; however, there are several intervals in which the preservation is only moderate. Samples with moderate preservation are most commonly found in the upper part of the section within Core 320-U1335-7H (lowermost upper Miocene) and in Cores 320-U1335-12H through 15H (middle Miocene), 25H through 29H (lower Miocene), and 37H and 38H (lowermost lower Miocene). This intermittent decrease in preservation is not clearly associated with any particular lithologic observation, such as the occurrence of turbidites or color changes. Nor is it associated with reworked older microfossils. Reworked older radiolarians are found mixed within younger assemblages most commonly in Cores 320-U1335-1H through 4H, an interval with lower average accumulation rates (Fig. F14). In the remainder of the section, reworking of older microfossils is minor and found mainly in the lower middle Miocene part of the section.

The lack of a clear association of preservation and reworking with the occurrence of turbidites in the section (see "Lithostratigraphy") suggests that the

material transported by these turbidites was nearly the same age as the levels at which they were deposited. However, the frequent occurrence of these turbidites could have an effect on the upper limit (last occurrence) of some of the stratigraphically important species (Table **T5**) by extending their apparent range upsection. Therefore, the first occurrence of a species is generally considered a more reliable datum in Zones RP18 through RP20.

In the expanded lower Miocene and Oligocene section it becomes clear that some of the species used in the radiolarian stratigraphy are discontinuous in their appearance. This was noticed in the Leg 199 material in such common and robust species as *Acrocubus octopylus* and *Didymocyrtis tubaria* (Nigrini et al., 2006). In Site U1335 we also see the discontinuous occurrences of these species, as well as in *Dorcadospyris ateuchus* and *Lychnocanoma elongata*. This may reflect large variation in the abundance of these species with time and changing ecologic conditions. However, there is also the possibility that at least some of these intermittent disappearances of a species may reflect genetic changes in the lineage that give rise to either "iterative evolution" or changing ecological preferences.

As at Sites U1331–U1334, the lower part of the succession (Cores 320-U1335A-40X through the upper part of 44X) has only moderate radiolarian preservation and the lowermost samples (Samples 320-U1335A-44X-CC through 45X-CC) are completely barren of radiolarians.

Diatoms

Diatoms were examined in core catcher samples from Hole U1335A and represent the interval from the *Fragilariopsis reinholdii* Zone through the *Rocella gelida* Zone of Barron (1985, 2006) and Barron et al. (2006). Diatoms range in abundance from rare to abundant. Diatom preservation is variable but generally moderate to good. Several intervals as discussed below reflect much poorer preservation, whereas others are better. Typical zonal indicators are not always present, requiring the use of secondary markers for zonal placement. Specific zonal assignments are as follows.

Sample 320-U1335A-1H-CC contains a Pleistocene diatom assemblage typified by *Actinocyclus ellipticus, Asteromphalus elegans, Azpeitia nodulifera, Hemidiscus cuneiformis, Nitzschia fossilis, F. reinholdii, Thalassiosira eccentrica,* and *Fragilariopsis doliolus*. The occurrences of *F. reinholdii* with *F. doliolus* allows placement of this sample into the *F. reinholdii* Zone.

Sample 320-U1335A-2H-CC is assigned to the *Nitzschia jouseae* Zone based on the occurrence of *N. jouseae* without *Rhizosolenia praebergonii*. The *R. praebergonii* Zone was not observed as a result of sample spacing.

The *Thalassiosira convexa* Zone is represented in Samples 320-U1335A-3H-CC and 4H-CC. Sample 320-U1335A-3H-CC is assigned to the upper portion of this zone based on the occurrences of *Fragilariopsis cylindrica, T. convexa* var. *aspinosa,* and *Thalassiosira oestrupii* without *N. jouseae*. The suggestion of this sample being equivalent to the upper portion of this zone is based on the presence of specimens transitional between *F. cylindrica* and *N. jouseae*. Sample 320-U1335A-4H-CC is assigned to Subzone A of the *T. convexa* Zone based on the occurrences of *Thalassiosira praeconvexa, Nitzschia miocenica, T. convexa* var. *aspinosa,* and *Asterolampra acutiloba*. The *N. miocenica* Zone was not observed because of sample spacing.

The occurrences of *Nitzschia porteri* and *F. cylindrica* without *N. miocenica* allows placement of Sample U1335A-5H-CC into the *N. porteri* Zone. *Thalassiosira burckliana* was not observed in the sample, suggesting placement of the sample in Subzone B of the *N. porteri* Zone.

Sample 320-U1335A-6H-CC is assigned to the *Thalassiosira yabei* Zone based on the occurrences of *T. yabei, A. ellipticus* var. *javanica,* and *A. nodulifera* var. *cyclopsa*. *T. burckliana* was not observed in the sample, suggesting placement of the sample in Subzone A of the *T. yabei* Zone.

The last occurrence of *Denticulopsis simonsenii* was recognized to have a chronostratigraphic occurrence similar to that of *Actinocyclus moronensis* and as such was identified as a useful datum for determining the top of the *A. moronensis* Zone. The common occurrence of *D. simonsenii* in Sample 320-U1335A-7H-CC suggests placement of this sample in the *A. moronensis* Zone.

The co-occurrence of *Craspedodiscus coscinodiscus* and *Coscinodiscus gigas* var. *diorama* allows placement of Sample 320-U1335A-8H-CC in the *C. coscinodiscus* Zone. The occurrence of *A. ellipticus* var. *spiralis* and *Rossiella praepaleacea* without *H. cuneiformis* suggests placement in the middle portion of this zone.

Samples 320-U1335A-9H-CC and 10H-CC are assigned to the *C. gigas* var. *diorama* Zone. The zonal assignment of Sample 320-U1335A-9H-CC is tentative. This sample is characterized by the presences of *D. simonsenii, Rossiella paleacea, Cavitatus jouseanus, C. coscinodiscus, Crucidenticula punctata,* and *C. gigas* var. *diorama*. The absence of *Coscinodiscus temperi* var. *delicata* suggests placement in the *C. gigas* var. *diorama* Zone, whereas the absence of *Cestodiscus pulchellus* suggests placement in the younger *C. coscinodiscus* Zone. Sample 320-U1335A-10H-CC is as-

signed to the *C. gigas* var. *diorama* Zone based on the occurrence of *Annellus californicus* and *C. pulchellus* without *Coscinodiscus lewisianus*.

Samples 320-U1335A-11H-CC and 12H-CC are assigned to the *C. lewisianus* Zone based on the occurrence of *C. lewisianus*. The occurrence of *Thalassiosira tappanae* in Sample 320-U1335A-12H-CC supports this zonal assignment and suggests that this sample is equivalent to the lower portion of this zone.

The interval from Samples 320-U1335A-13H-CC through 18H-CC contains few to common diatoms with poor to moderate preservation. *Cestodiscus peplum*, the marker for the *Coscinodiscus peplum/C. lewisianus* boundary, was not observed. As such, zonal assignment for this interval is tentative. Samples 320-U1335A-13H-CC through 15H-CC are assigned to the lowermost portion of the *C. lewisianus* Zone through Subzone B of the *C. peplum* Zone based on stratigraphic position. Zonal diagnostic species were not observed in this interval. The occurrence of *A. californicus* in Samples 320-U1335A-16H-CC and 17H-CC allow placement of these samples into Subzone A of the *C. peplum* Zone. The occurrence of *Cavitatus miocenica* in Sample 320-U1335A-18H-CC suggests placement of this sample in Subzone B of the *Crucidenticulopsis nicobarica* Zone.

Sample 320-U1335A-19H-CC contains *Crucidenticula kanayae, Coscinodiscus blysmos, C. jouseanus, Thalassiosira fraga,* and *C. lewisianus* var. *similis*. The occurrences of *C. kanayae* and *C. blysmos* without *C. miocenica* suggest that this sample approximates the *C. peplum*/*C. nicobarica* Zonal boundary.

Samples 320-U1335A-20H-CC and 21H-CC are assigned to the *C. nicobarica* Zone. The occurrence of *Raphidodiscus marylandicus* and *C. miocenica* in Sample 320-U1335A-20H-CC suggests placement of this sample in the lower portion of Subzone B of the *C. nicobarica* Zone or older. The co-occurrence of *C. lewisianus* var. *robustus* and *C. lewisianus* var. *similis* in Sample 320-U1335A-21H-CC suggests assignment of this sample into the upper portion of Subzone A of the *C. nicobarica* Zone.

The zonal assignment for Sample 320-U1335A-22H-CC is tentative given the minimal number of zonal indicators observed in this sample. The occurrence of *Triceratium pileus* suggests assignment to the lower portion of Subzone A of the *C. nicobarica* Zone or to the *T. pileus* Zone. Samples 320-U1335A-23H-CC and 24H-CC are assigned to the *T. pileus* Zone based on the occurrence of *Actinocyclus radionovae* in both samples. The occurrence of *Thalassiosira spinosa* in Sample 320-U1335A-23H-CC supports this zonal assignment.

The occurrences of *Coscinodiscus rhombicus* and *T. fraga* in Samples 320-U1335A-25H-CC and 26H-CC allow assignment of these samples to the *Craspedodiscus elegans* Zone. Other species observed include *T. spinosa, C. miocenica,* and *C. lewisianus*.

Zonal assignments for Samples 320-U1335A-27H-CC through 30H-CC are tentative, as this interval is characterized by diatoms with poor to moderate preservation. Diatom fragments are typical in this interval. Species observed include *C. rhombicus, C. lewisianus, C. miocenica,* and *A. radionovae*. The occurrence of *Actinocyclus hajosiae* in Sample 320-U1335A-30H-CC suggests that this section is equivalent to the lower portion of this zone or upper portion of the *Rossiella fennerae* Zone. The absence of *Bogorovia veniamini* in this sample and the occurrence of *B. veniamini* in Sample 320-U1335A-31-CC stratigraphically below this interval supports the *C. elegans* Zone assignment for Sample 320-U1335A-30H-CC.

The *R. fennerae* Zone is assigned to Samples 320-U1335A-31H-CC through 36H-CC based on the occurrence of *B. veniamini* with *R. fennerae*. Subzones were not differentiated within this interval given the amount of fragmentation. The assemblage is characterized by *Coscinodiscus barronii, C. rhombicus, B. veniamini, R. fennerae, C. miocenica,* and *C. jouseanus*. *R. paleacea* occurs in Section 320-U1335A-32H-CC, suggesting placement in the upper portion of this zone.

Samples 320-U1335A-37X-CC through 42X-CC are assigned to the *R. gelida* Zone based on the occurrence of *R. gelida*. The occurrence of *Rocella schraderi* in Sample 320-U1335A-40X-CC suggests that Samples 320-U1335A-37X-CC through 40X-CC are equivalent to the upper portion of this zone. The occurrence of *C. lewisianus* var. *rhomboides* and *Craspedodiscus baronii* without *R. schraderi* in Sample 320-U1335A-42X-CC suggests the equivalent of the lower portion of the zone.

Sample 320-U1335A-43X-CC is assigned to the *B. veniamini* Zone based on the occurrence of *Rocella vigilans* and *Cestodiscus kugleri* without *R. gelida*. Diatoms were not observed in Sample 320-U1335A-44X-CC.

Planktonic foraminifers

Micropaleontological samples from the core catchers were taken from both holes of Site U1335. High-resolution biostratigraphy was undertaken on additional samples from Hole U1335A (two per core). Planktonic foraminifer biostratigraphy indicates a nearly continuous succession of zones ranging from the Pleistocene (Zone PT1a) throughout the upper Oligocene (Zone O6) (Fig. **F13**), which agree well with calcareous nannofossil and radiolarian biostra-

tigraphy (Fig. F14). Preservation and abundance of planktonic foraminifers are generally good from the Pliocene through Miocene with samples frequently containing >70% planktonic foraminifers, but there are exceptions within this interval and lower preservation and abundances of planktonic foraminifers are recorded during the late Oligocene. The depths of the main datum biostratigraphic events and age estimates are shown in Table T8. Preservation and presence of planktonic foraminifers are shown in Table T9.

The topmost Samples 320-U1335A-1H-3, 100–102 cm, and 1H-5, 42–44 cm, are assigned to the first Pleistocene Zone PT1a that is distinguished between the top of *G. fistulosus* in Sample 320-U1335A-1H-CC and the top of *Globorotalia (Truncorotalia) tosaensis*. Accurate assignment of Zones PL1–PL6 is difficult because although planktonic foraminifers are abundant and assemblages are diverse (frequently >20 species), a number of age-diagnostic marker species were not found or were too rare to be employed as reliable datums (e.g., *Globoturborotalita nepenthes, Globorotalia [Hirsutella] margaritae,* and *Dentoglobigerina altispira*). Furthermore, in Core 320-U1335A-1H and Sample 320-U1335-2H-CC the <250 µm size fraction is composed almost entirely of planktonic foraminifer fragments. In these same cores there is also evidence of dissolution/fragmentation with only the "skeleton" of some species being preserved (i.e., individuals of the subgenus *Menardella* are frequently observed with only the keel and limbate sutures and missing walls of the final whorl chambers). Consequently, these assemblages are biased toward more robust taxa (i.e., *Globorotalia tumida, Pulleniatina* spp., and *Sphaeroidinella dehiscens*). In such cases, both primary datums and additional age-diagnostic species were employed to assign zones. Zone PL6 was identified between the LO of *Globorotalia pseudomiocenica* in Sample 320-U1335B-2H-CC (3.43 m CSF) and the top of *G. fistulosus*. Zones PL4–PL5 were identified between the top of *Sphaeroidinellopsis seminulina* in Sample 320-U1335A-3H-4, 38–40 cm, and the top of *Globoturborotalita woodi* and *G. pseudomiocenica* in Sample 320-U1335A-2H-2, 104–106 cm. It was not possible to further subdivide the zones because of the absence of the age-diagnostic taxon *D. altispira* within the high-resolution samples taken from Zones PL4 and PL5 in this sediment interval. Moreover, the last occurrence of this taxon, which is easily identifiable and often abundant, is recorded ~20 m deeper in Holes U1335A and U1335B than expected based on previous calibration studies in the equatorial Pacific that utilize the top of *D. altispira* as a datum event to define the Zone PL4/PL5 boundary (Chaisson and Pearson, 1997) at 3.47 Ma. Zones PL1–PL3 were identified between the base of *G. tumida* (Sample 320-U1335A-3H-CC; 28.13 m CSF) and the top of *S. seminulina* (Sample 320-U1335A-2H-4, 104–106 cm; 14.44 m CSF). The absence or rarity of *G. (Hirsutella) margaritae* and *G. nepenthes* prevented further subdivision. However, a number of supplementary age-diagnostic events were identified, including the base of *S. dehiscens* at 5.54 Ma (Chaisson and Pearson, 1997) and the top of *Sphaeroidinellopsis kochi* at 4.53 Ma (Curry et al., 1995), indicating the presence of Zone PL1.

Upper Miocene Zone M14 was determined between the lowest occurrence of *G. tumida* in Section 320-U1335A-3H-CC and the base of *G. (Hirsutella) margaritae* in Sample 320-U1335A-4H-CC. The first occurrence of *Globorotalia plesiotumida* is recorded in Sample 320-U1335A-6H-2, 38–40 cm, and defines the base of Zone M13b. Zones M13a and M12 were not divided because of the rare occurrence of *Neogloboquadrina acostaensis* toward the base of its stratigraphic range. Zone M11 was delimited by the top of *Paragloborotalia mayeri* (10.57 Ma) in Sample 320-U1335A-7H-6, 95–97 cm, and the base of *Globoturborotalita decoraperta* (11.49 Ma) in Section 320-U1335A-8H-CC, which falls just above the base of Zone M11. Above the last occurrence of *Globorotalia (Fohsella) fohsi* s.l. in Sample 320-U1335A-9H-2, 38–40 cm, is Zone M10 (N13). Zone M9b/N12 is defined by the total range of *Globorotalia (Fohsella) fohsi robusta* between Samples 320-U1335A-9H-4, 38–40 cm, and 11H-CC. Zone M9a/N12 was identified in Sample 320-U1335A-12H-2, 38–40 cm, by the base of *G. (Fohsella) fohsi* s.l. The base of Zone N10 was defined by the first occurrence of *Globorotalia (Fohsella) "praefohsi."* Secondary datum events such as the tops of *Clavatorella bermudezi* (13.82 Ma), *Globorotalia (Fohsella) peripheroronda* (13.80 Ma), and *Globorotalia praescitula* (13.73 Ma) take place within Zone M7 (N10–N11). The base of Zone M7 (N10) is defined by the base of *Globorotalia (Fohsella) peripheroacuta*. The base of *Praeorbulina sicana* occurs in Sample 320-U1335A-18H-CC, defining Zone M5, but further differentiation of Zones M5 and M6 was problematic given the absence of *Praeorbulina glomerosa, Orbulina* spp., and *Globigerinatella insueta,* which could be explained by the low preservation potential of these taxa. The latter may also account for the very shallow base of *C. bermudezi* recorded here. As a result, the exact position of some of the datums belonging to these zones might be slightly biased. The base of *Globorotalia (Menardella) archeomenardii* at 16.26 Ma (Curry et al., 1995) was identified in Sample 320-U1335A-16H-CC, indicating topmost Zone M5b or Zone M6/N9. The top of *Catapsydrax dissimilis* that defines the base of Zone M4 was difficult to deter-

mine because of low abundance toward the top of its stratigraphic range, but it was identified in Sample 320-U1335B-20H-CC. The absence of *G. insueta* prevented accurate determination of the M2/M3 zonal boundary. The datum event marked by the top of *Globoquadrina binaiensis* (19.09 Ma) was identified in Sample 320-U1335A-20H-CC (185.19 m CSF) and falls toward the very top of the undifferentiated Zones M2–M3, higher than expected. Zone M1b was determined by the co-occurrence of *P. kugleri, Paragloborotalia pseudokugleri,* and *Globoquadrina dehiscens* between Samples 320-U1335A-28H-CC and 33H-CC. Zone M1a occurs between the bases of *G. dehiscens* in Sample 320-U1335A-33H-CC at 22.4 Ma and *P. kugleri* in Sample 320-U1335A-37X-4, 136–138 cm, at 23.0 Ma. The Oligocene/Miocene boundary was also well defined in Hole U1335B between Samples 320-U1335B-37X-CC and 38X-CC using the base of *P. kugleri.* The lowest zone defined is Zone O6 in the late Oligocene and the presence of *P. pseudokugleri* indicates that only the upper part of the zone is present.

Benthic foraminifers

Benthic foraminifers from core catcher samples were examined semiquantitatively in all holes at Site U1335. Benthic foraminifers occurred almost continuously, except in Sample 320-U1335B-3H-CC and several other samples in the early Miocene and late Oligocene. The occurrence of benthic foraminifers at this site is shown in Table **T10.**

From Samples 320-U1335A-1H-CC to 9H-CC (8.84–85.05 m CSF), *Oridorsalis umbonatus, Cibicidoides mundulus,* and *Globocassidulina subglobosa* are common with a few subordinate *Anomalinoides* sp. A, *Gyroidinoides* spp., *Latcarinina pauperata, Melonis pompilioides,* and *Melonis barleeanum.* A similar fauna is found between Samples 320-U1335B-1H-CC and 9H-CC (3.46–79.96 m CSF). Preservation of the foraminifer tests is moderate to good. Pliocene and middle Miocene taxa recorded here indicate lower bathyal and abyssal paleodepths (van Morkhoven et al., 1986).

Samples 320-U1335A-10H-CC through 44X-CC (104.56–417.80 m CSF) generally contain common *O. umbonatus, C. mundulus, G. subglobosa,* and *Gyroidinoides* spp. with a few subordinate *Anomalinoides* sp. A, *Astrononion echolsi, L. pauperata,* and *Pullenia* spp. in several horizons. Several samples in the lower part of the interval (early Miocene and late Oligocene) were barren of benthic foraminifers (Samples 320-U1335A-28H-CC, 29H-CC, and 37X-CC; 265.99, 275.59, and 350.04 m CSF, respectively) or rare (Samples 320-U1335A-32H-CC, 33H-CC, and 44X-CC; 297.98, 313.51, and 394.90 m CSF, respectively), where present assemblages in these samples are often dominated by small individuals. Preservation of the foraminifer tests is moderate to good. Similar benthic foraminifer assemblages were also recognized in Hole U1335B (Samples 320-U1335B-10H-CC through 45X-CC; 89.06–411.88 m CSF), including a number of barren or rare horizons of benthic foraminifers (Samples 320-U1335B-32H-CC, 35H-CC, 36H-CC, and 43X-CC; 297.98, 326.87, 336.55, and 394.90 m, respectively); however, these were not always contemporaneous with those observed in Hole U1335A. These faunal compositions indicate lower bathyal and abyssal paleodepths during the middle Miocene to late Oligocene.

Paleomagnetism

We studied the paleomagnetism of sediments from Site U1335 with a primary focus on determining a preliminary magnetostratigraphy, which can be used to assist in dating the stratigraphic section. To accomplish this, we measured the natural remanent magnetization (NRM) of archive-half sections from 78 APC cores recovered from Holes U1335A and U1335B. Measurements were made along each section at 5 cm intervals before and after AF demagnetization at 20 mT. Many sections were measured at 2.5 cm intervals following 20 mT AF demagnetization, as we found higher resolution data to be more useful than measuring the 5, 10, or 15 mT demagnetization steps with ordinary resolution (see **"Paleomagnetism"** in the "Site U1334" chapter). For some of the archive-half sections from deeper intervals in Hole U1335B, we only measured the NRM before demagnetization because of their extremely weak magnetizations. No XCB cores were measured at this site.

We processed the paleomagnetic data by removing measurements made within 5 cm of section ends and data from disturbed intervals (Table **T11**). Cleaned data are presented in Tables **T12, T13, T14,** and **T15** and in Figures **F7** and **F15.**

Azimuthal core orientation was determined solely by correlating distinct reversals patterns as recorded by the paleomagnetic declination in each hole with the geomagnetic polarity timescale (GPTS) (See **"Paleomagnetism"** in the "Methods" chapter and **"Paleomagnetism"** in the "Site U1331" chapter). This process is aided by detailed biostratigraphic age constraints, which significantly limit the range of possible correlations with the GPTS (see **"Biostratigraphy"**). Once we had confidently identified a unique, unambiguous reversals pattern, the mean paleomagnetic directions for each core were calculated using Bingham statistics (Table **T16**) with

the same procedure described in "Paleomagnetism" in the "Site U1332" chapter. Subsequently the data were reoriented so that normal and reversed polarity intervals had declinations of ~0° and ~180°, respectively (see "Paleomagnetism" in the "Site U1331" chapter). Reoriented declinations are provided for Holes U1335A and U1335B in Tables T13 and T15, respectively, for the data collected after AF demagnetization at 20 mT.

We measured magnetic properties of 257 discrete paleomagnetic samples. Of these, 70 samples were subjected to progressive AF demagnetization up to 60 mT. Remanence measurements and characteristic remanent magnetization (ChRM) directions computed using principal component analysis (PCA) are given in Tables T17 and T18, respectively. Magnetic susceptibilities and masses, along with volumes estimated using MAD data (see "Physical properties"), are given in Table T19. This table also includes magnetic susceptibilities from the whole-core data for the depth intervals corresponding to that of the discrete samples, which is useful for checking the scale factor, 0.68×10^{-5} SI (see "Paleomagnetism" in the "Methods" chapter), for converting the whole-core raw susceptibility meter measurements into volume-normalized susceptibility values.

Results

Downhole variations in paleomagnetic data from split cores and discrete samples and magnetic susceptibility from whole-core and discrete samples are shown in Figures F7 and F15. The most prominent feature of the records is the magnetic intensity and susceptibility low that occurs between ~70 and 110 m and ~210 and 410 m CSF, referred to as the magnetic-low zone. We could not retrieve any reliable paleomagnetic directions from the magnetic-low zone because the remanent magnetic intensity of the zone after 20 mT AF demagnetization is on the order of 10^{-5} A/m, which is comparable to the noise level of the super-conducting rock magnetometer onboard the *JOIDES Resolution* (see "Paleomagnetism" in the "Methods" chapter). Similar to Site U1334, the magnetic-low zone can be attributed to reduction diagenesis (see "Paleomagnetism" in the "Site U1334" chapter).

The drilling overprint was generally weak for Site U1335 cores when nonmagnetic core barrels were used (Cores 320-U1335A-1H through 16H and 320-U1335B-1H through 19H). This is evidenced by relatively shallow inclinations observed before demagnetization (Figs. F7, F15). In contrast, cores collected with steel core barrels are highly overprinted, as noted by the steep inclinations prior to demagnetization (Figs. F7, F15), which is similar to those observed at Sites U1333 (see Fig. F17 in the "Site U1333" chapter) and U1334 (see Figs. F16, F17, and F18 in the "Site U1334" chapter). Regardless of which type of core barrel was used, shallow inclinations and distinct reversal patterns in the declinations were observed after 20 mT demagnetization, except within the magnetic-low zone. In the magnetic-low zone, the overprint appears more severe, which might be related to mineralogy (replacement of the primary iron oxides with iron sulfides). Similar to Site U1334, inclinations remain steep within the magnetic-low zone even after 20 mT demagnetization, in spite of associated large decrease in the remanent intensity (Figs. F7, F15), indicating that steel core barrels have completely remagnetized these sediments.

Discrete sample demagnetization data indicate that the ChRM of the sediments can be resolved by AF demagnetization above 5–15 mT (Fig. F16) except for samples from the magnetic-low zone. We interpret this ChRM to be the primary depositional remanent magnetization. Similar to the Site U1334 samples, many of the Site U1335 samples have poorly resolved ChRM directions (scattered directions along a linear demagnetization path in the orthogonal demagnetization plot) due to weak magnetization of Site U1335 sediments. Nonetheless the ChRM declinations agree well with those of coeval intervals of the archive-half measurements (Fig. F15), indicating that the declinations from the split cores after 20 mT demagnetization provide a reliable indicator of the ChRM of the sediments.

Magnetostratigraphy

The cleaned paleomagnetic data provide a series of distinct ~180° alternations in declination except for the magnetic-low zone. When combined with biostratigraphic age constraints (see "Biostratigraphy"), the data give a continuous magnetostratigraphy from Chrons C1n (0–0.781 Ma) to C5n.2n (9.987–11.040 Ma) from 0 to 65.95 m CSF in Hole U1335A and from Chrons C1n to C5r.1n (11.118–11.154 Ma) from 0 to 66.225 m CSF in Hole U1335B. Below the bottom of the first magnetic-low zone (~70–110 m CSF), the magnetostratigraphy is again interpretable downhole: Chrons C5Br (15.160–15.974 Ma) to C6n (18.748–19.722 Ma) from 155.35 to 208.40 m CSF in Hole U1335A and from Chron C5AAn (13.015–13.183 Ma) to Chron C5Er (18.524–18.748 Ma) from 107.95 to 202.60 m CSF in Hole U1335B. The magnetostratigraphy of the two holes is presented in Table T20 and Figures F17A, F17B, F18A, and F18B. The magnetostratigraphy could not be determined for the second magnetic-low zone (below ~210 m CSF).

Highlights of the magnetostratigraphy at Site U1335 are the identifications of (1) 123 reversals, (2) a previously observed cryptochron (C5Dr-1n) in both holes, and (3) 40 possible geomagnetic excursions (10 of these are recorded in both holes). The Site U1335 paleomagnetic record has high quality and resolution within the Miocene from 0 to 70 m CSF and 110 to 210 m CSF, whereas it has poor quality in the magnetic-low zones. The resolution is high owing to the high sedimentation rates at Site U1335 throughout the Miocene (see Fig. **F14**). The high-quality, high-resolution records made it possible to recognize the many potential excursions. Not all of the 40 potential excursions may be real geomagnetic features because a few are possibly associated with turbidites even though we excluded the intervals interpreted as turbidites. Considering the relatively high frequency of turbidites at this site, it is possible that some were not identified. Careful shore-based paleo- and rock magnetic investigations are necessary to confirm the reliability of these records.

Geochemistry

Sediment gas sampling and analysis

Headspace gas samples were taken at a frequency of one sample per core in Hole U1335A as part of the routine environmental protection and safety monitoring program. All headspace samples resulted in nondetectable levels of methane (C_1; <2 ppmv), with no higher hydrocarbons, consistent with the low organic carbon content of these sediments.

Interstitial water sampling and chemistry

A total of 48 interstitial water samples were collected using the whole-round squeezing method, 45 from Hole U1335A and 3 from Hole U1335B (Table **T21**). Chemical constituents were determined according to the procedures outlined in **"Geochemistry"** in the "Methods" chapter.

Chlorinity shows relatively little variability with depth, with values ranging from 554 to 565 mM (Fig. **F19**). However, chlorinity values reveal a distinct increase from 554 to 565 mM in the uppermost 40 m CSF, most clearly seen in previous IODP Sites U1332 and U1334, potentially reflecting the change from the more saline ocean at the Last Glacial Maximum to the present (Adkins and Schrag, 2003). Alkalinity shows little variability, with values ranging from 2.5 to 4.3 mM. Sulfate concentrations vary between 23 and 28 mM, with slightly decreasing values with depth. Dissolved phosphate concentrations are ~2 µM in the shallowest sample, decreasing to values ~0.5 µM in the uppermost ~50 m CSF. Dissolved manganese shows three distinct peaks with concentrations of up to 44, 13, and 5 µM between ~0 and 40, 50 and 80, and 150 and 210 m CSF, respectively. Generally, Mn peaks are sharp in the shallower part and broad at greater depth. Dissolved iron spikes to 6 µM at 6 m CSF and peaks with concentrations ~6 µM between 90 and 170 m CSF and between 190 and 370 m CSF. As with manganese, iron peaks become broader with increasing depth. Minima in dissolved Fe correspond to elevated Mn concentrations. The alternating pattern of dissolved Mn and Fe corresponds well to apparent color changes of the sediment (see **"Lithostratigraphy"**).

Because of the relatively high sulfate concentrations, dissolved Ba concentrations are low and relatively homogeneous, with values below 2.2 µM. Concentrations of dissolved silicate increase with depth from ~500 to ~820 µM.

Calcium and magnesium concentrations are relatively uniform, with values ranging from 9.5 to 12 mM and from 44 to 51 mM, respectively (Fig. **F19**).

Lithium concentrations decrease from ~26 µM at the surface to 5 µM at ~300 m CSF. Lithium strongly increases below 300 m CSF toward basement. Strontium concentrations range between 82 and 250 µM, and this profile mirrors the lithium profile. Values increase from the top toward 200 m CSF, followed by a decrease toward basement. Boron concentrations range between 440 and 490 µM, slightly decreasing from the top to the basement.

Bulk sediment geochemistry: major and minor elements

At Site U1335, bulk sediment samples for minor and major element analyses were distributed over the core depth to characterize the major lithologic units (0–400 m CSF; Hole U1335A). We analyzed concentrations of silicon, aluminum, iron, manganese, magnesium, calcium, sodium, potassium, titanium, phosphorus, barium, copper, chromium, scandium, strontium, vanadium, yttrium, and zirconium by inductively coupled plasma–atomic emission spectroscopy (ICP-AES) (Table **T22**).

SiO_2 ranges between 6 and 34 wt%, with generally higher concentrations in the upper sediment. Similar patterns to SiO_2 are displayed by Al_2O_3, with concentrations ranging from below detection limit to 3.6 wt%, TiO_2 (0.002–0.2 wt%), K_2O (0.1–1 wt%), Zr (12–90 ppm), and Sc (up to 14 ppm).

Concentrations of Fe_2O_3 vary between 0.4 and 2.7 wt%, following the general pattern of SiO_2. Similar trends are also shown by MnO (0.04 to >0.2 wt%), MgO (0.3–1.5 wt%), copper (below detection limit to >140 ppm), and vanadium (up to 20 ppm). Peak con-

centrations of Mn and Cu could not be quantified because they exceeded the calibrated range (values in brackets in Table T22).

Calcium (CaO) ranges from 26 to 43 wt%, with high values corresponding to the minima in SiO_2 and Al_2O_3. Strontium concentrations are >700 ppm, showing a similar pattern to that of CaO. Barium concentrations are >566 ppm, and P_2O_5 values range from below detection limit to 0.5 wt%, showing minima at high CaO concentrations.

Bulk sediment geochemistry: sedimentary inorganic and organic carbon

$CaCO_3$, IC, and TC concentrations were determined on sediment samples from Hole U1335A (Table T23; Fig. F5). Calcium carbonate concentrations ranged between 13 and 96 wt%. In the uppermost ~67 m CSF, $CaCO_3$ concentrations vary greatly between 12 and 87 wt%. From 67 to 157 m CSF, calcium carbonate concentrations are consistently high (72–92 wt%), and then $CaCO_3$ concentrations show more variation, ranging between 37 and 89 wt% from 157 to 222 m CSF. Below 222 m CSF, $CaCO_3$ concentrations are consistently high again (75–96 wt%). Variations in $CaCO_3$ concentrations correspond to lithostratigraphic changes (see "Lithostratigraphy").

TOC concentrations were determined by acidification (see "Geochemistry" in the "Methods" chapter) (Table T23; Fig. F5) and are very low throughout the sediment column, from below the detection limit to 0.10 wt% (Fig. F5).

Physical properties

Physical properties at Site U1335 were measured on whole cores, split cores, and discrete samples. WRMSL (GRA bulk density, magnetic susceptibility, *P*-wave velocity), thermal conductivity, and NGR measurements comprised the whole-core measurements. Compressional wave velocity measurements on split cores and MAD analyses on discrete core samples were made at a frequency of one per undisturbed section in Cores 320-U1335A-1H through 45X. Compressional wave velocities were measured toward the bottom of sections. MAD analyses were located 10 cm downsection from carbonate analyses (see "Geochemistry"). Lastly, the Section Half Multisensor Logger (SHMSL) was used to measure spectral reflectance on archive section halves. The Ocean Optics sensor was used in place of the Minolta, and the resolution was reduced from 2.5 to 5 cm because of time constraints.

Density and porosity

Two methods were used to evaluate wet bulk density at Site U1335. GRA provided an estimate from whole cores (Fig. F20). MAD samples gave a second, independent measure of wet bulk density, along with providing dry bulk density, grain density, water content, and porosity from discrete samples (Table T24). MAD and GRA bulk density measurements display the same trends and are also similar in absolute values through the entire section (Fig. F21B). Crossplots of wet and dry bulk density versus interpolated GRA density (Fig. F22) show excellent correlation between MAD and GRA density data.

Generally, wet bulk density corresponds with changes in lithology. Wet bulk density is lowest in Unit I (1.2–1.6 g/cm^3), which contains the lowest calcium carbonate content. A prominent decrease in wet bulk density occurs at 58 m CSF, coinciding with an interval of clay-rich radiolarian ooze with diatoms within the major lithology of nannofossil ooze. Wet bulk density increases at the top of Unit II to values around 1.7 g/cm^3. A small increase in wet bulk density occurs around 215 m CSF to values close to 1.8 g/cm^3 in the lower portion of Unit II.

Variation in grain density in Hole U1335A generally matches changes in lithology (Fig. F21C). Grain density ranges from 2.0 to 3.0 g/cm^3 in Unit I. In Unit II the grain density of the sediments is much more uniform in comparison, averaging 2.7 g/cm^3 with variation up to 3.0 g/cm^3. This average reflects the carbonates that dominate Unit II (calcite = 2.7 g/cm^3).

Porosity ranges from 70% to 90% in Unit I, reflecting intervals of clayey radiolarian ooze within the major lithology of nannofossil ooze. In Unit II porosity gradually decreases to values of 50%–60% downhole over this ~300 m section. Porosity and water content vary inversely with wet bulk density (Fig. F21A).

Magnetic susceptibility

Whole-core magnetic susceptibility measurements correlate well with the major differences in lithology in Unit I. In Unit II, magnetic susceptibility variability follows changes in geochemistry and reflectance spectroscopy. Loss of the magnetic susceptibility signal results from suboxic diagenesis that develops below 70 m CSF (Fig. F20). Magnetic susceptibility values range from 5×10^{-5} to 20×10^{-5} SI in the upper portion of Unit I. In the lower portion of Unit I, magnetic susceptibility values increase to 25×10^{-5} SI, which coincides with the occurrence of clayey radiolarian ooze within the major lithology of nannofossil ooze. Magnetic susceptibility values begin to

decrease at the top of Unit II (64 m CSF) and then fall to values that are slightly negative (-1×10^{-5} SI) in the zone of suboxic diagenesis as Fe reduction removes the ferromagnetic component of the sediment (see **"Geochemistry"**). Magnetic susceptibility values increase slightly and become highly variable (0 to 10×10^{-5} SI) between 110 and 150 m CSF. Magnetic susceptibility values are higher in the interval from 160 to 200 m CSF, coinciding with a decrease in Fe reduction that is also accompanied by a color change from green to brown (see **"Lithostratigraphy"**). Below 200 m CSF the magnetic susceptibility signature is largely diamagnetic, with values close to zero, reflecting a return to Fe reduction in the lower section of Unit II. Magnetic susceptibility values increase to 15×10^{-5} SI at the base of Unit II.

Compressional wave velocity

Shipboard results

Whole-core *P*-wave logger (PWL) data and discrete velocity measurements made on split cores follow similar trends, with key transitions reflecting increasing compaction with depth and the transition from ooze to chalk that occurs deep in the section (~220 m CSF) (Fig. **F23**). Discrete velocity measurements along the *x*-axis are in excellent agreement with PWL results, though *y*- and *z*-axis measurements generally overestimate by 10 m/s (Table **T25;** Fig. **F23**). Differences between whole-core and split-core measurements possibly reflect the presence of water in the space between the core liner and sediment in the whole cores and the slight compaction of the sediment in the contact probe technique.

Velocities are between 1460 and 1490 m/s in Unit I and the upper portion of Unit II. Below 200 m CSF, velocities begin to increase above 1500 m/s. At the base of Unit II, slightly below the described ooze/chalk boundary (345 m CSF; see **"Lithostratigraphy"**) velocities increase dramatically, reaching values of 1600–1800 m/s at the bottom of Unit II.

Postcruise correction

The *x*-direction velocities at Site U1335 were determined using a liner thickness of 3.2 mm, the correction that was initially applied at Site U1334 (see **"Physical properties"** in the "Site U1334" chapter). During the analysis of Hole U1337A cores, it was determined that high *x*-direction velocities do not result from thicker than expected core liner but instead are the result of using an incorrect value for the system delay associated with the contact probe (see **"Physical properties"** in the "Site 1337" chapter). Critical parameters used in this correction are system delay = 19.811 µs, liner thickness = 2.7 mm, and liner delay = 1.26 µs. During the analysis of Hole U1337A cores, it also was determined that consistently low PWL velocities required the addition of a constant value that would produce a reasonable velocity of water (~1495 m/s) for the quality assurance/quality control (QA/QC) liner (see **"Physical properties"** in the "Site U1337" chapter). These corrections have not been applied to the velocity data presented in this chapter.

Natural gamma radiation

NGR was measured on all cores at Site U1335 (Fig. **F20**). The highest NGR values are present at the seafloor (~73 cps). NGR values decrease rapidly with depth in Unit I, reaching values of 3 cps at the base of Unit I. In Unit II, NGR is very low (~1–2 cps) with low variability to the base of the section.

Thermal conductivity

Thermal conductivity was measured on the third section of each core from Hole U1335A (Table **T26**). Thermal conductivity shows a strong dependence on porosity downhole through the succession (Figs. **F24, F25**). Decreased conductivity occurs with increasing porosity as increased interstitial spacing attenuates the applied current from the probe. Thermal conductivity ranges from 0.8 to 1.0 W/(m·K) in Unit I and increases to 1.1 W/(m·K) in the upper portion of Unit II. Below 200 m CSF, thermal conductivity increases to 1.2 W/(m·K) and again to 1.3 W/(m·K) below 280 m CSF. These depths also coincide with increased *P*-wave velocity and decreased porosity. Below 380 m CSF, thermal conductivity decreases, possibly resulting from increasing fractures in the sediment core (see **"Lithostratigraphy"**).

Reflectance spectroscopy

Spectral reflectance was measured on split archive-half sections from all three holes using the Ocean Optics sensor with the SHMSL (Fig. **F26**). L* variations correspond to pronounced lithologic changes, the main example being the interval of clay-rich radiolarian ooze within the lower portion of Unit I (~60 m CSF) where L* values drop from ~90 to ~30. Variations in a* (green–red) and b* (blue–yellow) reflect changes in lithology but also covary with changes in magnetic susceptibility, as color change in these cores is largely driven by pore water geochemistry below 70 m CSF (see **"Geochemistry"**). In Unit I both a* and b* are relatively high (4 and 15, respectively). Below 70 m CSF, both parameters drop to minimum values reflecting color change in the interval of iron reduction.

Stratigraphic correlation and composite section

Special Task Multisensor Logger (STMSL) data were collected at 5 cm intervals from Hole U1335B and compared to the WRMSL data obtained at 2.5 cm resolution from Hole U1335A. In this way we monitored drilling in Hole U1335B in real time to maximize the opportunity for the recovery and construction of a stratigraphically complete composite section. The overall good to excellent overlap between Holes U1335A and U1335B did not require drilling a third hole.

The correlation was refined once magnetic susceptibility and GRA density data were available at 2.5 cm resolution from the WRMSL, and NGR and color reflectance data were available from the NGR track and the SHMSL (see **"Physical properties"**). Visual inspection of cores, comparison with core imagery, and biostratigraphic datums were used to establish and verify hole to hole correlation where track data lacked clearly identifiable features. Magnetic susceptibility and GRA density proved most useful for correlating between holes at Site U1335 (Figs. **F27, F28**). Features in the magnetic susceptibility and GRA density are well aligned between Holes U1335A (337 m CSF) and U1335B (344 m CSF) to ~398 m CCSF-A. Flow-in at the bottom half of Core 320-U1335A-16H between Sections 320-U1335A-16H-4 and 16H-7 (146.4–151.46 m CSF) made it impossible to construct a complete stratigraphic section below 165.15 m CCSF-A and required appending the remainder of the section. Between ~230 and ~398 m CCSF-A, GRA density data allowed confident alignment of cores despite very low magnetic susceptibility values. The section below 398 m CCSF-A was mostly XCB-cored, lacked clearly identifiable features, and had to be appended for these reasons.

Offsets and composite depths are listed in Table **T27.** Following construction of the composite depth section for Site U1335, a single spliced record was assembled for the aligned cores to Section 320-U1335B-37H-6 at 398.15 m CCSF-A (top panels of Figs. **F27, F28**). The sections of core used for the splice are identified in Table **T28** and displayed in Figures **F27** and **F28.**

We avoided intervals with significant disturbance or distortion and missing intervals where whole-round samples for interstitial water chemistry were taken (see **"Paleomagnetism;"** Table **T11**). The Site U1335 splice can be used as a sampling guide to recover a single sedimentary sequence from 0 to 398 m CCSF-A with gaps between 165 and 166 m CCSF-A, although it is advisable to overlap a few decimeters from different holes when sampling to accommodate anticipated ongoing development of the depth scale. Stretching and compression of sedimentary features in aligned cores indicates distortion of the cored sequence. Because much of the distortion occurs within individual cores on scales of <9 m, it was not possible to align every single feature in the magnetic susceptibility, GRA, NGR, and color reflectance records. However, at crossover points along the splice (Table **T28**), care was taken to align highly identifiable features from cores in each hole.

A growth factor of 1.16 is calculated by linear regression for all holes at Site U1335, indicating a 16% increase in CCSF-A relative to CSF depth (Fig. **F29**). We used this value to calculate CCSF-B, the compressed composite depth presented in Table **T27** to calculate sedimentation rates and aid in the calculation of mass accumulation rates.

Sedimentation rates

All the principal biostratigraphic datums and a set of 71 paleomagnetic reversals (restricted to the APC-cored section of the site) are defined in Holes U1335A and U1335B (Table **T29;** see **"Biostratigraphy"** and **"Paleomagnetism"**) and were used in establishing age control (Fig. **F14**). Paleomagnetic reversals were used to calculate the average linear sedimentation rates (LSRs) for the upper 200 m of the section at Site U1335 on CCSF-B depth scale, as depicted in Figure **F14.** Below 200 m CCSF-B all available biostratigraphic datums were used to calculate the average LSRs.

LSRs at Site U1335 are high, 25 m/m.y. on the average throughout the late Oligocene and early Miocene. Sedimentation rates decrease to 17 m/m.y. in the middle early Miocene and drop to 6 m/m.y. in late to middle Miocene to recent (Fig. **F14**).

Downhole measurements

Heat flow

Five APCT-3 downhole temperature measurements in Hole U1335B ranged from 1.64°C at 22.3 m to 2.22°C at 98.3 m (Table **T30**), giving a low geothermal gradient of 7.5°C/km (Fig. **F30**). The bottom water temperature was 1.469°C, based on the average of the minimum temperature in the five APCT-3 temperature profiles. Thermal conductivity under in situ conditions was estimated from laboratory-determined thermal conductivity using the method of Hyndman et al. (1974) (see **"Physical properties"** in the "Methods" chapter). The calculated in situ values are up to 2.5% less than the measured laboratory values. Thermal resistance was then calculated by cumulatively adding the inverse of the in situ

thermal conductivity values over depth intervals downhole (Fig. F30). A heat flow of 7.0 mW/m^2 was obtained from the linear fit between temperature and thermal resistance (Fig. F30) (Pribnow et al., 2000), which is a low value compared to nearby sites in the global heat flow database and an order of magnitude lower that the heat flow at Site U1332.

References

Adkins, J.F., and Schrag, D.P., 2003. Reconstructing Last Glacial Maximum bottom water salinities from deep-sea sediment pore fluid profiles. *Earth Planet Sci. Lett.,* 216:109–123. **doi:10.1016/S0012-821X(03)00502-8**

Amante, C., and Eakins, B.W., 2008. *ETOPO1 1 Arc-Minute Global Relief Model: Procedures, Data Sources and Analysis:* Washington, DC (DOC/NOAA/NESDIS/NGDC).

Barron, J.A., 1985. Late Eocene to Holocene diatom biostratigraphy of the equatorial Pacific Ocean, Deep Sea Drilling Project Leg 85. *In* Mayer, L., Theyer, F., Thomas, E., et al., *Init. Repts. DSDP,* 85: Washington, DC (U.S. Govt. Printing Office), 413–456. **doi:10.2973/dsdp.proc.85.108.1985**

Barron, J.A., 2006. Diatom biochronology for the Early Miocene of the Equatorial Pacific. Stratigraphy, vol. 2, no. 4, 281–309.

Barron, J.A, Fourtanier, E., and Bohaty, S.M., 2006, Oligocene and earliest Miocene diatom biostratigraphy of ODP Leg 199, Site 1220, Equatorial Pacific., *In* Wilson, P.A., Lyle, M., Janecek, T.R., and Firth, J.V. (Eds.) *Proceedings of the Ocean Drilling Program, Scientific Results* Volume 199, 1–25.

Billups, K., Pälike, H., Channell, J.E.T., Zachos, J.C., and Shackleton, N.J., 2004. Astronomic calibration of the late Oligocene through early Miocene geomagnetic polarity time scale. *Earth Planet. Sci. Lett.,* 224(1–2):33–44. **doi:10.1016/j.epsl.2004.05.004**

Busch, W.H., Vanden Berg, M.D., and Masau, P.E., 2006. Velocity and density of Paleogene equatorial sediments: variation with sediment composition. *In* Wilson, P.A., Lyle, M., and Firth, J.V. (Eds.), *Proc. ODP, Sci. Results,* 199: College Station, TX (Ocean Drilling Program), 1–31. **doi:10.2973/odp.proc.sr.199.226.2006**

Cande, S.C., LaBrecque, J.L., Larson, R.L., Pitmann, W.C., III, Golovchenko, X., and Haxby, W.F., 1989. *Magnetic Lineations of the World's Ocean Basins.* AAPG Map Ser., 13.

Chaisson, W.P., and Pearson, P.N., 1997. Planktonic foraminifer biostratigraphy at Site 925: middle Miocene–Pleistocene. *In* Shackleton, N.J., Curry, W.B., Richter, C., and Bralower, T.J. (Eds.), *Proc. ODP, Sci. Results,* 154: College Station, TX (Ocean Drilling Program), 3–31. **doi:10.2973/odp.proc.sr.154.104.1997**

Coxall, H.K., Wilson, P.A., Pälike, H., Lear, C.H., and Backman, J., 2005. Rapid stepwise onset of Antarctic glaciation and deeper calcite compensation in the Pacific Ocean. *Nature (London, U. K.),* 433(7021):53–57. **doi:10.1038/nature03135**

Curry, W.B., Shackleton, N.J., Richter, C., et al., 1995. *Proc. ODP, Init. Repts.,* 154: College Station, TX (Ocean Drilling Program). **doi:10.2973/odp.proc.ir.154.1995**

Engebretson, D.C., Cox, A., and Gordon, R.G., 1985. *Relative Motions between Oceanic and Continental Plates in the Pacific Basin.* Spec. Pap.—Geol. Soc. Am., 206.

Hays, J.D., et al., 1972. *Init. Repts. DSDP,* 9: Washington, DC (U.S. Govt. Printing Office). **doi:10.2973/dsdp.proc.9.1972**

Holbourn, A., Kuhnt, W., Schulz, M., and Erlenkeuser, H., 2005. Impacts of orbital forcing and atmospheric CO_2 on Miocene ice-sheet expansion. *Nature (London, U.K.),* 438(7067):483–487. **doi:10.1038/nature04123**

Hyndman, R.D., Erickson, A.J., and Von Herzen, R.P., 1974. Geothermal measurements on DSDP Leg 26. *In* Davies, T.A., Luyendyk, B.P., et al., *Init. Repts. DSDP,* 26: Washington, DC (U.S. Govt. Printing Office), 451–463. **doi:10.2973/dsdp.proc.26.113.1974**

Knappenberger, M., 2000. Sedimentation rates and Pacific plate motion calculated using seismic cross sections of the Neogene equatorial sediment bulge [M.Sc. thesis]. Boise State Univ., Idaho.

Koppers, A.A.P., Phipps Morgan, J., Morgan, J.W., and Staudigel, H., 2001. Testing the fixed hotspot hypothesis using $^{40}Ar/^{39}Ar$ age progressions along seamount trails. *Earth Planet. Sci. Lett.,* 185(3–4):237–252. **doi:10.1016/S0012-821X(00)00387-3**

Lear, C.H., Rosenthal, Y., Coxall, H.K., and Wilson, P.A., 2004. Late Eocene to early Miocene ice sheet dynamics and the global carbon cycle. *Paleoceanography,* 19(4):PA4015. **doi:10.1029/2004PA001039**

Lear, C.H., Bailey, T.R., Pearson, P.N., Coxall, H.K., and Rosenthal, Y., 2008. Cooling and ice growth across the Eocene–Oligocene transition. *Geology,* 36(3):251–254. **doi:10.1130/G24584A.1**

Lind, I.L., Janecek, T.R., Krissek, L.A., Prentice, M.L., and Stax, R., 1993. Color bands in Ontong Java Plateau carbonate oozes and chalks. *In* Berger, W.H., Kroenke, L.W., Mayer, L.A., et al., *Proc. ODP, Sci. Results,* 130: College Station, TX (Ocean Drilling Program), 453–470. **doi:10.2973/odp.proc.sr.130.007.1993**

Lyle, M.W., Pälike, H., Moore, T.C., Mitchell, N., and Backman, J., 2006. *Summary Report of R/V Roger Revelle Site Survey AMAT03 to the IODP Environmental Protection and Safety Panel (EPSP) in Support for Proposal IODP626:* Southampton, U.K. (Univ. Southampton). **http://eprints.soton.ac.uk/45921/**

Lyle, M., Wilson, P.A., Janecek, T.R., et al., 2002. *Proc. ODP, Init. Repts.,* 199: College Station, TX (Ocean Drilling Program). **doi:10.2973/odp.proc.ir.199.2002**

Mayer, L.A., Shipley, T.H., Theyer, F., Wilkens, R.H., and Winterer, E.L., 1985. Seismic modeling and paleoceanography at Deep Sea Drilling Project Site 574. *In* Mayer, L., Theyer, F., Thomas, E., et al., *Init. Repts. DSDP,* 85: Washington, DC (U.S. Govt. Printing Office), 947–970. **doi:10.2973/dsdp.proc.85.132.1985**

Miller, K.G., Wright, J.D., and Fairbanks, R.G., 1991. Unlocking the ice house: Oligocene–Miocene oxygen isotopes, eustasy, and margin erosion. *J. Geophys. Res.,* 96(B4):6829–6848. **doi:10.1029/90JB02015**

Müller, R.D., Roest, W.R., Royer, J.-Y., Gahagan, L.M., and Sclater, J.G., 1997. Digital isochrons of the world's ocean floor. *J. Geophys. Res.,* 102(B2):3211–3214. **doi:10.1029/96JB01781**

Nigrini, C., Sanfilippo, A., and Moore, T.C., Jr., 2006. Cenozoic radiolarian biostratigraphy: a magnetobiostratigraphic chronology of Cenozoic sequences from ODP Sites 1218, 1219, and 1220, equatorial Pacific. *In* Wilson, P.A., Lyle, M., and Firth, J.V. (Eds.), *Proc. ODP, Sci. Results,* 199: College Station, TX (Ocean Drilling Program), 1–76. **doi:10.2973/odp.proc.sr.199.225.2006**

Pälike, H., Lyle, M.W., Ahagon, N., Raffi, I., Gamage, K., and Zarikian, C.A., 2008. Pacific equatorial age transect. IODP Sci. Prosp., 320/321. **doi:10.2204/iodp.sp.320321.2008**

Pälike, H., Norris, R.D., Herrle, J.O., Wilson, P.A., Coxall, H.K., Lear, C.H., Shackleton, N.J., Tripati, A.K., and Wade, B.S., 2006. The heartbeat of the Oligocene climate system. *Science,* 314(5807):1894–1898. **doi:10.1126/science.1133822**

Pälike, H., Frazier, J., and Zachos, J.C., 2006. Extended orbitally forced palaeoclimatic records from the equatorial Atlantic Ceara Rise. *Quat. Sci. Rev.,* 25(23–24):3138–3149. **doi:10.1016/j.quascirev.2006.02.011**

Petronotis, K.E., 1991. Paleomagnetic studies of the skewness of Pacific plate marine magnetic anomalies 25–32R: implications for anomalous skewness and the motion of the Pacific plate and hotspots [Ph.D. thesis]. Northwestern Univ., Evanston, IL.

Petronotis, K.E., Gordon, R.G., and Acton, G.D., 1994. A 57 Ma Pacific plate paleomagnetic pole determined from a skewness analysis of crossings of marine magnetic anomaly 25r. *Geophys. J. Int.,* 118(3):529–554. **doi:10.1111/j.1365-246X.1994.tb03983.x**

Pribnow, D.F.C., Kinoshita, M., and Stein, C.A., 2000. *Thermal Data Collection and Heat Flow Recalculations for ODP Legs 101–180:* Hanover, Germany (Inst. Joint Geosci. Res., Inst. Geowiss. Gemeinschaftsauf. [GGA]). **http://www-odp.tamu.edu/publications/heatflow/ODPReprt.pdf**

Raffi, I., Backman, J., Fornaciari, E., Pälike, H., Rio, D., Lourens, L., and Hilgen, F., 2006. A review of calcareous nannofossil astrobiochronology encompassing the past 25 million years. *Quat. Sci. Rev.,* 25(23–24):3113–3137. **doi:10.1016/j.quascirev.2006.07.007**

Sager, W.W., and Pringle, M.S., 1988. Mid-Cretaceous to early Tertiary apparent polar wander path of the Pacific plate. *J. Geophys. Res., [Solid Earth],* 93(B10):11753–11771. **doi:10.1029/JB093iB10p11753**

Shackleton, N.J., Hall, M.A., Raffi, I., Tauxe, L., and Zachos, J., 2000. Astronomical calibration age for the Oligocene–Miocene boundary. *Geology,* 28(5):447–450. **doi:10.1130/0091-7613(2000)28<447:ACAFTO>2.0.CO;2**

van Morkhoven, F.P.C.M., Berggren, W.A., and Edwards, A.S., 1986. *Cenozoic Cosmopolitan Deep-Water Benthic Foraminifera.* Bull. Cent. Rech. Explor.—Prod. Elf-Aquitaine, Mem. 11.

Young, J.R., 1999. Neogene. *In* Bown, P.R. (Ed.), *Calcareous Nannofossil Biostratigraphy:* Dordrecht, The Netherlands (Kluwer Academic Publ.), 225–265.

Zachos, J., Pagani, M., Sloan, L., Thomas, E., and Billups, K., 2001. Trends, rhythms, and aberrations in global climate 65 Ma to present. *Science,* 292(5517):686–693. **doi:10.1126/science.1059412**

Zachos, J.C., Flower, B.P., and Paul, H., 1997. Orbitally paced climate oscillations across the Oligocene/Miocene boundary. *Nature (London, U. K.),* 388(6642):567–570. **doi:10.1038/41528**

Zachos, J.C., Shackleton, N.J., Revenaugh, J.S., Pälike, H., and Flower, B.P., 2001. Climate response to orbital forcing across the Oligocene–Miocene boundary. *Science,* 292(5515):274–278. **doi:10.1126/science.1058288**

Publication: 30 October 2010
MS 320321-107

Figure F1. A. ETOPO1 (Amante and Eakins, 2008) bathymetric overview map of Site U1335 and PEAT drilling locations, with previous ODP and DSDP sites. **B.** Swath map bathymetry for Site U1335 region from the AMAT-03 site survey. Black labels = seismic shotpoints, white labels = bathymetric contours. White line = survey Line 8 (Fig. F2). F.Z. = fracture zone.

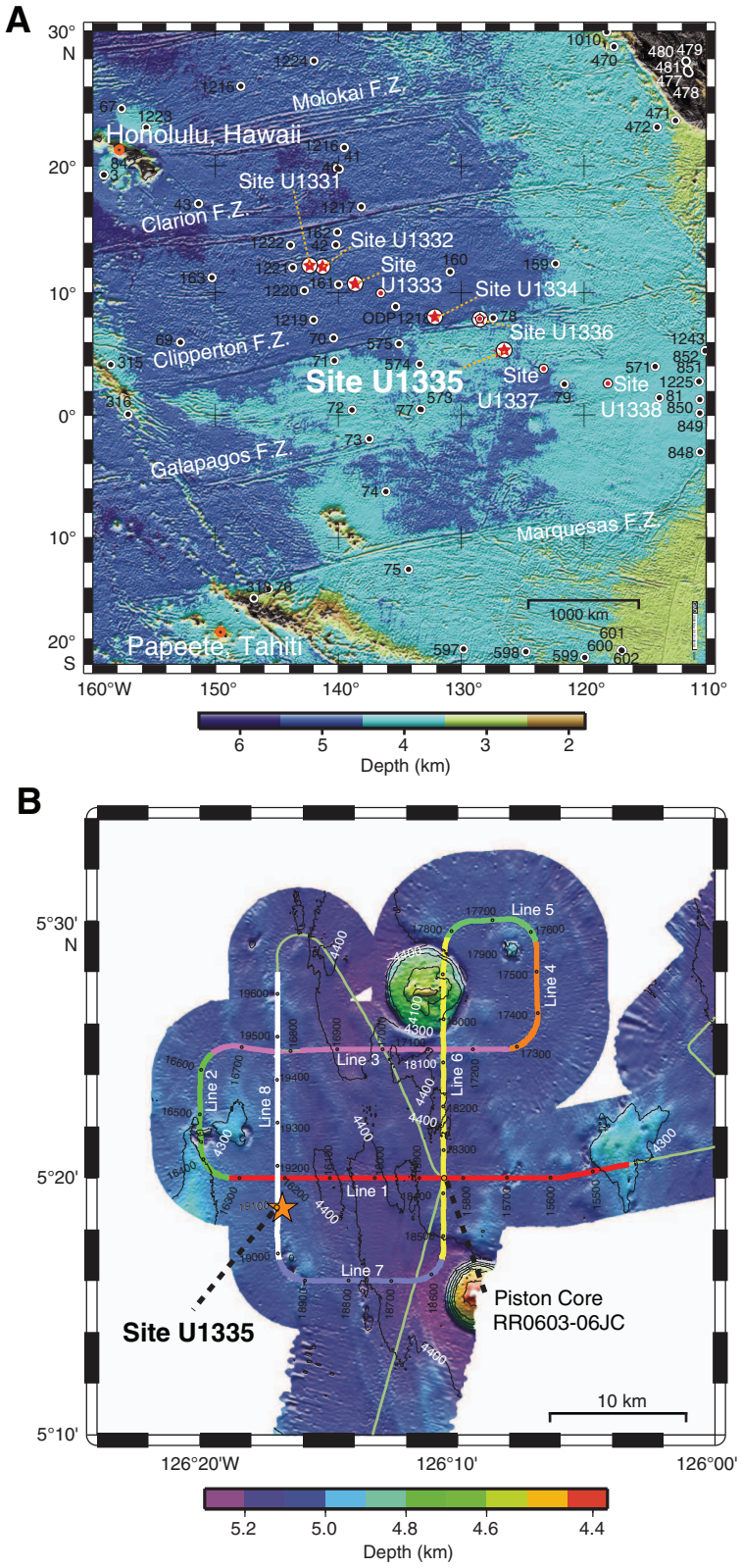

Figure F2. Seismic reflection profile PEAT-6C (Site U1335) Line 8 from the 48-channel seismic reflection survey, annotated in shotpoints (Lyle et al., 2006). Data are filtered, stacked, and migrated. Tentative conversion from two-way traveltime to depth uses velocity model of Busch et al. (2006). SP = shotpoint. mbsl = meters below sea level. TD = total depth.

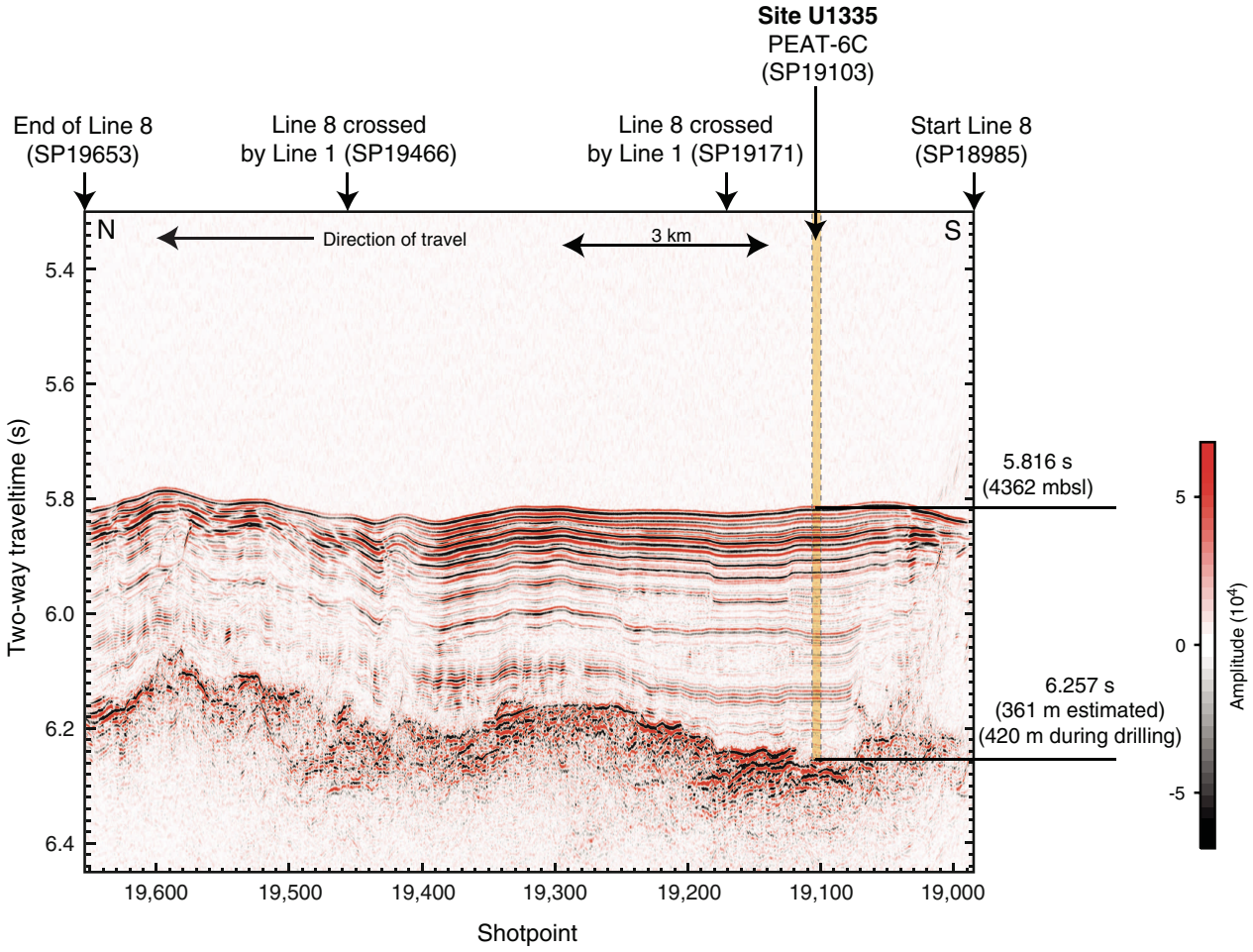

Figure F3. Site U1335 summary. At Site U1335, planktonic foraminifer Zone O6 is informally divided into an upper and lower part using the base of *Paragloborotalia pseudokugleri*.

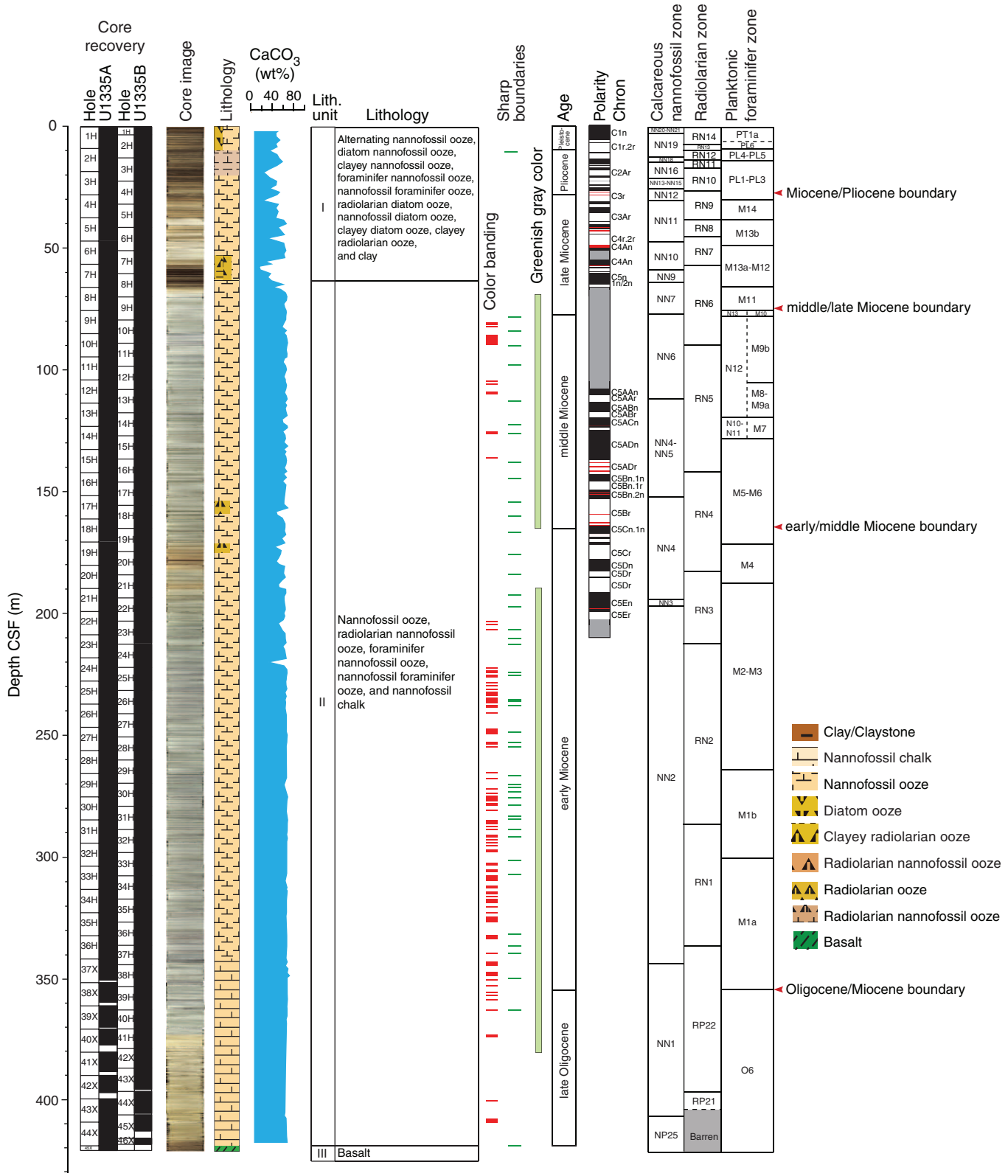

Figure F4. Lithologic summary, Site U1335. Magnetic stratigraphy data based on Hole U1335B. Geomagnetic polarity: red interval = possible geomagnetic excursions (cryptochron), gray interval = undetermined interval. L*, b* = reflectance value of sediment as defined in the LAB color model.

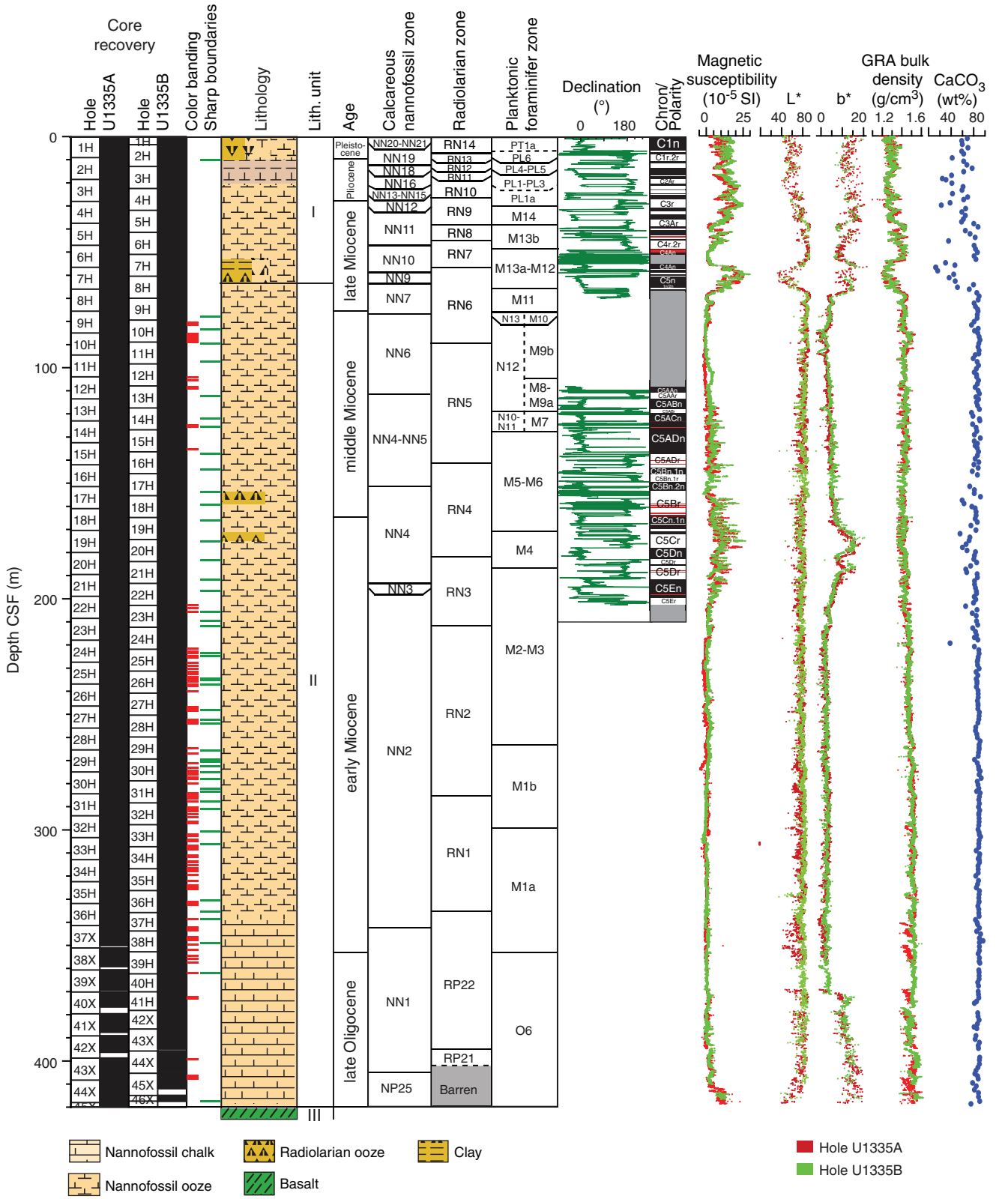

Figure F5. Calcium carbonate ($CaCO_3$), total carbon (TC), inorganic carbon (IC), and total organic carbon (TOC) determined by normal and acidification methods in sediments from Hole U1335A. (See **"Lithostratigraphy"** for information on unit boundaries.)

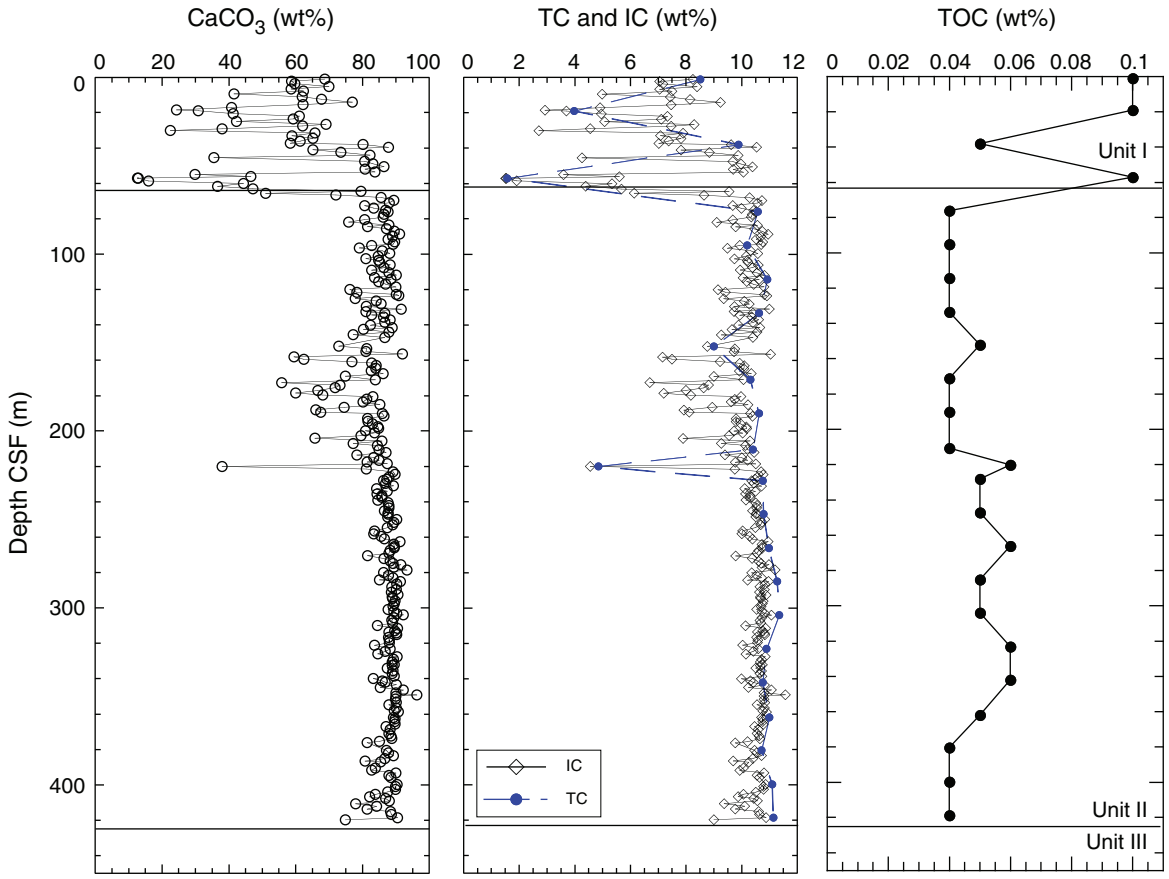

Figure F6. Color reflectance and magnetic susceptibility, Hole U1335A. Line scan images from Cores 320-U1335A-7H through 8H, 18H through 22H, and 39X through 45X highlight observed color changes. L*, a*, b* = reflectance value of sediment as defined in the LAB color model.

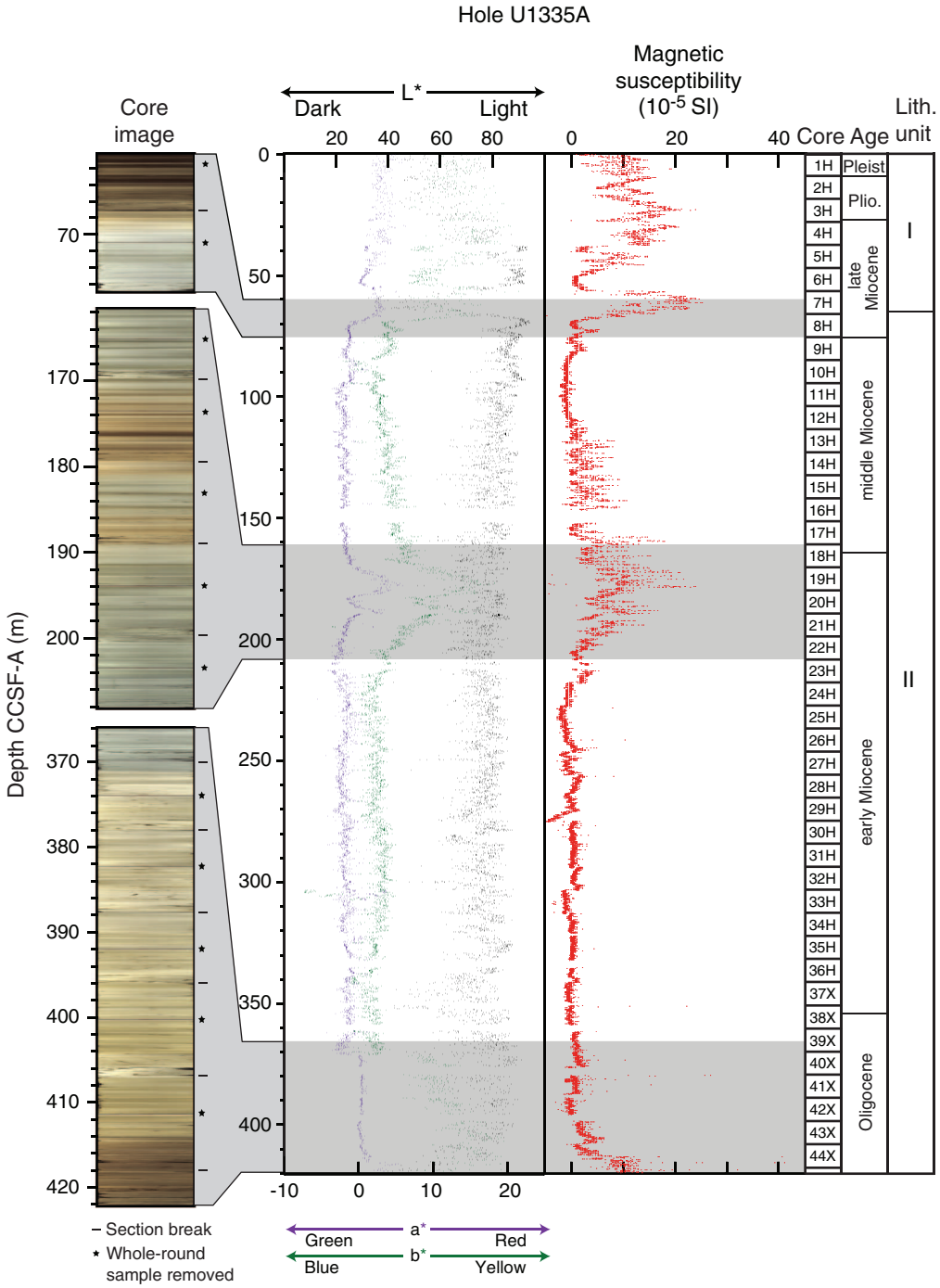

Figure F7. Summary of magnetic susceptibility and paleomagnetic results, Hole U1335B. Declinations are shown in sample coordinates (not reoriented to geographical coordinates).

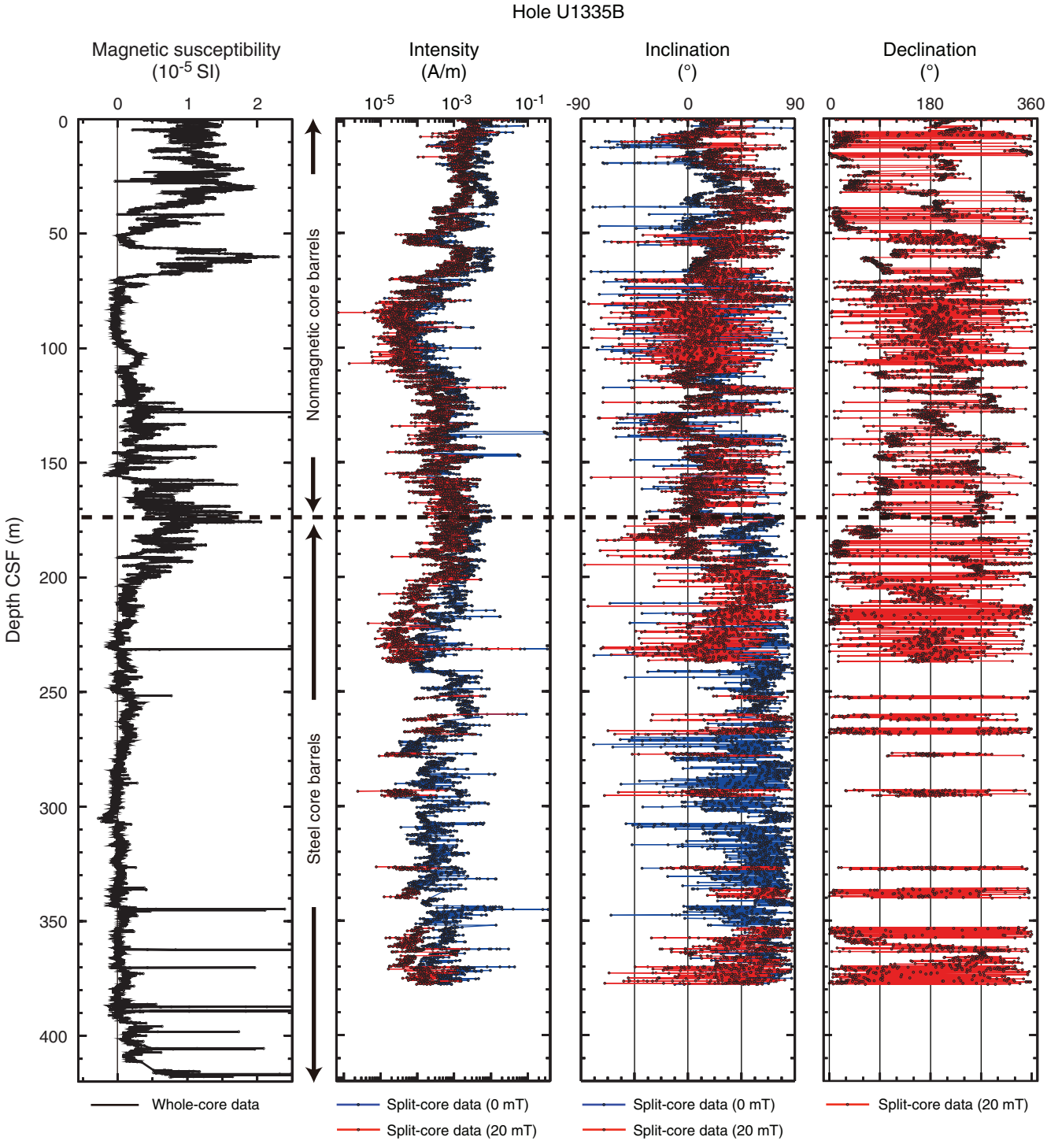

Figure F8. Line scan images of nannofossil ooze interbedded with nannofossil diatom ooze. **A.** Interval 320-U1335B-10H-3, 54–90 cm. **B.** Interval 320-U1335B-24H-6, 34–70 cm. Note that the beds of nannofossil diatom ooze are characterized by rough surfaces (both sections were scraped in the same way with a glass slide in preparation for line image scanning).

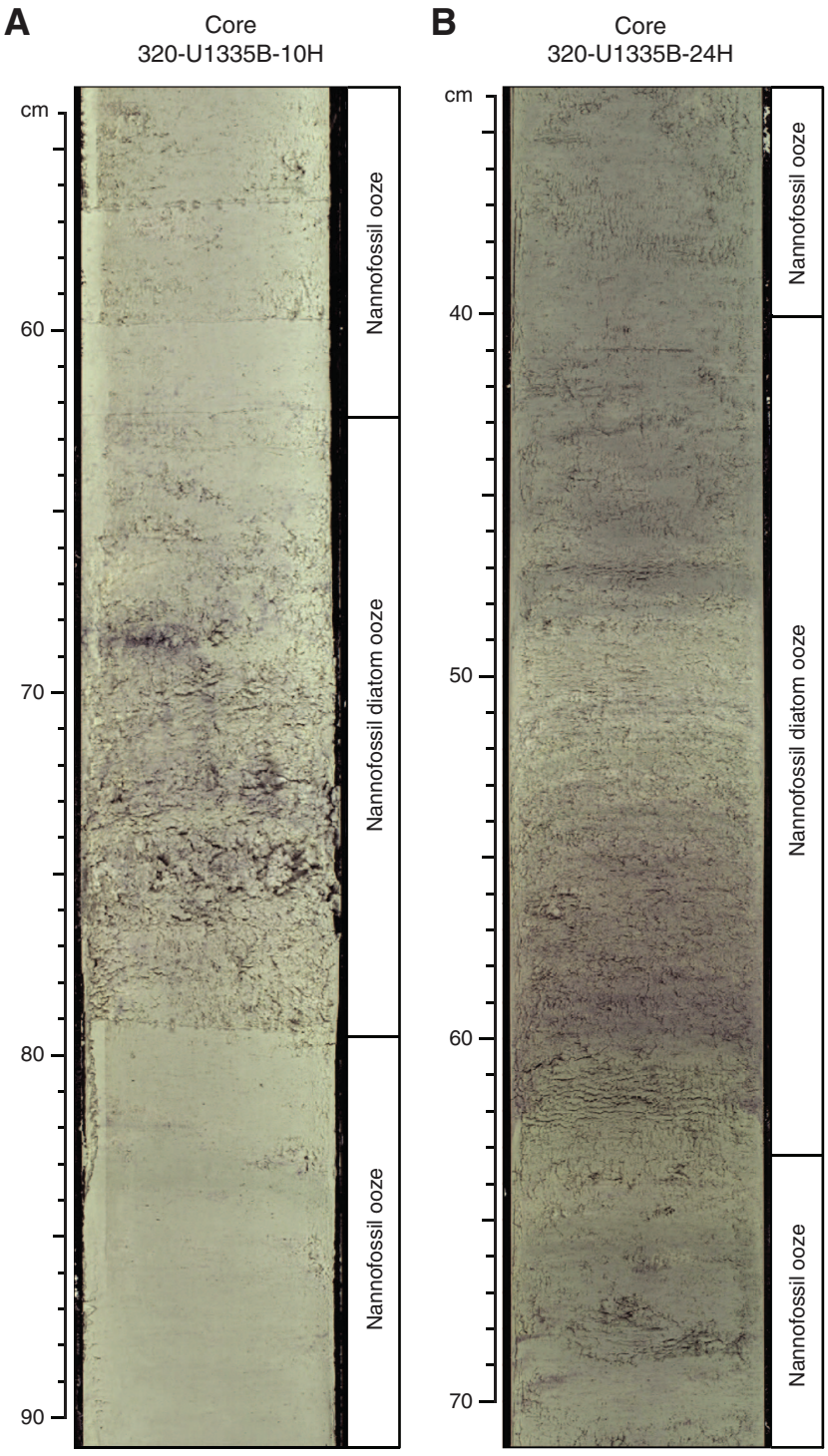

Figure F9. Photomicrographs of smear slides, Site U1335. Left image = plane-polarized light, right image = cross-polarized light. **A.** Nannofossil ooze (Sample 320-U1335B-10H-1, 110 cm). **B.** Nannofossil diatom ooze (Sample 320-U1335B-10H-3, 70 cm). See **"Site U1335 smear slides"** in "Core descriptions" for full descriptions.

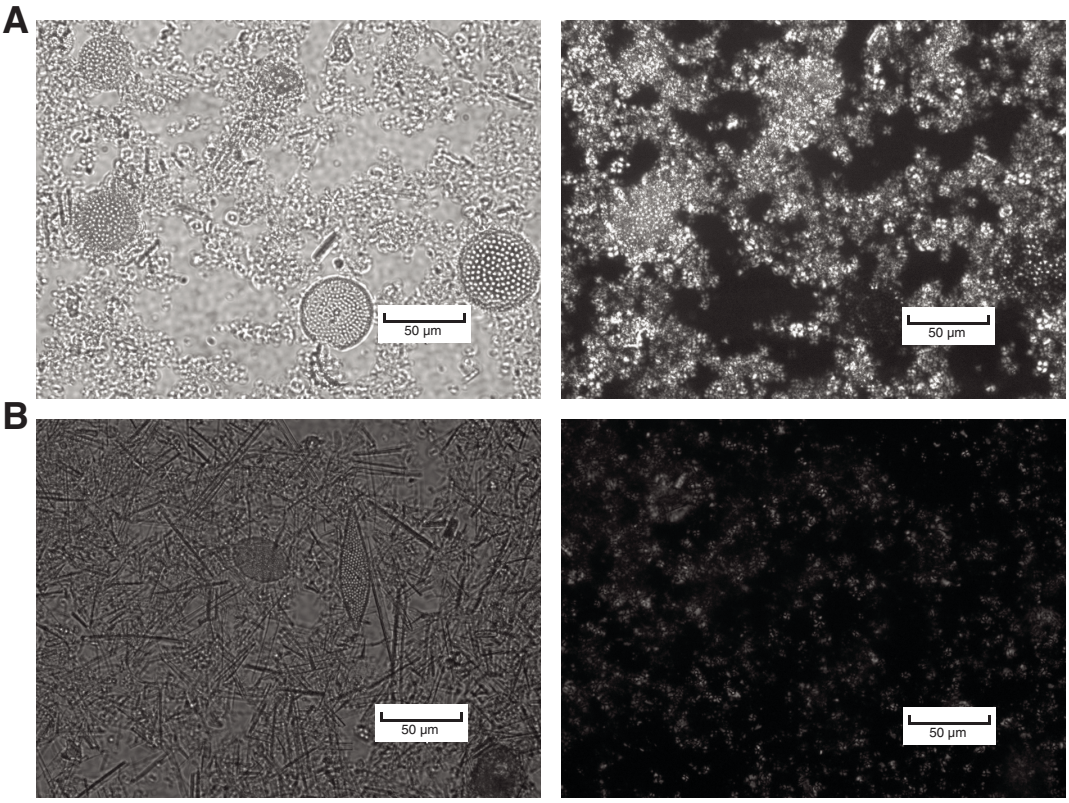

Figure F10. A. Line scan image of interval 320-U1335A-12H-6, 62–144 cm, including a nannofossil foraminifer ooze bed. **B, C.** Photomicrographs of angular basalt fragments (Sample 320-U1335A-12H-6, 134 cm). Basalt fragment containing glass groundmass and lath-shaped minerals inside. **D.** Close-up line scan image around the base of nannofossil foraminifer ooze.

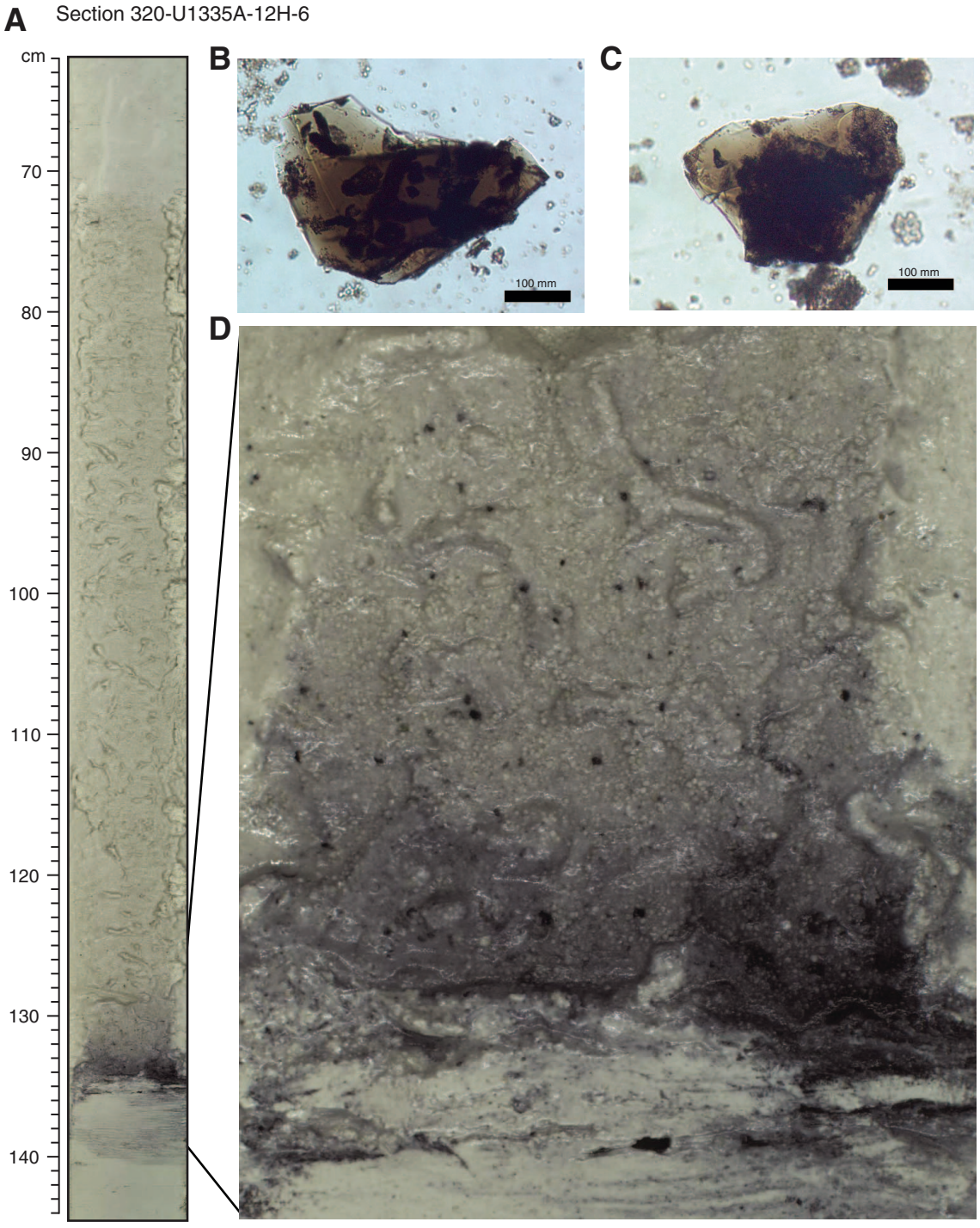

Figure F11. Line scan image of color bands in partially consolidated interval (interval 320-U1335A-39X-1, 102–115 cm).

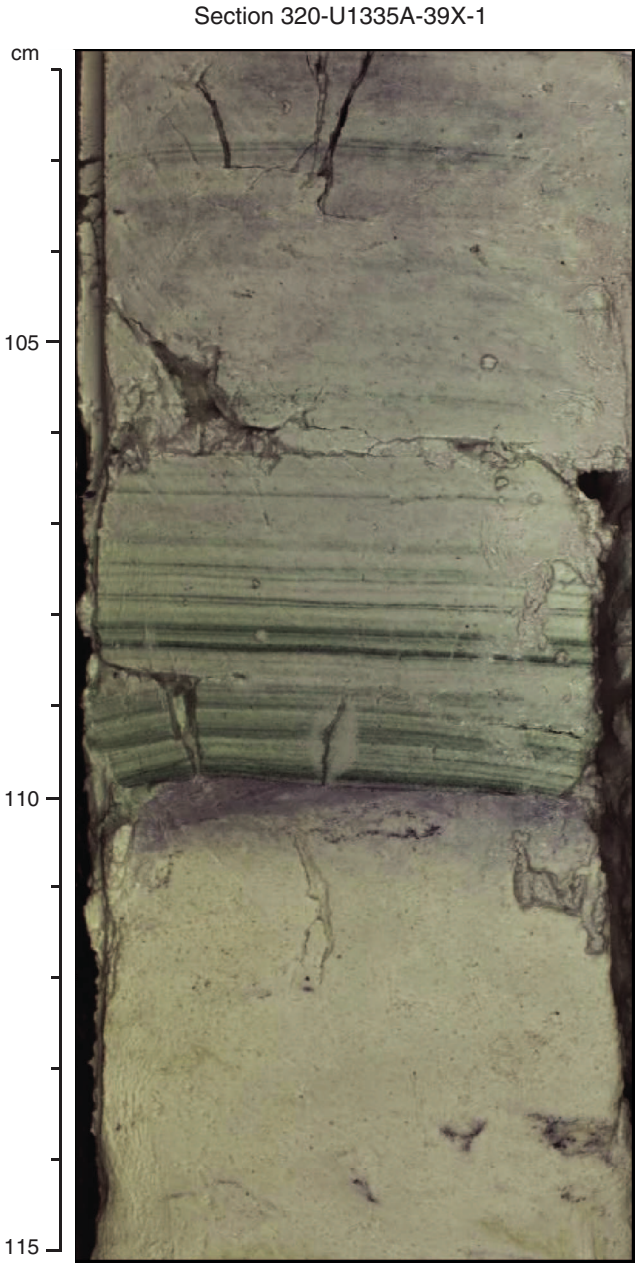

Figure F12. Line scan images of sharp boundary and overlying nannofossil foraminifer ooze. **A.** Boundary at 28 cm in interval 320-U1335A-2H-1, 116–133 cm. **B.** Boundary at 54 cm in interval 320-U1335B-2H-6, 41–59 cm.

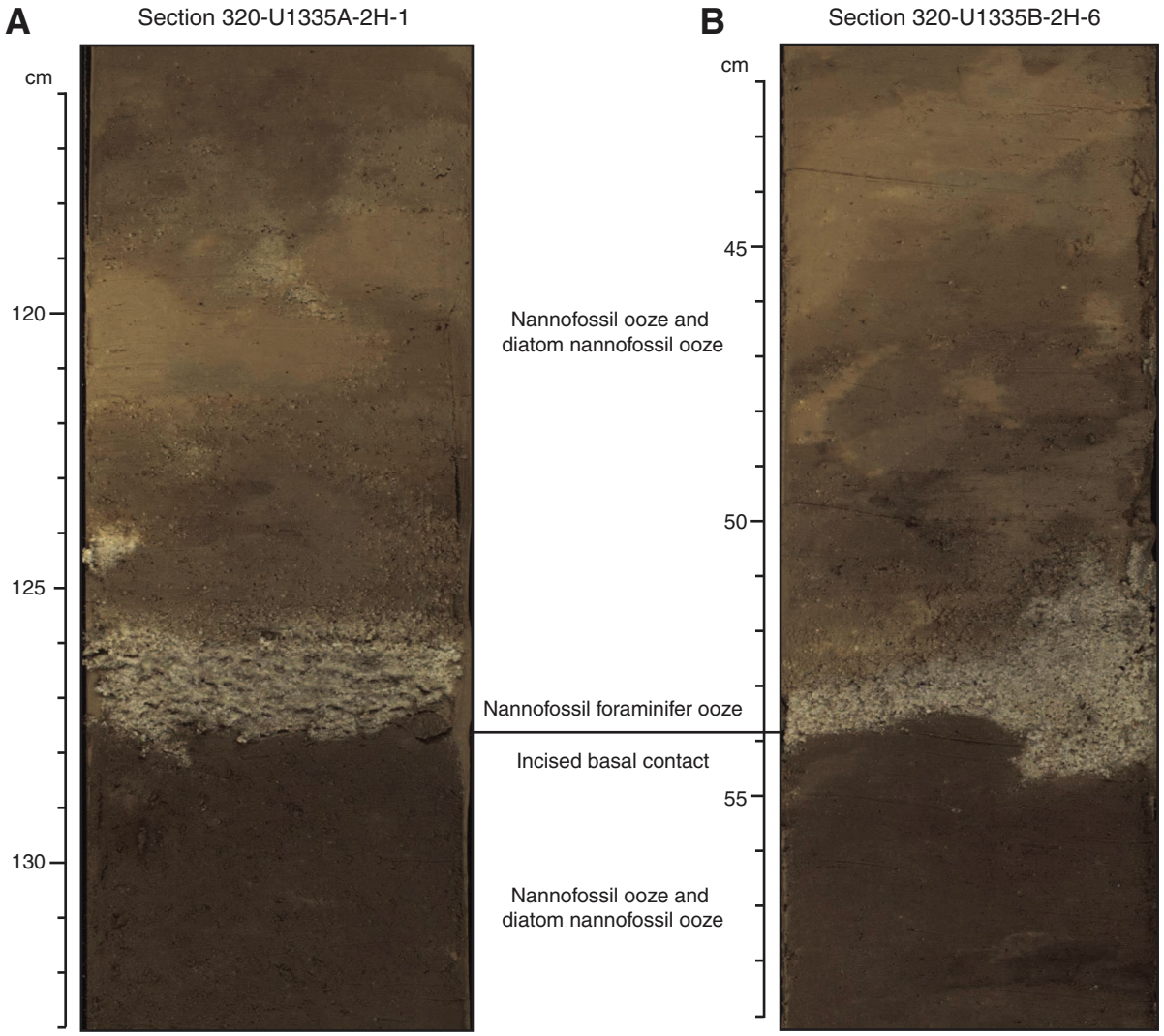

Figure F13. Integrated calcareous and siliceous microfossil biozonation, Site U1335.

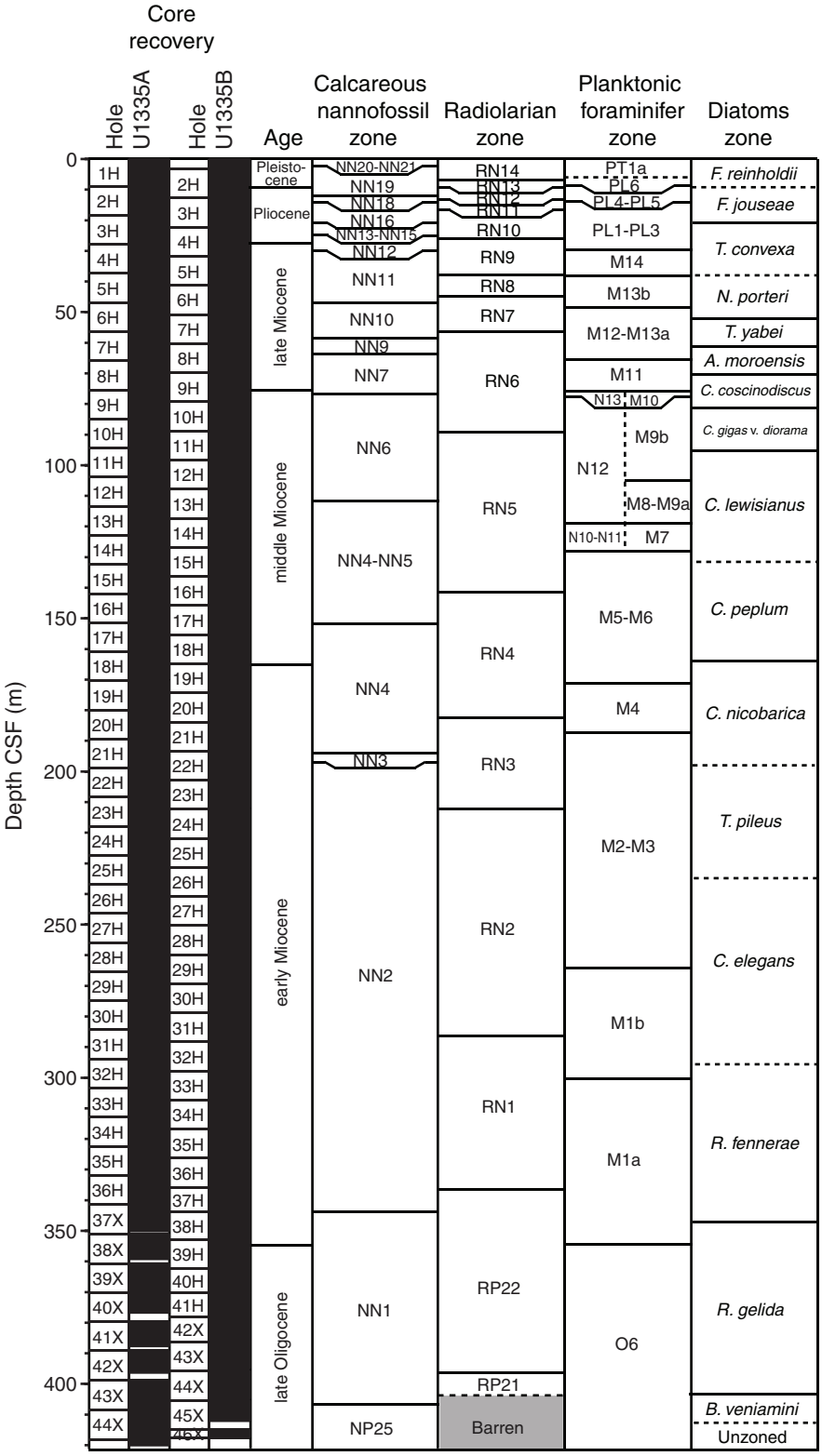

Figure F14. Linear sedimentation rates and chronostratigraphic markers, Site U1335.

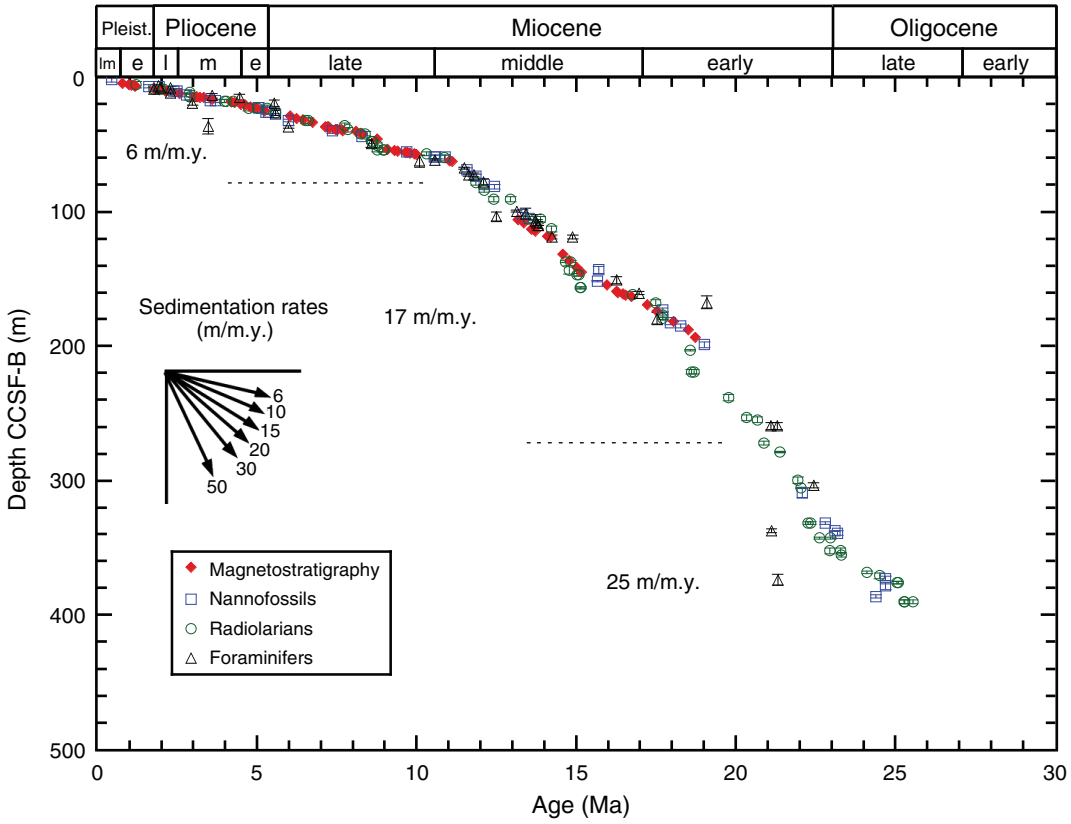

Figure F15. Summary of magnetic susceptibility and paleomagnetic results, Hole U1335A. Declinations are shown in sample coordinates (not reoriented to geographical coordinates). PCA = principle component analysis.

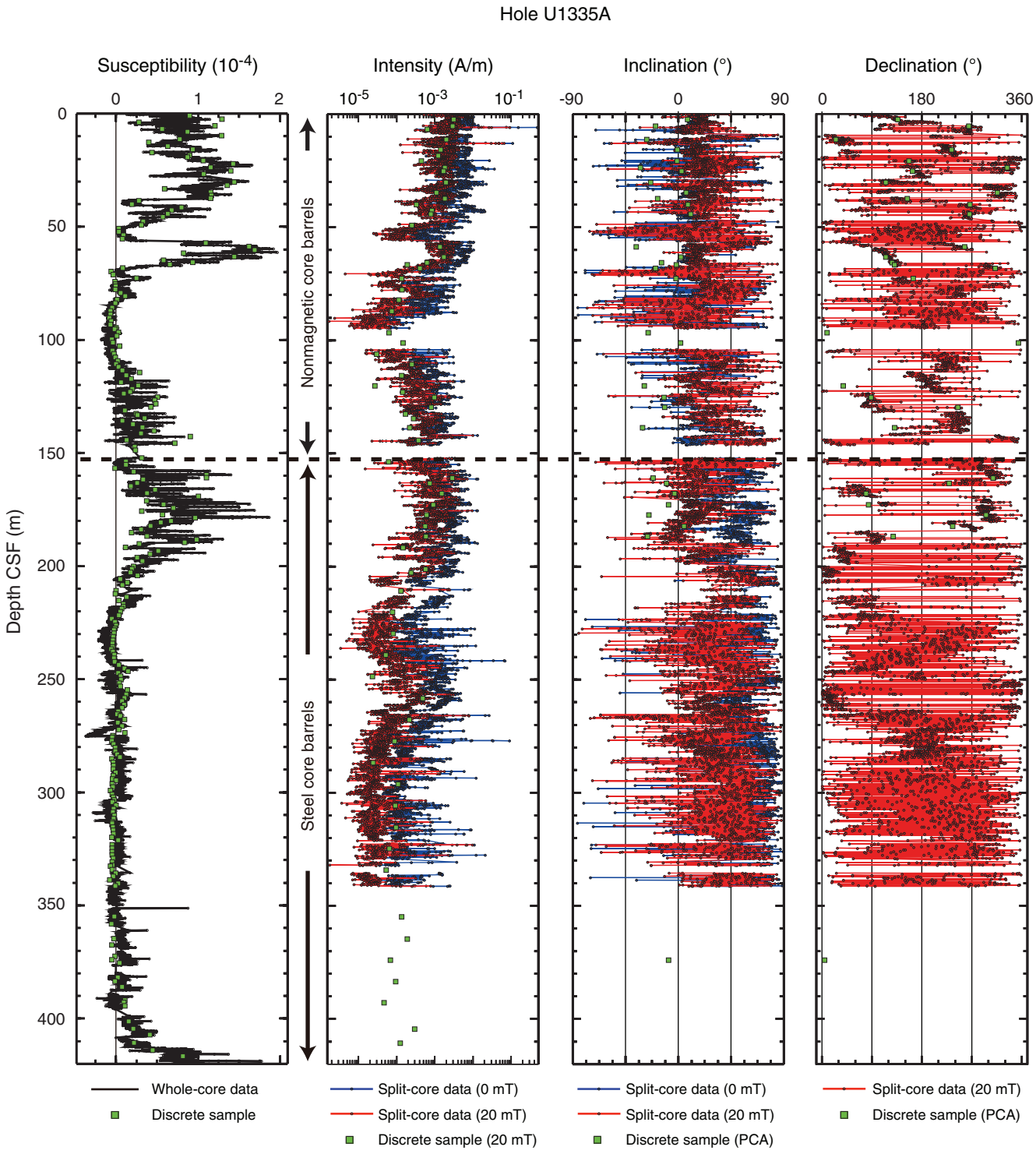

Figure F16. Representative alternating-field demagnetization (demag) results for Site U1335 samples. Left plot = vector endpoints of paleomagnetic directions on vector demagnetization diagrams or Zijderveld plots (solid circles = horizontal projections, open circles = vertical projections, gray circles = data not used in computing ChRM, black dashed line = ChRM direction), middle plot = intensity variation with progressive demagnetization, right plot = directions plotted on an equal-angle stereonet. Vector demagnetization diagrams of A and B show relatively well resolved characteristic remanent magnetizations, whereas that of C does not. **A.** Normal polarity sample (320-U1335A-1H-2, 90 cm) (2.40 m CSF) **B.** Reversed polarity sample (320-U1335A-17H-7, 50 cm) (160.90 m CSF). **C.** Weakly magnetized sample from the magnetic-low zone (Sample 320-U1335A-10H-2, 85 cm) (87.25 m CSF). NRM = natural remanent magnetization. Inc = inclination, Dec = declination, MAD = maximum angular deviation.

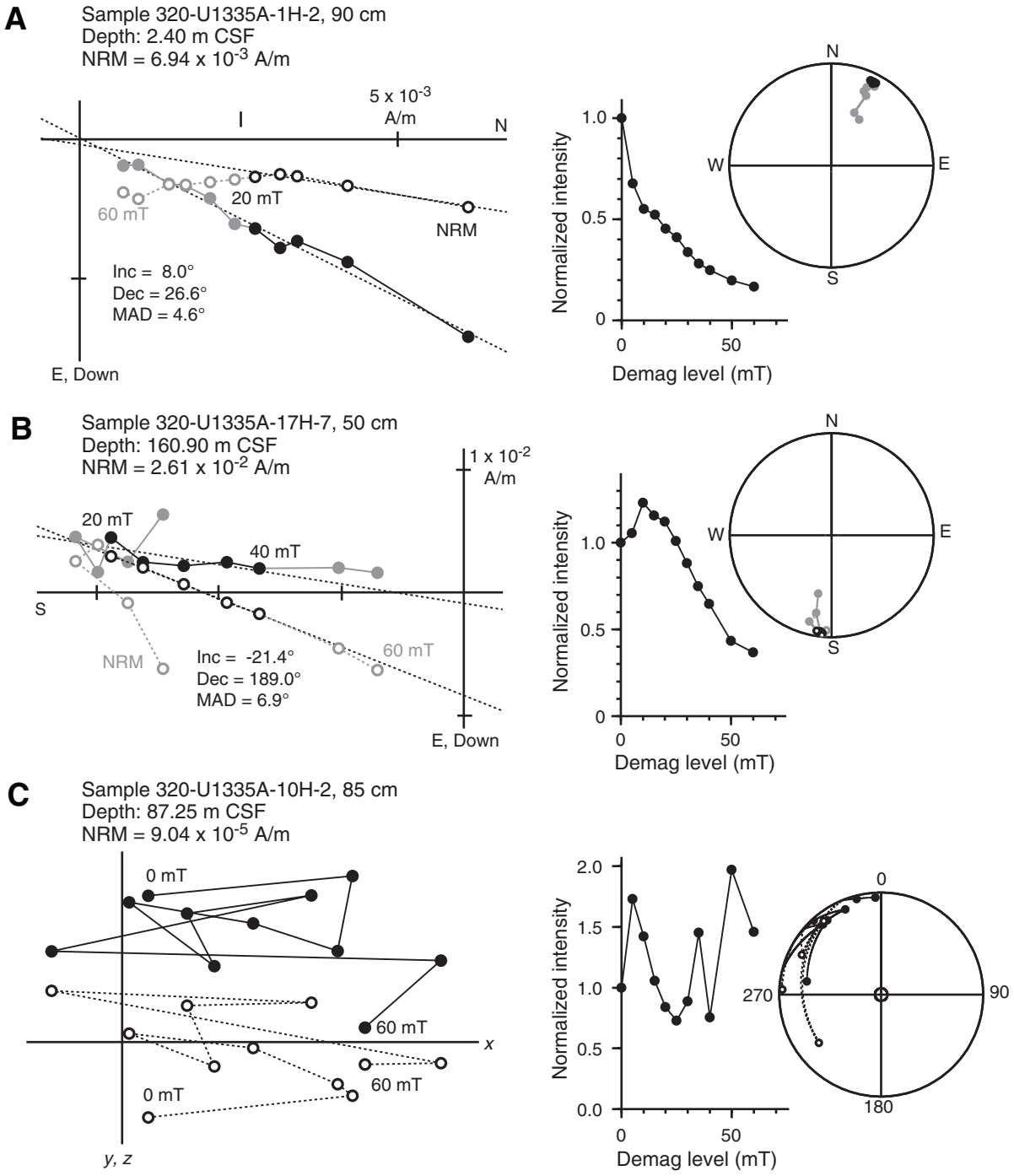

Figure F17. Latitude of the virtual geomagnetic pole (VGP), Hole U1335A. North latitudes = normal polarity (black), south latitudes = reversed polarity (white). Red bars = intervals of possible geomagnetic excursions. Gray bars = indeterminate polarity, such as in the magnetic-low zone. **A.** 0–70 m CSF. (**Continued on next page.**)

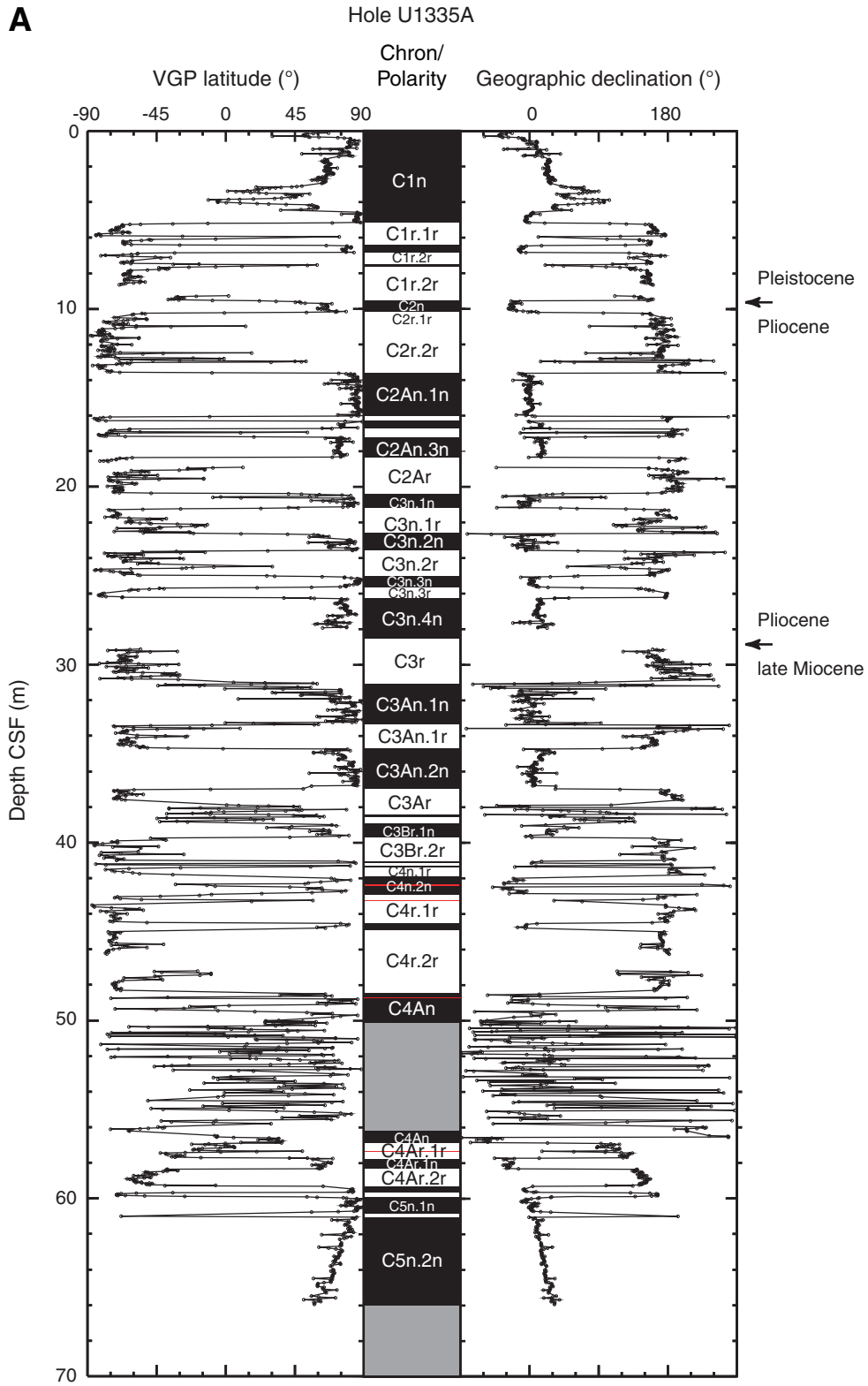

Figure F17 (continued). B. 150–210 m CSF.

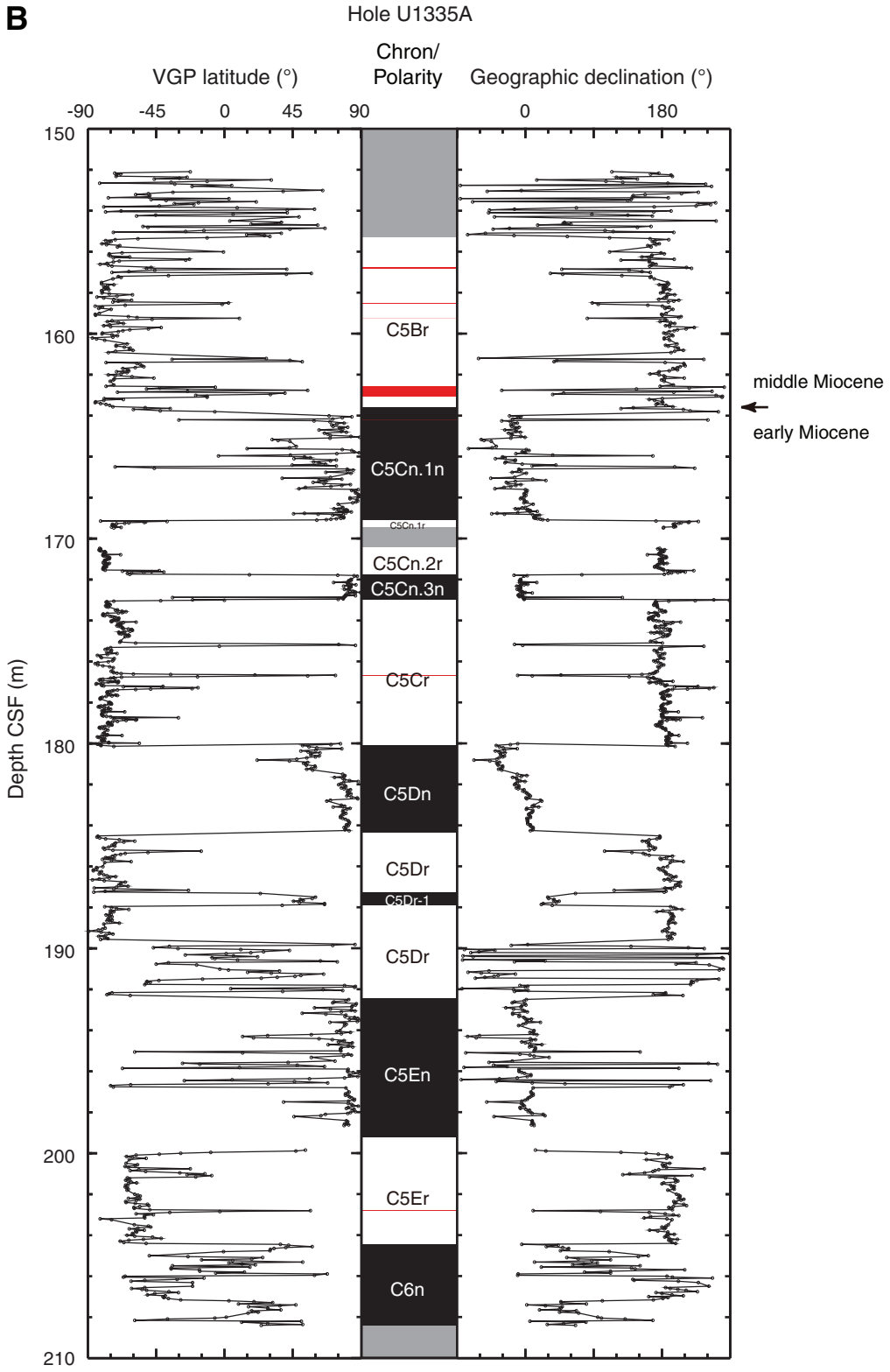

Figure F18. Latitude of the virtual geomagnetic pole (VGP), Hole U1335B. North latitudes = normal polarity (black), south latitudes = reversed polarity (white). Red bars = intervals of possible geomagnetic excursions. Gray bars = indeterminate polarity, such as in the magnetic-low zone. **A.** 0–70 m CSF. (**Continued on next page.**)

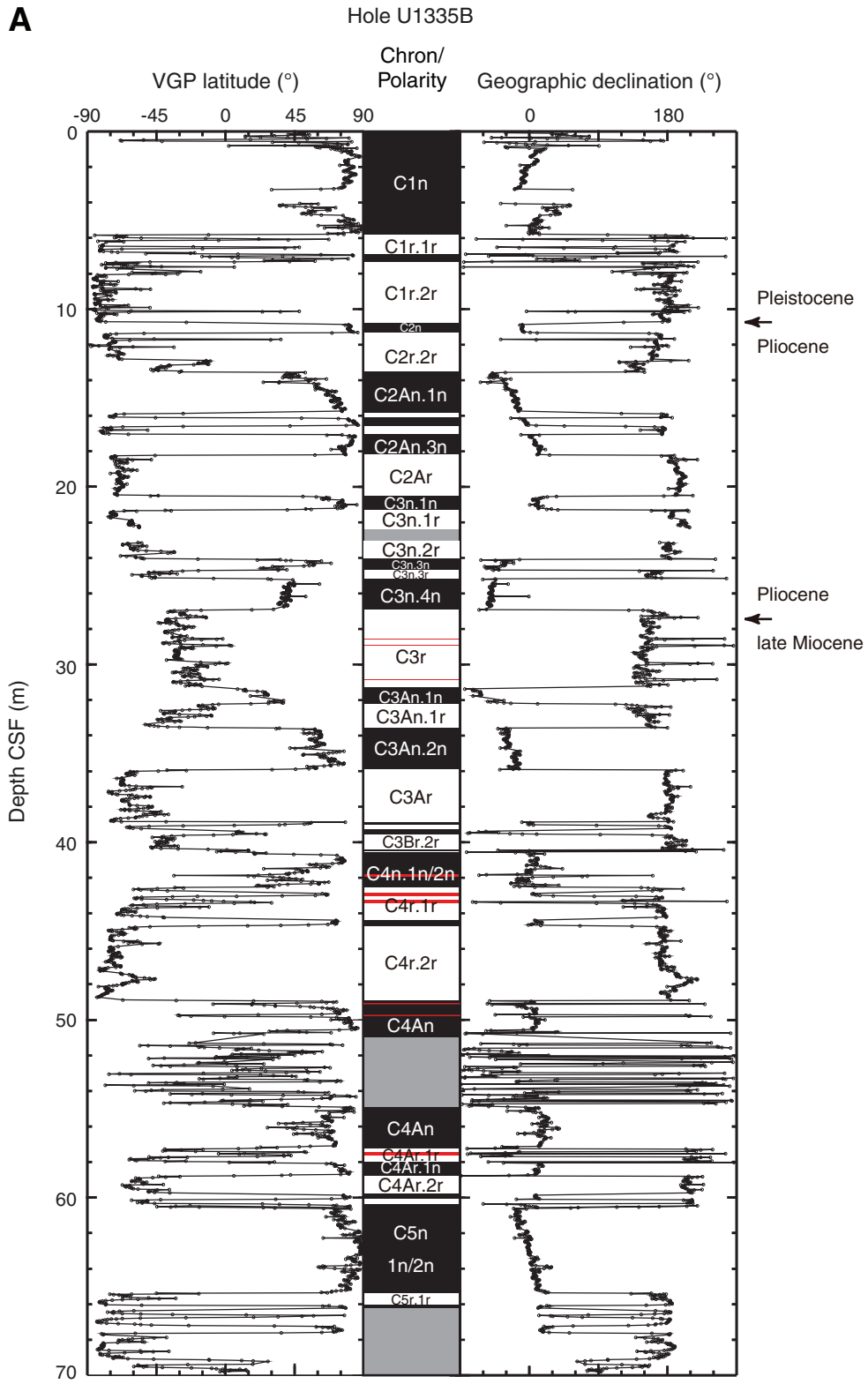

Figure F18 (continued). B. 105–205 m CSF.

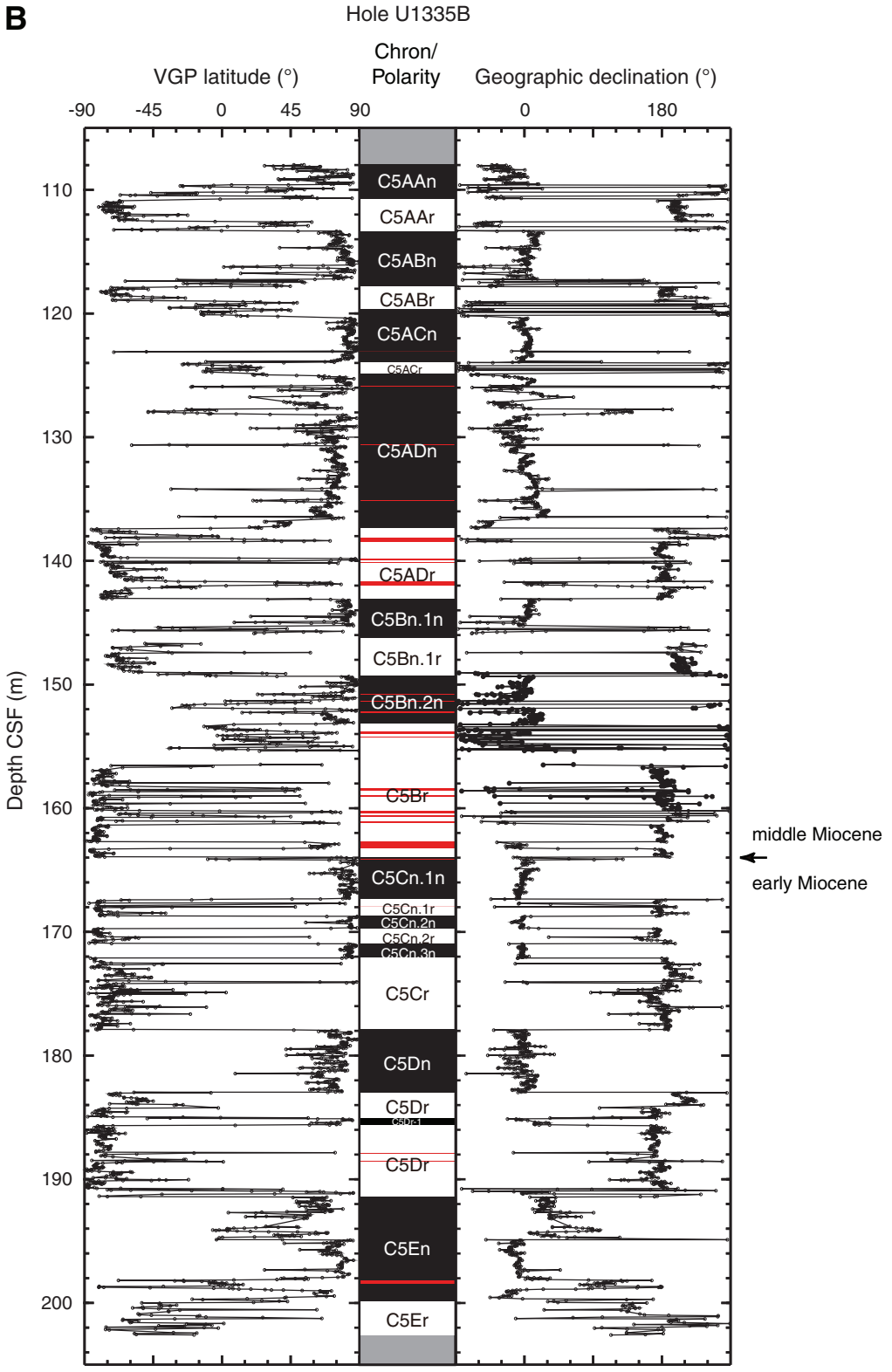

Figure F19. Interstitial water chemistry, Holes U1335A and U1335B. Values below the detection limit (see Table T21) are plotted as zero. (See "Lithostratigraphy" for information on unit boundaries.)

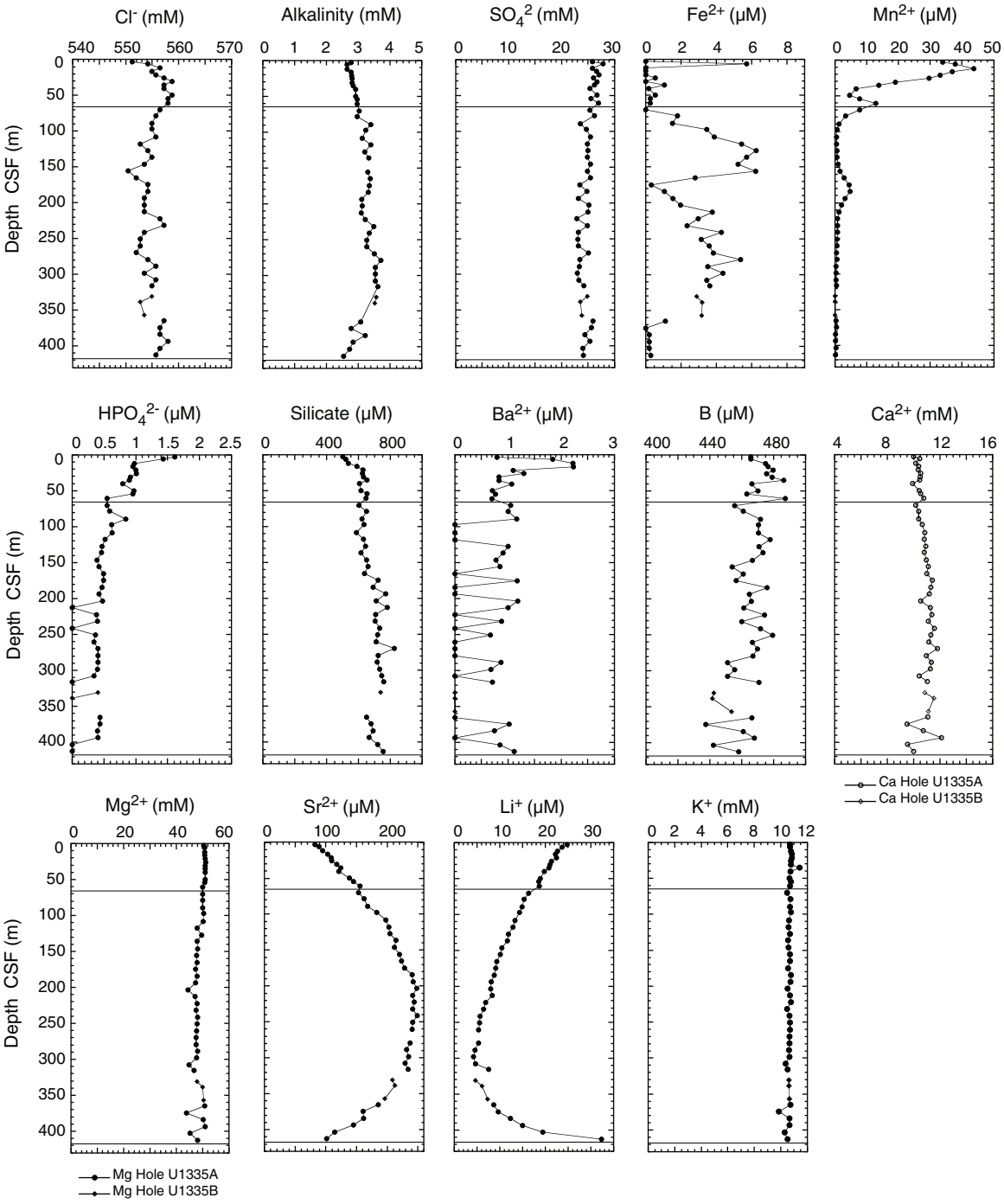

Figure F20. Whole-Round Multisensor Logger (WRMSL) and natural gamma radiation (NGR) data, Holes U1335A and U1335B. Data for Hole U1335B are plotted using offsets (0.5 g/cm^3 for bulk density; 10 × 10^{-5} SI for magnetic susceptibility; 100 m/s for *P*-wave velocity; 10 cps for NGR).

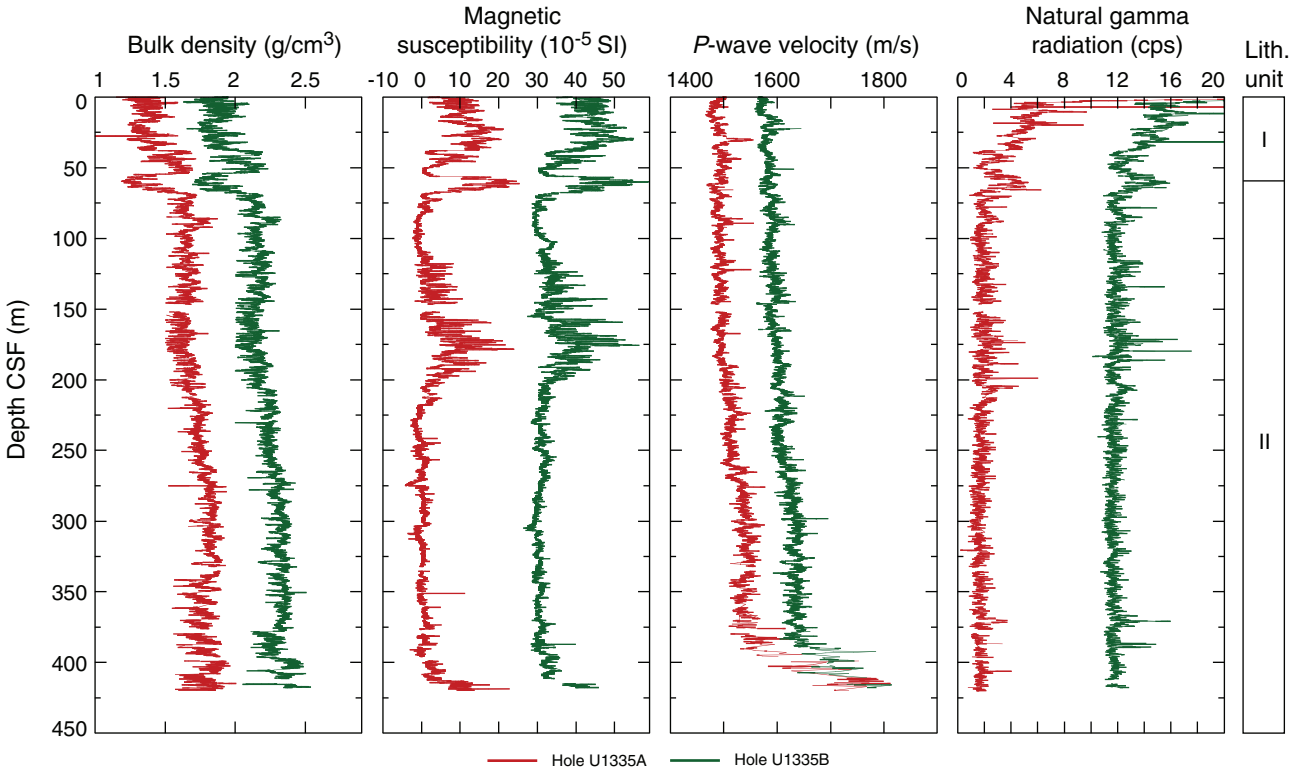

Figure F21. Moisture and density (MAD) measurements, Hole U1335A. **A.** Porosity and water content. **B.** MAD and gamma ray attenuation (GRA) bulk density. **C.** Grain density.

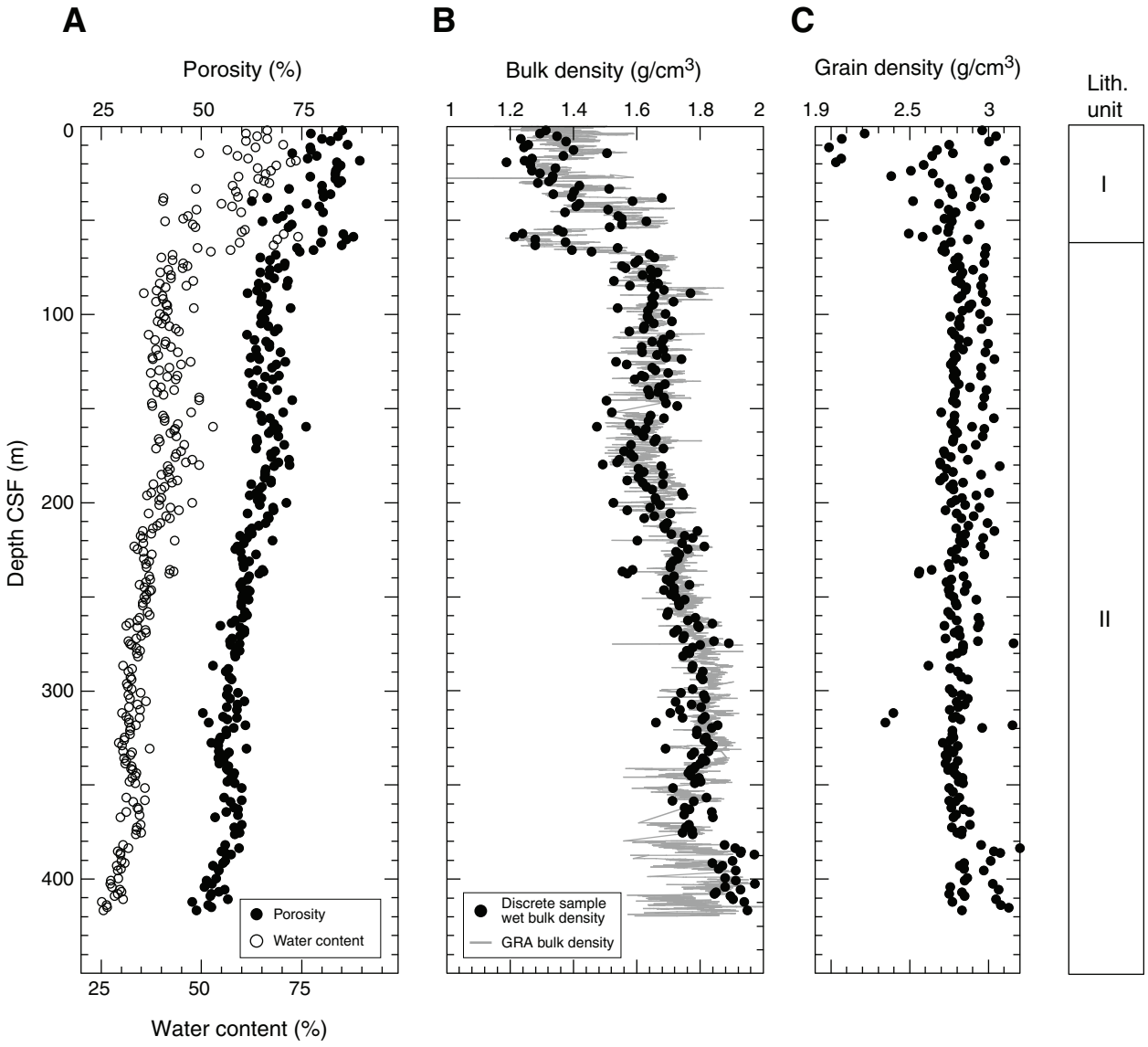

Figure F22. Moisture and density (MAD) analysis of discrete samples, Hole U1335A. Gamma ray attenuation (GRA) density interpolated with a 20 cm wide Gaussian window.

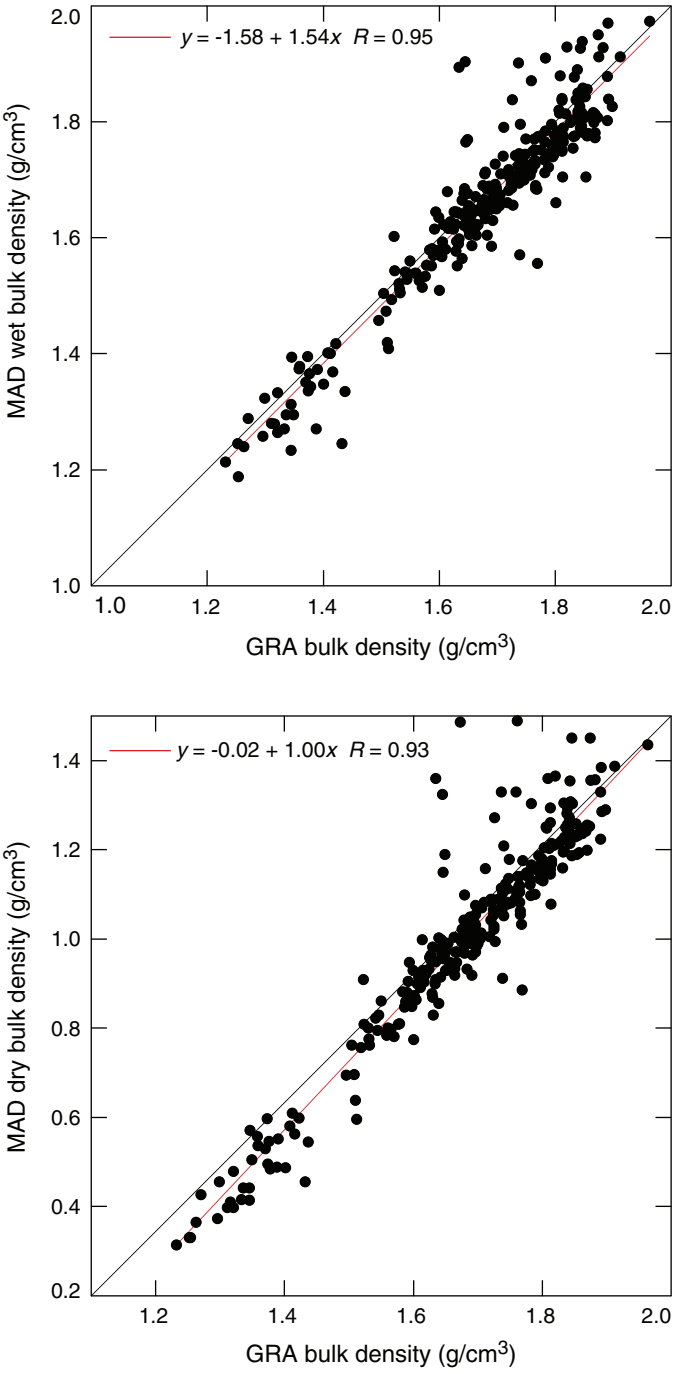

Figure F23. Compressional wave velocity from the *P*-wave logger (PWL) and discrete velocity measurements on split core from Hole U1335A, using the contact probe for *x*-axis measurements and insertion probes for *y*- and *z*-axis measurements (see **"Compressional wave velocity"** for a note on postcruise velocity correction.)

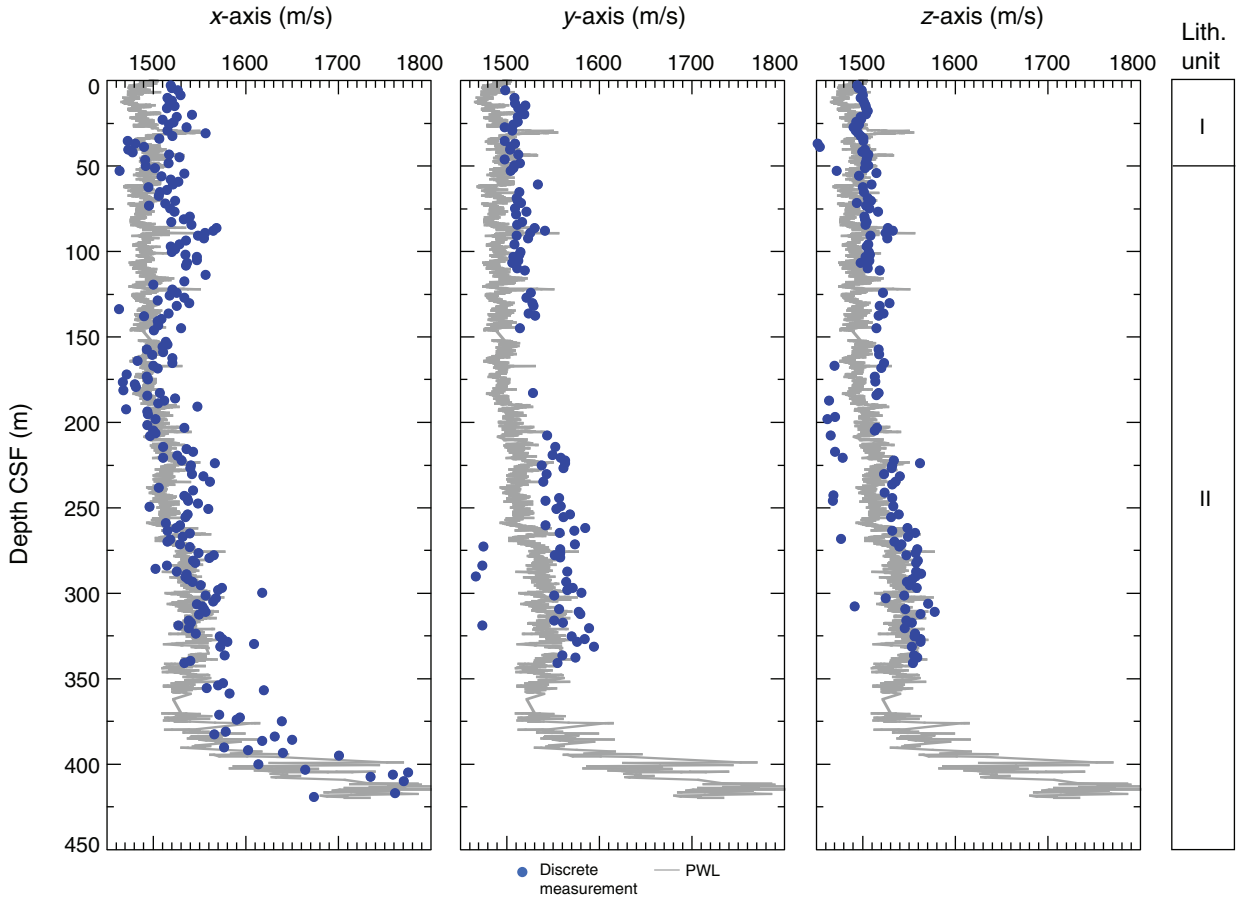

Figure F24. Porosity and thermal conductivity measurements, Hole U1335A.

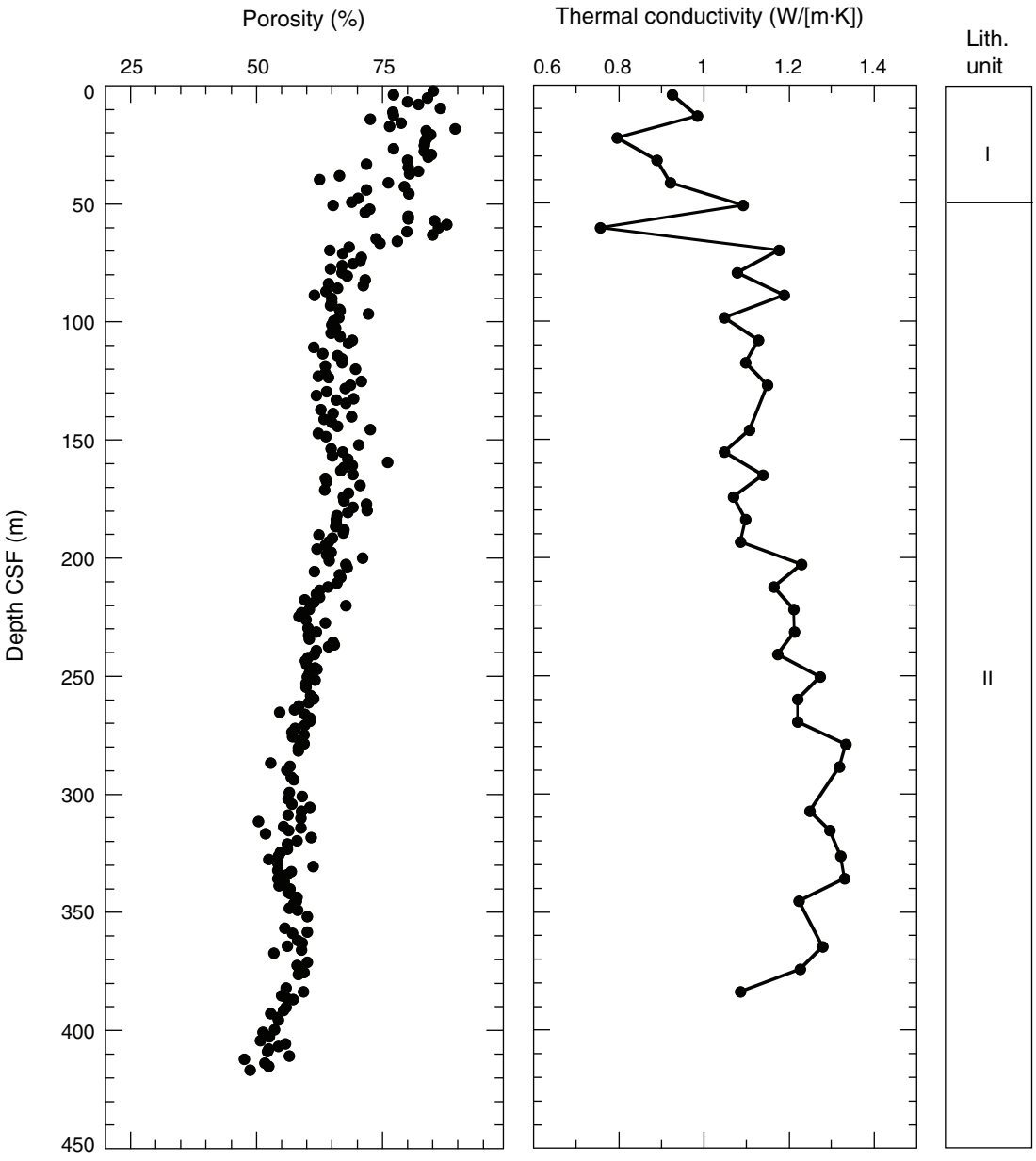

Figure F25. Thermal conductivity vs. porosity, from moisture and density analysis of discrete samples, Hole U1335A.

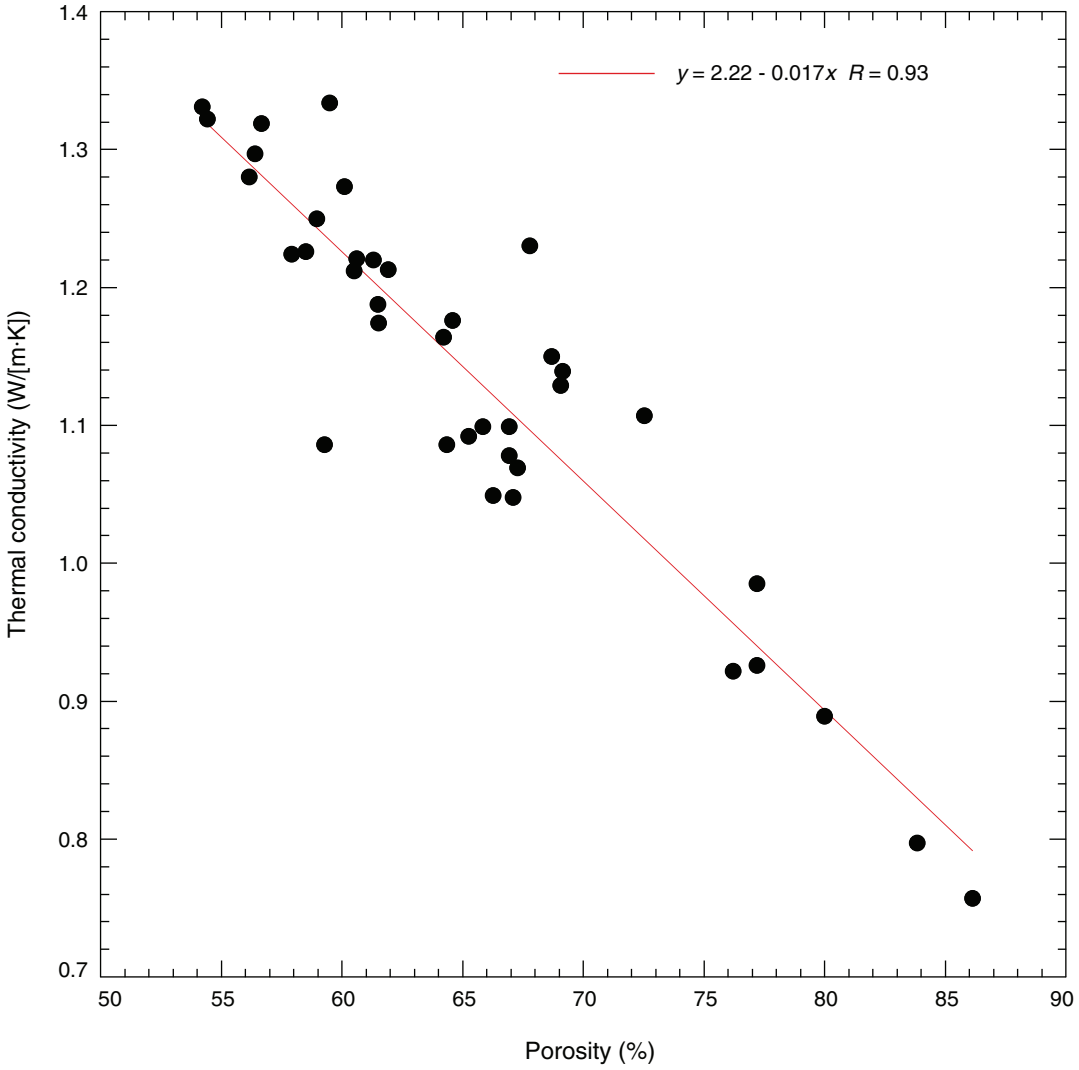

Figure F26. Reflectance spectrophotometer (RSC) data, Holes U1335A and U1335B. RSC for Hole U1335B has been offset (20 for L*, 4 for a*, and 8 for b*) for core to core comparison. L*, a*, b* = reflectance value of sediment as defined in the LAB color model.

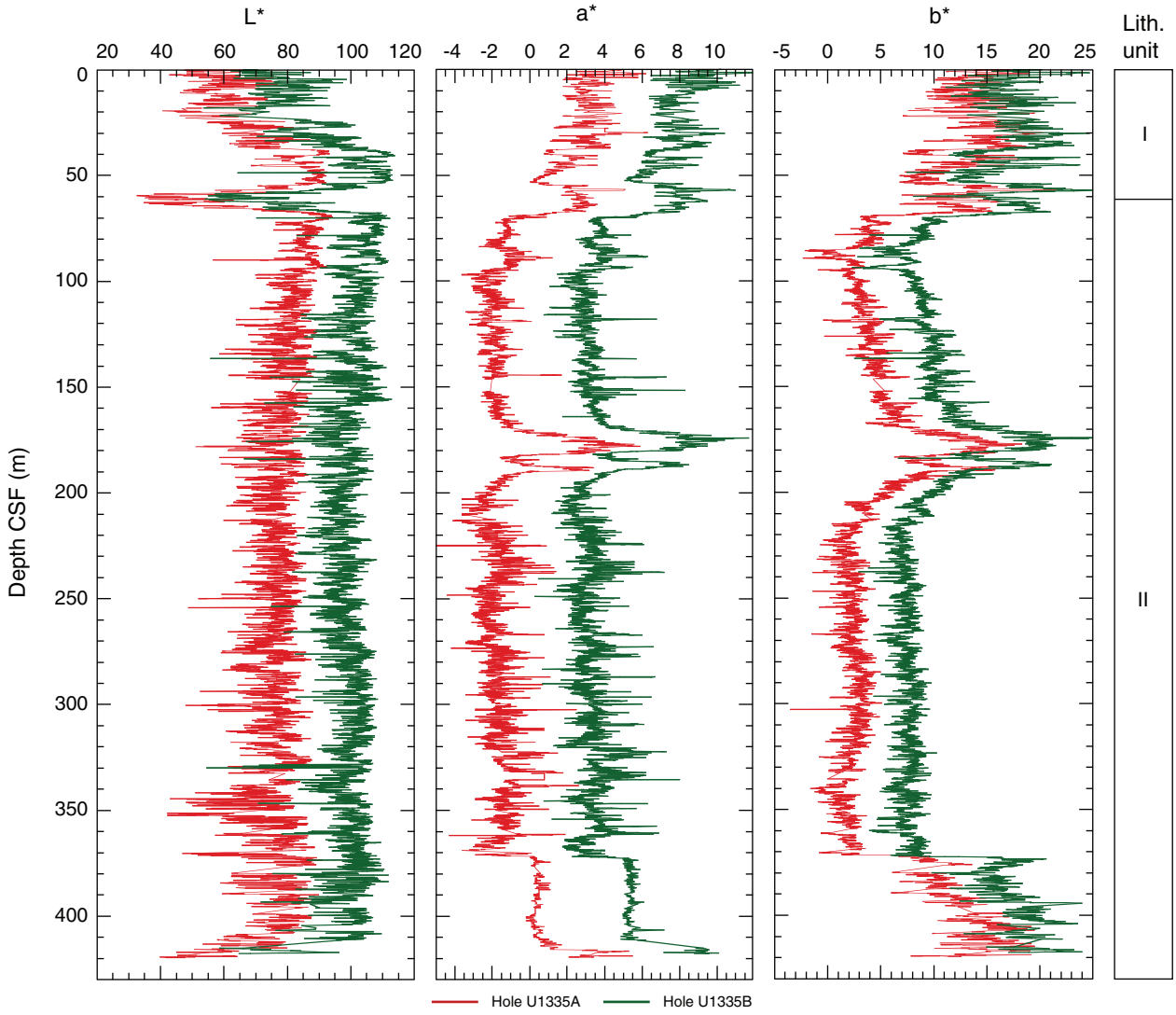

Figure F27. Magnetic susceptibility data, Site U1335. Top panel = spliced section with core breaks (triangles) and hole designations, bottom panel = Holes U1335A (red) and U1335B (blue), offset from each other by a constant (150 × 10^{-6} SI). **A.** 0–50 CCSF-A. (**Continued on next seven pages.**)

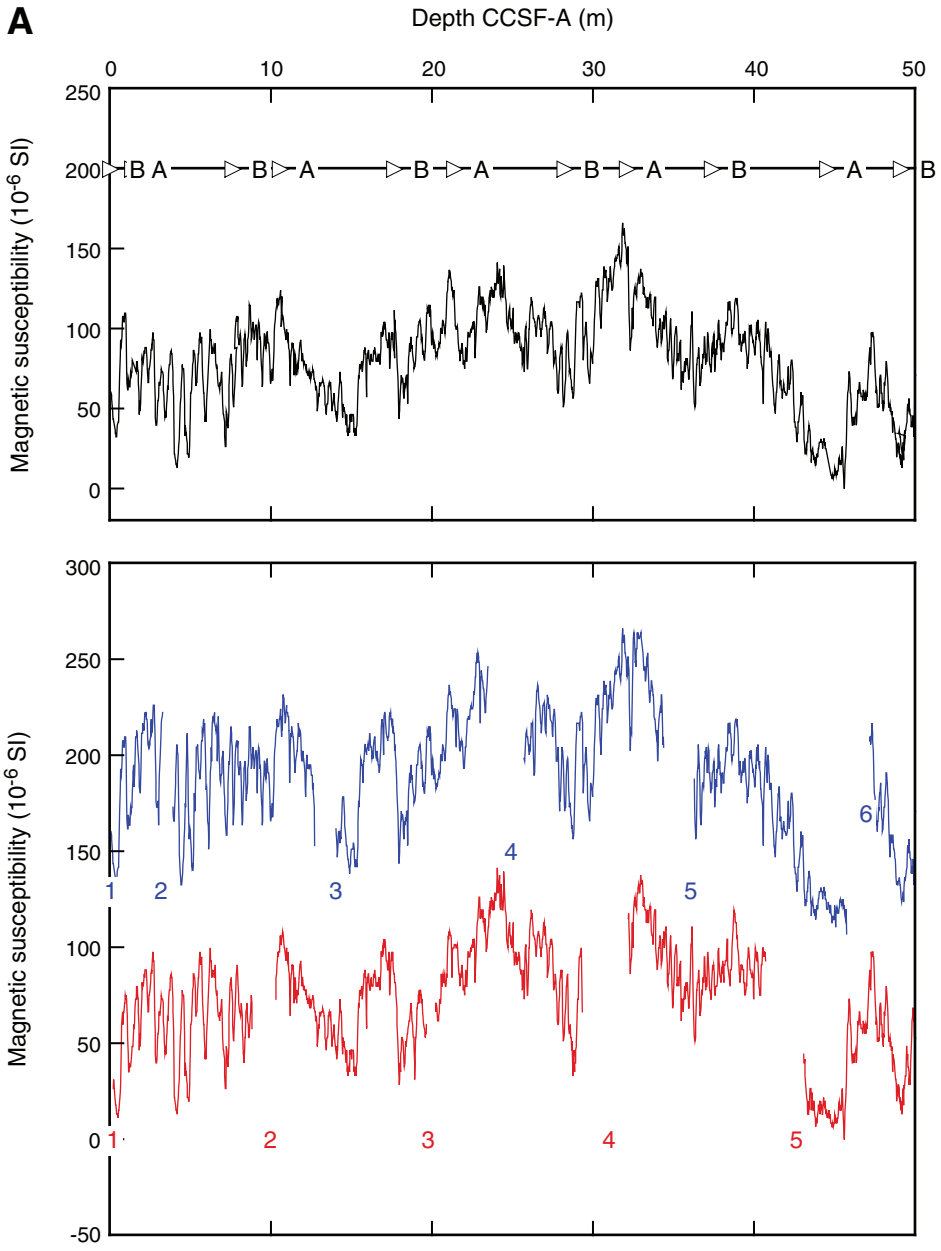

Figure F27 (continued). B. 50–100 CCSF-A. (Continued on next page.)

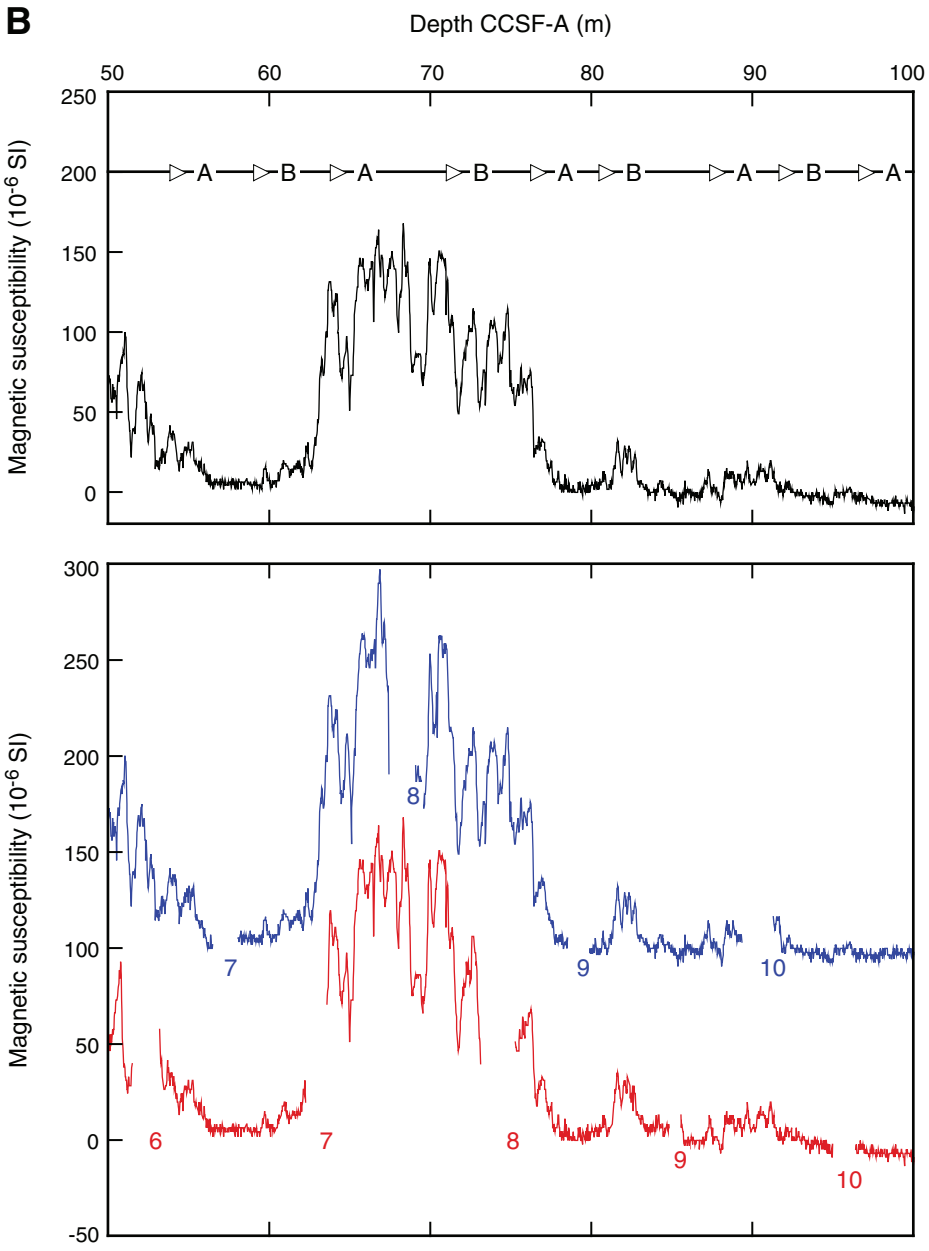

Figure F27 (continued). C. 100–150 CCSF-A. (Continued on next page.)

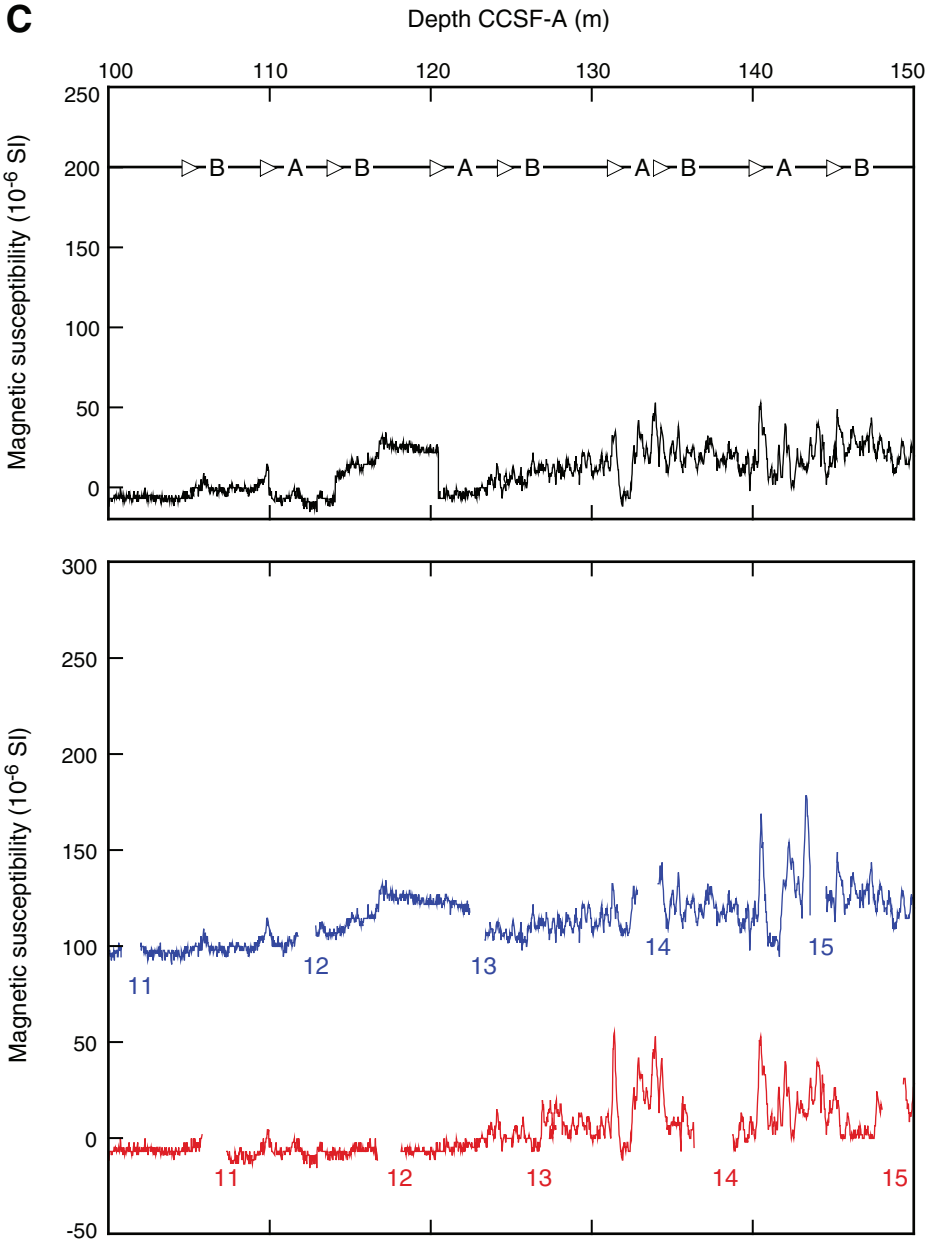

Figure F27 (continued). D. 150–200 CCSF-A. (Continued on next page.)

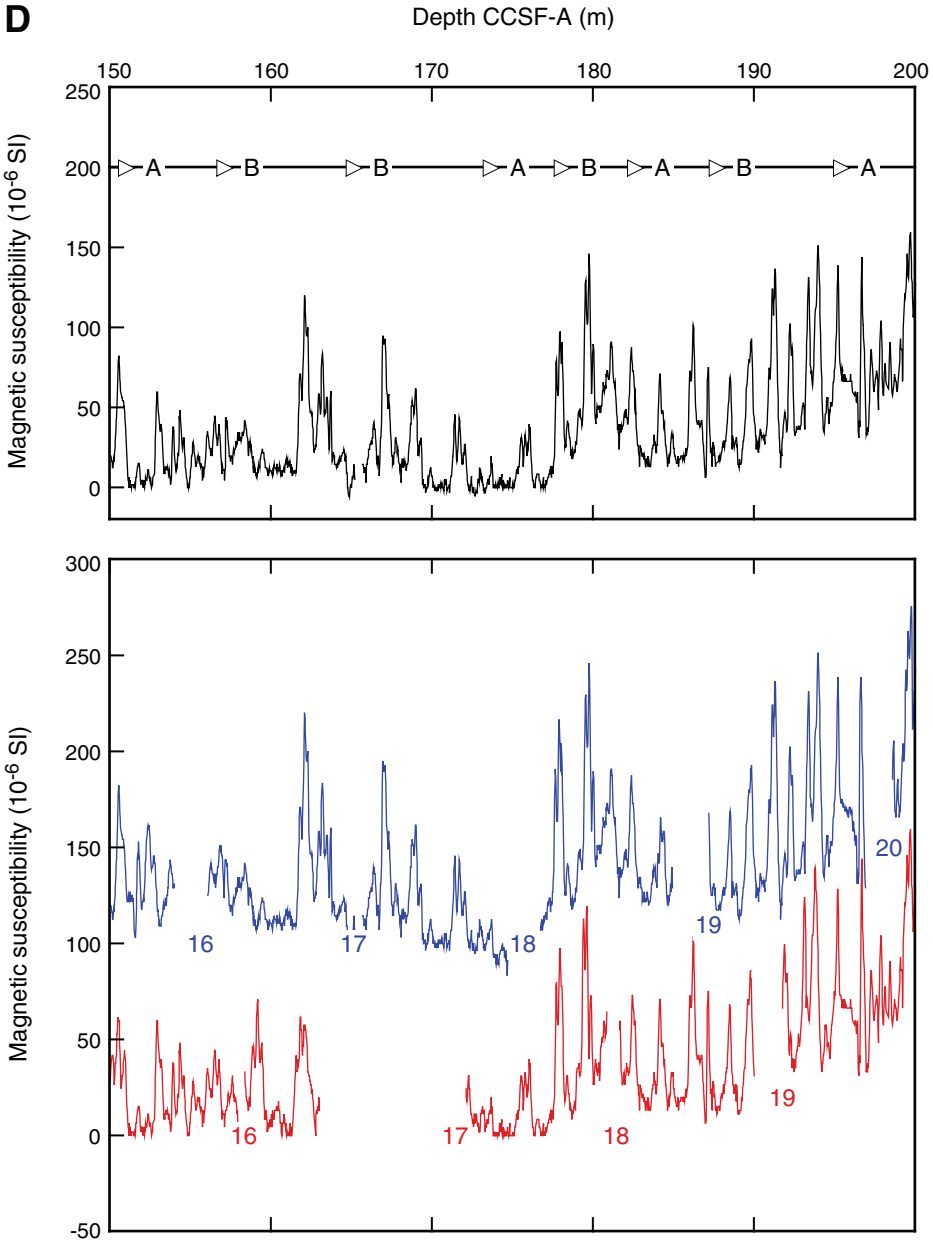

Figure F27 (continued). E. 200–250 CCSF-A. (Continued on next page.)

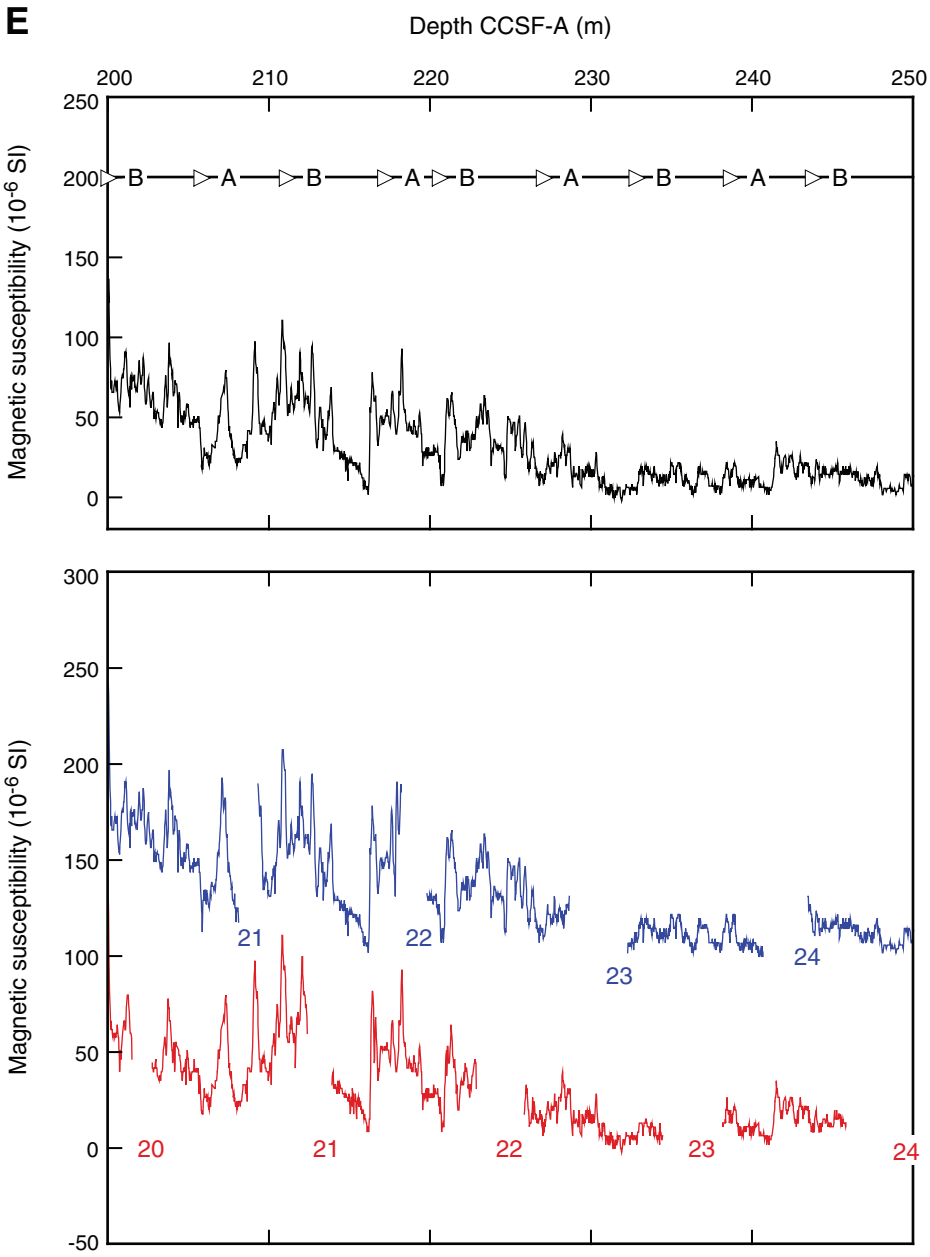

Figure F27 (continued). F. 250–300 CCSF-A. (Continued on next page.)

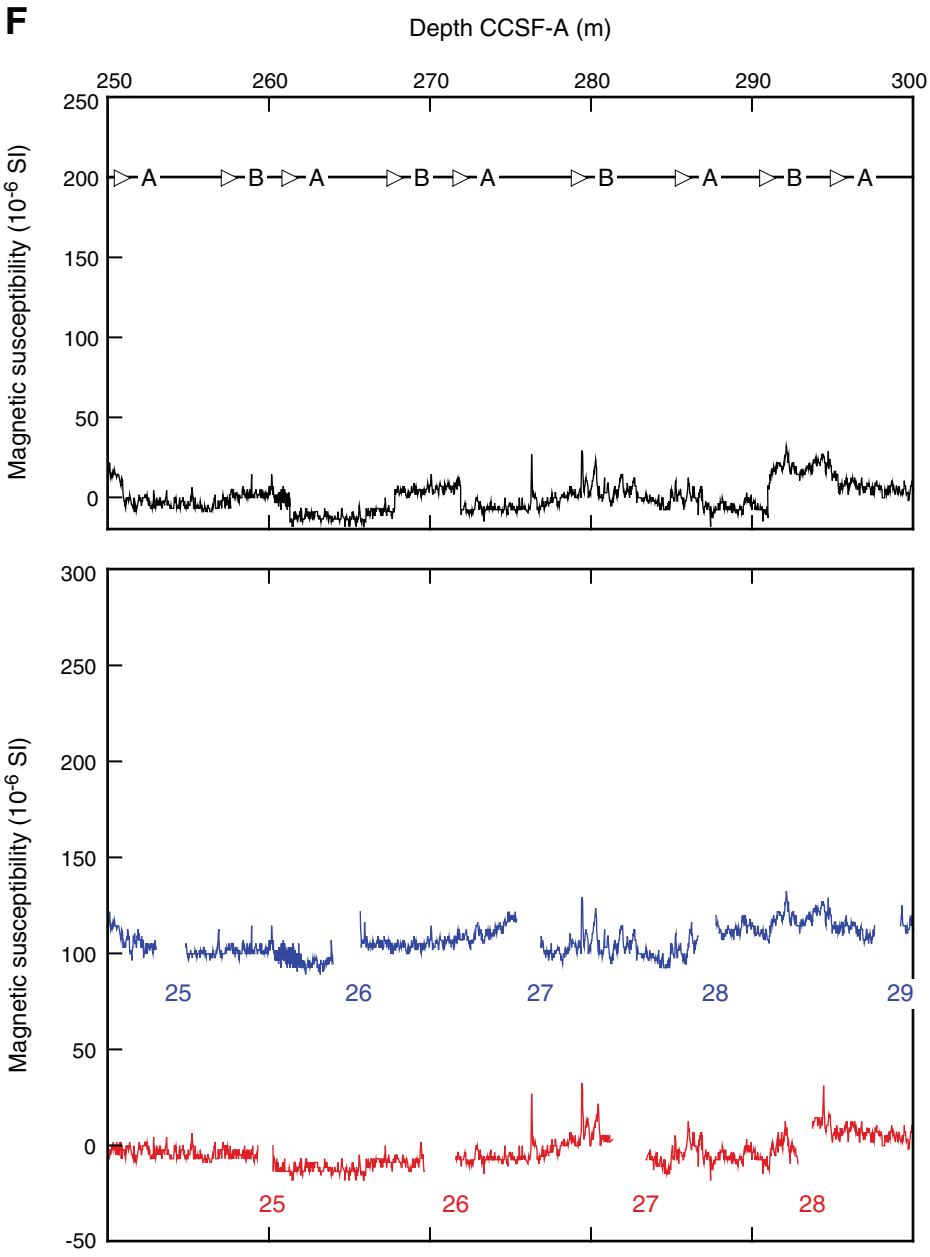

Figure F27 (continued). G. 300–350 CCSF-A. (Continued on next page.)

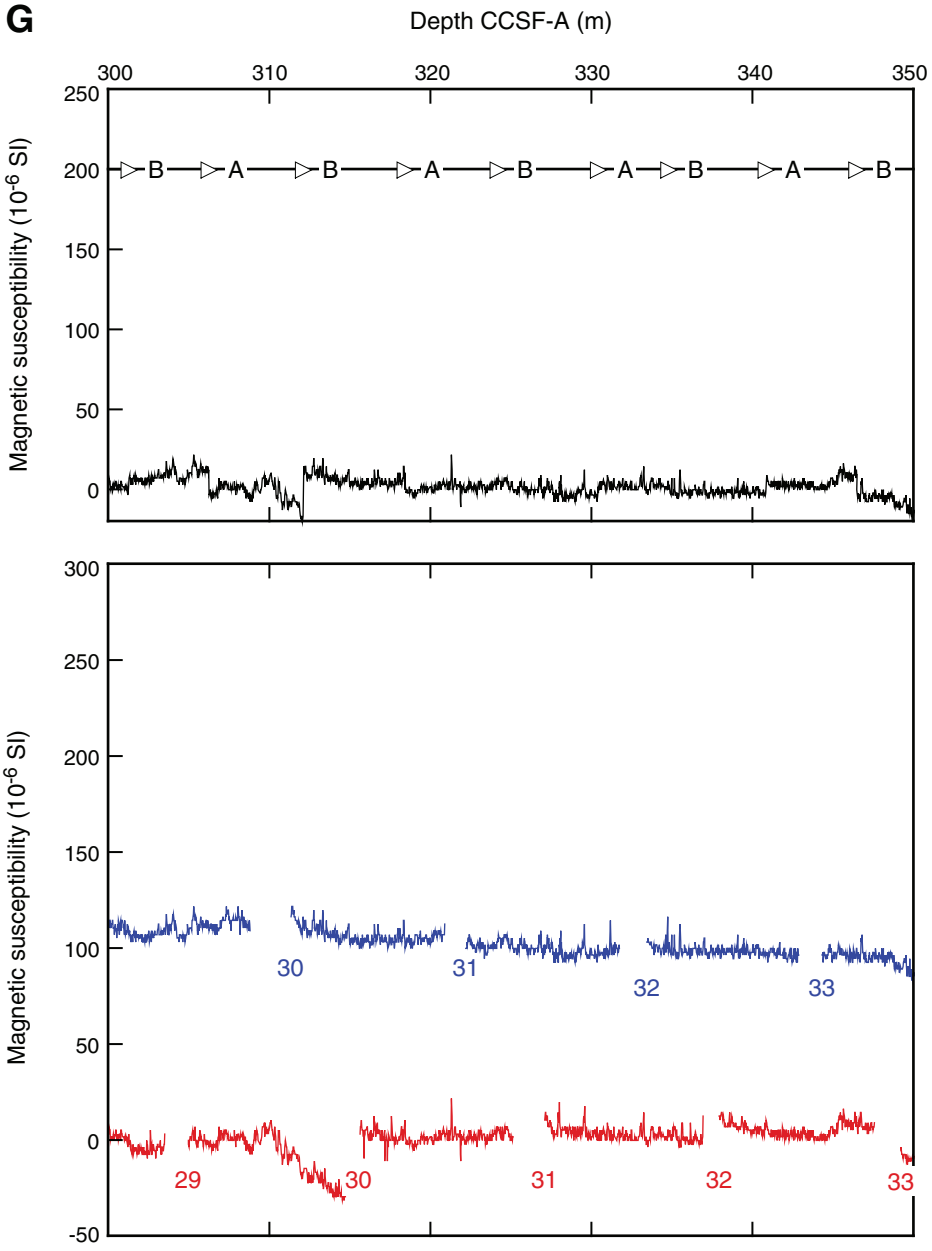

Figure F27 (continued). H. 350–400 CCSF-A.

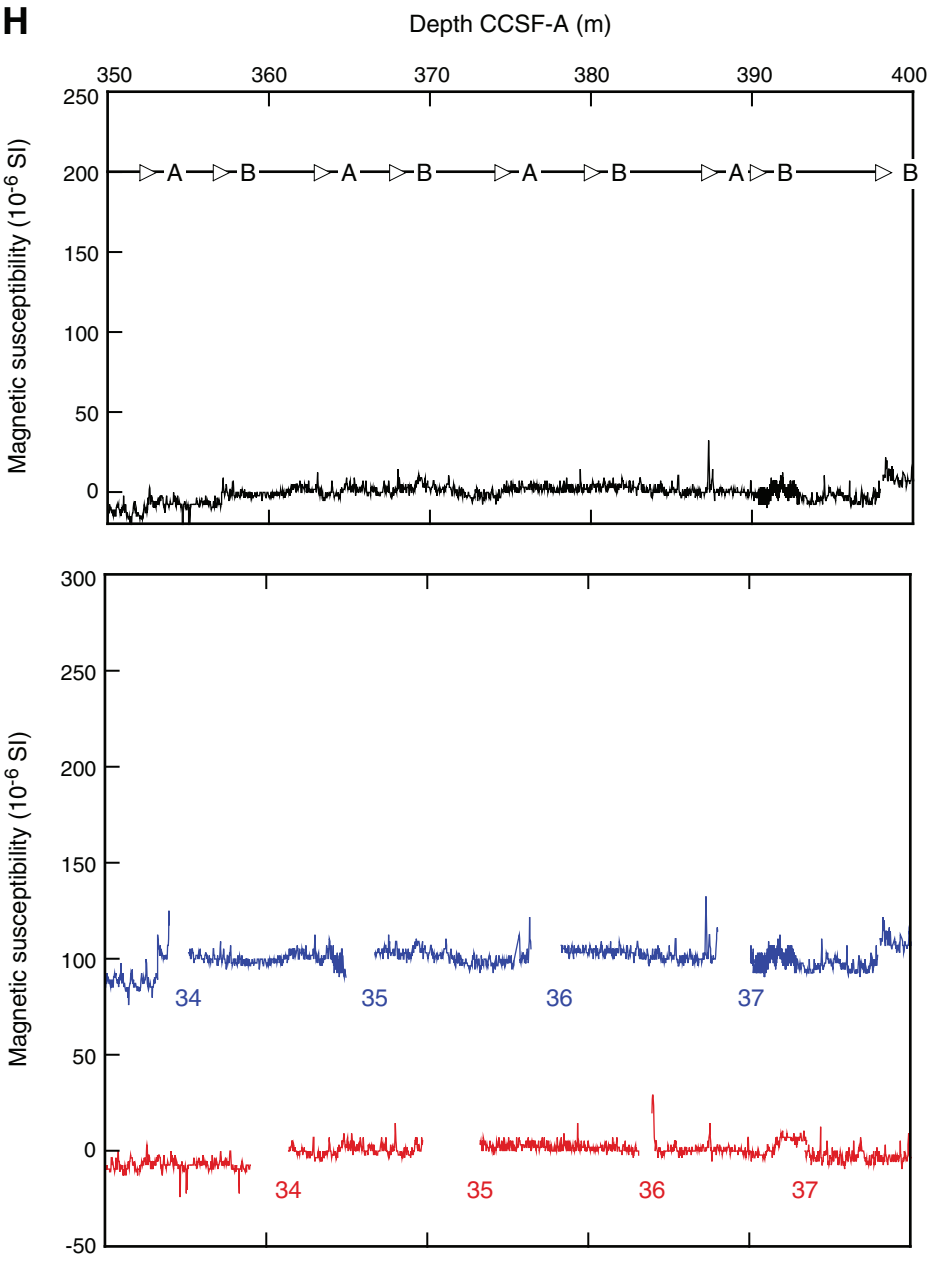

Figure F28. Gamma ray attenuation (GRA) density data, Site U1335. Top panel = spliced section with core breaks (triangles) and hole designations, bottom panel = Holes U1335A (red) and U1335B (blue), offset from each other by a constant (0.8 g/cm³). **A.** 0–50 CCSF-A. (**Continued on next seven pages.**)

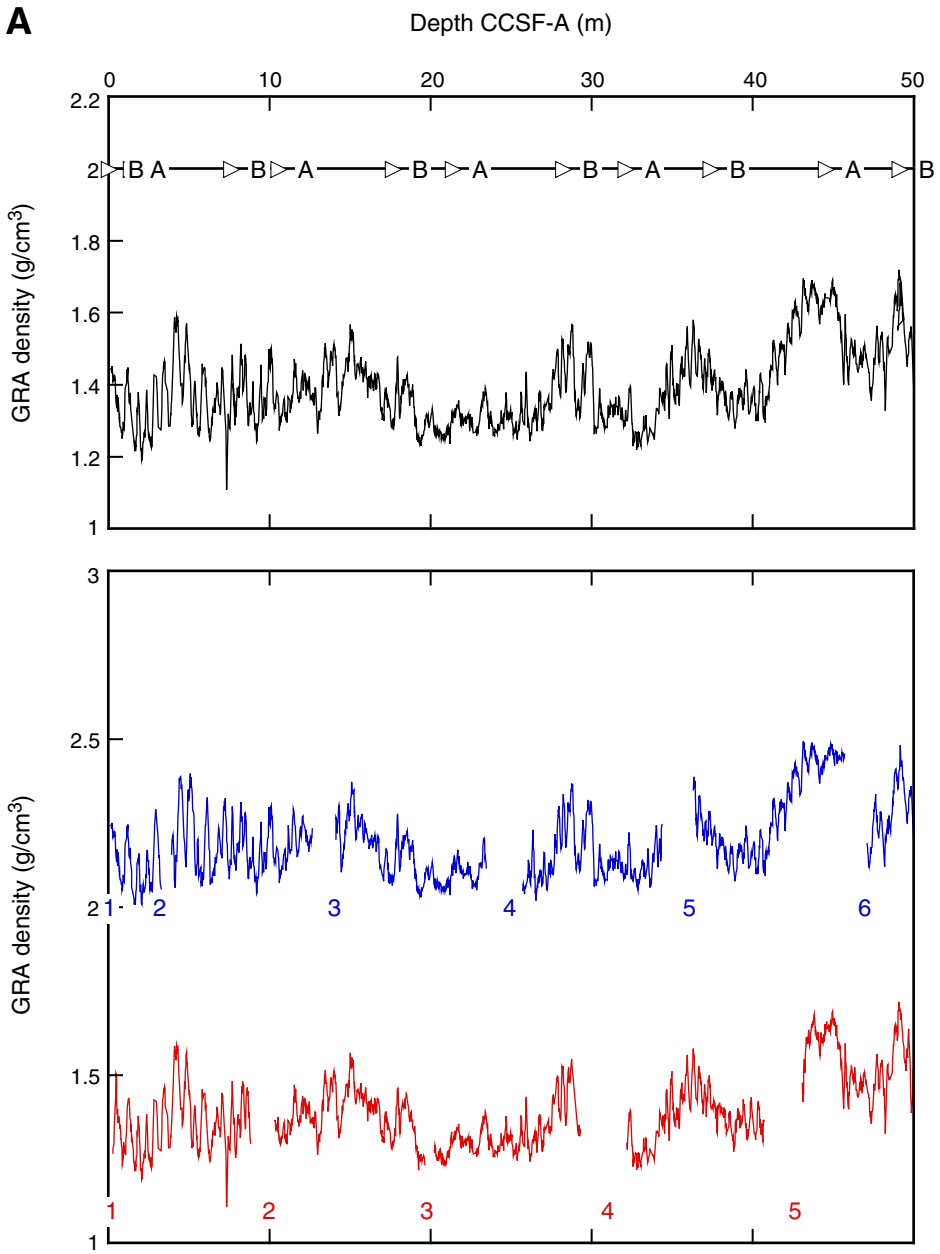

Figure F28 (continued). B. 50–100 CCSF-A. (Continued on next page.)

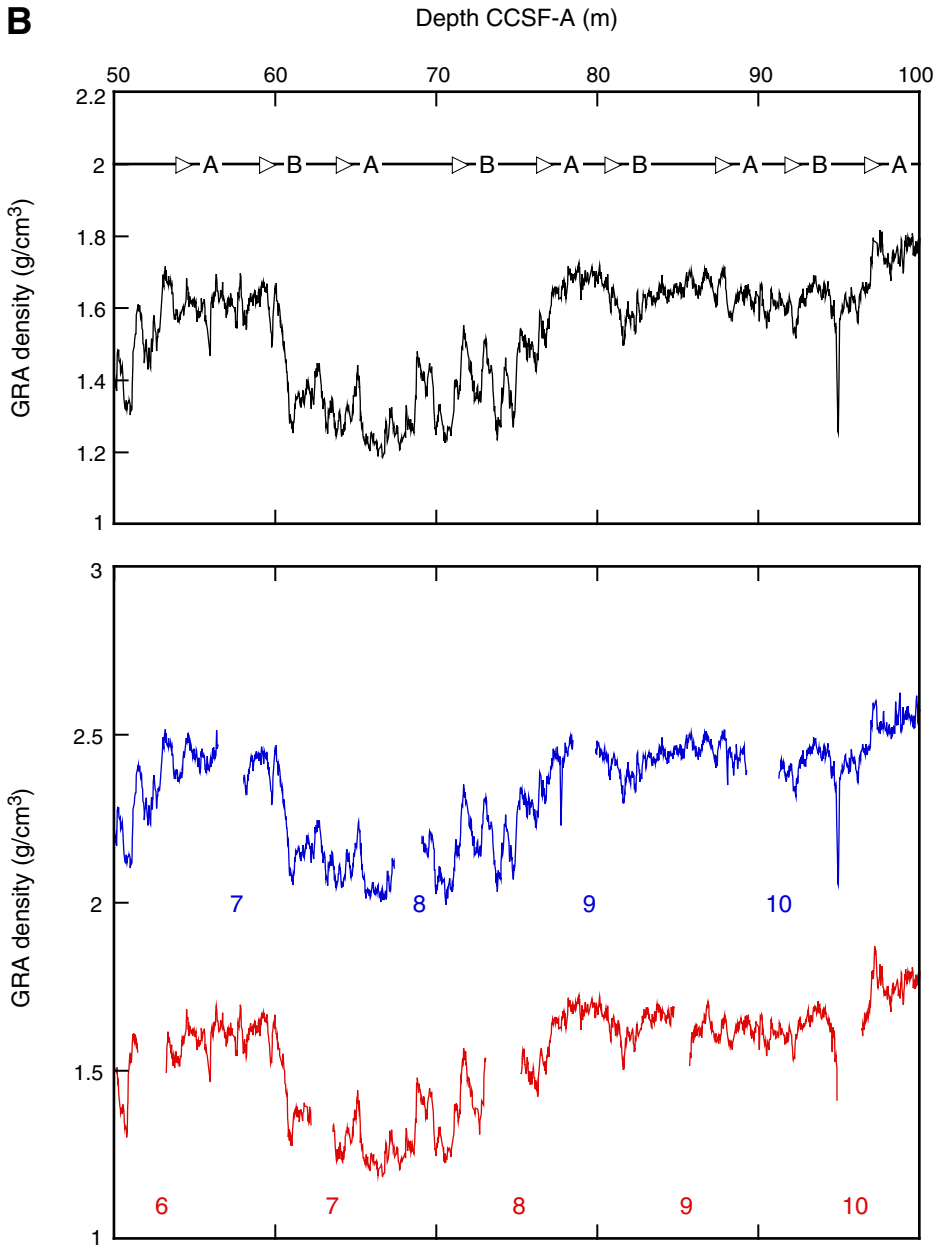

Figure F28 (continued). C. 100–150 CCSF-A. (Continued on next page.)

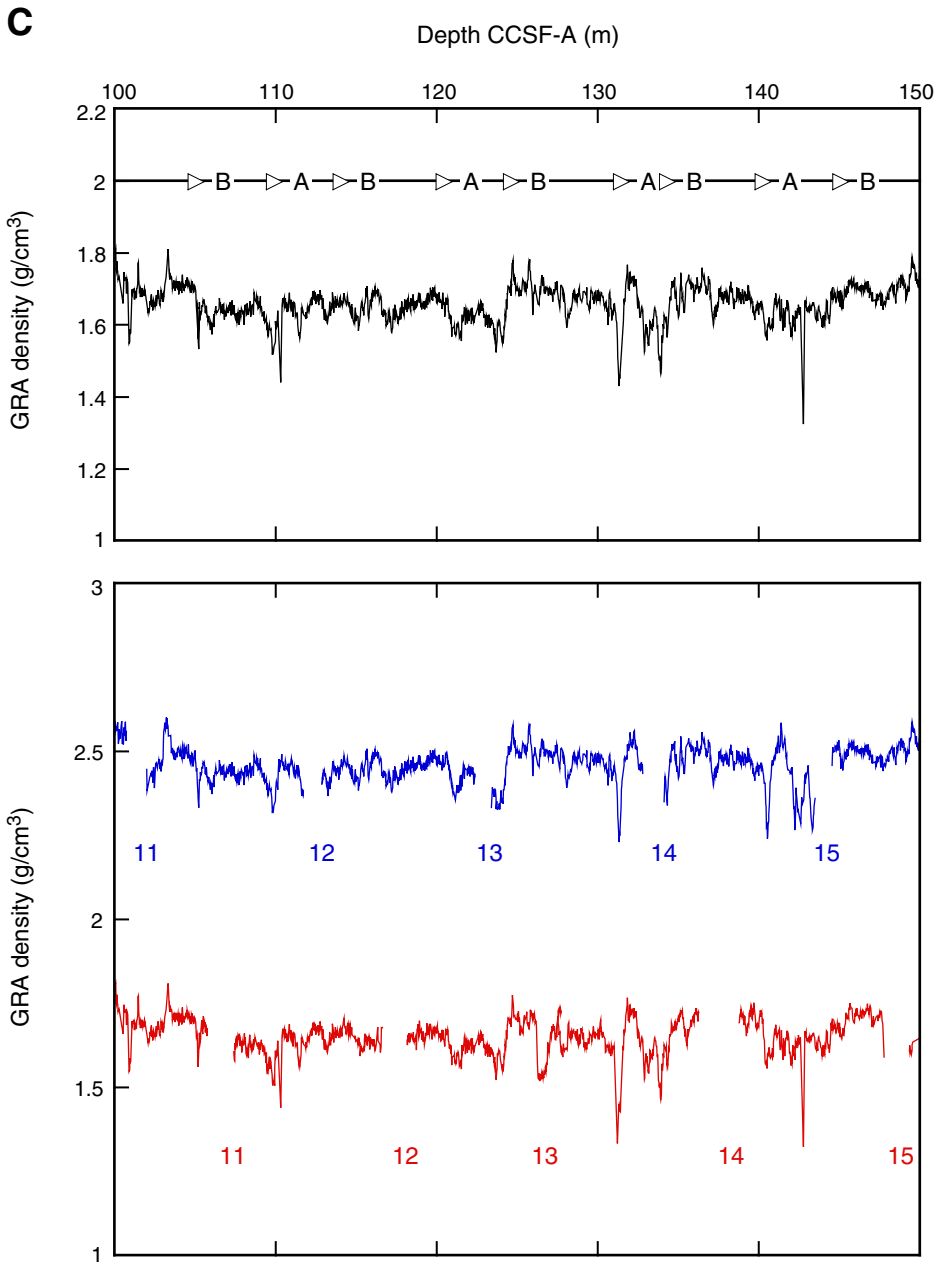

Figure F28 (continued). D. 150–200 CCSF-A. (Continued on next page.)

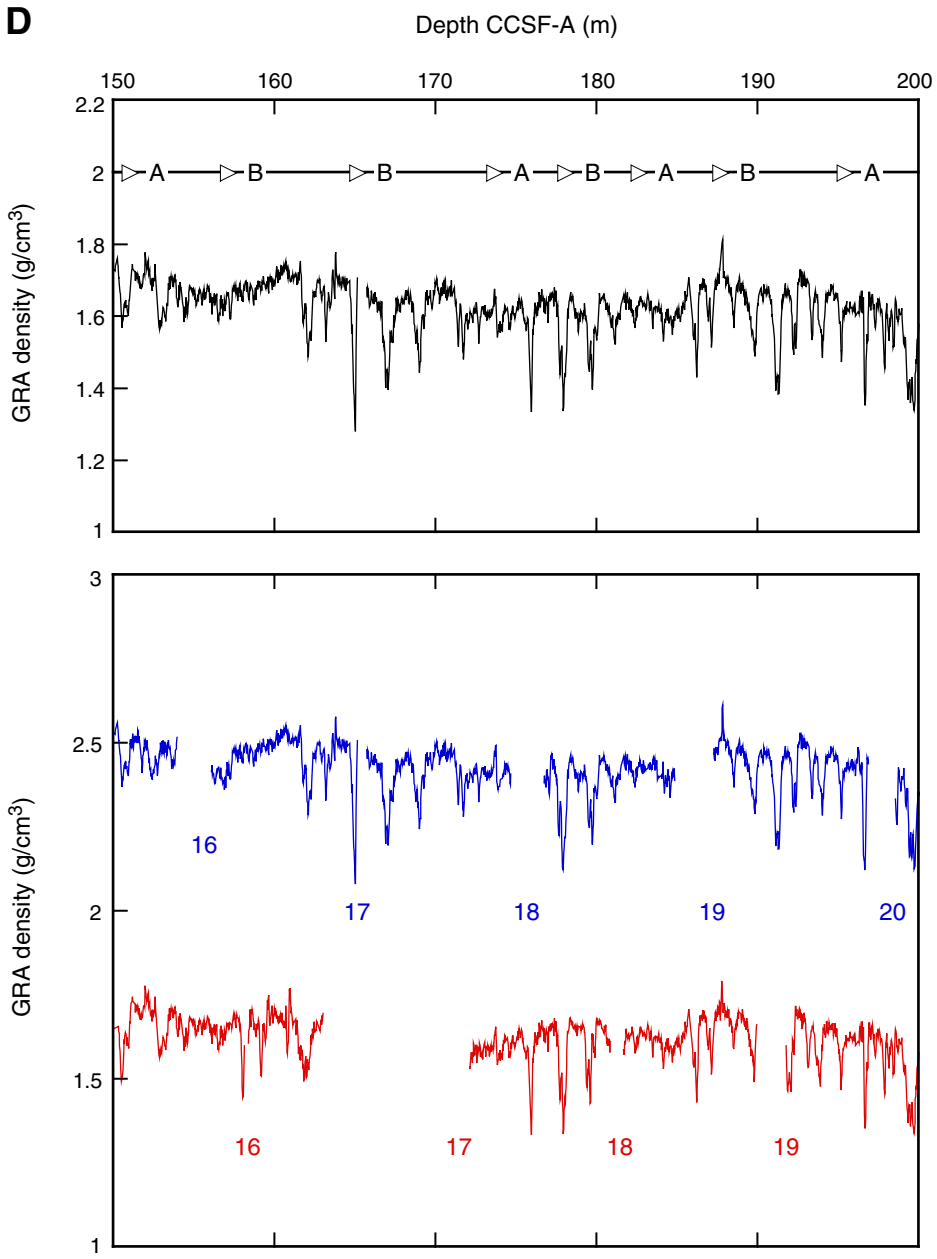

Figure F28 (continued). E. 200–250 CCSF-A. (Continued on next page.)

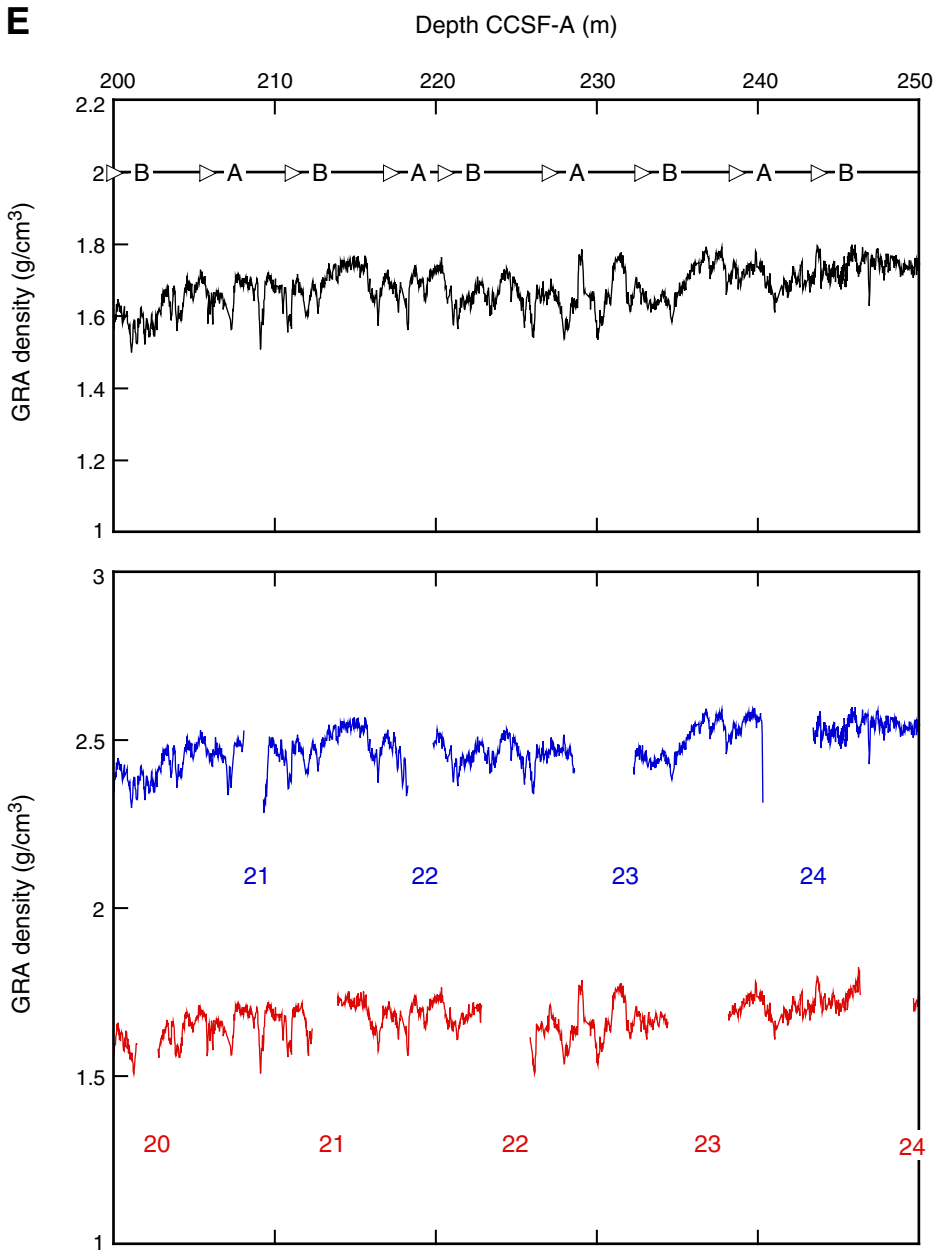

Figure F28 (continued). F. 250–300 CCSF-A. (Continued on next page.)

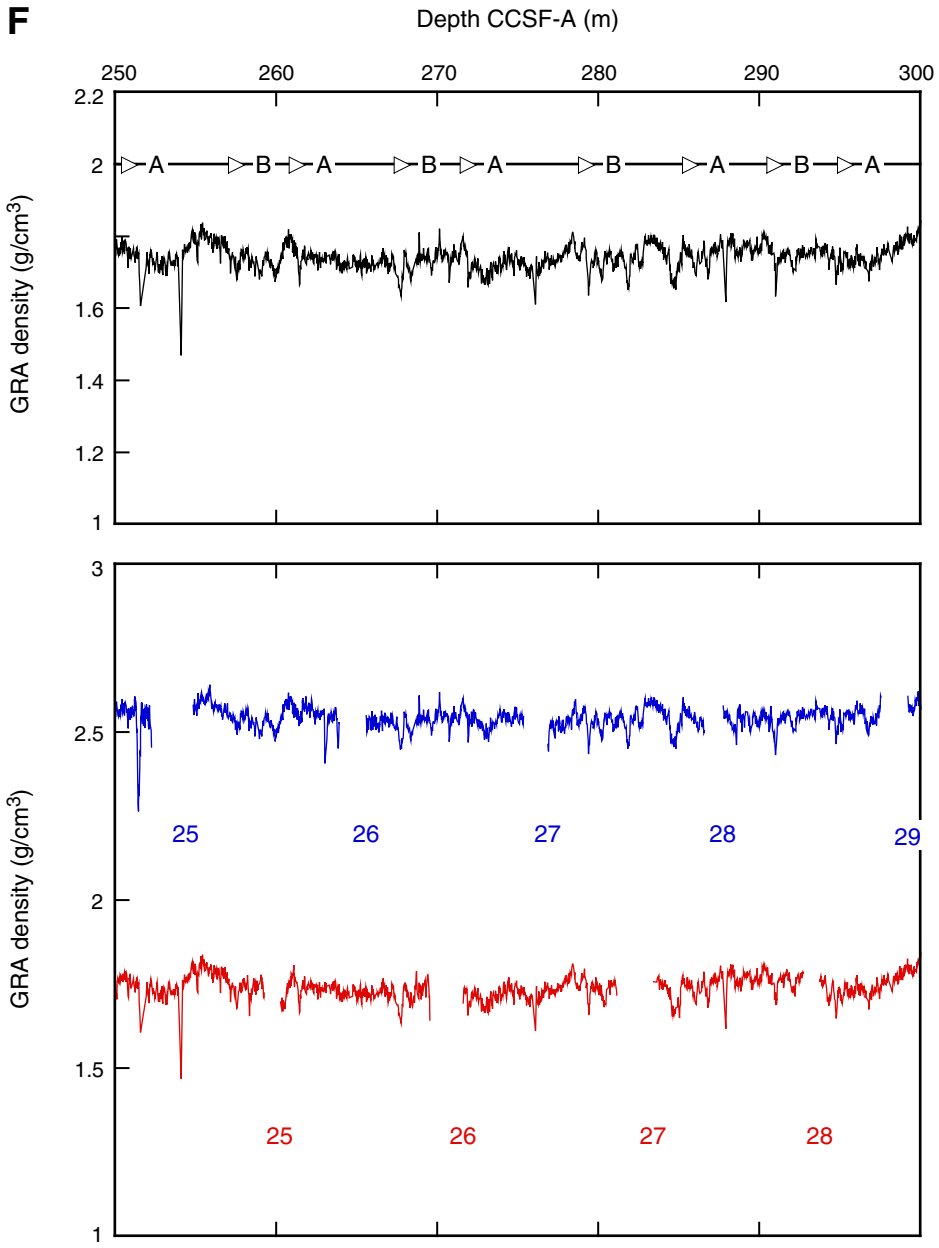

Figure F28 (continued). G. 300–350 CCSF-A. (Continued on next page.)

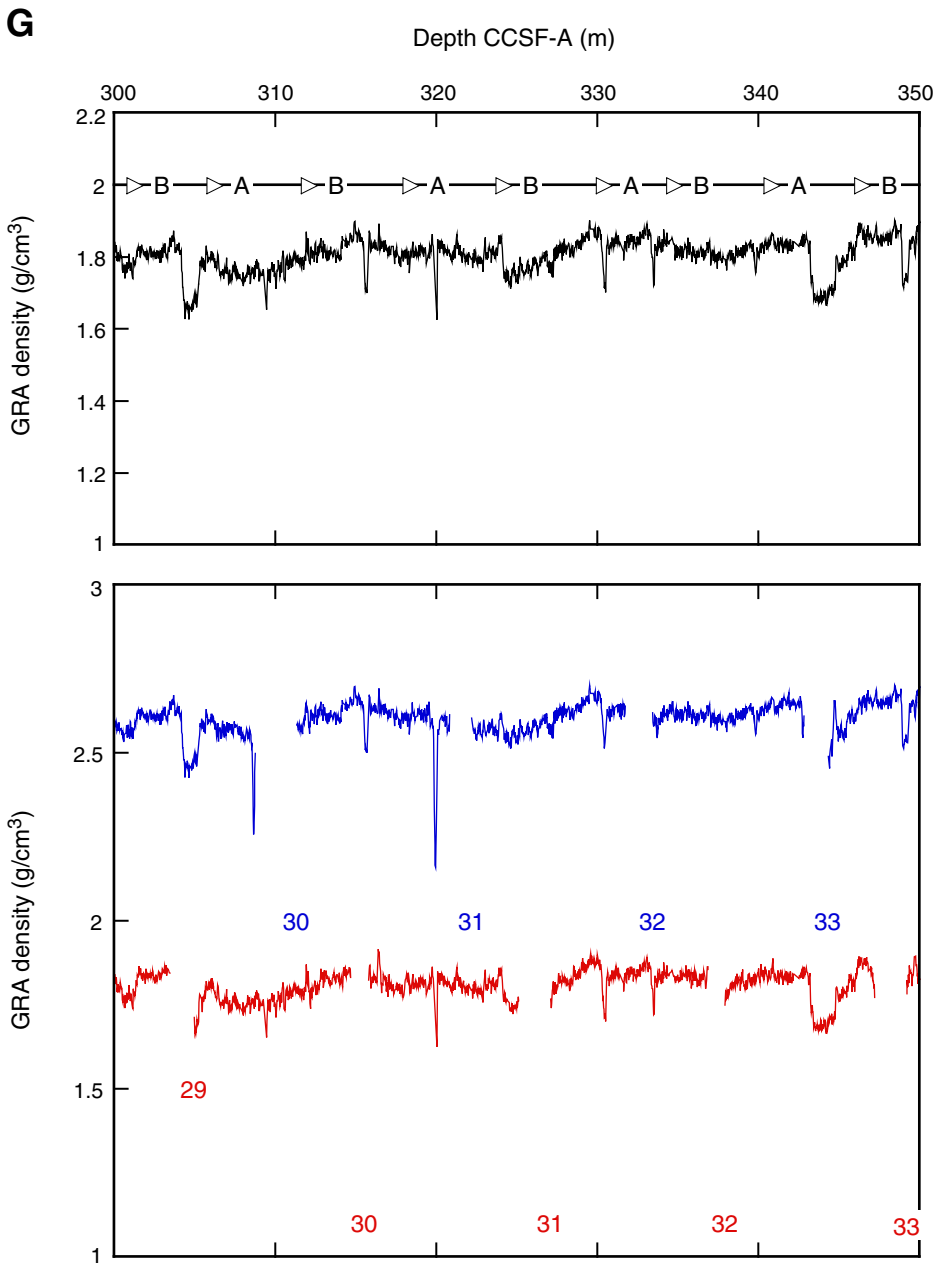

Figure F28 (continued). H. 350–400 CCSF-A.

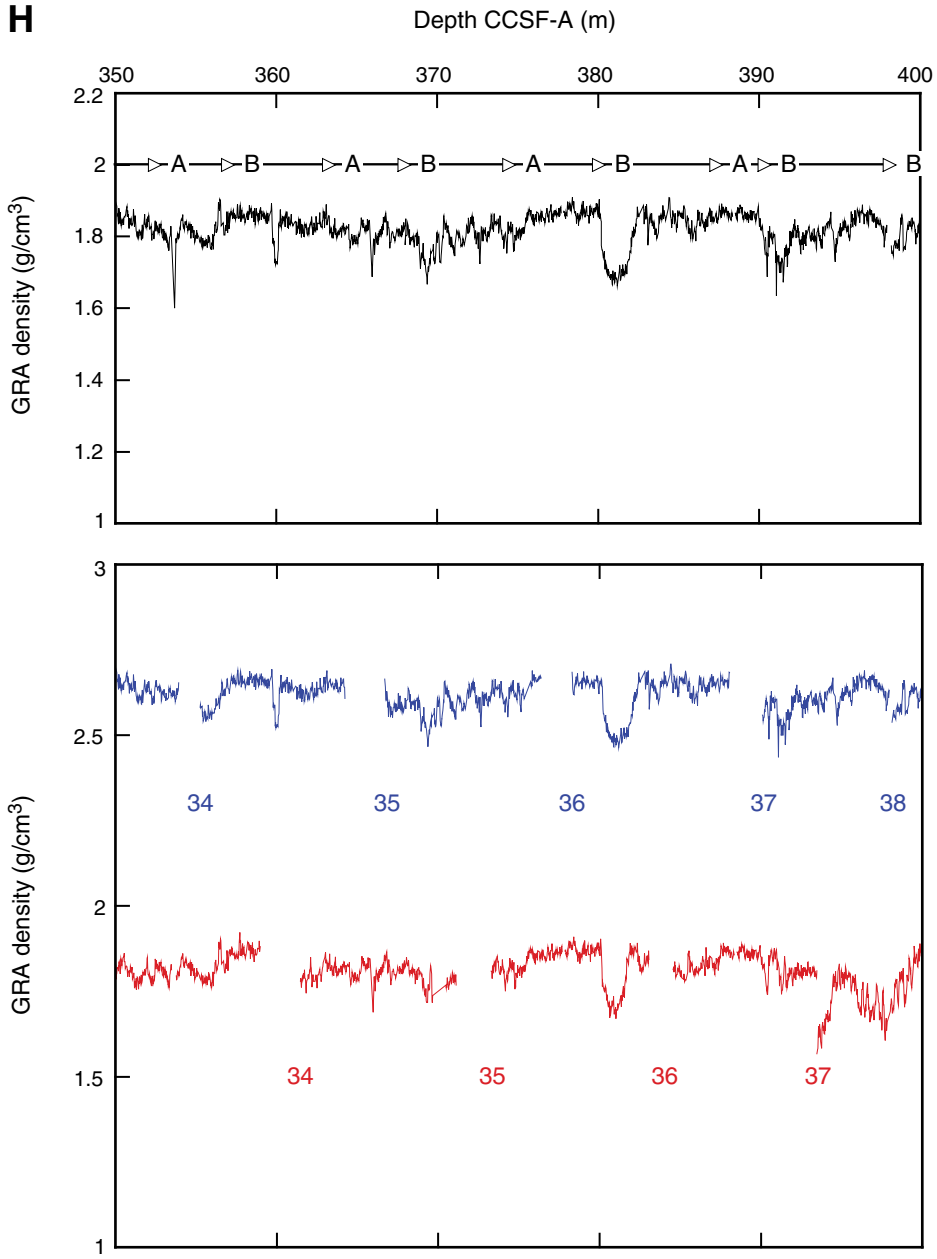

Figure F29. CSF depth vs. CCSF-A depth for tops of cores, Site U1335. Growth factor = slope of the regression line. On average, CCSF-A depth of spliced section is 16% greater than CSF depth.

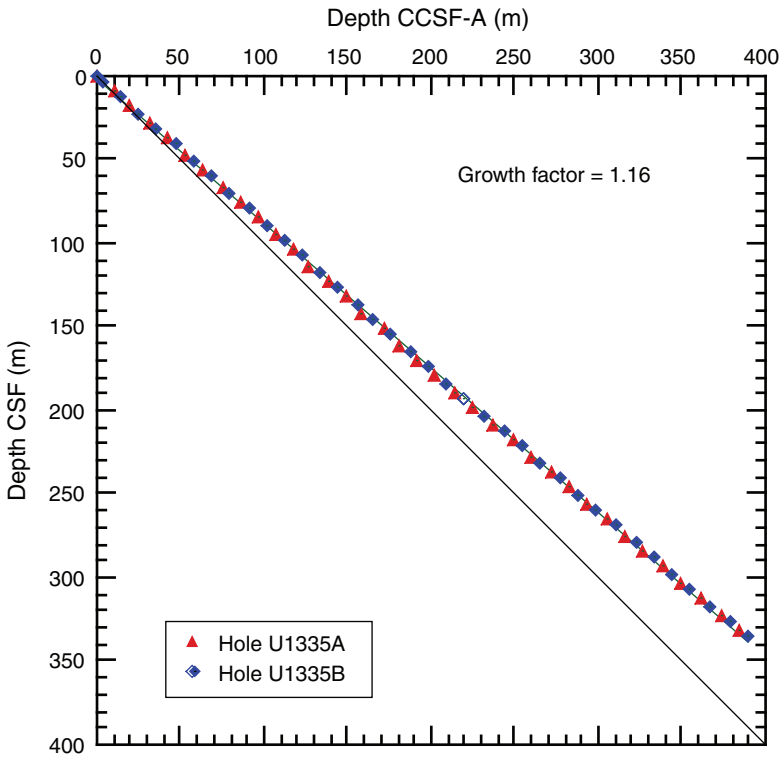

Figure F30. Heat flow calculation, Site U1335. **A.** Sediment temperatures, Hole U1335B. **B.** Thermal resistance based on laboratory thermal conductivity data, Hole U1335A. **C.** Bullard plot where heat flow is calculated from a linear fit of the temperature data. APCT-3 = advanced piston corer temperature tool.

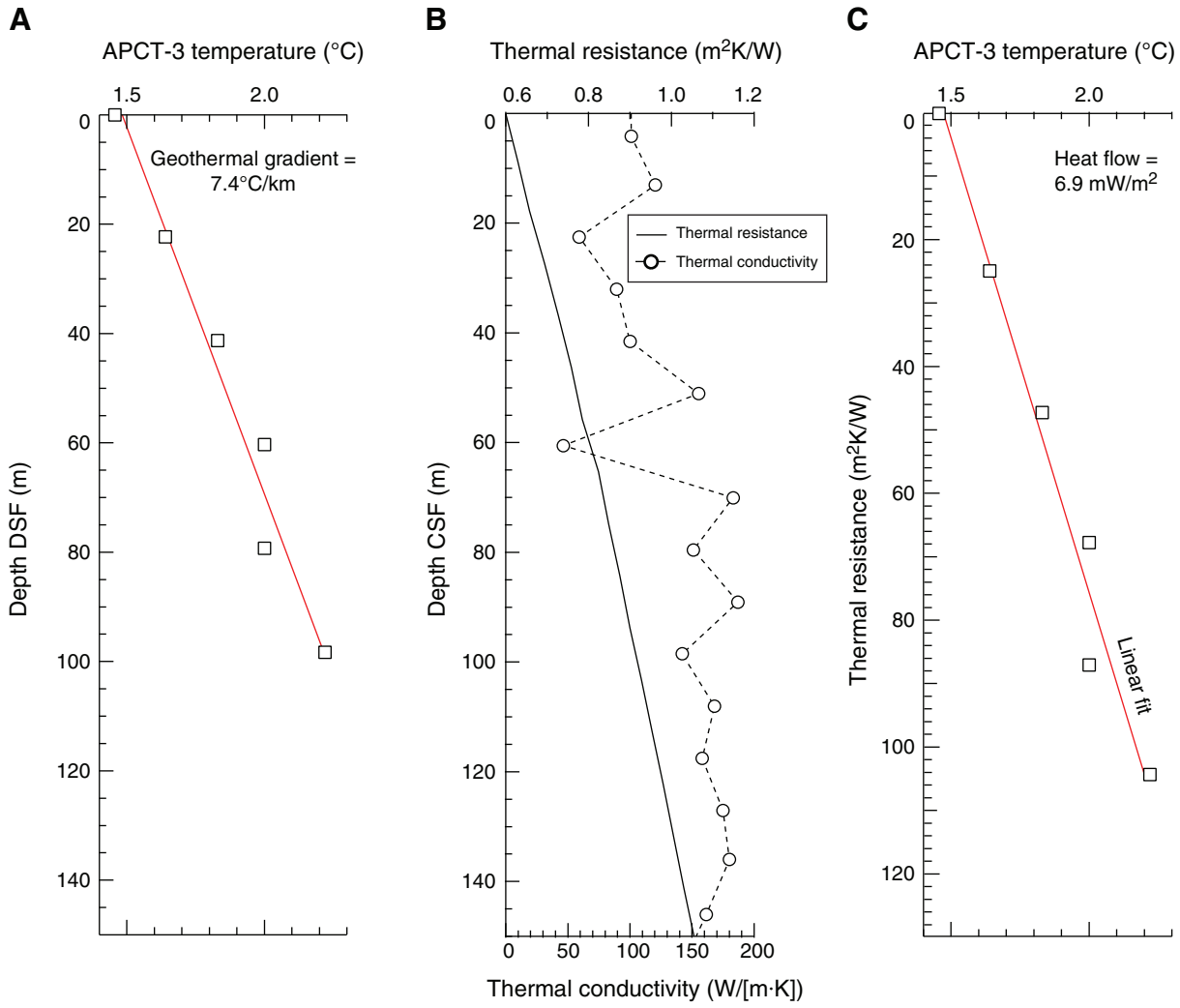

Table T1. Coring summary, Site U1335. (See table notes.) (Continued on next page.)

Site U1335
Time on site (h): 149.3 (1630 h, 15 April–2145 h, 21 April 2009)

Hole U1335A
Latitude: 5°18.734′N
Longitude: 126°16.995′W
Time on hole (h):72.9 (1630 h, 15 April–1725 h, 18 April 2009)
Seafloor (drill pipe measurement below rig floor, m DRF): 4339.0
Distance between rig floor and sea level (m): 11.5
Water depth (drill pipe measurement from sea level, mbsl): 4327.5
Total depth (drill pipe measurement from rig floor, m DRF): 4760.1
Total penetration (drilling depth below seafloor, m DSF): 421.1
Total length of cored section (m): 421.1
Total core recovered (m): 422.1
Core recovery (%): 101
Total number of cores: 45

Hole U1335B
Latitude: 5°18.736′N
Longitude: 126°17.009′W
Time on hole (h): 76.3 (1725 h, 18 April–2145 h, 21 April 2009)
Seafloor (drill pipe measurement below rig floor, m DRF): 4339.6
Distance between rig floor and sea level: 11.5 m
Water depth (drill pipe measurement from sea level, mbsl): 4328.1
Total depth (drill pipe measurement from rig floor, m DRF): 4757.1
Total penetration (drilling depth below seafloor, m DSF): 417.5
Total length of cored section (m): 417.5
Total core recovered (m): 428.7
Core recovery (%): 103
Total number of cores: 46

			Depth DSF (m)			Depth CSF (m)			
Core	Date (2009)	Local time (h)	Top of cored interval	Bottom of cored interval	Interval advanced (m)	Top of cored interval	Bottom of cored interval	Length of core recovered (m)	Recovery (%)
320-U1335A-									
1H	16 Apr	0420	0.0	8.9	8.9	0.00	8.90	8.86	100
2H	16 Apr	0530	8.9	18.4	9.5	8.90	18.90	10.00	105
3H	16 Apr	0620	18.4	27.9	9.5	18.40	28.20	9.78	103
4H	16 Apr	0725	27.9	37.4	9.5	27.90	37.85	9.95	105
5H	16 Apr	0820	37.4	46.9	9.5	37.40	46.50	9.10	96
6H	16 Apr	0915	46.9	56.4	9.5	46.90	56.50	9.60	101
7H	16 Apr	1010	56.4	65.9	9.5	56.40	66.30	9.89	104
8H	16 Apr	1110	65.9	75.4	9.5	65.90	75.91	10.01	105
9H	16 Apr	1215	75.4	84.9	9.5	75.40	85.10	9.67	102
10H	16 Apr	1320	84.9	94.4	9.5	84.90	95.00	10.09	106
11H	16 Apr	1420	94.4	103.9	9.5	94.40	104.58	9.84	107
12H	16 Apr	1600	103.9	113.4	9.5	103.90	113.90	9.99	105
13H	16 Apr	1655	113.4	122.9	9.5	113.40	123.44	10.04	106
14H	16 Apr	1755	122.9	132.4	9.5	122.90	133.04	10.14	107
15H	16 Apr	1855	132.4	141.9	9.5	132.40	142.13	9.73	102
16H	16 Apr	1955	141.9	151.4	9.5	141.90	151.53	9.63	101
17H	16 Apr	2135	151.4	160.9	9.5	151.40	161.24	9.84	104
18H	16 Apr	2225	160.9	170.4	9.5	160.90	169.80	8.87	94
19H	16 Apr	2335	170.4	179.9	9.5	170.40	180.50	10.06	106
20H	17 Apr	0055	179.9	189.4	9.5	179.90	189.92	10.02	105
21H	17 Apr	0210	189.4	198.9	9.5	189.40	199.00	9.60	101
22H	17 Apr	0335	198.9	208.4	9.5	198.90	208.70	9.80	103
23H	17 Apr	0435	208.4	217.9	9.5	208.40	218.20	9.76	103
24H	17 Apr	0605	217.9	227.4	9.5	217.90	227.90	9.99	105
25H	17 Apr	0710	227.4	236.9	9.5	227.40	236.90	9.50	100
26H	17 Apr	0835	236.9	246.4	9.5	236.90	246.83	9.93	105
27H	17 Apr	1005	246.4	255.9	9.5	246.40	256.24	9.84	104
28H	17 Apr	1110	255.9	265.4	9.5	255.90	266.01	10.11	106
29H	17 Apr	1210	265.4	274.9	9.5	265.40	275.61	10.21	107
30H	17 Apr	1310	274.9	284.4	9.5	274.90	284.82	9.92	104
31H	17 Apr	1415	284.4	293.9	9.5	284.40	294.55	10.15	107
32H	17 Apr	1520	293.9	303.4	9.5	293.90	303.80	9.85	104
33H	17 Apr	1625	303.4	312.9	9.5	303.40	313.53	10.13	107
34H	17 Apr	1750	312.9	322.4	9.5	312.90	323.05	10.15	107
35H	17 Apr	1940	322.4	331.9	9.5	322.40	332.64	10.24	108

Table T1 (continued).

Core	Date (2009)	Local time (h)	Depth DSF (m) Top of cored interval	Depth DSF (m) Bottom of cored interval	Interval advanced (m)	Depth CSF (m) Top of cored interval	Depth CSF (m) Bottom of cored interval	Length of core recovered (m)	Recovery (%)
36H	17 Apr	2125	331.9	341.4	9.5	331.90	341.85	9.95	105
37X	17 Apr	2245	341.4	351.1	9.7	341.40	350.10	8.66	90
38X	18 Apr	0000	351.1	360.7	9.6	351.10	359.20	8.06	84
39X	18 Apr	0105	360.7	370.2	9.5	360.70	369.41	8.71	92
40X	18 Apr	0245	370.2	379.7	9.5	370.20	376.65	6.45	68
41X	18 Apr	0350	379.7	389.2	9.5	379.70	387.66	7.96	84
42X	18 Apr	0525	389.2	398.8	9.6	389.20	396.33	7.13	74
43X	18 Apr	0700	398.8	408.4	9.6	398.80	408.23	9.43	98
44X	18 Apr	0915	408.4	418.1	9.7	408.40	417.81	9.41	97
45X	18 Apr	1505	418.1	421.1	3.0	418.10	420.13	2.03	68
				Advanced total:	421.1			422.08	100
				Total interval cored:	421.1				
320-U1335B-									
1H	18 Apr	2020	0.0	3.3	3.3	0.00	3.48	3.48	105
2H	18 Apr	2130	3.3	12.8	9.5	3.30	13.07	9.77	103
3H	18 Apr	2245	12.8	22.3	9.5	12.80	22.71	9.91	104
4H	18 Apr	2345	22.3	31.8	9.5	22.30	31.98	9.68	102
5H	19 Apr	0105	31.8	41.3	9.5	31.80	41.89	10.09	106
6H	19 Apr	0205	41.3	50.8	9.5	41.30	51.08	9.78	103
7H	19 Apr	0331	50.8	60.3	9.5	50.80	60.95	10.15	107
8H	19 Apr	0425	60.3	69.8	9.5	60.30	70.06	9.76	103
9H	19 Apr	0535	69.8	79.3	9.5	69.80	79.97	10.17	107
10H	19 Apr	0640	79.3	88.8	9.5	79.30	89.07	9.77	103
11H	19 Apr	0755	88.8	98.3	9.5	88.80	99.00	10.20	107
12H	19 Apr	0855	98.3	107.8	9.5	98.30	108.11	9.81	103
13H	19 Apr	0955	107.8	117.3	9.5	107.80	117.68	9.88	104
14H	19 Apr	1050	117.3	126.8	9.5	117.30	127.04	9.74	103
15H	19 Apr	1150	126.8	136.3	9.5	126.80	136.83	10.03	106
16H	19 Apr	1255	136.3	145.8	9.5	136.30	146.22	9.92	104
17H	19 Apr	1355	145.8	155.3	9.5	145.80	155.69	9.89	104
18H	19 Apr	1455	155.3	164.8	9.5	155.30	164.83	9.53	100
19H	19 Apr	1620	164.8	174.3	9.5	164.80	174.86	10.06	106
20H	19 Apr	1745	174.3	183.8	9.5	174.30	184.40	10.10	106
21H	19 Apr	1855	183.8	193.3	9.5	183.80	193.47	9.67	102
22H	19 Apr	1955	193.3	202.8	9.5	193.30	202.86	9.56	101
23H	19 Apr	2100	202.8	212.3	9.5	202.80	211.83	9.03	95
24H	19 Apr	2210	212.3	221.8	9.5	212.30	222.16	9.86	104
25H	19 Apr	2320	221.8	231.3	9.5	221.80	231.47	9.67	102
26H	20 Apr	0050	231.3	240.8	9.5	231.30	241.43	10.13	107
27H	20 Apr	0255	240.8	250.3	9.5	240.80	250.93	10.13	107
28H	20 Apr	0450	250.3	259.8	9.5	250.30	260.43	10.13	107
29H	20 Apr	0600	259.8	269.3	9.5	259.80	269.72	9.92	104
30H	20 Apr	0700	269.3	278.8	9.5	269.30	279.12	9.82	103
31H	20 Apr	0810	278.8	288.3	9.5	278.80	288.55	9.75	103
32H	20 Apr	0910	288.3	297.8	9.5	288.30	297.99	9.69	102
33H	20 Apr	1015	297.8	307.3	9.5	297.80	307.90	10.10	106
34H	20 Apr	1125	307.3	316.8	9.5	307.30	317.00	9.70	102
35H	20 Apr	1305	316.8	326.3	9.5	316.80	326.89	10.09	106
36H	20 Apr	1430	326.3	335.8	9.5	326.30	336.57	10.27	108
37H	20 Apr	1600	335.8	343.8	8.0	335.80	344.11	8.31	104
38H	20 Apr	1725	343.8	352.8	9.0	343.80	352.89	9.09	101
39H	20 Apr	1850	352.8	362.3	9.5	352.80	362.51	9.71	102
40H	20 Apr	2000	362.3	370.1	7.8	362.30	370.39	8.09	104
41H	20 Apr	2200	370.1	378.2	8.1	370.10	378.35	8.25	102
42X	21 Apr	0010	378.2	386.2	8.0	378.20	386.67	8.47	106
43X	21 Apr	0140	386.2	395.8	9.6	386.20	394.91	8.71	91
44X	21 Apr	0345	395.8	405.4	9.6	395.80	404.75	8.95	93
45X	21 Apr	0620	405.4	415.0	9.6	405.40	412.01	6.61	69
46X	21 Apr	1015	415.0	417.5	2.5	415.00	418.27	3.27	131
				Advanced total:	417.5			428.70	103
				Total interval cored:	417.5				

Notes: DRF = drilling depth below rig floor, DSF = drilling depth below seafloor, CSF = core depth below seafloor. H = APC core, X = XCB core. Local time = UTC – 10 h.

Table T2. Lithologic unit boundaries, Site U1335. (See table notes.)

Unit	Core, section, interval (cm)	Depth CSF (m)	Core, section, interval (cm)	Depth CSF (m)
	320-U1331A-		320-U1331B-	
I	7H-6, 44	64.34	8H-5, 75	67.05
II	45X-CC, 20*	420.13	46X-CC, 8	418.04
III	—	—	46X-CC, 46*	418.42

Notes: Interval/depth are given for basal boundary of each unit. * = unit extends through at least given interval and depth, but boundary was not cored. — = boundary not cored.

Table T3. Positions of sharp contacts and thickness and textures of overlying nannofossil foraminifer ooze bed, Site U1335. (**See table notes.**)

Unit	Contact position Core, section, interval (cm)	Depth CSF (m)	Thickness (cm)	Texture	Contact position Core, section, interval (cm)	Depth CSF (m)	Thickness (cm)	Texture
	320-U1335A-				320-U1335B-			
I	2H-1, 126	10.16	2	1, 2	2H-6, 55	11.35	5	1, 2
II	9H-2, 103	77.96	2	1, 2	8H-6, 133	69.13	3	1, 2
	9H-6, 55	83.47	2	1, 2	9H-6, 112	78.42	7	1, 2
	10H-4, 57	89.97	21	1, 2	10H-2, 93	81.73	4	1, 2
	11H-3, 50	97.90	2	1, 2	11H-4, 38	93.68	4	1, 2†
	12H-6, 135	112.75	66	1, 2, 3, 4	12H-3, 75	102.05	2	1, 2
	13H-6, 132	122.27	5	1, 2	13H-2, 127	110.57	7	1, 2
	14H-3, 29	126.19	9	1, 2	15H-1, 94	127.74	11	1, 2
	15H-4, 104	137.44	4	1, 2	15H-5, 145	134.25	5	1, 2
	16H-2, 113	144.54	22	1, 2, 5	16H-7, 32	145.62	18	1, 2
	17H-2, 92	153.82	3	1, 2	17H-2, 13	147.43	3	1, 2
	17H-6, 84	159.75	1	1, 2	17H-4, 136	151.66	2	1, 2
	18H-4, 117	166.57	14	1, 2, 6	17H-6, 122	154.52	4	1, 2
	19H-4, 39	175.29	15	1, 2, 6	17H-CC, 10	155.54	6	1, 2
	20H-3, 28	183.18	12	1, 2	19H-2, 37	166.67	2	1, 2
	21H-2, 129	192.19	67	1, 2, 3, 4, 5	19H-6, 39	172.69	15	1, 2
	21H-5, 135	196.75	40	1, 2, 4	20H-6, 5	181.85	15	1, 2
	22H-5, 107	205.97	17	1, 2	21H-5, 144	191.24	49	1, 2, 3
	23H-1, 130	209.70	30	1, 2	22H-1, 125	194.55	35	1, 2
	23H-3, 141	212.81	41	2, 4*	22H-4, 93	198.73	10	1, 2
	24H-4, 106	223.46	3	1, 2	22H-6, 35	201.15	6	1, 2
	24H-5, 102	224.92	2	1, 2	23H-5, 40	209.02	28	1, 2
	25H-6, 16	235.06	22	1, 2	24H-1, 51	212.81	4	1, 2
	25H-6, 63	235.53	6	1, 2	24H-3, 53	215.83	7	1, 2
	26H-1, 38	237.28	2	1, 2	25H-2, 92	224.22	7	1, 2
	27H-2, 16	248.06	53	1, 2, 4	25H-4, 12	226.42	4	1, 2
	27H-4, 131	252.21	4	1, 2	25H-6, 126	230.56	3	1, 2
	27H-4, 144	252.34	2	1, 2	26H-2, 85	233.65	35	1, 2
	27H-6, 24	254.14	10	1, 2	26H-5, 42	237.72	6	1, 2
	29H-1, 35	265.75	35	1	27H-2, 107	243.37	3	1, 2
	29H-3, 102	269.42	3	1	27H-5, 76	247.56	10	1, 2
	29H-4, 115	271.05	3	1	27H-6, 68	248.98	52	1, 2
	29H-5, 119	272.59	3	1	28H-1, 120	251.5	4	1, 2
	30H-1, 22	275.12	8	1	28H-1, 135	251.65	1	1, 2
	30H-2, 147	277.87	4	1	28H-3, 42	253.72	20	1, 2
	30H-6, 8	282.48	1	1	29H-1, 51	260.31	1	1, 2
	30H-6, 113	283.53	4	1†	29H-5, 13	265.93	113	1, 2
	31H-3, 49	287.89	22	1	29H-CC, 12	269.55	1	1, 2
	31H-5, 50	290.90	22	1	30H-1, 78	270.08	1	1, 2
	31H-5, 86	291.26	1	1	30H-3, 150	273.8	30	1, 2
	32H-5, 91	300.81	162	1, 2	31H-2, 49	280.79	2	1, 2
	33H-3, 3	306.43	2	1	31H-6, 97	287.27	43	1, 2
	35H-6, 81	330.71	3	1	33H-1, 40	298.2	40	1, 2
	36H-3, 63	335.53	3	1	33H-4, 54	302.4	44	1, 2
	36H-5, 56	338.46	12	1, 2	34H-4, 54	312.34	32	1, 2
	37X-6, 44	349.34	18	1, 6	34H-5, 115	314.45	2	1, 2
	38X-1, 77	351.87	3	1, 2	35H-1, 22	317.02	0	1, 2
	39X-1, 95	361.65	15	1, 2, 6	36H-3, 71	330.11	176	1, 2
					38H-1, 90	344.7	4	1, 2
					39H-4, 26	357.56	18	1, 2
					39H-6, 51	360.81	6	1, 2

Notes: Textures: 1 = sharp basal boundary, 2 = normal grading, 3 = millimeter-scale angular fragments of basalt at base (rip-up clast?), 4 = decreasing foraminifer content observed upward, 5 = millimeter-scale pyritized foraminifers at base, 6 = laminations in upper-middle part of bed. * = thickness may be >41 cm, as the base of coarse layer is within interstitial water sampling interval, † = inclined basal boundary.

Table T4. Calcareous nannofossil datums, Site U1335. (See table notes.)

Core, section, interval (cm)		Marker species	Age (Ma)	Depth CSF (m)			
Top	Bottom			Top	Bottom	Midpoint	±
320-U1335A-	320-U1335A-						
1H-1, 40	1H-3, 100	T *Pseudoemiliania lacunosa*	0.44	0.40	4.00	2.20	1.80
1H-5, 90	1H-CC	T *Calcidiscus macintyrei*	1.61	6.90	8.81	7.86	0.96
		Pliocene/Pleistocene boundary					
1H-5, 90	1H-CC	T *Discoaster brouweri*	1.93	6.90	8.81	7.86	0.96
2H-1, 30	2H-3, 123	T *Discoaster pentaradiatus*	2.39	9.20	13.13	11.17	1.97
2H-1, 30	2H-3, 123	T *Discoaster surculus*	2.49	9.20	13.13	11.17	1.97
2H-3, 123	2H-5, 107	T *Discoaster tamalis*	2.80	13.13	15.97	14.55	1.42
2H-CC	3H-2, 80	T *Sphenolithus* spp.	3.54	18.85	20.70	19.78	0.92
2H-CC	3H-2, 80	T *Reticulofenestra pseudoumbilicus*	3.70	18.85	20.70	19.78	0.92
3H-5, 18	3H-6, 88	T *Ceratolithus acutus*	5.04	24.58	26.78	25.68	1.10
3H-5, 18	3H-6, 88	B *Ceratolithus rugosus*	5.05	24.58	26.78	25.68	1.10
3H-CC	4H-1, 66	T *Triquetrorhabdulus rugosus*	5.28	28.13	29.22	28.68	0.55
		Miocene/Pliocene boundary					
3H-CC	4H-1, 66	B *Ceratolithus acutus*	5.35	28.13	29.22	28.68	0.55
4H-1, 66	4H-2, 66	T *Discoaster quinqueramus*	5.58	29.22	30.37	29.80	0.58
4H-5, 37	4H-6, 66	Tc *Nicklithus amplificus*	5.98	34.27	36.06	35.17	0.89
5H-3, 10	5H-5, 50	B *Amaurolithus* spp.	7.36	40.50	43.90	42.20	1.70
5H-CC	6H-1, 60	B *Discoaster berggrenii*	8.29	46.45	47.50	46.45	0.52
7H-2, 10	7H-3, 65	T *Discoaster hamatus*	9.69	58.00	60.05	59.03	1.02
7H-2, 10	7H-3, 65	T *Catinaster coalitus*	9.69	58.00	60.05	59.03	1.02
7H-4, 82	7H-6, 79	B *Discoaster hamatus*	10.55	61.72	64.69	63.21	1.49
7H-4, 82	7H-6, 79	T *Coccolithus miopelagicus*	10.60	61.72	64.69	63.21	1.49
7H-4, 82	7H-6, 79	B *Catinaster coalitus*	10.89	61.72	64.69	63.21	1.49
8H-4, 90	8H-6, 90	Tc *Discoaster kugleri*	11.58	71.30	74.30	72.80	1.50
9H-1, 70	9H-3, 70	Bc *Discoaster kugleri*	11.86	76.10	79.10	77.60	1.50
9H-7, 70	9H-CC	T *Coronocyclus nitescens*	12.12	84.70	85.02	84.86	0.16
9H-CC	10H-2, 100	T *Calcidiscus premacintyrei*	12.45	85.02	87.40	86.21	1.19
12H-2, 90	12H-3, PAL	Tc *Cyclicargolithus floridanus*	13.33	106.30	108.39	107.35	1.05
12H-4, 90	12H-6, 90	T *Sphenolithus heteromorphus*	13.53	109.30	112.30	110.80	1.50
16H-CC	17H-2, 70	B *Discoaster petaliformis*	15.70	151.48	153.60	152.54	1.00
17H-6, 120	17H-CC	Tc *Discoaster deflandrei*	15.66	161.10	161.19	160.65	0.55
20H-2, 70	20H-4, 70	Bc *Sphenolithus heteromorphus*	17.71	182.10	185.10	183.60	1.50
21H-2, 80	21H-4, 80	Tc *Sphenolithus belemnos*	17.95	191.70	194.70	193.20	1.50
21H-4, 80	21H-6, 80	T *Triquetrorhabdulus carinatus*	18.28	194.70	197.70	196.20	1.50
22H-CC	23H-2, 90	B *Sphenolithus belemnos*	19.03	208.65	210.80	209.73	1.08
34H-3, 149	34H-CC	Tc *Triquetrorhabdulus carinatus*	22.09	316.00	323.00	319.50	3.50
36H-CC	37X-2, 90	B *Sphenolithus disbelemnos*	22.8	341.80	343.80	342.80	1.00
		Oligocene/Miocene boundary					
37X-6, 50	37X-CC	T *Sphenolithus delphix*	23.1	349.40	350.00	349.70	0.30
37X-CC	38X-2, 90	B *Sphenolithus delphix*	23.2	350.00	353.50	351.75	1.75
43X-2, 81	43X-4, 37	T *Sphenolithus ciperoensis*	24.4	401.11	403.67	402.39	1.28
42X-CC	43X-2, 81	X *T. longus/T. carinatus*	24.7	396.30	401.10	398.70	2.40
42X-2, 74	42X-4, 114	Tc *Cyclicargolithus abisectus*	24.7	391.44	394.84	393.14	1.70

Notes: PAL = paleontology sample. T = top, B = bottom, Tc = top common, Bc = bottom common, X = abundance crossover.

Table T5. Radiolarian datums, Site U1335. (See table note.) (Continued on next page.)

Geologic age	Zone	Marker species	Age (Ma)	Core, section, interval (cm)		Depth CSF (m)				Depth CCSF-A (m)			
				Top	Bottom	Top	Bottom	Midpoint	±	Top	Bottom	Midpoint	±
Pleistocene	RN14			320-U1335A-	320-U1335A-								
		T *A. angulare*	1.214	1H-3, 103–105	1H-CC	4.04	8.82	6.43	2.39	4.18	8.96	6.57	2.39
	RN13	B *T. trachelium*	1.757	1H-CC	2H-2, 38–40	8.82	10.79	9.81	0.98	8.96	11.80	10.38	1.42
		B *A. angulare*	1.972	1H-CC	2H-2, 38–40	8.82	10.79	9.81	0.98	8.96	11.80	10.38	1.42
		T *P. prismatium*	2.077	1H-CC	2H-2, 38–40	8.82	10.79	9.81	0.98	8.96	11.80	10.38	1.42
	RN12	B *C. davisiana*	2.889	2H-2, 38–40	2H-4, 38–40	10.79	13.79	12.29	1.50	11.80	14.80	13.30	1.50
		T *S. peregrina*	2.902	2H-4, 38–40	2H-CC	13.79	18.86	16.33	2.54	14.80	19.87	17.34	2.54
Pliocene	RN11	T *S. pentas*	3.977	2H-CC	3H-2, 105–107	18.86	20.96	19.91	1.05	19.87	22.27	21.07	1.20
		T *P. doliolum*	4.032	2H-CC	3H-2, 105–107	18.86	20.96	19.91	1.05	19.87	22.27	21.07	1.20
	RN10	T *D. penultima*	4.264	2H-CC	3H-2, 105–107	18.86	20.96	19.91	1.05	19.87	22.27	21.07	1.20
		B *P. prismatium*	4.729	3H-4, 105–107	3H-CC	23.96	28.14	26.05	2.09	25.27	29.45	27.36	2.09
		B *N. renilla*	5.024	3H-4, 105–107	3H-CC	23.96	28.14	26.05	2.09	25.27	29.45	27.36	2.09
	RP9	T *S. omnitubus*	5.319	3H-4, 105–107	3H-CC	23.96	28.14	26.05	2.09	25.27	29.45	27.36	2.09
		T *S. berminghami*	5.573	3H-CC	4H-2. 100–102	28.14	30.41	29.28	1.14	29.45	33.45	31.45	2.00
		T *S. johnsoni*	6.534	4H-4. 100–102	4H-CC	33.41	37.81	35.61	2.20	36.45	40.85	38.65	2.20
		T *C. caepa*	6.599	4H-4. 100–102	4H-CC	33.41	37.81	35.61	2.20	36.45	40.85	38.65	2.20
		S. delmontensis > *S. peregrina*	7.75	4H-CC	5H-2, 100–102	37.81	39.91	38.86	1.05	40.85	45.08	42.97	2.11
		B *S. peregrina*	7.84	5H-2, 100–102	5H-4, 100–102	39.91	42.91	41.41	1.50	45.08	48.08	46.58	1.50
		B *S. omnitubus*	8.25	5H-4, 100–102	5H-CC	42.91	46.46	44.69	1.78	48.08	51.63	49.86	1.78
upper Miocene	RN7	T *D. hughesi*	8.392	5H-4, 100–102	5H-CC	42.91	46.46	44.69	1.78	48.08	51.63	49.86	1.78
		T *B. miralestensis*	8.587	6H-2, 105–107	6H-4, 105–107	49.46	52.46	50.96	1.50	55.45	58.45	56.95	1.50
		T *D. petterssoni*	8.63	6H-2, 105–107	6H-4, 105–107	49.46	52.46	50.96	1.50	55.45	58.45	56.95	1.50
		D. petterssoni > *D. hughesi*	8.76	6H-4, 105–107	6H-CC	52.46	56.46	54.46	2.00	58.45	62.45	60.45	2.00
		B *S. berminghami*	8.76	6H-CC	7H-2, 102–104	56.46	58.93	57.70	1.24	62.45	66.02	64.24	1.78
		T *S. wolffii*	8.95	6H-CC	7H-2, 102–104	56.46	58.93	57.70	1.24	62.45	66.02	64.24	1.78
	RN6	B *D. hughesi*	8.99	6H-CC	7H-2, 102–104	56.46	58.93	57.70	1.24	62.45	66.02	64.24	1.78
		T *C. japonica*	10.31	7H-2, 102–104	7H-4, 102–104	58.93	61.93	60.43	1.50	66.02	69.02	67.52	1.50
		T *C. cristata*	10.88	7H-4, 102–104	7H-CC	61.93	66.25	64.09	2.16	69.02	73.34	71.18	2.16
		T *C. cornuta*	11.86	9H-4, 105–107	9H-CC	80.96	85.03	83.00	2.04	91.05	95.12	93.09	2.04
		B *D. petterssoni*	12.11	10H-2, 105–107	10H-4, 105–107	87.46	90.46	88.96	1.50	98.51	101.51	100.01	1.50
		B *C. japonica*	12.41	10H-CC	11H-2, 104–106	94.95	96.95	95.95	1.00	106.00	109.81	107.91	1.91
		B *L. neotera*	12.95	10H-CC	11H-2, 104–106	94.95	96.95	95.95	1.00	106.00	109.81	107.91	1.91
		T *S. armata*	13.5	12H-4, 104–106	12H-CC	109.45	113.85	111.65	2.20	122.31	126.71	124.51	2.20
	RN5	T *A. octopylus*	13.88	12H-4, 104–106	12H-CC	109.45	113.85	111.65	2.20	122.31	126.71	124.51	2.20
middle Miocene		T *C. costata*	14.229	13-4, 104–106	13H-CC	118.95	123.40	121.18	2.23	132.19	136.64	134.42	2.23
		T *D. dentata*	14.666	16H-3, 149–150	16H-4, 115–117	146.39	147.56	146.98	0.59	162.74	163.91	163.33	0.59
		T *L. stauropora*	14.826	16H-3, 149–150	16H-4, 115–117	146.39	147.56	146.98	0.59	162.74	163.91	163.33	0.59
		D. dentata > *D. alata*	14.78	16H-CC	17H-2, 104–106	151.49	153.95	152.72	1.23	167.84	173.95	170.90	3.05
		B *D. alata*	15.08	17H-2, 104–106	17H-3, 149–150	153.95	155.89	154.92	0.97	173.95	175.89	174.92	0.97
	RN4	B *L. parkerae*	15.03	17H-2, 104–106	17H-3, 149–150	153.95	155.89	154.92	0.97	173.95	175.89	174.92	0.97
		T *C. cingulata*	15.13	18H-3, 149–150	18H-4, 105–107	165.39	166.46	165.93	0.54	185.86	186.93	186.40	0.54
		T *L. elongata*	15.15	18H-3, 149–150	18H-4, 105–107	165.39	166.46	165.93	0.54	185.86	186.93	186.40	0.54
		B *L. renzae*	16.77	18H-CC	19H-2, 105–107	169.73	172.96	171.35	1.62	190.20	194.27	192.24	2.04
		B *C. costata*	17.49	19H-4, 105–107	19H-CC	175.96	180.42	178.19	2.23	197.27	201.73	199.50	2.23
lower Miocene	RN3	B *D. dentata*	17.72	20H-4, 104–106	20H-CC	185.45	189.88	187.67	2.22	208.18	212.61	210.40	2.22
		B *L. stauropora*	17.72	20H-CC	21H-1, 105–107	189.88	190.46	190.17	0.29	212.61	214.58	213.60	0.99
		B *S. wolffii*	18.57	23H-3, 149–150	23H-4, 105–107	212.89	213.96	213.43	0.54	241.31	242.38	241.85	0.53

Table T5 (continued).

Geologic age	Zone	Marker species	Age (Ma)	Core, section, interval (cm)		Depth CSF (m)				Depth CCSF-A (m)			
				Top	Bottom	Top	Bottom	Midpoint	±	Top	Bottom	Midpoint	±
lower Miocene	RN2	B *D. forcipata*	18.61	24H-CC	25H-2, 104–106	227.85	229.96	228.91	1.06	259.48	262.73	261.11	1.63
		T *D. simplex*	18.69	24H-CC	25H-2, 104–106	227.85	229.96	228.91	1.06	259.48	262.73	261.11	1.63
		T *D. praeforcipata*	19.77	26H-CC	27H-2, 100–102	246.79	248.91	247.85	1.06	281.43	285.85	283.64	2.21
		B *D. simplex*	20.34	28H-4, 105–107	28H-CC	261.46	265.97	263.72	2.26	299.24	303.75	301.50	2.25
		B *S. delmontensis*	20.68	29H-4, 105–107	29H-CC	261.46	265.97	263.72	2.26	300.95	305.46	303.21	2.26
		T *L. pegetrum*	20.89	30H-5, 104–106	30H-CC	281.95	284.78	283.37	1.41	322.51	325.34	323.93	1.41
		T *T. annosa*	21.38	31H-3, 149–150	31H-4, 105–107	288.89	289.96	289.43	0.53	331.52	332.59	332.06	0.53
	RN1	B *C. virginis*	21.39	31H-3, 149–150	31H-4, 105–107	288.89	289.96	289.43	0.53	331.52	332.59	332.06	0.53
		T *E. mitodes*	21.95	33H-4, 105–107	33H-CC	308.96	313.49	311.23	2.27	354.70	359.23	356.97	2.27
		B *C. serrata*	22.04	34H-2, 105–107	34H-3, 149–150	314.96	315.99	315.48	0.52	363.38	364.41	363.90	0.52
		B *C. cornuta*	22.26	36H-CC	37X-2, 104–106	341.81	343.95	342.88	1.07	393.81	395.95	394.88	1.07
		B *C. tetrapera*	22.35	36H-CC	37X-2, 104–106	341.81	343.95	342.88	1.07	393.81	395.95	394.88	1.07
	RP22	T *A. gracilis*	22.62	38H-3, 149–150	38H-4, 104–106	355.59	356.65	356.12	0.53	407.59	408.65	408.12	0.53
		B *E. diaphanes*	22.95	39X-3, 149–150	39X-CC	365.19	396.37	380.78	15.59	417.19	448.37	432.78	15.59
		T *D. cyclacantha*	22.98	38H-3, 149–150	38H-4, 104–106	355.59	356.65	356.12	0.53	407.59	408.65	408.12	0.53
upper Oligocene		B *D. cyclacantha*	23.29	39X-3, 149–150	39X-CC	365.19	396.37	380.78	15.59	417.19	448.37	432.78	15.59
		T *D. papilio*	23.31	39X-CC	40X-2, 104–106	369.37	372.75	371.06	1.69	421.37	424.75	423.06	1.69
		T *L. longicornuta*	24.12	41X-4, 104–106	41X-CC	385.25	387.62	386.44	1.19	437.25	439.62	438.44	1.19
		T *L. apodora*	24.5	41X-CC	42X-2, 104–106	387.62	391.75	389.69	2.06	439.62	443.75	441.69	2.06
	RP21	B *L. elongata*	25.05	42X-4, 104–106	42X-CC	394.75	396.29	395.52	0.77	446.75	448.29	447.52	0.77
		B *A. octopylus*	25.09	42X-4, 104–106	42X-CC	394.75	396.29	395.52	0.77	446.75	448.29	447.52	0.77
		B *C. robusta*	25.27	44X-2, 105–107	44X-4, 105–107	410.96	413.96	412.46	1.50	462.96	465.96	464.46	1.50
		B *L. longicornuta*	25.29	44X-2, 105–107	44X-4, 105–107	410.96	413.96	412.46	1.50	462.96	465.96	464.46	1.50
		B *L. apodora*	25.55	44X-2, 105–107	44X-4, 105–107	410.96	413.96	412.46	1.50	462.96	465.96	464.46	1.50

Note: T = top, B = bottom.

Table T6. Preservation and relative abundance of radiolarians, Hole U1335A. This table is available in an **oversized format.**

Table T7. Preservation and relative abundance of radiolarians, Hole U1335B. (See table notes.)

Core, section, interval (cm)	Radiolarian zone	Abundance	Preservation	Mixing	*Acrobotrys tritubus*	*Acrocubus octopylus*	*Amphirhopalum ypsilon*	*Anthocyrtidium angulare*	*Anthocyrtidium jenghisi*	*Artophormis gracilis*	*Botryostrobus miralestensis*	*Calocycletta caepa*	*Calocycletta costata*	*Calocycletta robusta*	*Calocycletta serrata*	*Calocycletta virginis*	*Carpocanopsis bramlettei*	*Carpocanopsis cingulata*	*Carpocanopsis cristata*	*Cycladophora davisiana*	*Cyrtocapsella cornuta*	*Cyrtocapsella japonica*	*Cyrtocapsella tetrapera*	*Diartus hughesi*
320-U1335B-																								
1H-CC	RN13	A	G	3			R	R												R				
2H-CC	RN12b	A	M	3																VR				
3H-CC	RN9	A	G	2					R															
4H-CC		A	G	2	VR				R															VR
5H-CC	RN8	A	G		VR							F												
6H-CC	RN7	A	G								R	R												F
7H-CC		A	G	1							R	R										R	VR	R
8H-CC	RN6	A	G								R	R							R			R		
9H-CC		A	G								R	R							R		R	R		
10H-CC		A	G								R	R							R		R	R	R	
11H-CC		A	G								R	F							R		F		R	
12H-CC		A	G								R	F		VR			R		R		F		R	
13H-CC	RN5	A	G			R						R				R	R				F		R	
14H-CC		A	G			R								R			R				F		R	
15H-CC		A	G			R							R	R		R	R				R		R	
16H-CC		A	G			R							R	R		R	R				R		R	
17H-CC		A	G			R							R	R		R	R				R		R	
18H-CC	RN4	A	G			R							R	R		R	R	R			R		R	
19H-CC		A	G										R	R		R	R	R			R		R	
20H-CC		A	G											R		F	R	R			C		F	
21H-CC	RN3	A	G											R		F	R	R			F		R	
22H-CC		A	G											R		R	R	R			F		R	
23H-CC		A	G											R		R	R	R			F		R	
24H-CC		A	G											F		R	R	R			F		R	
25H-CC		A	G											R		R	R	R			F		R	
26H-CC		A	G											R		R	R	R			F		R	
27H-CC	RN2	A	G											F		R	R	R			F		R	
28H-CC		A	G											F	R	R	R	R			F		R	
29H-CC		A	G											R	R	R	R	R			F		R	
30H-CC		A	G											R	R	R	R	R			F		R	
31H-CC		A	G											R	R		R	R			F		R	
32H-CC		A	M	3		VR				VR				R				R			F		R	
33H-CC	RN1	A	G											R				R			F		R	
34H-CC		A	G											R				R			F		R	
35H-CC		A	G							R				R				R			R		R	
36H-CC		A	G											R				R			R		R	
37H-CC		A	G											R				R						
38H-CC		A	G							R				R				R						
39H-CC	RP22	A	G							R				R				R						
40H-CC		A	G							R				R				R						
41H-CC		A	G							R				R				R						
42H-CC		A	G							R				C										
43H-CC	RP21	C	P			R				R				R										
44H-CC		C	P							R				R										
45H-CC	RP21?	R	P											VR										

Core, section, interval (cm)	*Diartus petterssoni*	*Didymocyrtis antepenultima*	*Didymocyrtis avita*	*Didymocyrtis bassanii*	*Didymocyrtis laticonus*	*Didymocyrtis mammifera*	*Didymocyrtis penultima*	*Didymocyrtis prismatica*	*Didymocyrtis tetrathalamus*	*Didymocyrtis tubaria*	*Didymocyrtis violina*	*Dorcadospyris alata*	*Dorcadospyris ateuchus*	*Dorcadospyris cyclacantha*	*Dorcadospyris dentata*	*Dorcadospyris forcipata*	*Dorcadospyris papilio*	*Dorcadospyris praeforcipata*	*Dorcadospyris riedeli*	*Dorcadospyris scambos*	*Dorcadospyris simplex s.s.*	*Eucyrtidium diaphanes*	*Eucyrtidium mitodes*	*Lamprocyrtis neoheteroporos*	*Lamprocyrtis nigriniae*
320-U1335B-																									
1H-CC									R															R	VR?
2H-CC			R						R															R	
3H-CC			R				R		R																
4H-CC		VR	R				R		R																
5H-CC							R																		
6H-CC		R			R		R																		
7H-CC	F	R			F																				
8H-CC	F				F																				
9H-CC	R				F																				
10H-CC					F																				
11H-CC					F																				
12H-CC					F							R													
13H-CC				R	F							R										R			
14H-CC					R	R																VR			
15H-CC					F	R				R	R	R													
16H-CC					F	R				R	R	R													
17H-CC					F	R				R	R				R	R									
18H-CC					R	R		R		R	R				R	R									
19H-CC						R		R		R	R				R	R						R			
20H-CC						R		R		R	R				R	R						R			
21H-CC						R		R		R	R					R						R			
22H-CC						R		R		R	R					R						R			
23H-CC								R		R	R							VR		R		R			
24H-CC				R				R		R	R					R				R		R			
25H-CC				R				R		R	R		R							R	R	R			
26H-CC				R				R		R	R							R		R		R			
27H-CC				R				R		R	R		R					R		R	R	R			
28H-CC				R				R			R					VR		R		R		R			
29H-CC				R				R												R		R			
30H-CC				R				R												R		R			
31H-CC				R				R												R		R			
32H-CC				R				R									VR	R		R		R	R		
33H-CC				R				R										R		R		R	R		
34H-CC				R				R										R		R		R	R		
35H-CC				R				R										R		R		R	R		
36H-CC				R				R										R		R		R	R		
37H-CC								R										R		R		R	R		
38H-CC								R										R		R		R	R		
39H-CC								R					R					R		R			R		
40H-CC								R					R	VR				R		R			R		
41H-CC								R					R				R	R		R			R		
42H-CC								R		R			R				R	R		R			R		
43H-CC													R				R	R							
44H-CC								R					R				R								
45H-CC																									

Core, section, interval (cm)	*Liriospyris longicornuta*	*Liriospyris parkerae*	*Liriospyris stauropora*	*Lithopera neotera*	*Lithopera renzae*	*Lophocyrtis leptetrum*	*Lophocyrtis pegetrum*	*Lychnocanoma apodora*	*Lychnocanoma elongata*	*Lychnodictyum audax*	*Phormostichoartus doliolum*	*Phormostichoartus fistula*	*Pterocanium prismatium*	*Solenosphaera omnitubus*	*Spongaster berminghami*	*Spongaster pentas*	*Spongaster tetras*	*Stichocorys armata*	*Stichocorys delmontensis*	*Stichocorys johnsoni*	*Stichocorys peregrina*	*Stichocorys wolffii*	*Stylatractus universus*	*Theocorythium trachelium*	*Theocyrtis annosa*
320-U1335B-																									
1H-CC																	R						R	R	
2H-CC													R				R		R		R		R		
3H-CC										R			R			R			R	VR	F		R		
4H-CC										R	R	R		R	R	R			VR		F				
5H-CC										R	R			R	R				F	R			R		
6H-CC										R	R				R				F	R					
7H-CC				R						R									F			R			
8H-CC				VR						R									F			R			
9H-CC				VR	VR					R									R			R			
10H-CC					R					R									F			R			
11H-CC					R					R									F						
12H-CC		R		VR	R					R									F			R			
13H-CC		R			R	R												R	F			R			
14H-CC		R			R													R	F			R			
15H-CC		R			R													R	R			R			
16H-CC		R			R													R	R			R			
17H-CC			R		R													R	R			R			
18H-CC			R		R				R									R	R			R			
19H-CC			R						R									R	R			R			
20H-CC			R						R									R	R			R			
21H-CC									R									R	R			R			
22H-CC			VR						R									R	R			R			
23H-CC									R									R	F			R			
24H-CC									R									R	F						
25H-CC						R			R																
26H-CC						R			R																
27H-CC						F			R										F						
28H-CC						R			R										F						
29H-CC						R			R										R						
30H-CC						R			R																
31H-CC							R		R																R
32H-CC							R		R																R
33H-CC							R		R																R
34H-CC							R		R																R
35H-CC							R		R																R
36H-CC							R		R																R
37H-CC							R		R																R
38H-CC							R		R																R
39H-CC							R		R																R
40H-CC							R		R																R
41H-CC							R		R																R
42H-CC							R		F																R
43H-CC							R	R																	R
44H-CC	R						R	R																	R
45H-CC	VR						VR	VR																	VR

Notes: Abundance: A = abundant, C = common, F = frequent, R = rare, VR = very rare. Preservation: G = good, M = moderate, P = poor. Mixing: blank = no mixing of older specimens detected, 1 = 1–3 reworked specimens detected, 2 = 3–10 reworked specimens detected, 3 = >10 reworked specimens detected.

Table T8. Planktonic foraminifer datums, Site U1335. (See table note.) (Continued on next page.)

Core, section, interval (cm)		Marker species	Age (Ma)	Depth CSF (m)			
Top	Bottom			Top	Bottom	Midpoint	±
320-U1335A-	320-U1335A-						
		Pliocene/Pleistocene boundary					
1H-CC	2H-2, 104–106	T *Globigerinoides fistulosus*	1.77	8.81	11.44	10.13	1.32
1H-5, 42–44	1H-CC	B *Globorotalia (Truncorotalia) truncatulinoides*	1.92	6.42	8.81	7.62	1.20
1H-CC	2H-2, 104–106	T *Globigerinoides extremus*	1.98	8.81	11.44	10.13	1.32
1H-CC	2H-2, 104–106	T *Globorotalia pseudomiocenica*	2.30	8.81	11.44	10.13	1.32
2H-2, 104–106	2H-4, 104–106	T *Globoturborotalita woodi*	2.30	11.44	14.44	12.94	1.50
3H-2, 38–40	3H-4, 38–40	T *Globorotalia (Menardella) multicamerata*	2.98	20.28	23.28	21.78	1.50
4H-5, 120–1212	5H-CC	T *Dentoglobigerina altispira*	3.47	35.10	46.45	40.78	5.68
2H-2, 104–106	2H-4, 104–106	T *Sphaeroidinellopsis seminulina*	3.59	11.44	14.44	12.94	1.50
2H-4, 104–106	2H-CC	B *Globorotalia (Menardella) exilis*	4.45	14.44	18.85	16.65	2.21
3H-4, 38–40	3H-CC	B *Sphaeroidinella dehiscens* s.l.	5.54	23.28	28.13	25.71	2.42
		Miocene/Pliocene boundary					
3H-CC	4H-3, 100–102	B *Globorotalia tumida*	5.57	28.13	31.90	30.02	1.89
4H-CC	5H-2, 80–82	B *Globorotalia (Hirsutella) margaritae*	6.08	37.80	39.70	38.75	0.95
6H-2, 38–40	6H-4, 38–40	B *Globorotalia plesiotumida*	8.58	46.45	51.78	49.12	2.67
7H-6, 95–97	7H-CC	T *Paragloborotalia mayeri*	10.46	64.85	66.24	65.55	0.69
8H-CC	9H-2, 38–40	B *Globoturborotalita decoraperta*	11.49	75.86	77.28	76.57	0.71
9H-2, 38–40	9H-4, 38–40	T *Globorotalia (Fohsella) fohsi* s.l.	11.79	77.28	80.28	78.78	1.50
11H-CC	12-2H, 38–40	B *Globorotalia (Fohsella) fohsi robusta*	13.13	104.16	105.78	104.97	0.81
12-2H, 38–40	12H-CC	B *Globorotalia (Fohsella) fohsi* s.l.	13.41	105.78	113.84	109.81	4.03
12H-CC	13H-3, 149–150	B *Globorotalia (Fohsella) "praefohsi"*	13.77	113.84	117.89	115.87	2.03
13H-4, 38–40	13H-CC	T *Globorotalia (Fohsella) peripheroronda*	13.80	118.28	123.39	120.84	2.56
13H-3, 149–150	13H-4, 38–40	T *Clavatorella bermudezi*	13.82	117.89	118.28	118.09	0.20
14H-2, 38–40	14H-4, 38–40	B *Clavatorella bermudezi*	14.89	124.78	127.78	126.28	1.50
14H-2, 38–41	14H-4, 38–41	B *Globorotalia (Fohsella) peripheroacuta*	14.24	124.78	127.78	126.28	1.50
16H-CC	17H-3, 149–150	B *Globorotalia (Menardella) archeomenardii*	16.26	155.89	161.19	158.54	2.65
18H-CC	19H-2, 38–40	B *Praeorbulina sicana*	16.97	169.72	172.28	171.00	1.28
19H-CC	20H-CC	T *Globoquadrina binaiensis*	19.09	180.41	189.97	185.19	4.78
28H-4, 38–40	28H-CC	T *Paragloborotalia kugleri*	21.12	260.78	265.96	263.37	2.59
28H-4, 38–40	28H-CC	T *Paragloborotalia pseudokugleri*	21.31	260.78	265.96	263.37	2.59
37X-2, 48–50	37X-4, 136–138	B *Globoquadrina dehiscens*	22.44	343.38	347.26	345.32	1.94
		Oligocene/Miocene boundary					
37X-4, 136–138	37X-CC	B *Paragloborotalia kugleri*	23.00	347.26	350.01	348.64	1.38
320-U1335B-	320-U1335B-						
		Pliocene/Pleistocene boundary					
1H-CC	2H-CC	B *Globorotalia (Truncorotalia) truncatulinoides*	1.92	3.43	13.02	8.23	4.80
1H-CC	2H-CC	T *Globigerinoides extremus*	1.98	3.43	13.02	8.23	4.80
1H-CC	2H-CC	T *Globorotalia pseudomiocenica*	2.30	3.43	13.02	8.23	4.80
4H-CC	5H-CC	T *Dentoglobigerina altispira*	3.47	31.93	41.86	36.90	4.96
2H-CC	3H-CC	T *Sphaeroidinellopsis seminulina*	3.59	13.02	22.66	17.84	4.82
2H-CC	3H-CC	B *Sphaeroidinella dehiscens* s.l.	5.53	13.02	22.66	17.84	4.82
		Miocene/Pliocene boundary					
3H-CC	4H-CC	B *Globorotalia tumida*	5.57	22.26	31.93	27.10	4.83
6H-CC	7H-CC	B *Globorotalia plesiotumida*	8.58	51.05	60.92	55.99	4.94
7H-CC	8H-CC	T *Globorotalia (Menardella) praemenardii*	10.09	60.92	70.02	65.47	4.55
7H-CC	8H-CC	T *Paragloborotalia mayeri*	10.46	60.92	70.02	65.47	4.55
7H-CC	8H-CC	B *Globoturborotalita decoraperta*	11.49	60.92	70.02	65.47	4.55
8H-CC	9H-CC	T *Globorotalia (Fohsella) fohsi* s.l.	11.79	70.02	79.49	74.76	4.74
11H-CC	12H-CC	B *Globorotalia (Fohsella) fohsi robusta*	13.13	98.97	108.08	103.53	4.56
11H-CC	12H-CC	B *Globorotalia (Fohsella) fohsi* s.l.	13.41	98.97	108.08	103.53	4.56
12H-CC	13H-CC	T *Globorotalia praescitula*	13.73	108.08	117.65	112.87	4.79
12H-CC	13H-CC	B *Globorotalia (Fohsella) "praefohsi"*	13.77	108.08	117.65	112.87	4.79
12H-CC	13H-CC	T *Globorotalia (Fohsella) peripheroronda*	13.80	108.08	117.65	112.87	4.79
17H-CC	18H-CC	B *Globorotalia (Menardella) archeomenardii*	16.26	155.64	164.78	160.21	4.57
18H-CC	19H-CC	B *Praeorbulina sicana*	16.97	164.78	174.81	169.80	5.02
20H-CC	21H-CC	T *Catapsydrax dissimilis*	17.54	184.35	193.42	188.89	4.53
20H-CC	21H-CC	T *Globoquadrina binaiensis*	19.09	184.35	193.42	188.89	4.53
30H-CC	29H-CC	T *Paragloborotalia kugleri*	21.12	269.69	279.09	274.39	4.70
30H-CC	29H-CC	T *Paragloborotalia pseudokugleri*	21.31	269.69	279.09	274.39	4.70
30H-CC	31H-CC	B *Globoquadrina dehiscens*	22.44	279.09	288.52	283.81	4.71

Table T8 (continued).

Core, section, interval (cm)		Marker species	Age (Ma)	Depth CSF (m)			
Top	Bottom			Top	Bottom	Midpoint	±
		Oligocene/Miocene boundary					
37H-CC	38H-CC	B *Paragloborotalia kugleri*	23.00	344.06	352.84	348.45	4.39
42X-CC	43X-CC	B *Paragloborotalia pseudokugleri*	25.20	386.64	394.88	390.76	4.12

Note: T = top, B = bottom.

Table T9. Distribution of planktonic foraminifers, Site U1335. This table is available in an **oversized format.**

Table T10. Distribution of benthic foraminifers, Site U1335. This table is available in an **oversized format.**

Table T11. Coring-disturbed intervals and gaps, Site U1335. (See table notes.)

Core, section, interval (cm)	Type of disturbance
320-U1335A-	
1H-1, 0–9	Top of core
1H-2, 145–150	Interstitial water
1H-4, 145–150	Interstitial water
2H-1, 0–34	Top of core
2H-2, 145–150	Interstitial water
2H-5, 145–150	Interstitial water
3H-1, 0–48	Top of core
3H-2, 145–150	Interstitial water
3H-5, 145–150	Interstitial water
4H-1, 0–120	Top of core
4H-2, 145–150	Interstitial water
4H-5, 145–150	Interstitial water
5H-1, 0–45	Top of core
5H-2, 145–150	Interstitial water
6H-1, 0–28	Top of core
6H-2, 145–150	Interstitial water
6H-5, 145–150	Interstitial water
7H-3, 140–150	Interstitial water
8H-1, 0–9	Top of core
8H-3, 140–150	Interstitial water
9H-3, 18–23	Paleontology sample
10H-1, 0–41	Top of core
10H-3, 145–150	Interstitial water
11H-1, 0–150	Top of core
11H-2, 0–139	Disturbed
11H-2, 140–150	Interstitial water
11H-3, 0–150	Disturbed
11H-4, 0–150	Disturbed
11H-5, 0–150	Disturbed
11H-6, 0–150	Disturbed
11H-7, 0–42	Disturbed
12H-1, 0–12	Top of core
12H-3, 140–150	Interstitial water
13H-1, 0–68	Top of core
13H-3, 140–150	Interstitial water
13H-3, 149–150	Paleontology sample
14H-1, 0–51	Top of core
14H-3, 140–150	Interstitial water
15H-1, 0–56	Top of core
15H-3, 140–150	Interstitial water
16H-1, 0–10	Top of core
16H-3, 140–150	Interstitial water
16H-4, 25–150	Flow-in
16H-5, 0–150	Flow-in
16H-6, 0–150	Flow-in
16H-7, 0–45	Flow-in
17H-1, 0–69	Top of core
17H-3, 140–150	Interstitial water
18H-1, 0–25	Slurry
18H-3, 140–150	Interstitial water
19H-3, 140–150	Interstitial water
20H-1, 0–7	Top of core
20H-3, 140–150	Interstitial water
21H-1, 0–35	Top of core
21H-3, 140–150	Interstitial water
22H-1, 0–94	Top of core
22H-3, 140–150	Interstitial water
23H-1, 0–130	Top of core
23H-2, 70–150	Disturbed
23H-3, 0–100	Disturbed
23H-3, 100–141	Biscuits
23H-3, 140–150	Interstitial water
24H-1, 57–150	Biscuits
24H-2, 0–47	Biscuits
24H-2, 74–85	Flow-in
24H-2, 85–150	Biscuits
24H-3, 140–150	Interstitial water
24H-5, 0–79	Biscuits
25H-3, 140–150	Interstitial water
26H-3, 140–150	Interstitial water
27H-3, 140–150	Interstitial water
28H-3, 140–150	Interstitial water
29H-3, 140–150	Interstitial water
30H-1, 0–14	Top of core
30H-3, 140–150	Interstitial water
31H-3, 140–150	Interstitial water
32H-3, 140–150	Interstitial water
33H-3, 140–150	Interstitial water
34H-3, 140–150	Interstitial water
34H-7, 78–151	Flow-in
34H-8, 0–72	Flow-in
35H-5, 92–150	Flow-in
35H-6, 0–81	Flow-in
36H-1, 0–150	Top of core
36H-2, 0–150	Top of core
36H-3, 0–62	Top of core
37X–45X, all sections	Drilling biscuits
320-U1335B-	
2H-1, 0–74	Top of core
4H-1, 0–80	Top of core
5H-1, 0–20	Top of core
6H-1, 0–16	Top of core
7H-1, 0–46	Top of core
8H-1, 0–13	Top of core
9H-1, 0–40	Top of core
11H-5, 140–150	Whole-round sample
13H-1, 0–14	Top of core
15H-1, 0–32	Top of core
16H-1, 0–49	Top of core
17H-1, 0–84	Top of core
18H-1, 0–110	Top of core
20H-1, 0–20	Top of core
21H-1, 0–42	Top of core
22H-1, 0–51	Top of core
22H-2, 140–150	Whole-round sample
23H-1, 0–50	Top of core
25H-1, 0–46	Top of core
30H-1, 0–5	Top of core
31H-1, 8–12	Disturbed
31H-1, 83–91	Disturbed
33H-5, 140–150	Whole-round sample
36H-3, 140–150	Interstitial water
37H-2, 140–150	Interstitial water
38H-1, 0–2	Top of core
38H-6, 79–145	Flow-in
39H-1, 0–2	Top of core
39H-3, 140–150	Interstitial water
40H-1, 0–6	Top of core
41H-1, 0–3	Top of core
42X–46X, all sections	Drilling biscuits

Notes: Top of core = myriad forms of voids, disturbance, and debris from uphole that affect top portion of most cores. For that reason, probably the top 20 cm or so of all cores should be avoided.

Table T12. Paleomagnetic data from archive-half sections, Hole U1335A, at 0 mT AF demagnetization. (See table notes.)

Core, section	Offset (m)	Depth CSF (m)	Declination (°)	Inclination (°)	Intensity (A/m)	Time (s)
320-U1335A-						
1H-1	0.100	0.100	93.7	–6.6	6.445E–03	3322849274.76562
1H-1	0.150	0.150	62.2	3.6	2.542E–03	3322849280.09375
1H-1	0.200	0.200	336.5	72.6	1.930E–03	3322849285.42187
1H-1	0.250	0.250	81.7	24.5	3.273E–03	3322849290.75000
1H-1	0.300	0.300	74.6	26.2	1.734E–03	3322849296.06250
1H-1	0.350	0.350	106.1	30.4	1.484E–03	3322849301.39062
1H-1	0.400	0.400	102.1	26.2	2.012E–03	3322849306.71875
1H-1	0.450	0.450	110.3	14.5	3.365E–03	3322849312.03125
1H-1	0.500	0.500	104.6	17.0	4.146E–03	3322849317.35937
1H-1	0.550	0.550	114.2	16.9	5.322E–03	3322849322.68750
1H-1	0.600	0.600	122.1	20.2	5.628E–03	3322849328.01562
1H-1	0.650	0.650	126.4	23.9	5.074E–03	3322849333.34375
1H-1	0.700	0.700	119.1	20.9	6.714E–03	3322849338.65625
1H-1	0.750	0.750	118.8	17.9	7.110E–03	3322849343.98437
1H-1	0.800	0.800	119.1	17.6	6.510E–03	3322849349.31250
1H-1	0.850	0.850	118.1	20.4	6.783E–03	3322849354.64062
1H-1	0.900	0.900	127.5	24.7	5.409E–03	3322849359.96875
1H-1	0.950	0.950	110.1	14.3	4.068E–03	3322849365.28125
1H-1	1.000	1.000	101.6	16.4	3.064E–03	3322849370.60937
1H-1	1.050	1.050	134.7	22.5	4.764E–03	3322849375.93750
1H-1	1.100	1.100	139.5	22.2	5.204E–03	3322849381.26562
1H-1	1.150	1.150	122.8	21.1	4.343E–03	3322849386.57812
1H-1	1.200	1.200	125.5	19.8	4.728E–03	3322849391.90625
1H-1	1.250	1.250	147.6	4.0	6.640E–03	3322849397.23437
1H-1	1.300	1.300	114.5	–13.2	1.017E–02	3322849402.56250
1H-1	1.350	1.350	104.1	3.6	6.861E–03	3322849407.89062
1H-1	1.400	1.400	135.8	18.8	5.656E–03	3322849413.21875
1H-2	0.100	1.600	138.7	11.4	8.087E–03	3322850832.31250
1H-2	0.150	1.650	135.7	14.1	5.576E–03	3322850837.64062
1H-2	0.200	1.700	133.6	14.4	4.534E–03	3322850842.96875
1H-2	0.250	1.750	129.6	13.7	6.217E–03	3322850848.29687
1H-2	0.300	1.800	135.9	12.5	7.053E–03	3322850853.60937
1H-2	0.350	1.850	135.4	12.2	7.722E–03	3322850858.93750
1H-2	0.400	1.900	138.3	14.0	6.300E–03	3322850864.26562
1H-2	0.450	1.950	134.3	13.9	6.638E–03	3322850869.59375
1H-2	0.500	2.000	132.6	13.8	7.602E–03	3322850874.90625
1H-2	0.550	2.050	136.2	13.0	8.158E–03	3322850880.23437
1H-2	0.600	2.100	135.0	13.2	8.066E–03	3322850885.56250
1H-2	0.650	2.150	139.4	14.6	6.468E–03	3322850890.89062
1H-2	0.700	2.200	137.2	13.6	5.856E–03	3322850896.20312
1H-2	0.750	2.250	135.2	13.0	7.960E–03	3322850901.53125
1H-2	0.800	2.300	132.5	13.6	8.825E–03	3322850906.85937
1H-2	0.850	2.350	135.7	12.5	9.411E–03	3322850912.18750
1H-2	0.900	2.400	135.3	14.7	9.278E–03	3322850917.51562
1H-2	0.950	2.450	135.5	14.7	9.415E–03	3322850922.84375
1H-2	1.000	2.500	135.6	14.0	9.319E–03	3322850928.15625
1H-2	1.050	2.550	141.3	16.2	7.987E–03	3322850933.48437
1H-2	1.100	2.600	139.7	14.0	6.436E–03	3322850938.81250
1H-2	1.150	2.650	132.5	19.8	4.464E–03	3322850944.14062
1H-2	1.200	2.700	149.3	19.0	4.137E–03	3322850949.46875
1H-2	1.250	2.750	144.3	16.2	4.475E–03	3322850954.79687
1H-2	1.300	2.800	134.4	13.9	5.791E–03	3322850960.10937
1H-2	1.350	2.850	151.1	24.0	5.858E–03	3322850965.43750
1H-2	1.400	2.900	131.9	16.8	7.771E–03	3322850970.76562
1H-3	0.100	3.100	138.8	11.2	7.612E–03	3322851803.90625
1H-3	0.150	3.150	141.1	9.5	6.436E–03	3322851809.21875
1H-3	0.200	3.200	135.1	10.2	4.291E–03	3322851814.54687
1H-3	0.250	3.250	140.8	13.7	3.941E–03	3322851819.87500
1H-3	0.300	3.300	138.2	13.6	4.270E–03	3322851825.18750
1H-3	0.350	3.350	139.6	13.4	4.367E–03	3322851830.51562
1H-3	0.400	3.400	138.8	16.4	4.836E–03	3322851835.84375

Notes: Time = since 1 January 1904. Only a portion of this table appears here. The complete table is available in ASCII.

Table T13. Paleomagnetic data from archive-half sections, Hole U1335A, at 20 mT AF demagnetization. (See table notes.)

Core, section	Offset (m)	Depth CSF (m)	Declination (°)	Inclination (°)	Intensity (A/m)	Time (s)	Declination			CCSF offset (m)	Depth (m)		VGP (°)	
							Core mean (°)	Geographical coordinates			CCSF-A	CCSF-B	Latitude	Longitude
								0°–360°	–90°–270°					
320-U1335A-														
1H-1	0.100	0.100	87.0	2.8	2.112E–03	3322850308.59375	109.8	337.2	–22.8	0.14	0.24	0.21	66.9	134.9
1H-1	0.125	0.125	76.9	6.4	2.030E–03	3322850313.53125	109.8	327.1	–32.9	0.14	0.27	0.23	57.1	141.5
1H-1	0.150	0.150	72.8	10.1	2.249E–03	3322850318.45312	109.8	323.0	–37.0	0.14	0.29	0.25	53.2	–214.8
1H-1	0.175	0.175	71.3	8.3	2.037E–03	3322850323.39062	109.8	321.5	–38.5	0.14	0.32	0.27	51.6	–216.2
1H-1	0.200	0.200	70.4	10.0	1.574E–03	3322850328.32812	109.8	320.6	–39.4	0.14	0.34	0.29	50.8	–214.7
1H-1	0.225	0.225	70.0	13.4	1.220E–03	3322850333.25000	109.8	320.2	–39.8	0.14	0.37	0.32	50.4	–211.9
1H-1	0.250	0.250	71.3	18.7	1.033E–03	3322850338.18750	109.8	321.5	–38.5	0.14	0.39	0.34	51.6	–207.4
1H-1	0.275	0.275	50.8	43.8	5.224E–04	3322850343.12500	109.8	301.0	–59.0	0.14	0.42	0.36	30.2	–189.6
1H-1	0.300	0.300	73.6	23.7	8.704E–04	3322850348.06250	109.8	323.8	–36.2	0.14	0.44	0.38	53.6	–202.5
1H-1	0.325	0.325	75.1	27.0	7.409E–04	3322850352.98437	109.8	325.3	–34.7	0.14	0.47	0.40	54.7	–198.9
1H-1	0.350	0.350	82.0	30.4	6.924E–04	3322850357.92187	109.8	332.2	–27.8	0.14	0.49	0.42	60.6	–191.9
1H-1	0.375	0.375	95.5	28.2	8.162E–04	3322850362.85937	109.8	345.7	–14.3	0.14	0.52	0.45	72.9	–180.5
1H-1	0.400	0.400	99.4	24.8	1.055E–03	3322850367.78125	109.8	349.6	–10.4	0.14	0.54	0.47	77.2	–178.6
1H-1	0.425	0.425	102.5	21.0	1.389E–03	3322850372.71875	109.8	352.7	–7.3	0.14	0.57	0.49	80.9	–178.2
1H-1	0.450	0.450	102.2	18.6	1.652E–03	3322850377.65625	109.8	352.4	–7.6	0.14	0.59	0.51	81.4	–186.4
1H-1	0.475	0.475	100.9	15.0	2.098E–03	3322850382.59375	109.8	351.1	–8.9	0.14	0.62	0.53	80.9	–201.0
1H-1	0.500	0.500	102.6	20.5	2.087E–03	3322850387.51562	109.8	352.8	–7.2	0.14	0.64	0.55	81.1	–179.2
1H-1	0.525	0.525	104.4	16.9	2.070E–03	3322850392.45312	109.8	354.6	–5.4	0.14	0.67	0.58	83.7	–184.1
1H-1	0.550	0.550	109.5	16.9	2.152E–03	3322850397.39062	109.8	359.7	–0.3	0.14	0.69	0.60	86.7	–131.3
1H-1	0.575	0.575	118.9	15.4	2.484E–03	3322850402.31250	109.8	9.1	9.1	0.14	0.72	0.62	80.6	–52.3
1H-1	0.600	0.600	118.6	15.9	2.547E–03	3322850407.25000	109.8	8.8	8.8	0.14	0.74	0.64	80.8	–54.4
1H-1	0.625	0.625	119.9	17.0	2.516E–03	3322850412.17187	109.8	10.1	10.1	0.14	0.77	0.66	79.4	–55.4
1H-1	0.650	0.650	118.5	18.9	2.428E–03	3322850417.10937	109.8	8.7	8.7	0.14	0.79	0.68	80.3	–63.7
1H-1	0.675	0.675	112.3	22.0	2.613E–03	3322850422.03125	109.8	2.5	2.5	0.14	0.82	0.71	83.4	–104.3
1H-1	0.700	0.700	106.6	18.2	3.277E–03	3322850426.96875	109.8	356.8	–3.2	0.14	0.84	0.73	84.9	–164.3
1H-1	0.725	0.725	109.8	18.4	3.368E–03	3322850431.90625	109.8	0.0	0.0	0.14	0.87	0.75	85.9	–126.2
1H-1	0.750	0.750	113.8	17.2	3.425E–03	3322850436.82812	109.8	4.0	4.0	0.14	0.89	0.77	84.7	–77.7
1H-1	0.775	0.775	117.9	15.8	3.284E–03	3322850441.76562	109.8	8.1	8.1	0.14	0.92	0.79	81.5	–55.4
1H-1	0.800	0.800	119.0	15.7	3.058E–03	3322850446.68750	109.8	9.2	9.2	0.14	0.94	0.81	80.5	–53.1
1H-1	0.825	0.825	118.4	17.2	2.941E–03	3322850451.62500	109.8	8.6	8.6	0.14	0.97	0.83	80.8	–58.9
1H-1	0.850	0.850	118.2	19.1	2.980E–03	3322850456.54687	109.8	8.4	8.4	0.14	0.99	0.86	80.5	–65.1
1H-1	0.875	0.875	117.8	21.0	3.008E–03	3322850461.48437	109.8	8.0	8.0	0.14	1.02	0.88	80.3	–71.7
1H-1	0.900	0.900	119.2	22.7	2.838E–03	3322850466.40625	109.8	9.4	9.4	0.14	1.04	0.90	78.7	–71.8
1H-1	0.925	0.925	118.7	22.8	2.532E–03	3322850471.34375	109.8	8.9	8.9	0.14	1.07	0.92	79.0	–73.5
1H-1	0.950	0.950	108.3	19.2	2.321E–03	3322850476.28125	109.8	358.5	–1.5	0.14	1.09	0.94	85.2	–144.1
1H-1	0.975	0.975	80.8	10.6	2.254E–03	3322850481.20312	109.8	331.0	–29.0	0.14	1.12	0.96	61.1	–214.7
1H-1	1.000	1.000	76.4	8.9	1.150E–03	3322850486.14062	109.8	326.6	–33.4	0.14	1.14	0.99	56.7	–216.1
1H-1	1.025	1.025	93.9	9.8	1.508E–03	3322850491.06250	109.8	344.1	–15.9	0.14	1.17	1.01	74.2	143.2
1H-1	1.050	1.050	131.7	12.4	1.952E–03	3322850496.00000	109.8	21.9	21.9	0.14	1.19	1.03	68.2	–39.8
1H-1	1.075	1.075	123.7	14.5	2.059E–03	3322850500.93750	109.8	13.9	13.9	0.14	1.22	1.05	76.0	–45.4
1H-1	1.100	1.100	123.6	17.3	2.265E–03	3322850505.85937	109.8	13.8	13.8	0.14	1.24	1.07	75.9	–51.5
1H-1	1.125	1.125	123.6	16.4	2.247E–03	3322850510.79687	109.8	13.8	13.8	0.14	1.27	1.09	76.0	–49.5
1H-1	1.150	1.150	122.2	16.4	2.144E–03	3322850515.73437	109.8	12.4	12.4	0.14	1.29	1.12	77.3	–50.8
1H-1	1.175	1.175	120.1	15.5	2.088E–03	3322850520.65625	109.8	10.3	10.3	0.14	1.32	1.14	79.4	–50.9

Notes: Time = since 1 January 1904. VGP = virtual geomagnetic pole. Only a portion of this table appears here. The complete table is available in ASCII.

Table T14. Paleomagnetic data from archive-half sections, Hole U1335B, at 0 mT AF demagnetization. (See table notes.)

Core, section,	Offset (m)	Depth-CSF (m)	Declination (°)	Inclination (°)	Intensity (A/m)	Time (s)
320-U1335B-						
1H-1	0.100	0.100	241.7	–23.4	1.521E–02	3323143964.25450
1H-1	0.150	0.150	241.4	16.5	6.560E–03	3323143969.58262
1H-1	0.200	0.200	297.8	31.7	7.816E–03	3323143974.91075
1H-1	0.250	0.250	267.9	16.5	6.816E–03	3323143980.22325
1H-1	0.300	0.300	162.8	–7.3	5.043E–03	3323143985.55137
1H-1	0.350	0.350	215.2	–2.2	1.216E–02	3323143990.87950
1H-1	0.400	0.400	281.6	14.8	1.062E–02	3323143996.20762
1H-1	0.450	0.450	346.1	27.3	2.661E–02	3323144001.53575
1H-1	0.500	0.500	252.7	35.8	1.243E–02	3323144006.84825
1H-1	0.550	0.550	138.1	–12.9	3.402E–02	3323144012.17637
1H-1	0.600	0.600	133.7	12.0	5.697E–02	3323144017.50450
1H-1	0.650	0.650	191.3	37.3	8.961E–02	3323144022.83262
1H-1	0.700	0.700	236.5	23.5	3.344E–02	3323144028.16075
1H-1	0.750	0.750	309.4	65.1	3.304E–03	3323144033.47325
1H-1	0.800	0.800	166.8	5.8	1.026E–02	3323144038.80137
1H-1	0.850	0.850	188.9	19.4	6.260E–03	3323144044.12950
1H-1	0.900	0.900	221.1	19.6	6.313E–03	3323144049.45762
1H-1	0.950	0.950	218.9	18.7	6.722E–03	3323144054.77012
1H-1	1.000	1.000	213.5	16.8	6.649E–03	3323144060.09825
1H-1	1.050	1.050	207.6	16.8	4.581E–03	3323144065.42637
1H-1	1.100	1.100	208.0	22.8	2.816E–03	3323144070.75450
1H-1	1.150	1.150	210.6	20.9	3.395E–03	3323144076.08262
1H-1	1.200	1.200	208.5	23.9	4.012E–03	3323144081.39512
1H-1	1.250	1.250	205.1	18.5	4.632E–03	3323144086.72325
1H-1	1.300	1.300	203.1	15.8	5.234E–03	3323144092.05137
1H-1	1.350	1.350	204.8	16.5	5.093E–03	3323144097.37950
1H-1	1.400	1.400	209.9	19.5	5.489E–03	3323144102.70762
1H-2	0.100	1.600	220.6	12.1	8.470E–03	3323145023.41075
1H-2	0.150	1.650	228.1	15.1	7.126E–03	3323145028.73887
1H-2	0.200	1.700	222.5	19.4	7.549E–03	3323145034.06700
1H-2	0.250	1.750	221.2	17.4	7.890E–03	3323145039.39512
1H-2	0.300	1.800	222.4	18.4	7.527E–03	3323145044.72325
1H-2	0.350	1.850	226.9	18.6	6.061E–03	3323145050.03575
1H-2	0.400	1.900	221.9	16.5	5.695E–03	3323145055.36387
1H-2	0.450	1.950	218.4	13.5	7.212E–03	3323145060.69200
1H-2	0.500	2.000	215.3	13.1	8.220E–03	3323145066.02012
1H-2	0.550	2.050	213.4	13.8	8.322E–03	3323145071.34825
1H-2	0.600	2.100	216.1	14.9	7.534E–03	3323145076.67637
1H-2	0.650	2.150	218.2	14.9	7.228E–03	3323145081.98887
1H-2	0.700	2.200	215.3	14.2	7.334E–03	3323145087.31700
1H-2	0.750	2.250	213.2	12.9	7.788E–03	3323145092.64512
1H-2	0.800	2.300	214.1	11.3	7.983E–03	3323145097.97325
1H-2	0.850	2.350	215.0	10.6	8.143E–03	3323145103.30137
1H-2	0.900	2.400	215.8	11.5	8.095E–03	3323145108.62950
1H-2	0.950	2.450	215.8	13.4	7.962E–03	3323145113.94200
1H-2	1.000	2.500	215.3	15.2	8.135E–03	3323145119.27012
1H-2	1.050	2.550	212.1	17.7	9.047E–03	3323145124.59825
1H-2	1.100	2.600	210.3	18.8	9.152E–03	3323145129.91075
1H-2	1.150	2.650	209.7	19.1	9.207E–03	3323145135.23887
1H-2	1.200	2.700	209.6	17.8	9.752E–03	3323145140.56700
1H-2	1.250	2.750	212.0	17.5	9.672E–03	3323145145.89512
1H-2	1.300	2.800	216.5	14.7	8.434E–03	3323145151.22325
1H-2	1.350	2.850	222.2	16.5	6.775E–03	3323145156.55137
1H-2	1.400	2.900	224.8	16.2	5.793E–03	3323145161.87950
1H-3	0.075	3.075	184.9	20.9	5.988E–03	3323146071.20762
1H-3	0.100	3.100	174.4	20.3	6.969E–03	3323146076.14512
1H-3	0.125	3.125	170.5	17.9	8.804E–03	3323146081.06700
1H-3	0.150	3.150	162.2	16.2	1.086E–02	3323146086.00450
1H-3	0.175	3.175	150.2	13.8	1.381E–02	3323146090.92637
1H-3	0.200	3.200	143.2	13.9	1.601E–02	3323146095.86387
1H-3	0.225	3.225	155.5	23.2	1.107E–02	3323146100.78575
1H-3	0.250	3.250	280.9	11.5	2.617E–02	3323146105.72325
1H-3	0.275	3.275	289.4	3.3	7.721E–02	3323146110.66075
2H-1	0.750	4.050	142.1	31.5	4.702E–03	3323148890.89512

Notes: Time = since 1 January 1904. Only a portion of this table appears here. The complete table is available in ASCII.

Table T15. Paleomagnetic data from archive-half sections, Hole U1335B, at 20 mT AF demagnetization. (See table notes.)

Core, section	Offset (m)	Depth CSF (m)	Declination (°)	Inclination (°)	Intensity (A/m)	Time (s)	Declination			CCSF offset (m)	Depth (m)		VGP (°)	
							Core mean (°)	Geographical coordinates			CCSF-A	CCSF-B	Latitude	Longitude
								0°–360°	–90°–270°					
320-U1335B-														
1H-1A	0.075	0.075	169.8	–44.0	6.562E–03	3323144406.11387	200.6	329.2	–30.8	0.00	0.08	0.06	46.9	96.2
1H-1A	0.100	0.100	229.1	–35.3	1.022E–02	3323144411.05137	200.6	28.5	28.5	0.00	0.10	0.09	52.6	6.1
1H-1A	0.125	0.125	242.9	–20.6	1.158E–02	3323144415.98887	200.6	42.3	42.3	0.00	0.13	0.11	45.0	–15.4
1H-1A	0.150	0.150	249.3	–4.6	1.103E–02	3323144420.91075	200.6	48.7	48.7	0.00	0.15	0.13	40.8	–28.5
1H-1A	0.175	0.175	236.1	5.1	5.436E–03	3323144425.84825	200.6	35.5	35.5	0.00	0.18	0.15	54.5	–33.1
1H-1A	0.200	0.200	239.9	24.0	2.549E–03	3323144430.78575	200.6	39.3	39.3	0.00	0.20	0.17	50.6	–49.5
1H-1A	0.225	0.225	258.7	36.3	2.720E–03	3323144435.72325	200.6	58.1	58.1	0.00	0.23	0.19	31.7	–56.6
1H-1A	0.250	0.250	278.6	26.4	4.080E–03	3323144440.64512	200.6	78.0	78.0	0.00	0.25	0.22	12.9	–49.3
1H-1A	0.275	0.275	278.3	18.0	4.513E–03	3323144445.58262	200.6	77.7	77.7	0.00	0.28	0.24	13.0	–44.5
1H-1A	0.300	0.300	267.9	5.1	2.000E–03	3323144450.52012	200.6	67.3	67.3	0.00	0.30	0.26	22.8	–36.7
1H-1A	0.325	0.325	151.2	–0.1	1.474E–03	3323144455.45762	200.6	310.6	–49.4	0.00	0.33	0.28	40.4	139.2
1H-1A	0.350	0.350	164.3	–8.2	2.265E–03	3323144460.37950	200.6	323.7	–36.3	0.00	0.35	0.30	52.5	129.9
1H-1A	0.375	0.375	202.8	–8.3	4.345E–03	3323144465.31700	200.6	2.2	2.2	0.00	0.38	0.32	80.3	40.7
1H-1A	0.400	0.400	224.1	–1.0	7.813E–03	3323144470.23887	200.6	23.5	23.5	0.00	0.40	0.35	65.8	–23.0
1H-1A	0.425	0.425	237.4	5.5	7.694E–03	3323144475.17637	200.6	36.8	36.8	0.00	0.43	0.37	53.2	–33.7
1H-1A	0.450	0.450	275.1	17.0	5.486E–03	3323144480.11387	200.6	74.5	74.5	0.00	0.45	0.39	16.1	–43.7
1H-1A	0.475	0.475	348.8	24.9	6.479E–03	3323144485.03575	200.6	148.2	148.2	0.00	0.48	0.41	–53.5	–66.6
1H-1A	0.500	0.500	11.5	26.9	8.511E–03	3323144489.97325	200.6	170.9	170.9	0.00	0.50	0.43	–68.5	–101.5
1H-1A	0.525	0.525	15.2	30.8	7.448E–03	3323144494.91075	200.6	174.6	174.6	0.00	0.53	0.45	–67.4	–112.6
1H-1A	0.550	0.550	358.4	58.1	2.532E–03	3323144499.84825	200.6	157.8	157.8	0.00	0.55	0.48	–41.4	–103.1
1H-1A	0.575	0.575	208.3	11.4	2.461E–03	3323144504.78575	200.6	7.7	7.7	0.00	0.58	0.50	82.3	–39.9
1H-1A	0.600	0.600	141.7	–5.5	9.288E–03	3323144509.70762	200.6	301.1	–58.9	0.00	0.60	0.52	30.6	137.4
1H-1A	0.625	0.625	158.5	–0.7	2.001E–02	3323144514.64512	200.6	317.9	–42.1	0.00	0.63	0.54	47.6	137.5
1H-1A	0.650	0.650	174.9	7.3	2.590E–02	3323144519.58262	200.6	334.3	–25.7	0.00	0.65	0.56	64.3	141.2
1H-1A	0.675	0.675	183.8	16.9	3.047E–02	3323144524.52012	200.6	343.2	–16.8	0.00	0.68	0.58	73.0	–204.0
1H-1A	0.700	0.700	195.6	26.8	3.011E–02	3323144529.44200	200.6	355.0	–5.0	0.00	0.70	0.60	79.9	–154.9
1H-1A	0.725	0.725	205.6	27.4	2.329E–02	3323144534.48887	200.6	5.0	5.0	0.00	0.73	0.63	79.6	–98.5
1H-1A	0.750	0.750	224.0	19.8	1.472E–02	3323144539.59825	200.6	23.4	23.4	0.00	0.75	0.65	66.3	–49.5
1H-1A	0.775	0.775	251.8	29.2	4.489E–03	3323144544.91075	200.6	51.2	51.2	0.00	0.78	0.67	38.7	–52.0
1H-1A	0.800	0.800	291.2	47.5	1.794E–03	3323144549.84825	200.6	90.6	90.6	0.00	0.80	0.69	2.0	–64.7
1H-1A	0.825	0.825	198.2	34.8	1.274E–03	3323144554.78575	200.6	357.6	–2.4	0.00	0.83	0.71	76.0	–135.6
1H-1A	0.850	0.850	169.4	9.6	3.117E–03	3323144559.70762	200.6	328.8	–31.2	0.00	0.85	0.73	58.9	–215.6
1H-1A	0.875	0.875	170.5	7.5	3.913E–03	3323144564.64512	200.6	329.9	–30.1	0.00	0.88	0.76	60.0	142.2
1H-1A	0.900	0.900	172.1	10.9	3.524E–03	3323144569.56700	200.6	331.5	–28.5	0.00	0.90	0.78	61.6	–214.4
1H-1A	0.925	0.925	200.8	18.9	3.137E–03	3323144574.50450	200.6	0.2	0.2	0.00	0.93	0.80	85.6	–123.6
1H-1A	0.950	0.950	221.6	18.3	3.177E–03	3323144579.45762	200.6	21.0	21.0	0.00	0.95	0.82	68.8	–48.5
1H-1A	0.975	0.975	219.4	17.9	3.465E–03	3323144584.37950	200.6	18.8	18.8	0.00	0.98	0.84	71.0	–49.0
1H-1A	1.000	1.000	218.1	18.5	3.536E–03	3323144589.31700	200.6	17.5	17.5	0.00	1.00	0.86	72.2	–50.8
1H-1A	1.025	1.025	216.3	17.9	3.634E–03	3323144594.25450	200.6	15.7	15.7	0.00	1.03	0.89	74.0	–51.0
1H-1A	1.050	1.050	214.2	16.8	3.632E–03	3323144599.19200	200.6	13.6	13.6	0.00	1.05	0.91	76.1	–50.6
1H-1A	1.075	1.075	211.5	16.0	3.472E–03	3323144604.11387	200.6	10.9	10.9	0.00	1.08	0.93	78.8	–51.5
1H-1A	1.100	1.100	208.4	15.6	3.081E–03	3323144609.05137	200.6	7.8	7.8	0.00	1.10	0.95	81.8	–55.4
1H-1A	1.125	1.125	208.1	15.6	2.549E–03	3323144613.98887	200.6	7.5	7.5	0.00	1.13	0.97	82.1	–56.1

Notes: Time = since 1 January 1904. Only a portion of this table appears here. The complete table is available in ASCII.

Table T16. Mean paleomagnetic direction for each core, Site U1335. (See table notes.)

Core	Inclination (°)	Declination (°)	*N*	α95 (°)
320-U1335A-				
1H	10.7	109.8	317	3.1
2H	7.7	223.5	344	2.0
3H	1.1	164.2	331	3.1
4H	–2.7	315.0	310	2.8
5H	–8.9	87.6	173	5.2
6H	–0.2	191.9	224	11.6
7H	12.9	103.6	254	4.0
8H–16H	NA	NA	NA	NA
17H	–14.6	118.9	158	4.2
18H	4.2	76.7	171	3.4
19H	–10.5	116.9	327	1.4
20H	3.5	266.8	173	2.2
21H	17.8	38.3	159	4.0
22H	–57.8	179.5	153	4.1
23H–36H	NA	NA	NA	NA
320-U1335B-				
1H	19.8	200.6	119	2.9
2H	4.5	207.9	321	2.0
3H	2.5	15.1	343	2.7
4H	–75.9	251.0	313	3.0
5H	–64.6	9.9	347	7.2
6H	–16.3	206.1	344	5.6
7H	43.7	272.1	343	9.9
8H	4.1	81.8	346	2.1
9H–12H	NA	NA	NA	NA
13H	5.0	248.6	345	2.8
14H	4.7	284.8	346	4.4
15H	–10.2	187.7	348	2.0
16H	–9.2	292.6	332	2.7
17H	21.6	253.0	308	6.1
18H	–1.6	276.0	289	2.0
19H	0.5	272.8	358	1.3
20H	–13.3	71.3	350	1.6
21H	2.0	204.2	301	2.0
22H	45.6	272.1	231	5.9
23H–41H	NA	NA	NA	NA

Notes: Mean paleomagnetic directions and statistics calculated using Bingham statistics for each core. We used data from stable polarity intervals. Reversed polarity intervals were inverted prior to computing mean directions and statistics. Inclination = mean paleomagnetic inclination from stable polarity intervals in core, declination = mean paleomagnetic declination from stable polarity intervals in core. By subtracting this value from observed paleomagnetic declinations measured along core, core can be approximately reoriented back into geographic coordinates. After reorientation, normal polarity intervals will have ~0° declination and reversed polarity intervals will have ~180° declination. *N* = number of paleomagnetic observations used in calculating mean, α95 = 95% confidence angle for mean direction.

Table T17. Paleomagnetic results for discrete samples, Hole U1335A. (See table notes.)

Core, section, interval (cm)	Depth CSF (m)	Demag (mT)	Declination			Inclination (°)	Intensity (A/m)
			Azimuthally unoriented (°)	Geographical coordinates			
				0°–360°	–90°–270°		
320-U1335A-							
1H-2, 90	2.40	0	136.8	27.0	27.0	8.9	6.94E–03
1H-2, 90	2.40	5	134.5	24.7	24.7	8.9	4.69E–03
1H-2, 90	2.40	10	134.9	25.1	25.1	8.7	3.82E–03
1H-2, 90	2.40	15	138.3	28.5	28.5	8.7	3.62E–03
1H-2, 90	2.40	20	136.8	27.0	27.0	10.9	3.15E–03
1H-2, 90	2.40	25	138.5	28.7	28.7	12.8	2.85E–03
1H-2, 90	2.40	30	134.2	24.4	24.4	16.7	2.35E–03
1H-2, 90	2.40	35	133.5	23.7	23.7	21.5	1.95E–03
1H-2, 90	2.40	40	136.4	26.6	26.6	24.4	1.72E–03
1H-2, 90	2.40	50	133.3	23.5	23.5	43.0	1.37E–03
1H-2, 90	2.40	60	141.1	31.3	31.3	46.2	1.15E–03
1H-4, 85	5.35	0	–125.0	125.2	125.2	4.4	2.45E–03
1H-4, 85	5.35	5	–94.3	155.9	155.9	–3.6	2.89E–03
1H-4, 85	5.35	10	–89.2	161.0	161.0	–3.8	3.54E–03
1H-4, 85	5.35	15	–94.9	155.3	155.3	–3.4	3.35E–03
1H-4, 85	5.35	20	–89.9	160.3	160.3	–0.6	2.98E–03
1H-4, 85	5.35	25	–90.0	160.2	160.2	3.0	2.52E–03
1H-4, 85	5.35	30	–88.3	161.9	161.9	8.1	2.08E–03
1H-4, 85	5.35	35	–86.9	163.3	163.3	15.2	1.64E–03
1H-4, 85	5.35	40	–89.3	160.9	160.9	23.5	1.45E–03
1H-4, 85	5.35	50	–96.5	153.7	153.7	44.2	1.08E–03
1H-4, 85	5.35	60	–99.6	150.6	150.6	59.7	1.04E–03
1H-5, 85	6.85	0	108.6	358.8	–1.2	13.4	1.84E–03
1H-5, 85	6.85	5	91.0	341.2	–18.8	10.9	9.29E–04
1H-5, 85	6.85	10	90.6	340.8	–19.2	8.0	5.40E–04
1H-5, 85	6.85	15	60.3	310.5	–49.5	13.3	4.84E–04
1H-5, 85	6.85	20	36.1	286.3	–73.7	18.8	6.37E–04
1H-5, 85	6.85	25	68.0	318.2	–41.8	31.2	4.14E–04
1H-5, 85	6.85	30	46.0	296.2	–63.8	39.2	4.66E–04
1H-5, 85	6.85	35	73.2	323.4	–36.6	52.3	4.50E–04
1H-5, 85	6.85	40	49.5	299.7	–60.3	60.4	4.50E–04
1H-5, 85	6.85	50	50.2	300.4	–59.6	75.1	5.72E–04
1H-5, 85	6.85	60	13.0	263.2	263.2	57.7	6.24E–04
2H-2, 85	11.25	0	–1.2	135.3	135.3	–22.0	1.45E–03
2H-2, 85	11.25	5	22.3	158.8	158.8	–9.2	1.89E–03
2H-2, 85	11.25	10	23.7	160.2	160.2	–9.5	2.37E–03
2H-2, 85	11.25	15	23.7	160.2	160.2	–8.6	2.22E–03
2H-2, 85	11.25	20	24.2	160.7	160.7	–7.5	2.04E–03
2H-2, 85	11.25	25	23.4	159.9	159.9	–3.8	1.77E–03
2H-2, 85	11.25	30	23.1	159.6	159.6	3.8	1.37E–03
2H-2, 85	11.25	35	22.2	158.7	158.7	9.7	1.26E–03
2H-2, 85	11.25	40	21.9	158.4	158.4	20.4	9.56E–04
2H-2, 85	11.25	50	12.1	148.6	148.6	43.6	9.66E–04
2H-2, 85	11.25	60	25.9	162.4	162.4	72.4	6.18E–04
2H-5, 85	15.75	0	–136.5	0.0	0.0	11.4	4.14E–03
2H-5, 85	15.75	5	–128.6	7.9	7.9	4.9	2.69E–03
2H-5, 85	15.75	10	–131.8	4.7	4.7	2.9	2.11E–03
2H-5, 85	15.75	15	–127.2	9.3	9.3	5.5	1.79E–03
2H-5, 85	15.75	20	–124.5	12.0	12.0	9.2	1.43E–03
2H-5, 85	15.75	25	–138.3	–1.8	–1.8	8.8	1.45E–03
2H-5, 85	15.75	30	–125.6	10.9	10.9	17.5	1.03E–03
2H-5, 85	15.75	35	–128.4	8.1	8.1	24.9	8.68E–04
2H-5, 85	15.75	40	–121.5	15.0	15.0	39.9	7.31E–04
2H-5, 85	15.75	50	–139.3	–2.8	–2.8	53.1	5.51E–04
2H-5, 85	15.75	60	–105.0	31.5	31.5	74.3	6.01E–04
2H-7, 50	18.40	0	–162.8	–26.3	–26.3	29.8	7.63E–04
2H-7, 50	18.40	5	61.7	198.2	198.2	–5.4	7.14E–04
2H-7, 50	18.40	10	59.8	196.3	196.3	–5.6	1.23E–03
2H-7, 50	18.40	15	72.8	209.3	209.3	–7.4	1.03E–03
2H-7, 50	18.40	20	49.4	185.9	185.9	0.9	1.25E–03
2H-7, 50	18.40	25	60.5	197.0	197.0	7.6	9.33E–04
2H-7, 50	18.40	30	59.1	195.6	195.6	14.1	7.90E–04

Notes: Only a portion of this table appears here. The complete table is available in ASCII.

Table T18. Principal component analysis (PCA) results for paleomagnetic data, Hole U1335A. (**See table notes.**) (**Continued on next page.**)

Core, section, interval (cm)	Depth CSF (m)	PCA					NRM 20 mT (A/m)	Archive-half section at 20 mT AF demagnetization		
		Declination		Inclination (°)	MAD (°)	Range (mT)		Declination (°)	Inclination (°)	NRM (A/m)
		Azimuthally unoriented (°)	Geographical coordinates (0°–360°)							
320-U1335A-										
1H-2, 90	2.40	136.4	26.6	8.0	4.6	0–20	3.15E–03	129.8	17.5	4.459E–03
1H-4, 85	5.35	264.3	154.5	–19.3	8.3	10–35	2.98E–03	267.3	3.1	2.315E–03
1H-5, 85	6.85	NA	NA	NA	NA	NA	6.37E–04	239.6	40.9	7.587E–04
2H-2, 85	11.25	25.0	161.5	–27.0	2.0	10–30	2.04E–03	38.1	4.0	1.371E–03
2H-5, 85	15.75	233.2	9.7	–0.9	15.2	5–25	1.43E–03	221.7	8.9	2.845E–03
2H-7, 85	18.40	NA	NA	NA	NA	NA	1.25E–03	65.8	13.5	1.333E–03
3H-2, 85	20.75	156.9	352.7	–1.2	8.6	5–25	4.46E–04	170.6	42.5	1.205E–03
3H-4, 85	23.75	333.5	169.3	–32.2	8.7	10–60	1.87E–03	326.7	–2.4	2.283E–03
3H-5, 85	25.25	162.9	358.7	2.9	7.7	5–25	1.70E–03	166.9	12.2	2.465E–03
4H-2, 85	30.25	115.3	160.3	–23.6	8.4	10–30	1.97E–03	120.7	21.6	2.648E–03
4H-5, 85	34.75	315.5	0.4	6.7	14.2	5–25	1.12E–03	307.2	24.9	1.119E–03
4H-7, 60	37.50	153.8	198.8	–17.7	6.6	15–40	1.84E–03	142.9	20.9	1.724E–03
5H-2, 110	40.00	266.4	178.8	8.2	15.7	5–35	3.30E–04	256.9	21.2	1.932E–04
5H-4, 85	42.75	NA	NA	NA	NA	NA	8.45E–04	72.7	12.0	7.612E–04
5H-5, 85	44.25	265.7	178.1	10.5	17.0	5–40	7.97E–04	257.2	25.1	1.058E–03
6H-2, 85	49.25	NA	NA	NA	NA	NA	2.54E–04	290.9	32.0	2.733E–04
7H-2, 85	58.75	256.9	153.3	–35.8	7.4	10–30	1.38E–03	252.9	14.3	2.046E–03
7H-5, 85	63.25	115.3	11.7	2.1	11.1	5–25	1.74E–03	123.1	16.5	1.851E–03
7H-7, 40	65.80	126.7	23.1	–14.3	15.4	5–30	6.30E–04	131.7	20.9	1.153E–03
8H-1, 85	66.75	130.7	NA	–1.7	22.9	5–25	1.92E–04	131.7	51.5	4.609E–04
8H-2, 85	68.25	311.7	NA	–19.3	19.4	5–35	4.10E–04	310.6	11.3	3.837E–04
8H-5, 85	72.75	164.1	NA	–2.1	13.3	5–30	1.36E–04	136.6	15.8	4.854E–04
9H-2, 85	77.75	NA	NA	NA	NA	NA	1.39E–04	218.0	40.9	1.900E–04
9H-5, 85	82.25	NA	NA	NA	NA	NA	1.14E–04	124.4	–47.0	5.435E–05
10H-2, 85	87.25	NA	NA	NA	NA	NA	7.60E–05	290.5	25.5	1.363E–05
11H-2, 85	96.75	9.4	NA	–25.6	5.5	5–25	6.39E–05	NA	NA	NA
11H-5, 85	101.25	353.5	NA	2.0	19.3	10–30	1.47E–04	NA	NA	NA
12H-2, 85	106.25	NA	NA	NA	NA	NA	3.02E–05	226.5	51.3	5.679E–05
12H-5, 85	110.75	NA	NA	NA	NA	NA	2.54E–04	242.0	39.0	1.291E–04
13H-2, 85	115.75	NA	NA	NA	NA	NA	1.36E–04	187.0	1.5	2.100E–04
13H-5, 85	120.25	38.4	NA	–28.9	20.3	5–25	2.70E–05	186.3	23.0	2.738E–04
13H-7, 60	123.00	NA	NA	NA	NA	NA	1.47E–04	220.5	29.0	3.626E–04
14H-2, 85	125.25	88.7	NA	–12.2	11.0	10–35	9.88E–04	87.7	6.6	1.666E–03
14H-5, 85	129.75	244.5	NA	–11.7	10.8	5–30	8.05E–04	241.2	29.3	4.400E–04
14H-7, 75	132.60	NA	NA	NA	NA	NA	1.71E–04	238.8	18.8	3.491E–04
15H-2, 75	134.65	NA	NA	NA	NA	NA	2.78E–04	235.9	15.4	4.513E–04
15H-5, 85	138.75	131.0	NA	–30.5	32.5	5–25	2.23E–04	143.6	56.1	4.541E–04
16H-2, 85	144.25	NA	NA	NA	NA	NA	3.77E–04	151.8	61.0	2.167E–04
17H-2, 85	153.75	NA	NA	NA	NA	NA	6.18E–05	343.7	18.7	3.816E–04
17H-7, 50	160.90	307.9	189.0	–21.4	6.9	20–40	2.93E–03	310.6	2.8	3.584E–03
18H-2, 85	163.25	229.2	152.5	–10.2	16.9	5–50	7.49E–04	246.9	–3.2	6.911E–04
18H-5, 85	167.75	79.3	2.6	–3.1	4.3	10–40	1.52E–03	78.0	3.9	1.565E–03
19H-2, 85	172.75	84.2	327.3	–8.3	15.1	15–35	9.20E–04	107.5	17.9	1.336E–03
19H-5, 85	177.25	295.8	178.9	–25.1	16.0	15–50	6.11E–04	339.9	34.7	3.788E–04
20H-2, 85	182.25	235.6	328.8	5.0	14.8	5–25	5.68E–04	265.1	–2.7	6.262E–04
20H-5, 85	186.75	128.1	221.3	–26.2	26.7	5–50	5.85E–04	111.4	–15.1	3.742E–04
21H-2, 85	191.75	NA	NA	NA	NA	NA	1.50E–04	256.0	–9.5	1.186E–04
22H-2, 85	201.25	NA	NA	NA	NA	NA	5.82E–04	16.3	31.1	4.475E–04
22H-3, 85	202.75	NA	NA	NA	NA	NA	2.42E–04	13.3	52.6	4.269E–04
23H-2, 90	210.80	NA	NA	NA	NA	NA	1.30E–04	NA	NA	NA
24H-2, 85	220.25	NA	NA	NA	NA	NA	7.78E–05	NA	NA	NA
25H-2, 75	229.75	NA	NA	NA	NA	NA	8.15E–05	234.4	11.8	2.238E–05
26H-2, 85	239.25	NA	NA	NA	NA	NA	5.21E–05	135.7	26.6	1.128E–04
27H-2, 85	248.75	NA	NA	NA	NA	NA	2.37E–05	198.7	66.5	2.097E–04
28H-2, 85	258.25	NA	NA	NA	NA	NA	4.83E–04	44.4	31.8	6.934E–04
29H-2, 85	267.75	NA	NA	NA	NA	NA	2.18E–04	291.3	43.3	6.239E–05
30H-2, 85	277.25	NA	NA	NA	NA	NA	8.87E–05	207.7	20.5	5.990E–05
31H-2, 85	286.75	NA	NA	NA	NA	NA	2.43E–05	320.1	–27.0	2.427E–05
32H-2, 85	296.25	NA	NA	NA	NA	NA	1.11E–04	297.8	55.8	3.387E–05
33H-2, 85	305.75	NA	NA	NA	NA	NA	9.40E–05	243.8	73.4	1.260E–05
34H-3, 85	315.35	NA	NA	NA	NA	NA	9.65E–05	266.4	61.7	1.930E–05
35H-2, 85	324.75	NA	NA	NA	NA	NA	6.46E–05	241.0	53.3	1.277E–05
36H-2, 85	334.25	NA	NA	NA	NA	NA	5.37E–05	NA	NA	NA

Table T18 (continued).

Core, section, interval (cm)	Depth CSF (m)	PCA					NRM 20 mT (A/m)	Archive-half section at 20 mT AF demagnetization		
		Declination								
		Azimuthally unoriented (°)	Geographical coordinates (0°–360°)	Inclination (°)	MAD (°)	Range (mT)		Declination (°)	Inclination (°)	NRM (A/m)
38X-3, 88	354.97	NA	NA	NA	NA	NA	1.37E–04	NA	NA	NA
39X-3, 94	364.65	NA	NA	NA	NA	NA	1.92E–04	NA	NA	NA
40X-3, 90	374.10	5.0	NA	–8.2	17.6	15–40	6.93E–05	NA	NA	NA
41X-3, 90	383.60	NA	NA	NA	NA	NA	9.61E–05	NA	NA	NA
42X-3, 69	392.89	NA	NA	NA	NA	NA	4.71E–05	NA	NA	NA
43X-4, 127	404.57	NA	NA	NA	NA	NA	2.99E–04	NA	NA	NA
44X-2, 85	410.75	NA	NA	NA	NA	NA	1.24E–04	NA	NA	NA

Notes: MAD = maximum angular deviation, NRM = natural remanence magnetism. NA = not applicable.

Table T19. Magnetic susceptibility of discrete samples, Hole U1335A. (See table notes.) (Continued on next five pages.)

Core, section, interval (cm)	Depth CSF (m)	LIMS ID	Susceptibility Raw (10^{-6})	Susceptibility Corrected (10^{-6})	Total mass (g)	Bulk density (g/cm^3)	Volume (cm^3)	Susceptibility Volume normalized (10^{-5})	Susceptibility Mass normalized (m^3/kg)	Susceptibility Whole core (raw values)	Scale factor
320-U1335A-											
1H-1, 94–96	0.95	CUBE716101	69.5	74.4	12.14	1.30	5.81	8.97	4.288E–08	7.62	1.18E+00
1H-2, 89–91	2.40	CUBE716111	83.5	88.4	10.88	1.31	4.79	12.92	5.687E–08	10.68	1.21E+00
1H-3, 84–86	3.85	CUBE716121	22.8	27.7	13.78	1.33	6.91	2.80	1.405E–08	7.93	3.53E–01
1H-4, 84–86	5.35	CUBE716131	96.6	101.5	12.55	1.35	5.91	12.03	5.660E–08	10.66	1.13E+00
1H-5, 84–86	6.85	CUBE716141	51.3	56.2	14.17	1.37	6.99	5.63	2.778E–08	9.88	5.70E–01
1H-6, 84–86	8.05	CUBE716151	74.3	79.2	13.36	1.38	6.36	8.71	4.148E–08	9.94	8.76E–01
2H-1, 84–86	9.75	CUBE717291	106.1	111.0	12.20	1.26	6.05	12.85	6.369E–08	13.06	9.84E–01
2H-2, 84–86	11.25	CUBE717301	69.5	74.4	12.93	1.24	6.70	7.77	4.026E–08	11.04	7.04E–01
2H-3, 84–86	12.75	CUBE717311	34.3	39.2	14.26	1.40	6.90	3.97	1.924E–08	8.68	4.58E–01
2H-4, 94–96	14.35	CUBE717321	44.6	49.5	12.88	1.51	5.51	6.30	2.691E–08	8.82	7.14E–01
2H-5, 84–86	15.75	CUBE717331	51.1	56.0	10.32	1.37	4.19	9.36	3.796E–08	13.20	7.09E–01
2H-6, 84–86	17.25	CUBE717341	33.8	38.7	12.50	1.27	6.23	4.35	2.168E–08	8.86	4.91E–01
2H-7, 49–51	18.40	CUBE717351	70.2	75.1	11.92	1.25	5.89	8.94	4.412E–08	9.47	9.43E–01
3H-1, 84–86	19.25	CUBE720851	76.3	81.2	12.37	1.19	6.55	8.68	4.596E–08	12.67	6.85E–01
3H-2, 84–86	20.75	CUBE720861	89.5	94.4	12.46	1.26	6.22	10.61	5.301E–08	14.03	7.56E–01
3H-3, 84–86	22.25	CUBE720871	109.8	114.7	12.15	1.34	5.63	14.27	6.608E–08	18.20	7.84E–01
3H-4, 84–86	23.75	CUBE720881	96.2	101.1	12.39	1.27	6.14	11.52	5.712E–08	15.37	7.50E–01
3H-5, 84–86	25.25	CUBE720891	115.7	120.6	12.42	1.29	6.05	13.96	6.797E–08	15.29	9.13E–01
3H-6, 84–86	26.75	CUBE720901	88.6	93.5	12.80	1.33	6.15	10.65	5.115E–08	11.85	8.98E–01
4H-2, 84–86	30.25	CUBE722191	116.1	121.0	12.17	1.29	5.88	14.40	6.960E–08	17.35	8.30E–01
4H-3, 84–86	31.75	CUBE722211	106.7	111.6	12.78	1.42	5.78	13.53	6.113E–08	13.81	9.80E–01
4H-4, 84–86	33.25	CUBE722221	44.8	49.7	13.46	1.51	5.87	5.93	2.583E–08	11.73	5.05E–01
4H-5, 84–86	34.75	CUBE722231	87.4	92.3	12.44	1.40	5.60	11.53	5.191E–08	12.92	8.93E–01
4H-6, 84–86	36.25	CUBE722241	97.3	102.2	12.81	1.34	6.15	11.62	5.582E–08	14.14	8.22E–01
4H-7, 59–61	37.50	CUBE722201	88.0	92.9	12.47	1.39	5.65	11.52	5.217E–08	12.01	9.59E–01
5H-1, 109–111	38.50	CUBE722951	17.1	22.0	13.94	1.68	5.57	2.76	1.104E–08	2.69	1.03E+00
5H-2, 109–111	40.00	CUBE722991	12.1	17.0	14.33	1.59	6.14	1.94	8.309E–09	3.02	6.42E–01
5H-3, 109–111	41.50	CUBE723001	63.9	68.8	13.14	1.42	6.02	7.99	3.663E–08	9.05	8.83E–01
5H-4, 84–86	42.75	CUBE722961	53.7	58.6	13.11	1.41	6.05	6.78	3.127E–08	9.46	7.16E–01
5H-5, 84–86	44.25	CUBE722971	48.8	53.7	13.61	1.51	5.97	6.29	2.759E–08	5.67	1.11E+00
5H-6, 84–86	45.75	CUBE722981	48.3	53.2	13.56	1.37	6.53	5.70	2.745E–08	7.71	7.39E–01
6H-1, 84–86	47.75	CUBE723831	21.7	26.6	13.33	1.54	5.67	3.28	1.394E–08	5.41	6.07E–01
6H-2, 84–86	49.25	CUBE723841	19.2	24.1	13.13	1.55	5.50	3.07	1.285E–08	3.27	9.38E–01
6H-3, 84–86	50.75	CUBE723851	–1.7	3.2	15.02	1.63	6.40	0.35	1.496E–09	0.98	
6H-4, 84–86	52.25	CUBE723861	–2.6	2.3	11.64	1.55	4.54	0.35	1.361E–09	0.88	
6H-5, 84–86	53.75	CUBE723871	3.1	8.0	13.80	1.51	6.08	0.92	4.042E–09	1.04	
6H-6, 84–86	55.25	CUBE723881	2.1	7.0	13.33	1.35	6.47	0.76	3.684E–09	2.33	3.26E–01
7H-1, 84–86	57.25	CUBE724381	79.4	84.3	11.28	1.24	5.40	10.93	5.229E–08	12.74	8.58E–01
7H-2, 84–86	58.75	CUBE724391	143.9	148.8	12.40	1.21	6.43	16.19	8.400E–08	19.29	8.39E–01
7H-3, 84–86	60.25	CUBE724401	140.0	144.9	12.28	1.28	6.01	16.88	8.260E–08	20.77	8.13E–01
7H-4, 84–86	61.75	CUBE724411	61.9	66.8	12.40	1.37	5.68	8.23	3.773E–08	15.92	5.17E–01
7H-5, 84–86	63.25	CUBE724421	121.4	126.3	12.46	1.28	6.15	14.38	7.096E–08	19.07	7.54E–01
7H-6, 84–86	64.75	CUBE724431	41.3	46.2	13.20	1.54	5.59	5.78	2.449E–08	12.30	4.70E–01
7H-7, 39–41	65.80	CUBE724441	69.7	74.6	12.38	1.39	5.58	9.35	4.217E–08	11.41	8.19E–01
8H-1, 84–86	66.75	CUBE725011	49.4	54.3	13.02	1.46	5.78	6.57	2.917E–08	7.33	8.96E–01
8H-2, 84–86	68.25	CUBE725021	1.6	6.5	13.90	1.64	5.68	0.80	3.252E–09	2.46	3.24E–01
8H-3, 84–86	69.75	CUBE725031	–9.8	–4.9	14.18	1.66	5.79	–0.60	–2.434E–09	0.43	
8H-4, 84–86	71.25	CUBE725041	–7.6	–2.7	13.10	1.60	5.30	–0.36	–1.464E–09	0.82	
8H-5, 84–86	72.75	CUBE725051	13.6	18.5	12.88	1.59	5.20	2.49	1.006E–08	3.79	6.57E–01

Table T19 (continued). (Continued on next page.)

Core, section, interval (cm)	Depth CSF (m)	LIMS ID	Susceptibility Raw (10^{-6})	Susceptibility Corrected (10^{-6})	Total mass (g)	Bulk density (g/cm^3)	Volume (cm^3)	Susceptibility Volume normalized (10^{-5})	Susceptibility Mass normalized (m^3/kg)	Susceptibility Whole core (raw values)	Scale factor
8H-6, 84–86	74.25	CUBE725061	–6.0	–1.1	13.41	1.55	5.68	–0.14	–5.888E–10	1.38	
8H-7, 49–51	75.40	CUBE725071	–5.6	–0.7	14.16	1.56	6.12	–0.08	–3.470E–10	0.85	
9H-1, 84–86	76.25	CUBE726251	–5.3	–0.4	13.89	1.64	5.65	–0.04	–1.814E–10	–0.05	
9H-2, 84–86	77.75	CUBE726261	–5.7	–0.8	14.39	1.66	5.89	–0.09	–3.663E–10	0.60	
9H-3, 84–86	79.25	CUBE726271	–0.1	4.8	14.09	1.62	5.87	0.57	2.388E–09	1.36	
9H-4, 84–86	80.75	CUBE726281	2.7	7.6	12.37	1.64	4.73	1.13	4.308E–09	1.68	
9H-5, 84–86	82.25	CUBE726291	–4.0	0.9	13.64	1.53	5.92	0.11	4.588E–10	0.34	
9H-6, 84–86	83.75	CUBE726301	–5.6	–0.7	13.12	1.67	5.12	–0.09	–3.505E–10	–0.27	
10H-1, 84–86	85.75	CUBE727371	–7.7	–2.8	11.36	1.65	4.11	–0.48	–1.746E–09	–0.76	
10H-2, 84–86	87.25	CUBE727381	–10.1	–5.2	13.65	1.69	5.37	–0.68	–2.667E–09	–0.98	
10H-3, 84–86	88.75	CUBE727391	–9.7	–4.8	13.07	1.77	4.79	–0.71	–2.590E–09	–1.05	
10H-4, 84–86	90.25	CUBE727401	–11.6	–6.7	14.30	1.66	5.87	–0.80	–3.285E–09	–0.88	
10H-5, 84–86	91.75	CUBE727411	–9.0	–4.1	12.70	1.65	4.92	–0.59	–2.269E–09	–0.92	
10H-6, 84–86	93.25	CUBE727421	–7.9	–3.0	9.92	1.72	3.11	–0.67	–2.101E–09	–1.00	
10H-7, 74–76	94.65	CUBE727431	–4.9	–0.0	12.46	1.65	4.76	–0.00	–1.854E–11	–0.97	
11H-1, 84–86	95.25	CUBE728351	–6.0	–1.1	12.58	1.65	4.86	–0.16	–6.037E–10	–1.49	
11H-2, 84–86	96.75	CUBE728361	–2.1	2.8	14.62	1.54	6.52	0.30	1.345E–09	–0.82	
11H-3, 84–86	98.25	CUBE728371	–4.3	0.6	14.39	1.63	5.99	0.07	2.841E–10	–0.83	
11H-4, 84–86	99.75	CUBE728381	–9.3	–4.4	14.86	1.69	6.07	–0.51	–2.066E–09	–1.24	
11H-5, 84–86	101.25	CUBE728391	–7.9	–3.0	13.78	1.63	5.63	–0.38	–1.533E–09	–1.21	
11H-6, 84–86	102.75	CUBE728401	–1.2	3.7	14.22	1.64	5.88	0.44	1.814E–09	–0.83	
12H-1, 84–86	104.75	CUBE729601	–8.6	–3.7	14.66	1.65	6.09	–0.43	–1.767E–09	–0.93	
12H-2, 84–86	106.25	CUBE729611	–6.8	–1.9	13.39	1.62	5.42	–0.24	–9.818E–10	–0.90	
12H-3, 84–86	107.75	CUBE729621	–5.7	–0.8	14.29	1.62	5.98	–0.10	–4.076E–10	–0.63	
12H-4, 84–86	109.25	CUBE729631	–3.2	1.7	13.69	1.58	5.77	0.21	8.713E–10	0.14	
12H-5, 84–86	110.75	CUBE729641	–5.1	–0.2	14.74	1.71	5.95	–0.02	–8.548E–11	0.33	
12H-6, 59–61	112.00	CUBE729651	–2.4	2.5	14.98	1.70	6.11	0.29	1.182E–09	–0.08	
12H-7, 59–61	113.50	CUBE729661	1.2	6.1	14.02	1.68	5.60	0.76	3.038E–09	1.25	
13H-1, 104–106	114.45	CUBE730671	17.9	22.8	13.83	1.65	5.60	2.85	1.154E–08	1.32	
13H-2, 84–86	115.75	CUBE730681	5.8	10.7	14.53	1.68	5.93	1.26	5.133E–09	1.01	
13H-3, 84–86	117.25	CUBE730701	10.8	15.7	14.20	1.62	5.95	1.85	7.759E–09	0.79	
13H-4, 84–86	118.75	CUBE730711	–0.4	4.5	13.73	1.68	5.43	0.58	2.275E–09	1.57	
13H-5, 84–86	120.25	CUBE730721	19.2	24.1	14.68	1.62	6.24	2.71	1.151E–08	4.47	6.05E–01
13H-6, 84–86	121.75	CUBE730731	12.2	17.1	14.71	1.66	6.08	1.97	8.156E–09	1.79	
13H-7, 59–61	123.00	CUBE730691	8.2	13.1	13.72	1.69	5.40	1.70	6.697E–09	2.10	8.09E–01
14H-1, 84–86	123.75	CUBE731601	2.6	7.5	14.19	1.74	5.51	0.95	3.681E–09	0.43	
14H-2, 84–86	125.25	CUBE731611	35.1	40.0	13.11	1.53	5.55	5.04	2.135E–08	2.85	1.77E+00
14H-3, 84–86	126.75	CUBE731621	34.0	38.9	13.62	1.57	5.76	4.73	2.001E–08	2.09	2.26E+00
14H-4, 84–86	128.25	CUBE731631	34.4	39.3	13.97	1.65	5.69	4.83	1.969E–08	3.29	1.47E+00
14H-5, 84–86	129.75	CUBE731641	30.7	35.6	14.36	1.66	5.89	4.24	1.737E–08	1.87	
14H-6, 84–86	131.25	CUBE731651	3.5	8.4	14.11	1.70	5.60	1.05	4.173E–09	0.50	
14H-7, 69–71	132.60	CUBE731661	16.7	21.6	14.59	1.62	6.19	2.44	1.036E–08	2.75	8.86E–01
15H-1, 84–86	133.25	CUBE731781	17.8	22.7	14.40	1.62	6.04	2.63	1.102E–08	3.85	6.82E–01
15H-2, 74–76	134.65	CUBE731791	22.1	27.0	13.29	1.59	5.46	3.46	1.420E–08	3.84	9.01E–01
15H-3, 84–86	135.75	CUBE731801	0.6	5.5	12.81	1.64	5.01	0.77	2.993E–09	1.27	
15H-4, 84–86	137.25	CUBE731811	12.8	17.7	14.77	1.69	6.03	2.05	8.374E–09	3.72	5.52E–01
15H-5, 84–86	138.75	CUBE731821	22.7	27.6	14.66	1.67	6.02	3.21	1.318E–08	2.59	1.24E+00
15H-6, 84–86	140.25	CUBE731831	34.8	39.7	14.46	1.64	6.03	4.61	1.924E–08	3.79	1.22E+00
15H-7, 49–51	141.40	CUBE731841	21.0	25.9	14.58	1.67	5.99	3.03	1.245E–08	2.54	1.19E+00
16H-1, 84–86	142.75	CUBE732281	72.6	77.5	14.42	1.64	5.99	9.06	3.762E–08	4.75	1.91E+00

Table T19 (continued). (Continued on next page.)

Core, section, interval (cm)	Depth CSF (m)	LIMS ID	Susceptibility Raw (10^{-6})	Susceptibility Corrected (10^{-6})	Total mass (g)	Bulk density (g/cm^3)	Volume (cm^3)	Susceptibility Volume normalized (10^{-5})	Susceptibility Mass normalized (m^3/kg)	Susceptibility Whole core (raw values)	Scale factor
16H-2, 84–86	144.25	CUBE732291	5.5	10.4	14.07	1.69	5.62	1.30	5.193E–09	0.69	
16H-3, 84–86	145.75	CUBE732301	56.4	61.3	13.62	1.50	6.00	7.15	3.150E–08	5.18	1.38E+00
16H-4, 84–86	147.25	CUBE732311	13.9	18.8	14.44	1.69	5.82	2.27	9.128E–09	2.21	1.02E+00
16H-5, 84–86	148.75	CUBE732321	14.2	19.1	14.42	1.73	5.69	2.35	9.272E–09	2.81	8.36E–01
17H-1, 84–86	152.25	CUBE732671	22.3	27.2	13.83	1.52	6.07	3.13	1.376E–08	2.88	1.09E+00
17H-2, 84–86	153.75	CUBE732701	5.5	10.4	14.78	1.64	6.20	1.18	4.936E–09	0.91	
17H-3, 84–86	155.25	CUBE732711	5.3	10.2	14.70	1.69	6.00	1.20	4.879E–09	1.90	
17H-4, 84–86	156.75	CUBE732721	–6.2	–1.3	14.40	1.64	5.99	–0.15	–6.281E–10	1.23	
17H-5, 84–86	158.25	CUBE732731	14.8	19.7	14.75	1.58	6.43	2.14	9.354E–09	5.74	3.74E–01
17H-6, 74–76	159.65	CUBE732681	95.9	100.8	14.03	1.47	6.40	11.02	5.030E–08	8.73	1.26E+00
17H-7, 49–51	160.90	CUBE732691	85.9	90.8	13.98	1.63	5.77	11.03	4.548E–08	8.24	1.34E+00
18H-1, 84–86	161.75	CUBE733251	18.3	23.2	12.43	1.60	4.90	3.31	1.304E–08	5.87	5.63E–01
18H-2, 84–86	163.25	CUBE733261	16.1	21.0	13.89	1.62	5.76	2.55	1.057E–08	4.53	5.63E–01
18H-3, 84–86	164.75	CUBE733271	10.0	14.9	14.07	1.62	5.84	1.78	7.399E–09	3.48	5.12E–01
18H-4, 84–86	166.25	CUBE733281	35.6	40.5	14.50	1.66	5.97	4.75	1.954E–08	6.97	6.81E–01
18H-5, 84–86	167.75	CUBE733291	26.6	31.5	14.32	1.66	5.88	3.75	1.541E–08	4.19	8.95E–01
18H-6, 84–86	169.25	CUBE733301	77.7	82.6	13.70	1.58	5.76	10.04	4.218E–08	6.92	1.45E+00
19H-1, 84–86	171.25	CUBE733691	26.3	31.2	14.42	1.68	5.83	3.74	1.514E–08	9.69	3.86E–01
19H-2, 84–86	172.75	CUBE733701	43.1	48.0	13.68	1.56	5.82	5.76	2.454E–08	10.79	5.34E–01
19H-3, 84–86	174.25	CUBE733711	54.7	59.6	14.04	1.58	5.98	6.97	2.971E–08	10.61	6.58E–01
19H-4, 84–86	175.75	CUBE733721	17.3	22.2	12.53	1.59	4.99	3.11	1.237E–08	10.23	3.03E–01
19H-5, 84–86	177.25	CUBE733731	46.4	51.3	14.37	1.54	6.33	5.67	2.500E–08	10.25	5.53E–01
19H-6, 84–86	178.75	CUBE733741	81.0	85.9	14.19	1.54	6.24	9.63	4.237E–08	14.95	6.44E–01
19H-7, 59–61	180.00	CUBE733751	56.7	61.6	14.21	1.49	6.44	6.70	3.035E–08	8.48	7.89E–01
20H-1, 84–86	180.75	CUBE734301	37.0	41.9	13.65	1.68	5.40	5.43	2.150E–08	7.62	7.13E–01
20H-2, 84–86	182.25	CUBE734311	30.5	35.4	14.06	1.61	5.90	4.21	1.764E–08	6.37	6.60E–01
20H-3, 84–86	183.75	CUBE734321	21.1	26.0	14.30	1.62	5.98	3.04	1.272E–08	5.50	5.53E–01
20H-4, 84–86	185.25	CUBE734331	9.7	14.6	13.70	1.68	5.41	1.89	7.478E–09	5.50	3.45E–01
20H-5, 84–86	186.75	CUBE734341	27.1	32.0	14.10	1.60	5.92	3.78	1.590E–08	7.91	4.78E–01
20H-6, 84–86	188.25	CUBE734351	79.9	84.8	14.11	1.57	6.06	9.79	4.209E–08	10.54	9.29E–01
20H-7, 59–61	189.50	CUBE734361	66.4	71.3	14.23	1.62	5.96	8.38	3.507E–08	10.13	8.27E–01
21H-1, 84–86	190.25	CUBE734901	19.7	24.6	14.80	1.68	6.07	2.83	1.162E–08	4.42	6.41E–01
21H-2, 84–86	191.75	CUBE734911	4.2	9.1	13.65	1.63	5.56	1.15	4.682E–09	4.61	2.49E–01
21H-3, 84–86	193.25	CUBE734921	41.8	46.7	15.09	1.65	6.37	5.14	2.167E–08	7.76	6.62E–01
21H-4, 84–86	194.75	CUBE734931	27.7	32.6	14.14	1.74	5.48	4.16	1.614E–08	7.16	5.81E–01
21H-5, 84–86	196.25	CUBE734941	16.0	20.9	14.51	1.75	5.68	2.57	1.006E–08	4.34	5.91E–01
21H-6, 94–96	197.85	CUBE734951	21.5	26.4	14.12	1.66	5.75	3.21	1.307E–08	5.82	5.52E–01
22H-1, 119–121	200.10	CUBE735481	11.9	16.8	13.03	1.53	5.53	2.12	9.015E–09	3.62	5.86E–01
22H-2, 84–86	201.25	CUBE735531	9.3	14.2	13.31	1.67	5.21	1.91	7.455E–09	2.73	6.97E–01
22H-3, 84–86	202.75	CUBE735471	8.9	13.8	13.73	1.64	5.56	1.74	7.047E–09	3.23	5.39E–01
22H-4, 84–86	204.25	CUBE735491	16.3	21.2	13.51	1.57	5.68	2.61	1.097E–08	2.15	1.21E+00
22H-5, 84–86	205.75	CUBE735501	–0.8	4.1	14.56	1.71	5.84	0.50	1.992E–09	0.62	
22H-6, 84–86	207.25	CUBE735511	6.3	11.2	14.09	1.65	5.74	1.37	5.578E–09	1.51	
22H-7, 49–51	208.40	CUBE735521	1.9	6.8	14.53	1.62	6.12	0.78	3.298E–09	1.14	
23H-2, 89–91	210.80	CUBE736691	–4.8	0.1	13.43	1.70	5.21	0.01	3.909E–11	2.40	4.20E–03
23H-3, 84–86	212.25	CUBE736701	–5.7	–0.8	13.81	1.69	5.47	–0.11	–4.283E–10	1.37	
23H-4, 84–86	213.75	CUBE736711	6.2	11.1	14.63	1.69	5.95	1.30	5.294E–09	3.28	3.97E–01
23H-5, 84–86	215.25	CUBE736721	–2.1	2.8	14.76	1.79	5.68	0.35	1.338E–09	2.41	1.44E–01
23H-6, 84–86	216.75	CUBE736731	2.1	7.0	13.87	1.71	5.43	0.90	3.530E–09	2.16	4.18E–01
23H-7, 39–41	217.80	CUBE736741	2.5	7.4	14.66	1.75	5.75	0.90	3.516E–09	1.36	

Table T19 (continued). (Continued on next page.)

Core, section, interval (cm)	Depth CSF (m)	LIMS ID	Susceptibility Raw (10^{-6})	Susceptibility Corrected (10^{-6})	Total mass (g)	Bulk density (g/cm^3)	Volume (cm^3)	Susceptibility Volume normalized (10^{-5})	Susceptibility Mass normalized (m^3/kg)	Susceptibility Whole core (raw values)	Scale factor
24H-1, 84–86	218.75	CUBE738071	0.6	5.5	14.71	1.78	5.70	0.67	2.598E–09	–0.33	
24H-2, 84–86	220.25	CUBE738091	–0.6	4.3	14.02	1.60	5.88	0.51	2.141E–09	–0.34	
24H-3, 84–86	221.75	CUBE738101	–2.3	2.6	13.47	1.74	5.09	0.35	1.328E–09	–0.52	
24H-4, 84–86	223.25	CUBE738111	–8.9	–4.0	14.54	1.81	5.48	–0.51	–1.913E–09	–0.55	
24H-5, 84–86	224.75	CUBE738121	–5.9	–1.0	14.54	1.76	5.65	–0.12	–4.829E–10	–0.79	
24H-6, 84–86	226.25	CUBE738131	–5.0	–0.1	14.77	1.73	5.90	–0.02	–7.014E–11	–0.55	
24H-7, 59–61	227.50	CUBE738081	–5.8	–0.9	13.86	1.73	5.35	–0.11	–4.323E–10	–1.01	
25H-1, 84–86	228.25	CUBE738751	–7.1	–2.2	15.19	1.72	6.16	–0.24	–9.935E–10	–1.64	
25H-2, 84–86	229.75	CUBE738771	–6.7	–1.8	13.64	1.73	5.23	–0.25	–9.412E–10	–1.67	
25H-3, 84–86	231.25	CUBE738781	–7.8	–2.9	14.47	1.71	5.76	–0.35	–1.393E–09	–1.83	
25H-4, 84–86	232.75	CUBE738791	–8.0	–3.1	13.86	1.71	5.43	–0.39	–1.540E–09	–1.89	
25H-5, 84–86	234.25	CUBE738801	–8.1	–3.2	13.68	1.71	5.32	–0.42	–1.635E–09	–1.19	
25H-6, 84–86	235.75	CUBE738811	–8.7	–3.8	14.35	1.59	6.15	–0.43	–1.840E–09	–1.34	
25H-7, 34–36	236.75	CUBE738761	–9.7	–4.8	13.37	1.56	5.64	–0.59	–2.511E–09	–0.98	
26H-1, 84–86	237.75	CUBE739761	–8.4	–3.5	14.72	1.57	6.45	–0.38	–1.669E–09	–0.91	
26H-2, 84–86	239.25	CUBE739781	–6.6	–1.7	13.99	1.72	5.47	–0.22	–8.416E–10	–1.02	
26H-3, 84–86	240.75	CUBE739791	–7.1	–2.2	13.88	1.69	5.48	–0.28	–1.105E–09	–0.95	
26H-4, 84–86	242.25	CUBE739801	–6.1	–1.2	13.70	1.71	5.34	–0.16	–6.254E–10	–0.15	
26H-5, 84–86	243.75	CUBE739811	–2.2	2.7	14.65	1.77	5.70	0.33	1.281E–09	0.16	
26H-6, 84–86	245.25	CUBE739821	3.4	8.3	14.35	1.72	5.68	1.02	4.029E–09	1.42	
26H-7, 64–66	246.55	CUBE739771	7.3	12.2	14.34	1.69	5.78	1.47	5.946E–09	0.10	
27H-1, 84–86	247.25	CUBE740511	–2.9	2.0	14.64	1.72	5.85	0.24	9.563E–10	–1.51	
27H-2, 84–86	248.75	CUBE740521	–0.4	4.5	14.36	1.71	5.72	0.55	2.198E–09	–0.16	
27H-3, 84–86	250.25	CUBE740531	0.1	5.0	14.44	1.72	5.71	0.61	2.430E–09	–0.68	
27H-4, 84–86	251.75	CUBE740541	–1.8	3.1	14.26	1.75	5.52	0.39	1.524E–09	–0.92	
27H-5, 84–86	253.25	CUBE740551	–0.4	4.5	15.72	1.73	6.42	0.49	2.017E–09	–0.69	
27H-6, 84–86	254.75	CUBE740561	6.1	11.0	14.50	1.73	5.71	1.35	5.330E–09	–0.03	
28H-1, 84–86	256.75	CUBE741121	5.8	10.7	14.80	1.71	5.97	1.25	5.045E–09	1.47	
28H-2, 84–86	258.25	CUBE741141	3.8	8.7	14.57	1.70	5.87	1.03	4.163E–09	1.21	
28H-3, 84–86	259.75	CUBE741151	1.6	6.5	14.96	1.70	6.11	0.74	3.025E–09	0.83	
28H-4, 84–86	261.25	CUBE741161	3.4	8.3	15.11	1.78	5.90	0.99	3.850E–09	0.71	
28H-5, 84–86	262.75	CUBE741171	1.5	6.4	15.33	1.76	6.10	0.74	2.924E–09	0.43	
28H-6, 84–86	264.25	CUBE741181	–3.0	1.9	14.39	1.84	5.33	0.25	9.150E–10	–0.72	
28H-7, 59–61	265.50	CUBE741131	–4.0	0.9	13.90	1.79	5.19	0.12	4.563E–10	–0.33	
29H-1, 84–86	266.25	CUBE741711	–0.4	4.5	16.13	1.80	6.42	0.49	1.952E–09	–0.12	
29H-2, 84–86	267.75	CUBE741731	0.7	5.6	11.36	1.73	3.92	1.01	3.473E–09	0.19	
29H-3, 84–86	269.25	CUBE741741	–3.4	1.5	12.83	1.72	4.80	0.22	8.348E–10	–0.04	
29H-4, 84–86	270.75	CUBE741751	0.9	5.8	14.29	1.75	5.54	0.74	2.852E–09	0.29	
29H-5, 84–86	272.25	CUBE741761	–1.8	3.1	15.15	1.75	6.05	0.35	1.413E–09	–1.70	
29H-6, 84–86	273.75	CUBE741771	3.6	8.5	14.83	1.84	5.55	1.07	4.021E–09	–3.08	
29H-7, 59–61	275.00	CUBE741721	–7.9	–3.0	14.80	1.89	5.40	–0.39	–1.438E–09	–2.90	
30H-1, 84–86	275.75	CUBE742871	–9.2	–4.3	15.80	1.80	6.23	–0.49	–1.914E–09	0.51	
30H-2, 84–86	277.25	CUBE742891	–9.2	–4.3	15.11	1.78	5.92	–0.50	–1.978E–09	0.32	
30H-3, 84–86	278.75	CUBE742901	–7.6	–2.7	15.32	1.76	6.10	–0.31	–1.222E–09	–0.06	
30H-4, 84–86	280.25	CUBE742911	–5.5	–0.6	15.57	1.77	6.22	–0.07	–2.819E–10	0.42	
30H-5, 84–86	281.75	CUBE742921	–5.6	–0.7	14.70	1.75	5.79	–0.08	–3.338E–10	0.22	
30H-6, 84–86	283.25	CUBE742931	–3.8	1.1	15.76	1.76	6.35	0.13	5.081E–10	0.42	
30H-7, 59–61	284.50	CUBE742881	–1.3	3.6	14.38	1.76	5.56	0.45	1.746E–09	0.86	
31H-1, 84–86	285.25	CUBE744131	–9.2	–4.3	14.67	1.77	5.69	–0.53	–2.038E–09	0.86	
31H-2, 84–86	286.75	CUBE744141	–7.8	–2.9	15.66	1.78	6.23	–0.33	–1.305E–09	0.68	

Table T19 (continued). (Continued on next page.)

Core, section, interval (cm)	Depth CSF (m)	LIMS ID	Susceptibility Raw (10^{-6})	Susceptibility Corrected (10^{-6})	Total mass (g)	Bulk density (g/cm^3)	Volume (cm^3)	Susceptibility Volume normalized (10^{-5})	Susceptibility Mass normalized (m^3/kg)	Susceptibility Whole core (raw values)	Scale factor
31H-3, 84–86	288.25	CUBE744151	–7.3	–2.4	14.73	1.78	5.71	–0.29	–1.123E–09	0.44	
31H-4, 84–86	289.75	CUBE744161	–7.6	–2.7	14.60	1.81	5.54	–0.35	–1.318E–09	0.33	
31H-5, 94–96	291.35	CUBE744171	–5.3	–0.4	14.66	1.80	5.59	–0.06	–2.125E–10	0.41	
31H-6, 84–86	292.75	CUBE744181	–8.0	–3.1	15.37	1.80	5.98	–0.36	–1.389E–09	0.30	
31H-7, 69–71	294.10	CUBE744191	–8.3	–3.4	14.40	1.81	5.42	–0.44	–1.649E–09	0.59	
32H-1, 84–86	294.75	CUBE744711	–5.0	–0.1	14.63	1.80	5.58	–0.01	–4.163E–11	1.24	
32H-2, 84–86	296.25	CUBE744721	–8.9	–4.0	15.37	1.80	5.99	–0.46	–1.800E–09	0.87	
32H-3, 84–86	297.75	CUBE744731	–8.3	–3.4	15.42	1.80	6.02	–0.39	–1.541E–09	0.48	
32H-4, 84–86	299.25	CUBE744741	–9.9	–5.0	13.81	1.78	5.19	–0.67	–2.522E–09	0.43	
32H-5, 109–111	301.00	CUBE744751	–9.0	–4.1	15.28	1.74	6.14	–0.46	–1.866E–09	0.74	
32H-6, 84–86	302.25	CUBE744761	–7.8	–2.9	14.97	1.81	5.73	–0.35	–1.341E–09	1.44	
32H-7, 49–51	303.40	CUBE744771	–6.8	–1.9	15.23	1.81	5.88	–0.23	–8.871E–10	0.20	
33H-1, 94–96	304.35	CUBE745891	–8.3	–3.4	14.80	1.82	5.62	–0.42	–1.608E–09	–1.30	
33H-2, 84–86	305.75	CUBE745901	–4.8	0.1	14.67	1.72	5.85	0.01	4.867E–11	–1.19	
33H-3, 84–86	307.25	CUBE745911	–7.4	–2.5	14.54	1.77	5.61	–0.32	–1.219E–09	–0.87	
33H-4, 84–86	308.75	CUBE745921	–8.2	–3.3	14.89	1.80	5.71	–0.40	–1.532E–09	–1.30	
33H-5, 84–86	310.25	CUBE745931	–6.6	–1.7	14.88	1.74	5.93	–0.20	–7.969E–10	–1.03	
33H-6, 84–86	311.75	CUBE745941	–7.5	–2.6	15.68	1.71	6.50	–0.28	–1.179E–09	–0.98	
33H-7, 69–71	313.10	CUBE745951	–9.1	–4.2	15.40	1.76	6.14	–0.48	–1.919E–09	–0.85	
34H-1, 84–86	313.75	CUBE746381	–8.5	–3.6	14.24	1.81	5.32	–0.47	–1.765E–09	–0.11	
34H-3, 84–86	315.35	CUBE746391	–7.8	–2.9	14.31	1.81	5.38	–0.38	–1.411E–09	–0.23	
34H-4, 84–86	316.85	CUBE746401	–7.7	–2.8	14.29	1.66	5.84	–0.33	–1.365E–09	0.50	
34H-5, 84–86	318.35	CUBE746411	–7.3	–2.4	15.09	1.86	5.66	–0.30	–1.111E–09	0.13	
34H-6, 84–86	319.85	CUBE746421	–8.9	–4.0	14.64	1.84	5.47	–0.52	–1.932E–09	–0.02	
34H-7, 70–72	321.21	CUBE746431	–3.2	1.8	13.96	1.79	5.23	0.23	8.775E–10	0.51	
35H-1, 84–86	323.25	CUBE747471	–8.8	–3.9	15.10	1.79	5.87	–0.47	–1.813E–09	0.40	
35H-2, 84–86	324.75	CUBE747481	–8.5	–3.6	14.67	1.82	5.54	–0.46	–1.727E–09	0.42	
35H-3, 84–86	326.25	CUBE747501	–8.6	–3.7	14.69	1.81	5.57	–0.46	–1.754E–09	0.41	
35H-4, 84–86	327.75	CUBE747521	–8.7	–3.8	14.81	1.83	5.59	–0.48	–1.806E–09	0.45	
35H-5, 84–86	329.25	CUBE747531	–7.8	–2.9	15.12	1.84	5.72	–0.35	–1.325E–09	0.26	
35H-6, 84–86	330.75	CUBE747541	–9.4	–4.5	15.65	1.69	6.54	–0.48	–2.007E–09	0.27	
35H-7, 84–86	332.25	CUBE747551	–8.4	–3.5	15.15	1.83	5.78	–0.43	–1.621E–09	0.07	
36H-1, 84–86	332.75	CUBE747901	–10.6	–5.7	14.80	1.78	5.73	–0.69	–2.677E–09	0.51	
36H-2, 84–86	334.25	CUBE747911	–8.4	–3.5	14.29	1.77	5.47	–0.45	–1.738E–09	1.35	
36H-3, 84–86	335.75	CUBE747921	–5.4	–0.5	14.69	1.81	5.59	–0.06	–2.297E–10	0.81	
36H-4, 84–86	337.25	CUBE747931	–7.4	–2.5	14.29	1.82	5.34	–0.33	–1.215E–09	0.03	
36H-5, 84–86	338.75	CUBE747941	–11.0	–6.1	14.54	1.80	5.53	–0.77	–2.946E–09	–0.16	
36H-6, 84–86	340.25	CUBE747951	–2.6	2.3	15.44	1.78	6.08	0.26	1.028E–09	0.94	
36H-7, 54–56	341.45	CUBE747961	–5.7	–0.8	14.80	1.78	5.73	–0.10	–3.930E–10	–0.28	
38X-3, 86–88	354.97	CUBE749861	–6.2	–1.3	12.87	1.75	4.73	–0.20	–7.326E–10	–0.05	
38X-5, 113–115	358.24	CUBE749871	–9.1	–4.2	13.71	1.71	5.32	–0.55	–2.132E–09	0.48	
39X-3, 94–96	364.65	CUBE750471	–6.9	–2.0	13.75	1.84	4.99	–0.28	–1.014E–09	0.77	
39X-5, 80–82	367.51	CUBE750481	–8.0	–3.1	12.72	1.84	4.42	–0.50	–1.727E–09	1.18	
40X-2, 84–86	372.55	CUBE751501	–5.8	–0.9	12.38	1.75	4.44	–0.14	–5.174E–10	1.18	
40X-3, 89–91	374.10	CUBE751511	–8.2	–3.3	12.46	1.77	4.43	–0.52	–1.837E–09	1.74	
40X-4, 76–78	375.47	CUBE751521	–1.3	3.6	14.50	1.74	5.68	0.45	1.746E–09	5.10	8.75E–02
41X-2, 69–71	381.90	CUBE751981	–3.4	1.5	14.62	1.88	5.34	0.19	7.019E–10	7.42	2.59E–02
41X-3, 89–91	383.60	CUBE751991	–5.9	–1.0	15.63	1.91	5.78	–0.13	–4.622E–10	1.16	
41X-5, 36–38	386.07	CUBE752001	0.2	5.1	13.88	1.93	4.82	0.74	2.557E–09	0.44	
42X-2, 119–121	391.90	CUBE752811	3.1	8.0	14.15	1.84	5.20	1.07	3.945E–09	–0.34	

Table T19 (continued).

Core, section, interval (cm)	Depth CSF (m)	LIMS ID	Susceptibility Raw (10^{-6})	Susceptibility Corrected (10^{-6})	Total mass (g)	Bulk density (g/cm^3)	Volume (cm^3)	Susceptibility Volume normalized (10^{-5})	Susceptibility Mass normalized (m^3/kg)	Susceptibility Whole core (raw values)	Scale factor
42X-3, 68–70	392.89	CUBE752821	2.4	7.3	14.74	1.87	5.42	0.94	3.457E–09	–0.34	
42X-4, 74–76	394.45	CUBE752831	1.5	6.4	12.47	1.86	4.24	1.06	3.608E–09	0.26	
43X-2, 89–91	401.20	CUBE753431	6.5	11.4	14.39	1.91	5.12	1.56	5.539E–09	1.88	
43X-4, 126–128	404.57	CUBE753441	8.3	13.2	12.95	1.88	4.45	2.08	7.133E–09	3.02	6.88E–01
43X-6, 89–91	407.20	CUBE753451	20.8	25.7	12.72	1.85	4.39	4.10	1.416E–08	2.97	1.38E+00
44X-2, 84–86	410.75	CUBE754401	9.2	14.1	13.12	1.90	4.48	2.20	7.524E–09	2.64	8.34E–01
44X-4, 119–121	414.10	CUBE754411	23.4	28.3	13.56	2.02	4.45	4.45	1.460E–08	7.61	5.85E–01
44X-6, 74–76	416.65	CUBE754421	45.6	50.5	13.08	1.95	4.35	8.12	2.703E–08	10.09	8.05E–01
										Mean scale factor:	7.77E–01

Notes: Depth = depth to middle of discrete sample measured in meters using the core depth below seafloor, method A (CSF), depth scale. LIMS ID = sample identification within the Laboratory Information Management System (LIMS) database. Susceptibility raw = volume magnetic susceptibility (in SI units) of the discrete sample measured in the Kappabridge with the volume of the cube assumed to be 7 cm^3. Susceptibility corrected = the susceptibility of the plastic cube with a label was determined to be –4.9E–06 (SI) with a standard error of ±0.19E–06. Mass = mass of sample including mass of plastic cube, which has a mean of 4.5921 g. Bulk density = density from moisture and density (MAD) measurements. When these were not available or were obviously anomalous, we used a density of 1.2 m^3/kg. Volume = volume of sediments, calculated by subtracting mass of plastic cube from total mass and then dividing by bulk density. Volume normalized susceptibility = susceptibility of discrete samples normalized by true sample volume. These are unitless in the SI unit system. Mass normalized susceptibility = susceptibility of discrete samples normalize by mass of sediments in each sample cube. Scale factor = factor whole-core raw susceptibility values would need to be multiplied by to convert them to SI volume normalized susceptibilities.

Table T20. Magnetostratigraphy, Site U1335. (**Continued on next two pages.**)

Polarity chron	Age (Ma)	Hole U1335A				Hole U1335B			
		Range CSF (m)	Best estimate CSF (m)	Best estimate core, section, interval (cm)	Measurement type	Range CSF (m)	Best estimate CSF (m)	Best estimate core, section, interval (cm)	Measurement type
C1n	0.000	0.000–0.000	0.000	Mudline				Not recovered	
C1n–C1r.1r	0.781	5.125–5.225	5.175	1H-4, 67.50	Split core	5.775–5.850	5.813	2H-2, 101.25	Split core
C1r.1r–C1r.1n	0.988	6.375–6.450	6.413	1H-5, 41.25	Split core	6.875–6.925	6.900	2H-3, 60.00	Split core
C1r.1n–C1r.2r	1.072	6.825–6.875	6.850	1H-5, 85.00	Split core	7.275–7.375	7.325	2H-3, 102.50	Split core
C1r.2r–C1r.2n	1.173	7.450–7.525	7.488	1H-6, 28.75	Split core			Not identified	
C1r.2n–C1r.2r	1.185	7.575–7.650	7.613	1H-6, 41.25	Split core			Not identified	
C1r.2r–C2n	1.778	9.525–9.550	9.538	2H-1, 63.75	Split core	10.700–10.875	10.788	Between Sections 2H-5 and 6	Split core
C2n–C2r.1r	1.945	10.200–10.225	10.213	2H-1, 132.50	Split core	11.275–11.375	11.325	2H-6, 52.50	Split core
C2r.1r–C2r.1n	2.128	10.950–10.975	10.963	2H-2, 56.75	Split core	11.650–11.725	11.688	2H-6, 88.75	Split core
C2r.1n–C2r.2r	2.148	10.975–11.000	10.988	2H-2, 58.75	Split core	11.725–11.775	11.750	2H-6, 95.00	Split core
C2r.2r–C2An.1n	2.581	13.550–13.600	13.575	2H-4, 17.50	Split core	13.475–13.575	13.525	3H-1, 73.75	Split core
C2An.1n–C2An.1r	3.032	16.025–16.075	16.050	2H-5, 115.00	Split core	15.725–15.900	15.813	Between Sections 3H-2 and 3	Split core
C2An.1r–C2An.2n	3.116	16.275–16.300	16.288	2H-5, 138.75	Split core	16.075–16.150	16.113	3H-3, 31.25	Split core
C2An.2n–C2An.2r	3.207	16.725–16.750	16.738	2H-6, 33.75	Split core	16.525–16.625	16.575	3H-3, 77.50	Split core
C2An.2r–C2An.3n	3.330	17.175–17.225	17.200	2H-6, 80.00	Split core	17.025–17.050	17.038	3H-3, 123.75	Split core
C2An.3n–C2Ar	3.596	18.325–18.375	18.350	2H-7, 45.00	Split core	18.175–18.225	18.200	3H-4, 90.00	Split core
C2Ar–C3n.1n	4.187	20.350–20.475	20.413	3H-2, 51.25	Split core	20.500–20.550	20.525	3H-6, 22.50	Split core
C3n.1n–C3n.1r	4.300	21.125–21.275	21.200	3H-2, 130.00	Split core	21.275–21.300	21.288	3H-6, 98.75	Split core
C3n.1r–C3n.2n	4.493	22.475–22.675	22.575	3H-3, 117.50	Split core	22.275–23.125		Between Sections 3H-7 and 4H-1	Split core
C3n.2n–C3n.2r	4.631	23.575–23.625	23.600	3H-4, 70.00	Split core	22.275–23.125		Between Sections 3H-7 and 4H-1	Split core
C3n.2r–C3n.3n	4.799	24.975–25.075	25.025	3H-5, 62.50	Split core	24.025–24.075	24.050	4H-2, 25.00	Split core
C3n.3n–C3n.3r	4.896	25.650–25.700	25.675	3H-5, 127.50	Split core	24.675–24.725	24.700	4H-2, 90.00	Split core
C3n.3r–C3n.4n	4.997	26.200–26.300	26.250	3H-6, 35.00	Split core	25.125–25.175	25.150	4H-2, 135.00	Split core
C3n.4n–C3r	5.235	27.925–29.125	28.525	Between Sections 3H-7 and 4H-1	Split core	26.900–26.925	26.913	4H-4, 11.25	Split core
Excursion C3r-1 ?				Not identified		27.325–27.375	27.350	4H-4, 55.00	Split core
Excursion C3r-2 ?				Not identified		28.550–28.575	28.563	4H-5, 26.25	Split core
Excursion C3r-3 ?				Not identified		28.900–28.950	28.925	4H-5, 62.50	Split core
Excursion C3r-4 ?				Not identified		29.925–29.975	29.950	4H-6, 15.00	Split core
Excursion C3r-5 ?				Not identified		30.825–30.875	30.850	4H-6, 105.00	Split core
C3r–C3An.1n	6.033	30.775–31.400	31.088	4H-3, 25.00	Split core	31.225–31.375	31.300	Between Sections 4H-4 and 5	Split core
C3An.1n–C3An.1r	6.252	33.225–33.450	33.338	4H-4, 93.75	Split core	32.150–32.225	32.188	5H-1, 38.75	Split core
C3An.1r–C3An.2n	6.436	34.675–34.775	34.725	4H-5, 82.50	Split core	33.525–33.575	33.550	5H-2, 25.00	Split core
C3An.2n–C3Ar	6.733	36.975–37.025	37.000	4H-7, 10.00	Split core	35.875–35.950	35.913	5H-3, 112.50	Split core
C3Ar–C3Bn	7.140	38.400–38.450	38.425	5H-1, 102.50	Split core	38.850–38.875	38.863	5H-5, 106.25	Split core
C3Bn–C3Br.1r	7.212	38.575–38.625	38.600	5H-1, 120.00	Split core	39.025–39.075	39.050	5H-5, 125.00	Split core
C3Br.1r–C3Br.1n	7.251	38.825–39.000	38.913	Between Sections 5H-1 and 2	Split core	39.225–39.375	39.300	Between Sections 5H-5 and 6	Split core
C3Br.1n–C3Br.2r	7.285	39.700–39.750	39.725	5H-2, 82.5	Split core	39.550–39.600	39.575	5H-6, 27.50	Split core
C3Br.2r–C3Br.2n	7.454	41.000–41.050	41.025	5H-3, 62.5	Split core	40.375–40.450	40.413	5H-6, 111.25	Split core
C3Br.2n–C3Br.3r	7.489	41.150–41.200	41.175	5H-3, 77.5	Split core	40.475–40.500	40.488	5H-6, 118.75	Split core
C3Br.3r–C4n.1n	7.528	41.250–41.300	41.275	5H-3, 87.5	Split core	40.525–40.600	40.563	5H-6, 126.25	Split core
C4n.1n–C4n.1r	7.642	41.350–41.450	41.400	5H-3, 100.0	Split core			Not identified	
C4n.1r–C4n.2n	7.695	41.800–42.000	41.900	Between Sections 5H-3 and 4	Split core			Not identified	
Excursion C4n.2n-1 ?		42.350–42.450	42.400	5H-4, 102.5	Split core	41.825–41.950	41.888	6H-1, 58.75	Split core
C4n.2n–C4r.1r	8.108	42.850–43.000	42.925	5H-4, 50.00	Split core	42.525–42.550	42.538	6H-1, 123.75	Split core
Excursion C4r.1r-1 ?		43.250–43.300	43.275	5H-4, 137.5	Split core	42.875–43.050	42.963	6H-2, 16.25	Split core
Excursion C4r.1r-2 ?				Not identified		43.250–43.450	43.350	6H-2, 55.00	Split core
C4r.1r–C4r.1n	8.254	44.500–44.550	44.525	5H-5, 112.5	Split core	44.375–44.400	44.388	Between Sections 6H-2 and 3	Split core
C4r.1n–C4r.2r	8.300	44.800–45.000	44.900	Between 5H-5 and 6	Split core	44.650–44.750	44.700	6H-3, 40.00	Split core
C4r.2r–C4An	8.769	48.300–48.500	48.400	Between 6H-1 and 2	Split core	48.875–48.950	48.913	6H-6, 11.25	Split core
Excursion C4An-1 ?		48.700–48.750	48.725	6H-2, 32.5	Split core	49.075–49.125	49.100	6H-6, 30.00	Split core

Table T20 (continued). (Continued on next page.)

Polarity chron	Age (Ma)	Hole U1335A Range CSF (m)	Hole U1335A Best estimate CSF (m)	Hole U1335A Best estimate core, section, interval (cm)	Hole U1335A Measurement type	Hole U1335B Range CSF (m)	Hole U1335B Best estimate CSF (m)	Hole U1335B Best estimate core, section, interval (cm)	Hole U1335B Measurement type
Excursion C4An-2 ?				Not identified		49.700–49.800	49.750	6H-6, 95.00	Split core
C4An–C4Ar.1r	9.098	56.850–56.900	56.875	7H-1, 96.25	Split core	57.225–57.275	57.250	7H-5, 45.00	Split core
Excursion C4Ar.1r-1 ?				Not identified		57.425–57.500	57.463	7H-5, 66.25	Split core
Excursion C4Ar.1r-2 ?		57.350–57.375	57.363	7H-1, 47.50	Split core	57.550–57.675	57.613	7H-5, 81.25	Split core
C4Ar.1r–C4Ar.1n	9.312	57.700–57.775	57.738	7H-1, 133.75	Split core	57.925–58.075	58.000	7H-5, 120.00	Split core
C4Ar.1n–C4Ar.2r	9.409	58.300–58.350	58.325	7H-2, 42.50	Split core	58.725–58.800	58.763	7H-6, 42.50	Split core
C4Ar.2r–C4Ar.2n	9.656	59.300–59.325	59.313	7H-2, 141.25	Split core	59.725–59.875	59.800	Between Sections 7H-6 and 7	Split core
C4Ar.2n–C4Ar.3r	9.717	59.650–59.700	59.675	7H-3, 27.50	Split core	60.075–60.125	60.100	7H-7, 30.00	Split core
C4Ar.3r–C5n.1n	9.779	59.875–59.975	59.925	7H-3, 52.50	Split core	60.325–60.400	60.363	7H-7, 56.25	Split core
C5n.1n–C5n.1r	9.934	60.775–61.000	60.888	Between Sections 7H-3 and 4	Split core	60.600–60.625		Between Sections 7H-7 and 8H-1	Split core
C5n.1r–C5n.2n	9.987	61.000–61.050	61.025	7H-4, 12.50	Split core	60.600–60.625		Between Sections 7H-7 and 8H-1	Split core
C5n.2n–C5r.1r	11.040	Below 65.95		Below 7H-7, 55.00	Split core	65.350–65.375	65.363	8H-4, 56.25	Split core
C5r.1r–C5r.1n	11.118			Not identified		66.025–66.075	66.050	8H-4, 125.00	Split core
C5r.1n–C5r.2r	11.154			Not identified		Below 66.225		Below 8H-4 142.5	Split core
C5r.2r–C5r.2n	11.554			Not identified				Not identified	
C5r.2n–C5r.3r	11.614			Not identified				Not identified	
C5r.3r–C5An.1n	12.014			Not identified				Not identified	
C5An.1n–C5An.1r	12.116			Not identified				Not identified	
C5An.1r–C5An.2n	12.207			Not identified				Not identified	
C5An.2n–C5Ar.1r	12.415			Not identified				Not identified	
C5Ar.1r–C5Ar.1n	12.730			Not identified				Not identified	
C5Ar.1n–C5Ar.2r	12.765			Not identified				Not identified	
C5Ar.2r–C5Ar.2n	12.820			Not identified				Not identified	
C5Ar.2n–C5Ar.3r	12.878			Not identified				Not identified	
C5Ar.3r–C5AAn	13.015			Not identified		Above 107.95		Above 13H-1, 15.00	Split core
C5AAn–C5AAr	13.183			Not identified		110.675–110.900	110.788	Between Sections 13H-2 and 3	Split core
C5AAr–C5ABn	13.369			Not identified		113.275–113.350	113.313	13H-2, 101.25	Split core
C5ABn–C5ABr	13.605			Not identified		117.800–117.875	117.838	14H-1, 53.75	Split core
C5ABr–C5ACn	13.734			Not identified		118.975–120.375	119.675	14H-2, 87.50	Split core
Excursion C5ACn-1 ?				Not identified		123.075–123.100	123.088	14H-4, 128.75	Split core
C5ACn–C5ACr	14.095			Not identified		123.925–124.000	123.963	14H-5, 66.25	Split core
C5ACr–C5ADn	14.194			Not identified		124.700–125.025	124.863	Between Sections 14H-5 and 6	Split core
Excursion C5ADn-1 ?				Not identified		125.875–125.975	125.925	14H-6, 112.50	Split core
Excursion C5ADn-2 ?				Not identified		130.600–130.650	130.625	15H-3, 82.50	Split core
Excursion C5ADn-3 ?				Not identified		135.100–135.150	135.125	15H-6, 82.50	Split core
C5ADn–C5ADr	14.581			Not identified		137.350–137.425	137.388	16H-1, 108.75	Split core
Excursion C5ADr-1 ?				Not identified		138.175–138.450	138.313	16H-2, 51.25	Split core
Excursion C5ADr-2 ?				Not identified		139.775–140.000	139.888	16H-3, 58.75	Split core
Excursion C5ADr-3 ?				Not identified		140.125–140.200	140.163	16H-3, 86.25	Split core
Excursion C5ADr-4 ?				Not identified		141.650–142.025	141.838	16H-4, 103.75	Split core
C5ADr–C5Bn.1n	14.784			Not identified		143.050–143.150	143.100	16H-5, 80.00	Split core
C5Bn.1n–C5Bn.1r	14.877			Not identified		145.85–146.65		Between Sections 16H-7 and 17H-1	
C5Bn.1r–C5Bn.2n	15.032			Not identified		149.175–149.375	149.275	17H-3, 47.50	Split core
Excursion C5Bn.2n-1 ?				Not identified		150.750–150.850	150.800	17H-4, 50.00	Split core
Excursion C5Bn.2n-2 ?				Not identified		151.300–151.400	151.350	17H-4, 105.00	Split core
Excursion C5Bn.2n-3 ?				Not identified		152.200–152.300	152.250	17H-5, 45.00	Split core
C5Bn.2n–C5Br	15.160	Above 155.35		Above 17H-3, 95.0	Split core	153.150–153.225	153.188	17H-5, 138.75	Split core
Excursion C5Br-1 ?				Not identified		153.775–154.000	153.888	17H-6, 58.75	Split core
Excursion C5Br-2 ?				Not identified		154.250–154.350	154.300	17H-6, 100.00	Split core
Excursion C5Br-3 ?				Not identified		158.375–158.625	158.500	18H-3, 20.00	Split core

Table T20 (continued).

Polarity chron	Age (Ma)	Hole U1335A Range CSF (m)	Hole U1335A Best estimate CSF (m)	Hole U1335A Best estimate core, section, interval (cm)	Hole U1335A Measurement type	Hole U1335B Range CSF (m)	Hole U1335B Best estimate CSF (m)	Hole U1335B Best estimate core, section, interval (cm)	Hole U1335B Measurement type
Excursion C5Br-4 ?		156.750–156.850	156.800	17H-4, 90.0	Split core	159.000–159.100	159.050	18H-3, 75.00	Split core
Excursion C5Br-5 ?		157.050–157.100	157.075	17H-4, 117.5	Split core	159.600–159.625	159.613	18H-3, 131.25	Split core
Excursion C5Br-6 ?		158.500–158.550	158.525	17H-5, 112.5	Split core	160.225–160.400	160.313	18H-4, 51.25	Split core
Excursion C5Br-7 ?		159.250–159.250	159.250	17H-6, 35.0	Split core	160.600–160.700	160.650	18H-4, 85.00	Split core
Excursion C5Br-8 ?				Not identified		161.050–161.225	161.138	18H-4, 133.75	Split core
Excursion C5Br-9 ?		162.600–163.100	162.850	18H-2, 45.0	Split core	162.725–163.250	162.988	18H-6, 25.00	Split core
C5Br–C5Cn.1n	15.974	163.750–163.400	163.575	Between Sections 18H-2 and 3	Split core	163.925–163.950	163.938	18H-6, 113.75	Split core
Excursion C5Cn-1 ?		164.200–164.200	164.200	18H-3, 30.0	Split core	164.075–164.150	164.113	18H-6, 131.25	Split core
C5Cn.1n–C5Cn.1r	16.268	169.100–169.150	169.125	18H-6, 72.5	Split core	167.300–167.425	167.363	19H-2, 106.25	Split core
Excursion C5Cn.1r-1 ?				Not identified		167.675–167.725	167.700	19H-2, 140.00	Split core
Excursion C5Cn.1r-2 ?				Not identified		167.975–167.975	167.975	19H-3, 17.50	Split core
C5Cn.1r–C5Cn.2n	16.303	Below 169.475		Below 18H-6, 107.5	Split core	168.700–168.725	168.713	19H-3, 91.25	Split core
C5Cn.2n–C5Cn.2r	16.472	Above 170.475		Above 19H-1, 7.50	Split core	169.675–169.725	169.700	19H-4, 40.00	Split core
C5Cn.2r–C5Cn.3n	16.543	171.725–171.775	171.750	19H-1, 135.00	Split core	170.925–170.950	170.938	19H-5, 13.75	Split core
C5Cn.3n–C5Cr	16.721	172.950–173.075	173.013	19H-2, 111.25	Split core	172.100–172.125	172.113	19H-5, 131.25	Split core
Excursion C5Cr-1 ?		176.650–176.700	176.675	19H-5, 27.50	Split core			Not identified	
C5Cr–C5Dn	17.235	180.125–180.00	180.063	Between Sections 19H-7 and 20H-1	Split core	177.875–177.950	177.913	20H-3, 61.25	Split core
C5Dn–C5Dr	17.533	184.250–184.500	184.375	Between Sections 20H-3 and 4	Split core	182.950–183.025	182.988	20H-6, 118.75	Split core
C5Dr–C5Dr-1	17.825	187.250–187.300	187.275	20H-5, 137.5	Split core	184.975–185.100	185.038	21H-1, 123.75	Split core
C5Dr-1–C5Dr	17.853	187.900–187.950	187.925	20H-6, 52.5	Split core	185.600–185.650	185.625	21H-2, 32.50	Split core
Excursion C5Dr-2 ?				Not identified		187.850–187.900	187.875	21H-3, 107.50	Split core
Excursion C5Dr-3 ?				Not identified		188.525–188.600	188.563	21H-4, 26.25	Split core
C5Dr–C5En	18.056	192.300–192.500	192.400	Between Sections 21H-2 and 3	Split core	191.400–191.450	191.425	21H-6, 12.50	Split core
Excursion C5En-1 ?				Not identified		198.175–198.475	198.325	22H-4, 52.50	Split core
C5En–C5Er	18.524	198.65–199.85	199.250	Between Sections 21H-7 and 22H-1	Split core	199.600–200.050	199.825	22H-5, 52.50	Split core
Excursion C5Er-1 ?		202.800–202.850	202.825	22H-3, 92.50	Split core			Not identified	
C5Er–C6n	18.748	204.400–204.500	204.450	22H-4, 105.0	Split core	Below 202.60		Below 22H-7, 30.00	
C6n–C6r	19.722	Below 208.40		Below 22H-7, 50.0	Split core			Not identified	

Table T21. Interstitial water data from squeezed whole-round samples, Site U1335. (See table notes.) (Continued on next page.)

Core, section, interval (cm)	Depth CSF (m)	pH	Alkalinity (mM)	Salinity	Cl^- (mM)	Na^+ (mM)	SO_4^{2-} (mM)	HPO_4^{2-} (µM)	H_4SiO_4 (µM)	Mn^{2+} (µM)	Fe^{2+} (µM)	Ca^{2+} (mM)	Mg^{2+} (mM)	B (µM)	Sr^{2+} (µM)	Ba^{2+} (µM)	Li^+ (µM)	K^+ (mM)
320-U1335A-																		
1H-2, 145–150	2.95	7.53	2.77	—	555	478	25.8	1.94	500	33.91	BDL	10.0	50.4	466	82	0.79	24.8	10.7
1H-4, 145–150	5.95	7.54	2.65	—	559	484	27.9	1.72	519	37.93	5.72	10.5	50.7	466	89	1.84	23.7	10.7
2H-2, 145–150	11.85	7.54	2.65	—	562	483	25.8	1.17	535	43.82	BDL	10.1	50.8	475	95	2.22	22.8	10.8
2H-5, 145–150	16.35	7.52	2.78	—	560	482	26.6	1.14	590	36.91	BDL	10.4	50.8	477	103	2.23	22.3	10.8
3H-2, 145–150	21.35	7.54	2.79	—	561	484	27.1	1.20	627	33.14	BDL	10.3	50.9	480	109	1.10	22.5	10.8
3H-5, 145–150	25.85	7.54	2.80	—	563	483	26.0	1.21	626	29.59	0.55	10.5	51.1	476	110	1.30	21.4	10.8
4H-2, 145–150	30.85	7.75	2.81	—	565	487	26.7	1.10	630	18.96	BDL	10.5	51.0	479	118	0.83	21.0	10.8
4H-5, 145–150	35.35	7.52	2.84	—	563	484	26.2	1.08	654	13.75	1.05	10.5	50.9	486	124	0.83	20.8	11.4
5H-2, 145–150	40.35	7.48	2.92	—	563	484	25.4	0.95	604	6.62	BDL	9.9	50.9	467	121	1.07	19.8	10.7
6H-2, 145–150	49.85	7.52	2.92	—	565	487	26.7	1.16	615	4.59	0.53	10.4	51.0	470	139	0.71	18.9	10.6
6H-5, 145–150	54.35	7.89	2.96	—	564	485	25.6	1.14	654	7.71	0.26	10.5	50.7	463	145	0.76	18.5	10.8
7H-3, 140–150	60.80	7.50	2.97	—	564	488	27.0	0.66	648	12.77	0.26	10.8	50.0	487	156	0.70	18.7	10.7

Table T21 (continued).

Core, section, interval (cm)	Depth CSF (m)	pH	Alkalinity (mM)	Salinity	Cl^- (mM)	Na^+ (mM)	SO_4^{2-} (mM)	HPO_4^{2-} (µM)	H_4SiO_4 (µM)	Mn^{2+} (µM)	Fe^{2+} (µM)	Ca^{2+} (mM)	Mg^{2+} (mM)	B (µM)	Sr^{2+} (µM)	Ba^{2+} (µM)	Li^+ (µM)	K^+ (mM)
8H-3, 140–150	70.30	7.48	3.02	—	562	485	25.4	0.66	603	7.66	BDL	10.2	49.9	456	153	1.05	16.3	10.5
9H-3, 145–150	78.58	7.47	2.97	—	561	485	26.2	0.71	651	3.32	1.81	10.4	49.9	461	163	1.00	15.3	10.7
10H-3, 145–150	89.35	7.42	3.40	—	560	479	23.6	1.01	622	1.18	1.53	10.4	50.1	472	168	1.16	14.9	10.7
11H-2, 140–150	97.30	7.40	3.24	—	560	479	24.7	0.74	633	0.62	3.46	10.7	50.4	471	183	BDL	14.4	10.8
12H-3, 140–150	108.30	7.42	3.13	—	561	482	25.5	0.75	586	0.45	3.88	10.9	50.1	471	198	BDL	13.3	10.6
13H-3, 140–150	117.80	7.63	3.39	—	557	482	24.9	0.62	630	0.50	5.43	10.8	47.9	478	203	BDL	13.0	10.6
14H-3, 140–150	127.30	7.42	3.20	—	559	480	25.0	0.56	642	0.52	6.26	10.9	49.6	471	205	1.00	11.9	10.7
15H-3, 140–150	136.30	7.40	3.33	—	560	485	24.9	0.55	615	0.57	5.73	10.8	47.9	473	214	0.91	11.7	10.5
16H-3, 140–150	146.30	7.57	6.50	—	558	487	25.5	0.47	650	0.93	5.23	11.0	48.1	467	212	0.77	10.5	10.6
17H-3, 140–150	155.80	7.50	3.30	—	554	479	24.9	0.51	660	1.52	6.23	11.1	47.7	454	220	0.85	10.2	10.7
18H-3, 140–150	165.30	7.44	3.38	—	556	482	25.5	0.59	637	2.78	2.80	11.0	47.8	461	223	0.47	9.3	10.7
19H-3, 140–150	174.80	7.46	3.35	—	559	481	23.5	0.59	722	4.32	0.31	11.4	47.3	457	228	1.17	9.2	10.6
20H-3, 140–150	184.30	7.47	3.31	—	559	483	24.8	0.56	692	4.69	1.06	11.3	47.9	476	241	BDL	8.7	10.8
21H-3, 140–150	193.80	7.42	3.11	—	558	479	23.2	0.51	770	3.09	1.54	11.2	47.4	465	243	BDL	8.1	10.7
22H-3, 140–150	203.30	7.24	3.13	—	558	491	25.2	0.57	709	2.06	1.98	10.5	44.4	466	248	1.18	8.0	10.5
23H-3, 140–150	212.80	7.51	3.09	—	558	483	25.0	BDL	781	1.24	3.79	11.3	47.1	461	242	1.00	8.3	10.7
24H-3, 140–150	222.30	7.43	3.22	—	562	481	22.9	0.46	707	0.76	2.98	11.4	47.9	474	244	BDL	6.9	10.8
25H-3, 140–150	231.80	7.44	3.49	—	563	488	24.9	0.48	703	0.82	2.34	11.1	47.4	460	242	0.88	6.4	10.5
26H-3, 140–150	241.30	7.46	3.35	—	558	478	23.2	BDL	733	0.71	4.30	11.6	48.0	472	249	BDL	5.6	10.6
27H-3, 140–150	250.80	7.44	3.26	—	557	477	23.1	0.44	719	0.61	3.15	11.3	48.0	479	242	BDL	5.6	10.7
28H-3, 140–150	260.30	7.42	3.26	—	557	478	23.2	0.41	710	0.55	3.62	11.1	47.7	467	240	BDL	5.3	10.7
29H-3, 140–150	269.80	7.57	3.50	—	556	480	25.1	0.49	823	0.46	3.84	11.8	47.5	470	195	BDL	13.2	10.7
30H-3, 140–150	279.30	7.39	3.71	—	559	482	23.5	0.49	722	0.59	5.37	11.0	47.5	467	238	BDL	5.3	10.6
31H-3, 140–150	288.80	7.37	3.54	—	561	482	23.4	0.49	717	0.30	3.51	11.3	48.0	451	232	0.87	4.5	10.6
32H-3, 140–150	298.30	7.53	3.54	—	558	479	23.0	0.48	731	0.30	4.39	11.3	47.7	456	235	BDL	4.3	10.7
33H-3, 140–150	307.80	7.60	3.54	—	561	490	23.3	0.41	744	0.27	3.47	10.4	44.8	451	229	BDL	4.7	10.4
34H-3, 140–150	315.90	7.56	3.61	—	560	486	24.2	BDL	759	0.37	3.63	11.0	46.7	471	234	0.71	7.5	10.5
39X-3, 140–150	365.10	7.42	3.07	—	563	483	25.9	0.52	686	0.34	1.11	11.1	50.8	467	186	BDL	8.6	10.7
40X-3, 140–150	374.60	7.40	2.78	—	562	499	25.7	0.52	651	0.49	BDL	9.5	43.8	437	161	1.02	9.7	9.9
41X-3, 140–150	384.10	7.73	3.21	—	562	481	24.4	0.48	678	BDL	0.19	10.7	50.2	461	161	0.74	12.3	10.7
42X-3, 140–150	393.60	7.46	2.83	—	564	481	25.4	0.49	690	0.16	0.21	12.1	50.9	468	145	BDL	15.0	10.6
43X-3, 140–150	403.20	7.50	2.73	—	562	493	24.0	BDL	665	0.21	0.19	9.5	45.1	442	115	0.85	19.4	10.3
44X-3, 140–150	412.80	7.43	2.54	—	561	485	24.1	BDL	719	0.11	0.29	10.0	48.0	458	101	1.12	32.4	10.5
320-U1335B-																		
36H-3, 140–150	330.80	7.59	4.32	—	560	486	24.9	0.49	754	BDL	2.88	10.9	47.9	443	208	BDL	4.7	10.6
37H-2, 140–150	338.70	7.60	3.57	—	557	474	23.6	BDL	743	BDL	3.22	11.5	50.0	442	212	BDL	6.1	10.6
39H-3, 140–150	357.20	7.51	3.52	—	558	475	23.8	—	739	BDL	3.17	11.1	50.3	454	196	BDL	7.3	10.7

Notes: BDL = below detection limit (HPO_4^{2-} = 0.4 µM, Mn^{2+} = 0.1 µM, Fe^{2+} = 0.2 µM, B = 1.4 µM, Sr^{2+} = 0.2 µM, Ba^{2+} = 0.7 µM, Li^+ = 0.4 µM). H_4SiO_4 values measured by different techniques during Expeditions 320 and 321disagree significantly, especially for low values. Therefore, caution should be used concerning the H_4SiO_4 data and comparison between the different expeditions.

Table T22. Inorganic geochemistry of solid samples, Site U1335. (See table notes.)

Core, section, interval (cm)	Depth CSF (m)	Major element oxide (wt%)										Trace element (ppm)							
		SiO_2	Al_2O_3	Fe_2O_3 T	MnO	MgO	CaO	Na_2O	K_2O	TiO_2	P_2O_5	Ba	Cr	Cu	Sc	Sr	V	Y	Zr
320-U1335A-																			
1H-3, 65–66	3.65	21.76	3.56	2.31	(0.40)	1.15	31.2	3.06	0.88	0.17	0.30	3931	18.2	271	9.7	1031	20.6	54.9	65.3
7H-3, 65–66	60.05	34.22	2.96	2.66	(0.68)	1.46	26.1	3.34	0.76	0.14	0.49	7372	11.1	631	14.3	1448	10.8	151.4	91.7
12H-7, 40–41	113.30	6.85	0.42	0.54	0.05	0.37	40.5	1.40	0.24	0.02	0.20	2254	51.0	68	1.1	2061	BDL	23.3	24.7
18H-2, 65–66	163.05	7.76	0.06	0.43	0.10	0.37	41.4	1.54	0.11	0.00	0.24	1052	BDL	88	0.6	1526	BDL	10.0	15.2
19H-2, 65–65	172.55	29.14	1.73	1.83	0.09	0.81	31.7	2.14	0.55	0.07	0.31	5692	6.7	312	5.4	1640	BDL	50.0	43.0
22H-2, 65–66	201.05	9.10	0.08	0.47	0.08	0.32	36.7	1.07	0.09	0.00	0.18	1591	BDL	52	BDL	1366	BDL	13.7	13.7
30H-5, 65–66	281.55	6.01	BDL	0.40	0.04	0.28	40.5	0.93	0.07	0.00	0.16	1369	BDL	35	BDL	1668	BDL	10.3	12.0
34H-6, 65–66	319.65	5.93	BDL	0.41	0.04	0.26	42.5	0.98	0.07	0.00	0.18	1524	BDL	44	BDL	1927	BDL	11.0	12.6
41X-6, 33–35	387.13	9.03	0.17	0.45	0.05	0.42	40.6	0.86	0.08	0.01	BDL	1769	89.5	69	BDL	1942	BDL	12.2	15.3

Notes: BDL = below detection limit (SiO_2 = 3.5 wt%, Al_2O_3 = 0.04 wt%, Fe_2O_3 T = 0.003 wt%, MnO = 0.0004 wt%, MgO = 0.007 wt%, CaO = 0.1 wt%, Na_2O = 0.02 wt%, K_2O = 0.004 wt%, TiO_2 = 0.001 wt%, P_2O_5 = 0.1 wt%, Ba = 28 wt%, Cr = 5 wt%, Cu = 16 wt%, Sc = 0.4 wt%, Sr = 3 wt%, V = 4 wt%, Y = 1.7 wt%, Zr = 4 wt%). See Table T9 for maximum values of calibration.

Table T23. Calcium carbonate and organic carbon data, Site U1335. (See table notes). (Continued on next two pages.)

Core, section, interval (cm)	Depth CSF (m)	Carbon (wt%)			
		$CaCO_3$	IC	TC	TOC
320-U1335A-					
1H-1, 105–106	1.05	68.7	8.25	8.52	0.10
1H-2, 65–66	2.15	58.8	7.05	ND	ND
1H-3, 65–66	3.65	59.7	7.17	ND	ND
1H-4, 65–66	5.15	69.9	8.39	ND	ND
1H-5, 65–66	6.65	58.7	7.05	ND	ND
1H-6, 65–66	7.85	62.4	7.49	ND	ND
2H-1, 65–66	9.55	41.5	4.98	ND	ND
2H-2, 65–66	11.05	62.0	7.44	ND	ND
2H-3, 65–66	12.55	67.8	8.14	ND	ND
2H-4, 65–66	14.05	77.0	9.24	ND	ND
2H-5, 65–66	15.55	62.2	7.46	ND	ND
2H-6, 65–66	17.05	40.9	4.91	ND	ND
2H-7, 65–66	18.55	24.4	2.93	ND	ND
3H-1, 65–66	19.05	30.8	3.70	3.98	0.10
3H-2, 65–66	20.55	41.2	4.95	ND	ND
3H-3, 65–66	22.05	61.1	7.34	ND	ND
3H-4, 65–66	23.55	59.3	7.12	ND	ND
3H-5, 65–66	25.05	42.3	5.08	ND	ND
3H-6, 65–66	26.55	69.0	8.29	ND	ND
3H-7, 25–26	27.65	62.1	7.46	ND	ND
4H-1, 115–116	29.05	38.0	4.56	ND	ND
4H-2, 64–65	30.04	22.5	2.71	ND	ND
4H-3, 64–65	31.54	65.8	7.89	ND	ND
4H-4, 64–65	33.04	59.0	7.08	ND	ND
4H-5, 64–65	34.54	65.1	7.81	ND	ND
4H-6, 64–65	36.04	61.4	7.37	ND	ND
4H-7, 40–41	37.30	58.5	7.02	ND	ND
5H-1, 64–65	38.04	80.1	9.62	9.89	0.05
5H-2, 64–65	39.54	87.8	10.54	ND	ND
5H-3, 64–65	41.04	65.1	7.81	ND	ND
5H-4, 64–65	42.54	73.6	8.83	ND	ND
5H-5, 64–65	44.04	82.3	9.88	ND	ND
5H-6, 64–65	45.54	35.5	4.26	ND	ND
6H-1, 65–66	47.55	80.6	9.68	ND	ND
6H-2, 65–66	49.05	83.1	9.97	ND	ND
6H-3, 65–66	50.55	86.5	10.38	ND	ND
6H-4, 65–66	52.05	80.8	9.70	ND	ND
6H-5, 65–66	53.55	83.8	10.06	ND	ND
6H-6, 65–66	55.05	29.9	3.59	ND	ND
6H-7, 20–21	56.10	46.6	5.60	ND	ND
7H-1, 65–66	57.05	12.6	1.51	ND	ND
7H-1, 65–66	57.05	12.8	1.54	1.57	0.10
7H-2, 65–66	58.55	16.0	1.92	ND	ND
7H-3, 65–66	60.05	44.4	5.33	ND	ND
7H-4, 65–65	61.55	36.6	4.39	ND	ND
7H-5, 65–65	63.05	47.2	5.67	ND	ND
7H-6, 65–65	64.55	79.5	9.54	ND	ND
7H-7, 20–21	65.60	51.1	6.13	ND	ND
8H-1, 65–66	66.55	72.0	8.65	ND	ND
8H-2, 65–66	68.05	85.6	10.28	ND	ND
8H-3, 65–66	69.55	89.4	10.73	ND	ND
8H-4, 65–66	71.05	88.1	10.57	ND	ND
8H-5, 65–66	72.55	80.6	9.68	ND	ND
8H-6, 65–66	74.05	83.3	10.00	ND	ND
8H-7, 30–31	75.20	87.0	10.44	ND	ND
9H-1, 65–66	76.05	87.6	10.52	10.59	0.04
9H-2, 65–66	77.55	86.4	10.37	ND	ND
9H-3, 65–66	79.05	86.2	10.34	ND	ND
9H-4, 65–66	80.55	80.6	9.68	ND	ND
9H-5, 65–66	82.05	75.9	9.11	ND	ND
9H-6, 65–66	83.55	88.0	10.56	ND	ND
9H-7, 15–16	84.55	81.5	9.78	ND	ND
10H-1, 65–66	85.55	87.2	10.47	ND	ND
10H-2, 65–66	87.05	89.5	10.75	ND	ND
10H-3, 65–66	88.55	91.2	10.94	ND	ND
10H-4, 65–66	90.05	89.0	10.68	ND	ND
10H-5, 65–66	91.55	87.6	10.52	ND	ND
10H-6, 65–66	93.05	89.7	10.77	ND	ND
10H-7, 55–56	94.45	89.2	10.71	ND	ND
11H-1, 65–66	95.05	82.8	9.93	10.20	0.04
11H-2, 65–66	96.55	79.1	9.49	ND	ND
11H-3, 65–66	98.05	85.9	10.31	ND	ND
11H-4, 65–66	99.55	88.2	10.58	ND	ND
11H-5, 65–66	101.05	84.7	10.17	ND	ND
11H-6, 65–66	102.55	81.1	9.73	ND	ND
11H-7, 20–21	103.60	84.9	10.19	ND	ND
12H-1, 64–65	104.54	85.2	10.23	ND	ND
12H-2, 64–65	106.04	88.2	10.59	ND	ND
12H-3, 64–65	107.54	86.5	10.39	ND	ND
12H-4, 64–65	109.04	82.8	9.94	ND	ND
12H-5, 64–65	110.54	87.9	10.55	ND	ND
12H-6, 40–41	111.80	90.1	10.82	ND	ND
12H-7, 40–41	113.30	83.7	10.05	ND	ND
13H-1, 84–85	114.24	88.5	10.63	10.92	0.04
13H-2, 64–65	115.54	84.8	10.18	ND	ND
13H-3, 64–65	117.04	86.9	10.44	ND	ND
13H-4, 64–65	118.54	90.0	10.80	ND	ND
13H-5, 64–65	120.04	76.3	9.16	ND	ND
13H-6, 64–65	121.54	78.4	9.41	ND	ND
13H-7, 40–41	122.80	90.1	10.82	ND	ND
14H-1, 65–66	123.55	90.9	10.91	ND	ND
14H-2, 65–66	125.05	77.9	9.35	ND	ND
14H-3, 65–66	126.55	84.1	10.10	ND	ND
14H-4, 65–66	128.05	85.5	10.27	ND	ND
14H-5, 65–66	129.55	81.2	9.75	ND	ND
14H-6, 65–66	131.05	91.6	11.00	ND	ND
14H-7, 50–51	132.40	81.0	9.72	ND	ND
15H-1, 10–11	133.40	86.7	10.41	10.63	0.04
15H-2, 50–51	134.40	82.7	9.93	ND	ND
15H-3, 50–51	135.40	86.3	10.36	ND	ND
15H-4, 65–66	137.05	88.3	10.60	ND	ND
15H-5, 65–66	138.55	86.7	10.40	ND	ND
15H-6, 65–66	140.05	82.3	9.89	ND	ND
15H-7, 65–66	141.55	88.8	10.66	ND	ND
16H-1, 65–66	142.55	80.3	9.64	ND	ND
16H-2, 65–66	144.05	87.9	10.56	ND	ND
16H-3, 65–66	145.55	77.2	9.27	ND	ND
16H-4, 65–66	147.05	86.6	10.40	ND	ND
17H-1, 65–66	152.05	73.0	8.76	8.99	0.05
17H-2, 65–66	153.55	81.3	9.75	ND	ND
17H-3, 65–66	155.05	81.0	9.72	ND	ND
17H-4, 65–66	156.55	91.9	11.03	ND	ND
17H-5, 65–66	158.05	59.6	7.15	ND	ND
17H-6, 55–56	159.45	62.5	7.50	ND	ND
17H-7, 40–41	160.80	76.9	9.23	ND	ND
18H-1, 65–66	161.55	82.7	9.93	ND	ND
18H-2, 65–66	163.05	84.1	10.10	ND	ND
18H-3, 65–66	164.55	84.0	10.08	ND	ND
18H-4, 65–66	166.05	82.6	9.92	ND	ND
18H-5, 65–66	167.55	86.2	10.35	ND	ND
18H-6, 65–66	169.05	74.9	8.99	ND	ND
19H-1, 65–67	171.05	83.8	10.07	10.31	0.04
19H-2, 65–65	172.55	55.8	6.70	ND	ND
19H-3, 65–65	174.05	73.3	8.80	ND	ND
19H-4, 65–65	175.55	71.8	8.62	ND	ND
19H-5, 65–65	177.05	66.6	7.99	ND	ND
19H-6, 65–65	178.55	60.0	7.21	ND	ND
19H-7, 40–41	179.80	68.1	8.17	ND	ND
20H-1, 65–66	180.55	83.1	9.98	ND	ND
20H-2, 65–66	182.05	81.3	9.76	ND	ND
20H-3, 65–66	183.55	80.1	9.62	ND	ND
20H-4, 65–66	185.05	85.2	10.22	ND	ND
20H-5, 65–66	186.55	74.5	8.94	ND	ND

Table T23 (continued). (Continued on next page.)

Core, section, interval (cm)	Depth CSF (m)	Carbon (wt%)			
		$CaCO_3$	IC	TC	TOC
20H-6, 65–66	188.05	66.0	7.92	ND	ND
20H-7, 40–41	189.30	67.5	8.11	ND	ND
21H-1, 65–66	190.05	85.9	10.32	10.63	0.04
21H-2, 65–66	191.55	86.5	10.38	ND	ND
21H-3, 65–66	193.05	81.6	9.79	ND	ND
21H-4, 65–66	194.55	81.7	9.81	ND	ND
21H-5, 65–66	196.05	83.1	9.97	ND	ND
21H-6, 65–66	197.55	84.6	10.16	ND	ND
21H-7, 20–21	198.50	84.9	10.19	ND	ND
22H-1, 100–101	199.90	80.9	9.72	ND	ND
22H-2, 65–66	201.05	83.6	10.04	ND	ND
22H-3, 65–66	202.55	79.5	9.54	ND	ND
22H-4, 65–66	204.05	65.8	7.90	ND	ND
22H-5, 65–66	205.55	85.8	10.30	ND	ND
22H-6, 65–66	207.05	77.2	9.27	ND	ND
22H-7, 30–31	208.20	84.5	10.14	ND	ND
23H-2, 65–66	210.55	85.0	10.20	10.40	0.04
23H-3, 65–66	212.05	87.1	10.45	ND	ND
23H-4, 65–66	213.55	78.3	9.40	ND	ND
23H-5, 65–66	215.05	83.4	10.01	ND	ND
23H-6, 65–66	216.55	85.0	10.21	ND	ND
23H-7, 20–21	217.60	81.4	9.77	ND	ND
24H-1, 65–66	218.55	87.5	10.50	ND	ND
24H-2, 65–66	220.05	38.0	4.56	4.84	0.06
24H-3, 65–66	221.55	81.2	9.75	ND	ND
24H-4, 65–66	223.05	89.1	10.70	ND	ND
24H-5, 65–66	224.55	89.7	10.77	ND	ND
24H-6, 65–66	226.05	88.0	10.56	ND	ND
24H-7, 40–41	227.30	87.3	10.48	ND	ND
25H-1, 65–66	228.05	86.3	10.36	10.77	0.05
25H-2, 65–66	229.55	87.0	10.44	ND	ND
25H-3, 65–66	231.05	89.3	10.72	ND	ND
25H-4, 65–66	232.55	84.2	10.11	ND	ND
25H-5, 65–66	234.05	87.4	10.50	ND	ND
25H-6, 65–66	235.55	84.4	10.13	ND	ND
25H-7, 15–16	236.55	85.8	10.30	ND	ND
26H-1, 64–65	237.54	85.8	10.30	ND	ND
26H-2, 64–65	239.04	84.6	10.15	ND	ND
26H-3, 64–65	240.54	87.6	10.52	ND	ND
26H-4, 64–65	242.04	87.9	10.55	ND	ND
26H-5, 64–65	243.54	87.9	10.55	ND	ND
26H-6, 64–65	245.04	86.6	10.39	ND	ND
26H-7, 45–46	246.35	87.7	10.53	ND	ND
27H-1, 65–66	247.05	87.7	10.52	10.79	0.05
27H-2, 65–66	248.55	87.5	10.51	ND	ND
27H-3, 65–66	250.05	90.2	10.83	ND	ND
27H-4, 65–66	251.55	89.4	10.73	ND	ND
27H-5, 65–66	253.05	89.0	10.68	ND	ND
27H-6, 65–66	254.55	87.4	10.49	ND	ND
28H-1, 64–65	256.54	83.6	10.03	ND	ND
28H-2, 64–65	258.04	83.4	10.01	ND	ND
28H-3, 64–65	259.54	85.6	10.28	ND	ND
28H-4, 64–65	261.04	86.6	10.39	ND	ND
28H-5, 64–65	262.54	91.2	10.95	ND	ND
28H-6, 64–65	264.04	89.4	10.73	ND	ND
28H-7, 40–41	265.30	89.6	10.75	ND	ND
29H-1, 65–66	266.05	89.5	10.74	10.99	0.06
29H-2, 65–66	267.55	88.3	10.61	ND	ND
29H-3, 65–66	269.05	88.0	10.56	ND	ND
29H-4, 65–66	270.55	81.5	9.79	ND	ND
29H-5, 65–66	272.05	86.4	10.37	ND	ND
29H-6, 65–66	273.55	88.4	10.61	ND	ND
29H-7, 35–36	274.75	89.1	10.70	ND	ND
30H-1, 65–66	275.55	91.5	10.98	ND	ND
30H-2, 65–66	277.05	89.4	10.73	ND	ND
30H-3, 65–66	278.55	93.3	11.20	ND	ND
30H-4, 65–66	280.05	86.4	10.37	ND	ND
30H-5, 65–66	281.55	87.8	10.55	ND	ND
30H-6, 65–66	283.05	89.2	10.71	ND	ND
30H-7, 39–40	284.29	85.1	10.22	ND	ND
31H-1, 65–66	285.05	91.4	10.97	11.27	0.05
31H-2, 65–66	286.55	90.3	10.84	ND	ND
31H-3, 60–61	288.00	88.8	10.66	ND	ND
31H-4, 65–66	289.55	90.1	10.81	ND	ND
31H-5, 65–66	291.05	88.6	10.64	ND	ND
31H-6, 65–66	292.55	90.6	10.88	ND	ND
31H-7, 50–51	293.90	88.9	10.67	ND	ND
32H-1, 65–66	294.55	89.0	10.69	ND	ND
32H-2, 65–66	296.05	89.8	10.78	ND	ND
32H-3, 65–66	297.55	89.5	10.75	ND	ND
32H-4, 65–66	299.05	89.1	10.70	ND	ND
32H-5, 95–96	300.85	87.7	10.53	ND	ND
32H-6, 65–66	302.05	89.4	10.73	ND	ND
32H-7, 30–31	303.20	90.3	10.84	ND	ND
33H-1, 65–66	304.05	92.2	11.07	11.35	0.05
33H-2, 65–66	305.55	89.4	10.73	ND	ND
33H-3, 65–66	307.05	88.7	10.65	ND	ND
33H-4, 65–66	308.55	89.1	10.69	ND	ND
33H-5, 65–66	310.05	84.5	10.14	ND	ND
33H-6, 65–66	311.55	90.5	10.86	ND	ND
33H-7, 49–50	312.89	89.6	10.76	ND	ND
34H-1, 65–66	313.55	88.0	10.56	ND	ND
34H-2, 30–31	314.20	90.1	10.82	ND	ND
34H-3, 65–66	315.15	90.2	10.83	ND	ND
34H-4, 65–66	316.65	87.8	10.54	ND	ND
34H-5, 65–66	318.15	88.1	10.58	ND	ND
34H-6, 65–66	319.65	88.0	10.57	ND	ND
34H-7, 50–51	321.00	83.6	10.03	ND	ND
35H-1, 65–66	323.05	88.2	10.59	10.89	0.06
35H-2, 65–66	324.55	86.8	10.42	ND	ND
35H-3, 65–66	326.05	84.6	10.15	ND	ND
35H-4, 65–66	327.55	90.3	10.85	ND	ND
35H-5, 65–66	329.05	89.3	10.72	ND	ND
35H-6, 65–66	330.55	88.9	10.67	ND	ND
35H-7, 65–66	332.05	89.5	10.74	ND	ND
36H-1, 65–66	332.55	88.9	10.67	ND	ND
36H-2, 65–66	334.05	87.5	10.50	ND	ND
36H-3, 65–66	335.55	89.2	10.71	ND	ND
36H-4, 65–66	337.05	88.8	10.66	ND	ND
36H-5, 65–66	338.55	89.4	10.74	ND	ND
36H-6, 65–66	340.05	83.3	9.99	ND	ND
36H-7, 34–35	341.24	86.0	10.32	ND	ND
37X-1, 60–61	342.00	86.8	10.42	10.76	0.06
37X-2, 63–64	343.53	90.1	10.82	ND	ND
37X-3, 63–64	345.03	85.3	10.24	ND	ND
37X-4, 36–37	346.26	92.3	11.08	ND	ND
37X-5, 64–65	348.04	90.0	10.80	ND	ND
37X-6, 23–24	349.13	96.4	11.57	ND	ND
37X-CC, 15–16	349.89	90.0	10.81	ND	ND
38X-1, 52–53	351.62	89.9	10.80	ND	ND
38X-2, 85–86	353.45	90.2	10.83	ND	ND
38X-3, 68–69	354.78	87.9	10.55	ND	ND
38X-4, 102–103	356.62	90.2	10.82	ND	ND
38X-5, 102–103	358.12	89.6	10.75	ND	ND
38X-6, 20–21	358.80	90.8	10.90	ND	ND
39X-1, 120–121	361.90	89.2	10.71	10.99	0.05
39X-2, 57–58	362.77	89.7	10.77	ND	ND
39X-3, 59–60	364.29	89.7	10.77	ND	ND
39X-4, 52–53	365.72	89.8	10.78	ND	ND
39X-5, 46–47	367.16	87.1	10.46	ND	ND
39X-6, 50–51	368.70	88.2	10.59	ND	ND
40X-1, 90–91	371.10	87.9	10.55	ND	ND
40X-2, 75–76	372.45	88.5	10.62	ND	ND
40X-3, 70–71	373.90	88.8	10.66	ND	ND
40X-4, 80–81	375.50	85.1	10.21	ND	ND
40X-5, 37–38	376.17	81.3	9.77	ND	ND
41X-1, 78–79	380.48	87.2	10.46	10.71	0.04
41X-2, 75–76	381.95	87.8	10.54	ND	ND

Table T23 (continued).

Core, section, interval (cm)	Depth CSF (m)	Carbon (wt%)			
		$CaCO_3$	IC	TC	TOC
41X-3, 79–81	383.49	89.3	10.72	ND	ND
41X-4, 93–95	385.13	86.7	10.40	ND	ND
41X-5, 81–83	386.51	80.8	9.70	ND	ND
41X-6, 33–35	387.13	85.5	10.26	ND	ND
42X-1, 119–120	390.39	83.8	10.07	ND	ND
42X-2, 112–113	391.82	82.7	9.93	ND	ND
42X-3, 109–111	393.29	90.0	10.81	ND	ND
42X-4, 95–97	394.65	88.0	10.56	ND	ND
42X-5, 54–56	395.74	88.6	10.64	ND	ND
43X-1, 90–91	399.70	90.4	10.86	11.10	0.04
43X-2, 54–55	400.84	89.9	10.79	ND	ND
43X-3, 84–85	402.64	89.9	10.79	ND	ND
43X-4, 80–81	404.10	87.5	10.50	ND	ND
43X-5, 66–67	405.46	83.8	10.07	ND	ND
43X-6, 43–44	406.73	82.2	9.87	ND	ND
43X-7, 20–21	407.80	86.9	10.43	ND	ND
44X-1, 66–67	409.06	88.0	10.57	ND	ND
44X-2, 89–90	410.79	78.0	9.36	ND	ND
44X-3, 76–77	412.16	84.2	10.11	ND	ND
44X-4, 90–91	413.80	81.4	9.77	ND	ND
44X-5, 70–71	415.10	88.4	10.61	ND	ND
44X-6, 86–87	416.76	88.7	10.64	ND	ND
45X-1, 60–61	418.70	90.5	10.87	11.14	0.04
45X-2, 25–26	419.85	74.9	8.99	ND	ND

Notes: IC = inorganic carbon, TC = total carbon, TOC = total organic carbon determined by acidification method. ND = not determined. BDL = below detection limit ($CaCO_3$ = <1 wt%, TOC = <0.03 wt%) as determined by three times the standard deviation of replicate measures of a low concentration sample.

Table T24. Moisture and density measurements, Hole U1335A. (**Continued on next two pages.**)

Core, section, interval (cm)	Depth CSF (m)	Water content (%)	Density (g/cm^3) Wet bulk	Dry bulk	Grain	Porosity (%)
320-U1335A-						
1H-2, 75–76	2.25	66.4	1.31	0.44	2.96	85.1
1H-3, 75–76	3.75	61.1	1.29	0.50	2.21	77.2
1H-4, 75–76	5.25	63.9	1.35	0.49	3.05	84.0
1H-5, 75–76	6.75	66.4	1.23	0.41	2.07	80.0
1H-6, 75–76	7.95	61.1	1.38	0.54	3.00	82.1
2H-1, 75–76	9.65	70.4	1.26	0.37	2.75	86.5
2H-2, 75–76	11.15	63.4	1.24	0.46	1.99	77.1
2H-3, 75–76	12.65	56.5	1.40	0.61	2.67	77.2
2H-4, 75–76	14.15	49.3	1.51	0.76	2.78	72.5
2H-5, 75–76	15.65	58.9	1.37	0.56	2.64	78.7
2H-6, 75–76	17.15	61.6	1.27	0.49	2.07	76.4
2H-7, 40–41	18.30	73.5	1.25	0.33	3.11	89.4
3H-1, 75–76	19.15	72.2	1.19	0.33	2.03	83.7
3H-2, 75–76	20.65	68.6	1.26	0.40	2.59	84.7
3H-3, 75–76	22.15	63.9	1.34	0.48	3.00	83.8
3H-4, 75–76	23.65	67.3	1.27	0.42	2.51	83.4
3H-5, 75–76	25.15	65.9	1.29	0.44	2.65	83.3
3H-6, 75–76	26.65	59.2	1.33	0.54	2.38	77.1
3H-7, 45–46	27.85	64.1	1.33	0.48	2.88	83.4
4H-1, 125–126	29.15	65.6	1.32	0.46	2.98	84.7
4H-2, 75–76	30.15	66.9	1.29	0.43	2.69	84.1
4H-3, 74–75	31.64	57.8	1.42	0.60	2.99	80.0
4H-4, 75–76	33.15	48.7	1.51	0.78	2.76	71.9
4H-5, 75–76	34.65	58.5	1.40	0.58	2.92	80.1
4H-6, 75–76	36.15	63.0	1.34	0.49	2.77	82.1
4H-7, 50–51	37.40	59.0	1.39	0.57	2.91	80.4
5H-1, 75–76	38.15	40.5	1.68	1.00	2.98	66.4
5H-2, 75–76	39.65	40.3	1.59	0.95	2.52	62.5
5H-3, 75–76	41.15	55.0	1.42	0.64	2.69	76.2
5H-4, 75–76	42.65	57.7	1.41	0.60	2.89	79.4
5H-5, 75–76	44.15	48.7	1.51	0.77	2.75	71.8
5H-6, 75–76	45.65	59.9	1.37	0.55	2.79	80.3
6H-1, 75–76	47.65	46.6	1.54	0.82	2.76	70.2
6H-2, 75–76	49.15	45.4	1.55	0.85	2.72	68.8
6H-3, 75–76	50.65	41.0	1.63	0.96	2.77	65.2
6H-4, 75–76	52.15	47.8	1.55	0.81	2.94	72.5
6H-5, 75–76	53.65	48.4	1.51	0.78	2.75	71.6
6H-6, 75–76	55.15	60.8	1.35	0.53	2.67	80.2
6H-7, 30–31	56.20	60.1	1.37	0.55	2.74	80.1
7H-1, 75–76	57.15	70.5	1.24	0.37	2.49	85.3
7H-2, 75–76	58.65	74.1	1.21	0.31	2.58	87.8
7H-3, 75–76	60.15	68.9	1.28	0.40	2.87	86.1
7H-4, 75–76	61.65	59.5	1.37	0.56	2.76	79.8
7H-5, 75–76	63.15	68.0	1.28	0.41	2.72	85.0
7H-6, 75–76	64.65	49.0	1.54	0.78	2.99	73.7
7H-7, 30–31	65.70	57.2	1.39	0.60	2.70	77.9
8H-1, 75–76	66.65	52.3	1.46	0.69	2.72	74.5
8H-2, 75–76	68.15	42.8	1.64	0.94	2.98	68.5
8H-3, 75–76	69.65	39.9	1.66	0.99	2.81	64.6
8H-4, 75–76	71.15	42.8	1.60	0.92	2.79	67.1
8H-5, 75–76	72.65	45.4	1.59	0.87	2.97	70.7
8H-6, 75–76	74.15	46.6	1.55	0.83	2.82	70.6
8H-7, 40–41	75.30	45.3	1.56	0.86	2.78	69.2
9H-1, 75–76	76.15	41.7	1.64	0.96	2.90	67.0
9H-2, 75–76	77.65	39.7	1.66	1.00	2.83	64.6
9H-3, 75–76	79.15	42.3	1.62	0.93	2.82	66.9
9H-4, 75–76	80.65	42.4	1.64	0.95	2.97	68.0
9H-5, 75–76	82.15	47.9	1.53	0.80	2.80	71.6
9H-6, 75–76	83.65	39.5	1.67	1.01	2.82	64.3
9H-7, 75–76	84.65	46.2	1.58	0.85	2.95	71.3
10H-1, 75–76	85.65	41.1	1.65	0.97	2.86	66.1
10H-2, 75–76	87.15	38.8	1.69	1.03	2.85	63.9
10H-3, 75–76	88.65	35.6	1.77	1.14	2.96	61.5
10H-4, 75–76	90.15	40.2	1.66	0.99	2.83	65.0
10H-5, 75–76	91.65	40.3	1.65	0.98	2.81	64.9
10H-6, 75–76	93.15	38.6	1.72	1.05	2.98	64.7
10H-7, 65–66	94.55	41.2	1.65	0.97	2.89	66.4
11H-1, 75–76	95.15	41.4	1.65	0.96	2.88	66.6
11H-2, 75–76	96.65	48.0	1.54	0.80	2.87	72.2
11H-3, 75–76	98.15	41.5	1.63	0.96	2.83	66.3
11H-4, 75–76	99.65	39.6	1.69	1.02	2.95	65.3
11H-5, 75–76	101.15	40.7	1.63	0.97	2.76	64.9
11H-6, 75–76	102.65	41.1	1.64	0.96	2.82	65.8
11H-7, 30–31	103.70	39.0	1.71	1.04	3.00	65.2
12H-1, 75–76	104.65	40.1	1.65	0.99	2.81	64.8
12H-2, 75–76	106.15	42.0	1.62	0.94	2.82	66.6
12H-3, 75–76	107.65	43.6	1.62	0.91	2.96	69.1
12H-4, 75–76	109.15	44.3	1.58	0.88	2.77	68.3
12H-5, 75–76	110.65	36.8	1.71	1.08	2.79	61.3
12H-7, 50–51	113.40	38.4	1.68	1.04	2.82	63.2
13H-1, 95–96	114.35	41.1	1.65	0.97	2.87	66.2
13H-2, 75–76	115.65	40.9	1.68	0.99	3.00	66.9
13H-3, 75–76	117.15	42.4	1.62	0.93	2.81	66.9
13H-4, 75–76	118.65	38.7	1.68	1.03	2.84	63.6
13H-5, 75–76	120.15	44.1	1.62	0.90	2.98	69.7
13H-6, 75–76	121.65	39.2	1.66	1.01	2.79	63.7
13H-7, 50–51	122.90	37.7	1.69	1.05	2.80	62.3
14H-1, 75–76	123.65	37.9	1.74	1.08	3.04	64.4
14H-2, 75–76	125.15	47.3	1.53	0.81	2.77	70.8
14H-3, 75–76	126.65	44.9	1.57	0.86	2.76	68.7
14H-4, 75–76	128.15	42.0	1.65	0.96	2.95	67.6
14H-5, 75–76	129.65	39.4	1.66	1.01	2.78	63.9
14H-6, 75–76	131.15	37.3	1.70	1.07	2.80	61.9
14H-7, 60–61	132.50	44.0	1.62	0.90	2.95	69.3
15H-1, 75–76	133.15	41.5	1.62	0.95	2.78	65.8
15H-2, 65–66	134.55	43.6	1.59	0.90	2.79	67.8
15H-4, 75–76	137.15	38.1	1.69	1.05	2.81	62.8
15H-5, 75–76	138.65	39.9	1.67	1.00	2.88	65.2
15H-6, 75–76	140.15	43.1	1.64	0.93	2.99	68.9
15H-7, 40–41	141.30	39.0	1.67	1.02	2.79	63.5
16H-1, 75–76	142.65	40.5	1.64	0.98	2.78	64.9
16H-2, 75–76	144.15	49.4	1.69	1.01	2.98	66.1
16H-3, 75–76	145.65	49.4	1.50	0.76	2.77	72.5
16H-4, 75–76	147.15	37.7	1.69	1.06	2.79	62.2
16H-5, 75–76	148.65	37.8	1.73	1.07	2.96	63.7
17H-1, 75–76	152.15	47.4	1.52	0.80	2.70	70.3
17H-2, 75–76	153.65	40.3	1.64	0.98	2.78	64.7
17H-3, 75–76	155.15	40.8	1.69	1.00	3.03	67.1
17H-4, 75–76	156.65	40.7	1.64	0.97	2.78	65.1
17H-5, 75–76	158.15	44.2	1.58	0.88	2.76	68.1
17H-6, 65–66	159.55	52.8	1.47	0.70	2.90	76.0
17H-7, 40–41	160.80	43.4	1.63	0.92	2.97	69.0
18H-1, 75–76	161.65	43.2	1.60	0.91	2.79	67.4
18H-2, 75–76	163.15	42.3	1.62	0.93	2.80	66.7
18H-3, 75–76	164.65	43.7	1.62	0.91	2.96	69.2
18H-4, 75–76	166.15	39.3	1.66	1.01	2.78	63.7
18H-5, 75–76	167.65	39.5	1.66	1.00	2.77	63.9
18H-6, 75–76	169.15	45.7	1.58	0.86	2.92	70.6
19H-1, 75–76	171.15	38.6	1.68	1.03	2.83	63.5
19H-2, 75–76	172.65	44.8	1.56	0.86	2.72	68.3
19H-3, 75–76	174.15	43.6	1.58	0.89	2.72	67.3
19H-4, 75–76	175.65	43.4	1.59	0.90	2.76	67.4
19H-5, 75–76	177.15	47.7	1.54	0.81	2.87	71.8
19H-6, 75–76	178.65	46.0	1.54	0.83	2.69	69.2
19H-7, 50–51	179.90	49.3	1.49	0.76	2.70	72.0
20H-1, 75–76	180.65	41.6	1.68	0.98	3.07	68.1
20H-2, 75–76	182.15	42.1	1.61	0.93	2.73	66.0
20H-3, 75–76	183.65	41.6	1.62	0.95	2.78	65.9
20H-4, 75–76	185.15	40.0	1.68	1.01	2.95	65.8
20H-5, 75–76	186.65	41.9	1.60	0.93	2.72	65.7
20H-6, 75–76	188.15	43.9	1.57	0.88	2.69	67.3
20H-7, 50–51	189.40	42.6	1.62	0.93	2.84	67.3
21H-1, 75–76	190.15	38.0	1.68	1.04	2.78	62.4
21H-2, 75–76	191.65	40.9	1.63	0.96	2.76	65.0
21H-3, 75–76	193.15	40.0	1.65	0.99	2.78	64.3

Table T24 (continued). (Continued on next page.)

Core, section, interval (cm)	Depth CSF (m)	Water content (%)	Density (g/cm³) Wet bulk	Dry bulk	Grain	Porosity (%)
21H-4, 75–76	194.65	37.5	1.74	1.09	3.00	63.7
21H-5, 75–76	196.15	36.4	1.75	1.11	2.92	62.0
21H-6, 75–76	197.65	40.1	1.66	0.99	2.83	64.9
21H-7, 30–31	198.60	39.4	1.66	1.01	2.79	64.0
22H-1, 110–111	200.00	47.7	1.53	0.80	2.76	71.1
22H-2, 75–76	201.15	39.5	1.67	1.01	2.85	64.5
22H-3, 75–76	202.65	42.3	1.64	0.95	2.94	67.8
22H-4, 75–76	204.15	44.3	1.57	0.87	2.73	68.0
22H-5, 75–76	205.65	36.9	1.71	1.08	2.80	61.5
22H-6, 75–76	207.15	41.2	1.65	0.97	2.91	66.5
22H-7, 40–41	208.30	42.1	1.62	0.94	2.83	66.7
23H-2, 80–81	210.70	39.8	1.70	1.02	2.99	65.9
23H-3, 75–76	212.15	39.0	1.69	1.03	2.87	64.2
23H-4, 75–76	213.65	37.9	1.69	1.05	2.80	62.5
23H-5, 75–76	215.15	35.4	1.79	1.16	3.04	61.9
23H-6, 75–76	216.65	37.4	1.71	1.07	2.85	62.5
23H-7, 30–31	217.70	34.8	1.75	1.14	2.82	59.6
24H-1, 75–76	218.65	35.4	1.78	1.15	2.97	61.3
24H-2, 75–76	220.15	43.3	1.60	0.91	2.82	67.7
24H-3, 75–76	221.65	35.6	1.74	1.12	2.85	60.5
24H-4, 75–76	223.15	33.3	1.81	1.21	2.95	59.0
24H-5, 75–76	224.65	34.0	1.76	1.16	2.80	58.5
24H-6, 75–76	226.15	35.5	1.73	1.11	2.77	59.8
24H-7, 50–51	227.40	37.6	1.73	1.08	2.97	63.6
25H-2, 75–76	229.65	35.6	1.73	1.11	2.79	60.2
25H-3, 75–76	231.15	37.0	1.71	1.08	2.84	61.9
25H-4, 75–76	232.65	36.2	1.71	1.09	2.75	60.4
25H-5, 75–76	234.15	36.3	1.71	1.09	2.75	60.5
25H-6, 75–76	235.65	42.1	1.59	0.92	2.64	65.2
25H-7, 25–26	236.65	43.1	1.56	0.89	2.56	65.4
26H-1, 75–76	237.65	42.0	1.57	0.91	2.56	64.4
26H-2, 75–76	239.15	36.9	1.72	1.08	2.84	61.9
26H-3, 75–76	240.65	37.2	1.69	1.06	2.76	61.5
26H-4, 75–76	242.15	36.1	1.71	1.09	2.73	60.2
26H-5, 75–76	243.65	34.6	1.77	1.15	2.86	59.7
26H-6, 75–76	245.15	35.8	1.72	1.10	2.75	60.0
26H-7, 55–56	246.45	37.4	1.69	1.05	2.75	61.6
27H-1, 75–76	247.15	37.0	1.72	1.08	2.85	62.0
27H-2, 75–76	248.65	36.3	1.71	1.09	2.75	60.5
27H-3, 75–76	250.15	35.7	1.72	1.11	2.78	60.1
27H-4, 75–76	251.65	36.1	1.75	1.12	2.92	61.7
27H-5, 75–76	253.15	35.4	1.73	1.12	2.79	59.9
27H-6, 75–76	254.65	35.4	1.73	1.12	2.80	59.9
28H-2, 75–76	258.15	36.6	1.70	1.08	2.75	60.7
28H-3, 75–76	259.65	37.0	1.70	1.07	2.76	61.3
28H-4, 75–76	261.15	34.6	1.78	1.17	2.94	60.3
28H-5, 75–76	262.65	34.0	1.76	1.16	2.80	58.4
28H-6, 75–76	264.15	32.0	1.84	1.25	2.94	57.5
28H-7, 50–51	265.40	31.2	1.79	1.23	2.72	54.6
29H-1, 75–76	266.15	34.0	1.80	1.19	2.93	59.6
29H-2, 75–76	267.65	36.0	1.73	1.11	2.81	60.7
29H-3, 75–76	269.15	36.1	1.72	1.10	2.78	60.6
29H-4, 75–76	270.65	34.9	1.75	1.14	2.82	59.6
29H-5, 75–76	272.15	33.8	1.75	1.16	2.73	57.6
29H-6, 75–76	273.65	31.7	1.84	1.26	2.93	57.1
29H-7, 50–51	274.90	32.2	1.89	1.28	3.16	59.4
30H-1, 75–76	275.65	32.6	1.80	1.21	2.84	57.2
30H-2, 75–76	277.15	33.8	1.78	1.18	2.84	58.6
30H-3, 75–76	278.65	34.7	1.76	1.15	2.84	59.5
30H-4, 75–76	280.15	33.8	1.77	1.17	2.80	58.3
30H-5, 75–76	281.65	34.2	1.75	1.15	2.76	58.4
31H-2, 75–76	286.65	30.5	1.78	1.24	2.62	52.8
31H-3, 75–76	288.15	32.7	1.78	1.19	2.76	56.7
31H-4, 75–76	289.65	31.7	1.81	1.23	2.81	56.0
31H-6, 75–76	292.65	32.3	1.80	1.22	2.83	56.9
31H-7, 50–51	293.90	32.5	1.81	1.22	2.87	57.4
32H-4, 75–76	299.15	32.6	1.78	1.20	2.75	56.5
32H-5, 104–105	300.94	34.8	1.74	1.13	2.77	59.1
32H-6, 75–76	302.15	31.8	1.81	1.24	2.83	56.3
33H-1, 75–76	304.15	32.2	1.82	1.23	2.87	57.1
33H-2, 75–76	305.65	36.1	1.72	1.10	2.80	60.7
33H-3, 75–76	307.15	34.1	1.77	1.17	2.85	59.0
33H-4, 75–76	308.65	32.0	1.80	1.23	2.81	56.3
33H-5, 75–76	310.15	34.7	1.74	1.13	2.75	58.8
33H-6, 75–76	311.65	30.3	1.71	1.19	2.40	50.4
34H-1, 75–76	313.65	31.2	1.81	1.25	2.80	55.3
34H-2, 40–41	314.30	34.5	1.74	1.14	2.77	58.8
34H-3, 75–76	315.25	32.0	1.81	1.23	2.82	56.4
34H-4, 75–76	316.75	31.9	1.66	1.13	2.35	51.8
34H-5, 75–76	318.25	33.6	1.86	1.23	3.15	60.9
34H-6, 75–76	319.75	32.3	1.84	1.24	2.96	58.0
34H-7, 60–61	321.10	32.1	1.79	1.21	2.77	56.2
35H-1, 75–76	323.15	32.1	1.79	1.21	2.77	56.2
35H-2, 75–76	324.65	30.8	1.82	1.26	2.78	54.8
35H-3, 75–76	326.15	30.7	1.81	1.26	2.76	54.4
35H-4, 75–76	327.65	29.4	1.83	1.29	2.71	52.4
35H-5, 75–76	329.15	30.2	1.84	1.29	2.80	54.2
35H-6, 75–76	330.65	37.1	1.69	1.06	2.74	61.2
35H-7, 75–76	332.15	30.4	1.83	1.27	2.78	54.3
36H-1, 75–76	332.65	32.7	1.78	1.20	2.78	56.9
36H-2, 75–76	334.15	32.4	1.77	1.20	2.73	56.1
36H-3, 75–76	335.65	30.7	1.81	1.25	2.74	54.2
36H-4, 75–76	337.15	31.3	1.82	1.25	2.80	55.5
36H-5, 75–76	338.65	31.0	1.80	1.24	2.73	54.4
36H-6, 75–76	340.15	32.5	1.78	1.20	2.78	56.7
36H-7, 45–46	341.35	32.4	1.78	1.20	2.75	56.3
37X-1, 52–53	341.92	32.8	1.77	1.19	2.74	56.6
37X-2, 71–72	343.61	33.7	1.76	1.17	2.79	58.1
37X-3, 82–83	345.22	33.5	1.77	1.18	2.80	57.9
37X-4, 36–37	346.26	32.7	1.80	1.21	2.84	57.4
37X-5, 81–82	348.21	32.1	1.80	1.22	2.81	56.5
37X-6, 18–19	349.08	33.5	1.78	1.19	2.84	58.2
38X-1, 61–62	351.71	35.9	1.71	1.10	2.75	60.1
38X-2, 97–98	353.57	58.2	1.39	0.58	2.77	79.1
38X-4, 112–113	356.72	31.3	1.82	1.25	2.82	55.6
38X-5, 115–116	358.25	35.9	1.71	1.10	2.75	60.1
38X-6, 26–27	358.86	32.9	1.78	1.19	2.79	57.2
39X-1, 129–130	361.99	34.0	1.75	1.16	2.76	58.2
39X-2, 68–69	362.88	34.2	1.77	1.16	2.84	59.1
39X-3, 69-70	364.39	31.3	1.84	1.26	2.88	56.2
39X-4, 70–71	365.90	34.5	1.75	1.14	2.79	59.0
39X-5, 58–59	367.28	29.7	1.84	1.29	2.78	53.4
40X-1, 83–84	371.03	34.9	1.77	1.15	2.88	60.1
40X-2, 84–85	372.54	33.9	1.75	1.16	2.77	58.1
40X-3, 88–89	374.08	33.8	1.77	1.18	2.83	58.5
40X-4, 64–65	375.34	34.9	1.74	1.14	2.80	59.5
40X-5, 39–40	376.19	33.6	1.78	1.18	2.83	58.3
41X-2, 68–69	381.88	30.5	1.88	1.31	2.96	55.8
41X-3, 97–98	383.67	31.8	1.91	1.30	3.20	59.3
41X-4, 97–98	385.17	29.2	1.93	1.37	3.03	55.0
41X-5, 36–37	386.06	29.7	1.93	1.35	3.07	55.9
41X-6, 23–24	387.03	29.8	1.97	1.38	3.24	57.3
42X-1, 108–109	390.28	30.1	1.90	1.33	3.02	55.9
42X-2, 76–77	391.46	30.8	1.84	1.27	2.85	55.3
42X-3, 60–61	392.80	28.9	1.87	1.33	2.82	52.8
42X-4, 74–75	394.44	29.9	1.86	1.30	2.85	54.2
42X-5, 30–31	395.50	29.1	1.91	1.36	2.97	54.4
43X-1, 75–76	399.55	29.2	1.88	1.33	2.87	53.6
43X-2, 44–45	400.74	27.4	1.91	1.39	2.85	51.3
43X-3, 74–75	402.54	27.3	1.97	1.44	3.03	52.6
43X-4, 92–93	404.22	27.6	1.88	1.36	2.76	50.7
43X-5, 77–78	405.57	29.6	1.93	1.36	3.07	55.7
43X-6, 56–57	406.86	30.1	1.85	1.29	2.83	54.3
43X-7, 32–33	407.92	29.1	1.84	1.31	2.75	52.4
44X-1, 66–67	409.06	28.2	1.89	1.36	2.85	52.3
44X-2, 89–90	410.79	30.4	1.90	1.32	3.05	56.6

Table T24 (continued).

Core, section, interval (cm)	Depth CSF (m)	Water content (%)	Density (g/cm^3)			Porosity (%)
			Wet bulk	Dry bulk	Grain	
44X-3, 75–76	412.15	25.2	1.94	1.45	2.77	47.6
44X-4, 90–91	413.80	26.3	2.02	1.49	3.08	51.7
44X-5, 70–71	415.10	26.5	2.03	1.49	3.13	52.4
44X-6, 88–89	416.78	25.6	1.95	1.45	2.83	48.8

Table T25. Split-core *P*-wave velocity measurements, Hole U1335A. (**Continued on next two pages.**)

Core, section	Depth CSF (m)	Velocity (m/s)		
		x-axis	*y*-axis	*z*-axis
320-U1335A-				
1H-2	2.83			1495
1H-2	2.90	1519		
1H-3	4.37			1496
1H-3	4.46	1520		
1H-4	5.72	1527		
1H-4	5.87		1498	1499
1H-6	8.49	1530		
1H-6	8.58			1500
2H-1	10.23	1516		
2H-1	10.32		1508	1498
2H-2	11.71			1501
2H-2	11.80	1520		
2H-3	13.25		1509	1502
2H-3	13.35	1518		
2H-4	14.75		1520	1503
2H-4	14.86	1523		
2H-5	16.19		1512	1503
2H-5	16.30	1515		
2H-6	17.75			1506
3H-1	19.77		1519	1504
3H-1	19.86	1542		
3H-2	21.22		1512	1498
3H-2	21.30	1525		
3H-3	22.74		1404	1499
3H-3	22.85	1510		
3H-4	24.26		1512	1493
3H-4	24.35	1522		
3H-5	25.74		1508	1496
3H-5	25.81	1517		
3H-6	27.29		1498	1490
3H-6	27.36	1536		
4H-1	29.26		1506	1493
4H-1	29.35	1515		
4H-2	30.56		1414	1495
4H-2	30.81	1556		
4H-3	32.27		1397	1498
4H-3	32.34	1521		
4H-4	33.62		2638	1501
4H-4	33.86	1507		
4H-5	35.20		1498	1501
4H-5	35.29	1473		
4H-6	36.74		1509	1452
4H-6	36.85	1481		
5H-1	38.79		1504	1454
5H-1	38.86	1490		
5H-2	40.23		1503	1503
5H-2	40.30	1473		
5H-3	41.77			1500
5H-3	41.85	1478		
5H-4	43.25		1512	1506
5H-4	43.33	1517		
5H-5	44.77			1505
5H-5	44.85	1528		
5H-6	46.21		1498	1504
5H-6	46.28	1491		
6H-1	48.27		1514	1503
6H-1	48.34	1517		
6H-2	49.71		1508	1506
6H-2	49.80	1492		
6H-3	51.25		1508	1503
6H-3	51.34	1502		
6H-4	52.75		1504	1472
6H-4	52.85	1464		
6H-5	54.21		1400	1515
6H-5	54.29	1533		
6H-6	55.72		1419	1496
6H-6	55.85	1509		
7H-1	57.84	1519		
7H-2	59.34	1527		
7H-3	60.70		1534	1510
7H-3	60.79	1521		
7H-4	62.26			1500
7H-4	62.34	1495		
7H-5	63.85	1515		
7H-6	65.25		1514	1502
7H-6	65.34	1508		
8H-1	67.35	1506		
8H-2	68.78		1511	1506
8H-3	70.18		1512	1509
8H-3	70.24	1523		
8H-4	71.75		1515	1494
8H-4	71.84	1513		
8H-5	73.25		1403	1504
8H-5	73.34	1496		
8H-6	74.77		1509	1508
8H-6	74.84	1519		
9H-1	76.76		1522	1517
9H-1	76.85	1523		
9H-2	78.25		1510	
9H-2	78.35	3007		
9H-3	79.65		2366	1502
9H-3	79.73	1540		
9H-4	81.23	1533		
9H-4	81.31			1503
9H-5	82.73	1520		
9H-5	82.81		1517	1504
9H-6	84.24	1541		
9H-6	84.32		1511	1503
10H-1	86.24	1568		
10H-1	86.33		1531	1527
10H-2	87.73	1565		
10H-2	87.81		1541	1533
10H-3	89.15	1556		
10H-3	89.22		1525	1525
10H-4	90.71	1548		
10H-4	90.79		1511	1509
10H-5	92.22	1555		
10H-5	92.31		1523	1527
10H-6	93.71	1535		
10H-6	93.80		2696	1774
11H-1	95.73	1529		
11H-1	95.81		1508	1506
11H-2	97.11	1519		
11H-2	97.20			1504
11H-3	98.75	1524		
11H-4	100.25	1520		
11H-4	100.32		1515	1507
11H-5	101.74	1535		
11H-5	101.81		1514	1508
11H-6	103.21	1547		
11H-6	103.29		1507	1503
12H-1	105.24	1547		
12H-1	105.31		1513	1508
12H-2	106.73	1537		
12H-2	106.81		1506	1498
12H-3	108.11	1536		
12H-3	108.19			1505
12H-4	109.79		1512	1506
12H-5	111.31		1520	1519
12H-7	113.51	1557		
13H-3	117.64	1534		
13H-4	119.30		1388	
13H-4	119.37	1500		
13H-5	120.80		1408	
13H-5	120.86	2770		

Table T25 (continued). (Continued on next page.)

Core, section	Depth CSF (m)	Velocity (m/s)		
		x-axis	*y*-axis	*z*-axis
13H-6	122.35	1521		
14H-1	124.22	1525		
14H-1	124.30		1526	1522
14H-2	125.87	1518		
14H-3	127.14	1534		
14H-3	127.22		1521	
14H-4	128.72	1505		
14H-5	130.24	1539		
14H-5	130.32		1528	1529
14H-6	131.73	1525		
14H-6	131.81		1529	1518
15H-1	133.84	1464		
15H-3	136.18		1523	1522
15H-3	136.26	1517		
15H-4	137.75		1531	1517
15H-4	137.84	1490		
15H-5	139.35	1509		
15H-6	140.74		1406	
15H-6	140.84	1505		
16H-1	143.35	1506		
16H-2	144.76		1515	1515
16H-2	144.85	1530		
16H-3	146.25	1501		
17H-1	152.85	1514		
17H-2	154.34	1515		
17H-3	155.75	1510		
17H-4	157.25			1518
17H-4	157.35	1493		
17H-5	158.84	1511		
17H-6	160.25			1518
17H-6	160.35	1499		
18H-1	162.37	1521		
18H-2	163.86	1483		
18H-3	165.18		1421	1523
18H-3	165.26	1521		
18H-4	166.78			1469
18H-4	166.85	1500		
18H-5	168.27		1412	1520
18H-5	168.36	1505		
19H-1	171.86	1471		
19H-2	173.28			1513
19H-2	173.34	1493		
19H-3	174.68			1786
19H-3	174.75	1495		
19H-4	176.26			1514
19H-4	176.35	1467		
19H-5	177.76			1362
19H-5	177.85	1480		
19H-6	179.36	1482		
20H-1	181.35	1468		
20H-2	182.75		1529	1517
20H-2	182.86	1508		
20H-3	184.25	1494		
20H-4	185.78		1429	
20H-4	185.85	1524		
20H-5	187.23			1464
20H-5	187.35	1512		
20H-6	188.85	1506		
21H-1	190.76		1421	
21H-1	190.84	1548		
21H-2	192.36	1471		
21H-3	193.74	1494		
21H-4	195.27		1429	
21H-4	195.35	1494		
21H-5	196.81		1428	1470
21H-6	198.17		1442	1462
21H-6	198.25	1503		
22H-2	201.73	1494		
22H-3	203.17			1516
22H-3	203.25	1534		
22H-4	204.76		1447	1513
22H-4	204.84	1500		
22H-5	206.37	1503		
22H-6	207.78		1544	1466
22H-6	207.85	1497		
23H-4	214.22	1511		
23H-4	214.29		1552	
23H-5	215.72	1536		
23H-6	217.22	1543		
23H-6	217.29		1443	1470
24H-1	219.27		1550	
24H-1	219.35	1526		
24H-2	220.78		1558	1478
24H-2	220.86	1511		
24H-3	222.17		1563	1534
24H-3	222.25	1531		
24H-4	223.78		1563	1562
24H-4	223.86	1567		
24H-5	225.15	1541		
24H-5	225.23		1538	1532
24H-6	226.71	1540		
24H-6	226.79		1561	1531
25H-2	230.30		1543	1523
25H-2	230.37	1542		
25H-3	231.57	1554		
25H-3	231.65			1540
25H-4	233.27		1412	
25H-5	234.77		1539	1535
25H-5	234.84	1561		
25H-6	236.28			1532
26H-1	238.35	1506		
26H-2	239.77		1414	
26H-2	239.85	1543		
26H-3	241.17			1524
26H-3	241.24	2785		
26H-4	242.78			1469
26H-4	242.86	1534		
26H-5	244.26		1557	1532
26H-5	244.34	1537		
26H-6	245.78		1542	1468
26H-6	245.85	1538		
27H-1	247.65	1549		
27H-2	249.27		1558	1533
27H-2	249.35	1496		
27H-3	250.67		1554	
27H-3	250.75	1560		
27H-5	253.75		1569	1539
27H-5	253.84	1537		
27H-6	255.26		1561	1531
27H-6	255.35	1535		
28H-2	258.85	1513		
28H-3	260.15		1542	
28H-3	260.24	1529		
28H-4	261.75		1585	1549
28H-4	261.86	1525		
28H-5	263.28		1573	1532
28H-5	263.35	1515		
28H-6	264.76		1557	1557
28H-6	264.85	1539		
29H-1	266.77			1549
29H-1	266.85	1532		
29H-2	268.27			1477
29H-2	268.35	1518		
29H-3	269.66			1534
29H-3	269.74	1515		
29H-4	271.26		1574	1542
29H-4	271.35	3023		
29H-4	271.35	1529		

Table T25 (continued).

Core, section	Depth CSF (m)	Velocity (m/s)		
		x-axis	*y*-axis	*z*-axis
29H-5	272.72		1475	1539
29H-5	272.85	1540		
29H-6	274.24		1558	1559
30H-1	276.30		1558	1558
30H-1	276.36	1549		
30H-2	277.72		1552	1547
30H-2	277.81	1565		
30H-3	279.14		1558	
30H-3	279.24	1561		
30H-4	280.79			1560
30H-4	280.86	1543		
30H-5	282.25			1558
30H-5	282.35	1545		
30H-6	283.76		1474	
30H-6	283.85	1515		
31H-1	285.85	1503		
31H-2	287.27		1566	1558
31H-2	287.35	1525		
31H-3	288.66			1563
31H-3	288.74	1536		
31H-4	290.24		1467	1557
31H-4	290.34	1535		
31H-5	291.75			1554
31H-5	291.85	1538		
31H-6	293.27		1564	1548
31H-6	293.35	1543		
32H-1	295.24			1551
32H-1	295.35	1552		
32H-2	296.74		1571	1559
32H-2	296.84	1575		
32H-3	298.15		1566	
32H-3	298.25	1570		
32H-4	299.75		1581	
32H-4	299.85	1618		
32H-5	301.23		1551	1545
32H-5	301.34	1557		
32H-6	302.78			1525
32H-6	302.85	1568		
33H-1	304.72		1437	
33H-1	304.84	1565		
33H-2	306.25		2495	1571
33H-2	306.35	1547		
33H-3	307.66			1491
33H-3	307.74	1553		
33H-4	309.26		1557	1546
33H-4	309.35	1555		
33H-5	310.74		1578	1577
33H-5	310.84	1557		
33H-6	312.28		1579	1563
33H-6	312.36	1549		
34H-3	315.89		1551	1547
34H-3	315.95	1539		
34H-4	317.26		1561	1553
34H-4	317.32	3123		
34H-4	317.32	1541		
34H-5	318.88		1474	
34H-5	318.95	1528		
34H-6	320.39		1589	1546
34H-6	320.47	1538		
35H-1	323.70	1546		
35H-1	323.79		1434	1557
35H-2	325.26		1570	1556
35H-2	325.35	1572		
35H-3	326.76		1584	1563
35H-3	326.85	1575		
35H-4	328.27		1576	1562
35H-4	328.35	1580		
35H-5	329.85	1609		
35H-6	331.14	1572		
35H-6	331.22		1594	1553
36H-3	336.28		1560	1556
36H-3	336.36	1577		
36H-4	337.80		1574	1559
36H-5	339.35	1540		
36H-6	340.76		1555	1554
36H-6	340.85	1534		
38X-1	352.52	1575		
38X-2	353.99	1570		
38X-3	355.39	1558		
38X-4	356.78	1620		
38X-5	358.54	1583		
40X-1	370.93	1571		
40X-2	372.81	1593		
40X-3	374.11	1590		
40X-4	374.91	1639		
41X-1	381.03	1578		
41X-2	382.53	1566		
41X-3	383.89	1631		
41X-4	385.62	1650		
41X-5	386.35	1618		
42X-1	390.17	1577		
42X-2	391.90	1602		
42X-3	393.50	1640		
42X-4	394.84	1701		
43X-1	400.21	1613		
43X-2	401.69	1816		
43X-3	403.13	1664		
43X-4	404.68	1775		
43X-5	406.27	1759		
43X-6	407.24	1735		
44X-1	409.82	1771		
44X-2	411.35	1801		
44X-3	412.53	4832		
44X-5	415.51	4235		
44X-6	417.00	1761		
45X-1	419.20	1674		

Table T26. Thermal conductivity, Hole U1335A.

Core, section, interval (cm)	Depth CSF (m)	Thermal conductivity (W/[m·K])
320-U1335A-		
1H-3, 115	4.15	0.926
2H-3, 115	13.05	0.985
3H-3, 115	22.55	0.797
4H-3, 115	32.05	0.889
5H-3, 115	41.55	0.922
6H-3, 115	51.05	1.092
7H-3, 115	60.55	0.757
8H-3, 115	70.05	1.176
9H-3, 115	79.55	1.078
10H-3, 115	89.05	1.188
11H-3, 115	98.55	1.049
12H-3, 115	108.05	1.129
13H-3, 115	117.55	1.099
14H-3, 115	127.05	1.150
15H-3, 115	136.05	1.165
16H-3, 115	146.05	1.107
17H-3, 115	155.55	1.048
18H-3, 115	165.05	1.139
19H-3, 115	174.55	1.069
20H-3, 115	184.05	1.099
21H-3, 115	193.55	1.086
22H-3, 115	203.05	1.230
23H-3, 115	212.55	1.164
24H-3, 115	222.05	1.212
25H-3, 115	231.55	1.213
26H-3, 115	241.05	1.174
27H-3, 115	250.55	1.273
28H-3, 115	260.05	1.220
29H-3, 115	269.55	1.221
30H-3, 115	279.05	1.334
31H-3, 115	288.55	1.319
32H-3, 115	298.05	1.296
33H-3, 115	307.55	1.250
34H-3, 115	315.65	1.297
35H-3, 115	326.55	1.322
36H-3, 115	336.05	1.331
37X-3, 115	345.55	1.224
38X-3, 115	355.25	1.270
39X-3, 115	364.85	1.280
40X-3, 115	374.35	1.226
41X-3, 115	383.85	1.086
42X-3, 115	393.35	1.090

Table T27. Shipboard core top, composite, and corrected composite depths, Site U1335.

Core	Depth CSF (m)	Offset (m)	Top depth (m) CCSF-A	Top depth (m) CCSF-B
320-U1335A-				
1H	0.00	0.14	0.14	0.12
2H	8.90	1.01	9.91	8.56
3H	18.40	1.31	19.71	17.03
4H	27.90	3.04	30.94	26.73
5H	37.40	5.17	42.57	36.78
6H	46.90	5.99	52.89	45.70
7H	56.40	7.09	63.49	54.85
8H	65.90	9.19	75.09	64.88
9H	75.40	10.09	85.49	73.86
10H	84.90	11.05	95.95	82.90
11H	94.40	12.86	107.26	92.67
12H	103.90	14.09	117.99	101.94
13H	113.40	13.24	126.64	109.42
14H	122.90	15.30	138.20	119.40
15H	132.40	16.35	148.75	128.52
16H	141.90	16.35	158.25	136.73
17H	151.40	20.00	171.40	148.09
18H	160.90	20.47	181.37	156.70
19H	170.40	21.31	191.71	165.63
20H	179.90	22.73	202.63	175.07
21H	189.40	24.12	213.52	184.48
22H	198.90	25.98	224.88	194.30
23H	208.40	28.42	236.82	204.61
24H	217.90	31.63	249.53	215.60
25H	227.40	32.77	260.17	224.79
26H	236.90	34.64	271.54	234.61
27H	246.40	36.94	283.34	244.80
28H	255.90	37.78	293.68	253.74
29H	265.40	39.49	304.89	263.43
30H	274.90	40.56	315.46	272.56
31H	284.40	42.63	327.03	282.56
32H	293.90	43.96	337.86	291.91
33H	303.40	45.74	349.14	301.66
34H	312.90	48.42	361.32	312.18
35H	322.40	50.83	373.23	322.47
36H	331.90	52.00	383.90	331.69
37X	341.40	52.00	393.40	339.90
38X	351.10	52.00	403.10	348.28
39X	360.70	52.00	412.70	356.57
40X	370.20	52.00	422.20	364.78
41X	379.70	52.00	431.70	372.99
42X	389.20	52.00	441.20	381.20
43X	398.80	52.00	450.80	389.49
44X	408.40	52.00	460.40	397.79
45X	418.10	52.00	470.10	406.17

Core	Depth CSF (m)	Offset (m)	Top depth (m) CCSF-A	Top depth (m) CCSF-B
320-U1335B-				
1H	0.00	0.00	0.00	0.00
2H	3.30	-0.18	3.12	2.70
3H	12.80	1.17	13.97	12.07
4H	22.30	2.57	24.87	21.49
5H	31.80	4.23	36.03	31.13
6H	41.30	5.60	46.90	40.52
7H	50.80	6.77	57.57	49.74
8H	60.30	8.61	68.91	59.54
9H	69.80	9.65	79.45	68.65
10H	79.30	11.90	91.20	78.80
11H	88.80	13.11	101.91	88.05
12H	98.30	14.50	112.80	97.46
13H	107.80	15.40	123.20	106.44
14H	117.30	16.74	134.04	115.81
15H	126.80	17.36	144.16	124.56
16H	136.30	19.28	155.58	134.42
17H	145.80	19.28	165.08	142.63
18H	155.30	20.30	175.60	151.72
19H	164.80	22.31	187.11	161.67
20H	174.30	24.03	198.33	171.36
21H	183.80	25.05	208.85	180.45
22H	193.30	25.97	219.27	189.45
23H	202.80	28.92	231.72	200.21
24H	212.30	31.09	243.39	210.29
25H	221.80	32.54	254.34	219.75
26H	231.30	34.22	265.52	229.41
27H	240.80	36.01	276.81	239.17
28H	250.30	37.38	287.68	248.56
29H	259.80	39.36	299.16	258.47
30H	269.30	41.95	311.25	268.92
31H	278.80	43.33	322.13	278.33
32H	288.30	45.06	333.36	288.02
33H	297.80	46.44	344.24	297.43
34H	307.30	47.82	355.12	306.82
35H	316.80	49.88	366.68	316.81
36H	326.30	51.85	378.15	326.72
37H	335.80	54.25	390.05	337.01
38H	343.80	54.25	398.05	343.92
39H	352.80	54.25	407.05	351.69
40H	362.30	54.25	416.55	359.90
41H	370.10	54.25	424.35	366.64
42X	378.20	54.25	432.45	373.64
43X	386.20	54.25	440.45	380.55
44X	395.80	54.25	450.05	388.85
45X	405.40	54.25	459.65	397.14
46X	415.00	54.25	469.25	405.43

Table T28. Splice tie points, Site U1335. (**Continued on next page.**)

Hole, core, section, interval (cm)	Depth (m) CSF	Depth (m) CCSF-A		Hole, core, section, interval (cm)	Depth (m) CSF	Depth (m) CCSF-A
320-				320-		
U1335B-1H-2, 30	1.80	1.80	Tie to	U1335A-1H-2, 16	1.66	1.80
U1335A-1H-6, 55	7.75	7.89	Tie to	U1335B-2H-4, 26	8.06	7.89
U1335B-2H-6, 19	10.99	10.82	Tie to	U1335A-2H-1, 91	9.81	10.82
U1335A-2H-6, 53	16.93	17.93	Tie to	U1335B-3H-3, 97	16.77	17.93
U1335B-3H-6, 23	20.53	21.70	Tie to	U1335A-3H-2, 49	20.39	21.70
U1335A-3H-6, 132	27.22	28.52	Tie to	U1335B-4H-3, 65	25.95	28.52
U1335B-4H-5, 144	29.74	32.31	Tie to	U1335A-4H-1, 137	29.27	32.31
U1335A-4H-5, 68	34.58	37.62	Tie to	U1335B-5H-2, 9	33.39	37.62
U1335B-5H-6, 117	40.47	44.71	Tie to	U1335A-5H-2, 63	39.53	44.71
U1335A-5H-5, 56	43.96	49.13	Tie to	U1335B-6H-2, 73	43.53	49.13
U1335B-6H-6, 8	48.88	54.48	Tie to	U1335A-6H-2, 9	48.49	54.48
U1335A-6H-5, 82	53.72	59.71	Tie to	U1335B-7H-2, 64	52.94	59.71
U1335B-7H-5, 89	57.69	64.46	Tie to	U1335A-7H-1, 98	57.38	64.46
U1335A-7H-6, 74	64.64	71.73	Tie to	U1335B-8H-2, 132	63.12	71.73
U1335B-8H-6, 49	68.29	76.90	Tie to	U1335A-8H-2, 31	67.71	76.90
U1335A-8H-5, 9	71.99	81.19	Tie to	U1335B-9H-2, 24	71.54	81.19
U1335B-9H-6, 112	78.42	88.08	Tie to	U1335A-9H-2, 109	77.99	88.08
U1335A-9H-5, 64	82.04	92.13	Tie to	U1335B-10H-1, 93	80.23	92.13
U1335B-10H-5, 15	85.45	97.35	Tie to	U1335A-10H-1, 140	86.30	97.35
U1335A-10H-7, 25	94.15	105.20	Tie to	U1335B-11H-3, 29	92.09	105.20
U1335B-11H-6, 72	97.02	110.13	Tie to	U1335A-11H-2, 137	97.27	110.13
U1335A-11H-5, 92	101.32	114.18	Tie to	U1335B-12H-1, 138	99.68	114.18
U1335B-12H-6, 28	106.08	120.58	Tie to	U1335A-12H-2, 109	106.49	120.58
U1335A-12H-5, 68	110.58	124.67	Tie to	U1335B-13H-1, 148	109.28	124.67
U1335B-13H-6, 85	116.15	131.55	Tie to	U1335A-13H-4, 41	118.31	131.55
U1335A-13H-6, 27	121.17	134.41	Tie to	U1335B-14H-1, 38	117.68	134.41
U1335B-14H-5, 24	123.54	140.28	Tie to	U1335A-14H-2, 59	124.99	140.28
U1335A-14H-5, 95	129.85	145.15	Tie to	U1335B-15H-1, 99	127.79	145.15
U1335B-15H-5, 94	133.74	151.10	Tie to	U1335A-15H-2, 85	134.75	151.10
U1335A-15H-6, 145	140.85	157.20	Tie to	U1335B-16H-2, 12	137.92	157.20
U1335B-16H-7, 56	145.86	165.14	Append to	U1335B-17H-1, 63	146.43	165.70
U1335B-17H-6, 116	154.46	173.73	Tie to	U1335A-17H-2, 84	153.74	173.73
U1335A-17H-5, 75	158.15	178.14	Tie to	U1335B-18H-2, 104	157.84	178.14
U1335B-18H-5, 112	162.42	182.72	Tie to	U1335A-18H-1, 135	162.25	182.72
U1335A-18H-5, 47	167.37	187.84	Tie to	U1335B-19H-1, 72	165.52	187.84
U1335B-19H-6, 87	173.17	195.48	Tie to	U1335A-19H-3, 77	174.17	195.48
U1335A-19H-6, 89	178.79	200.10	Tie to	U1335B-20H-2, 27	176.07	200.10
U1335B-20H-5, 153	181.83	205.86	Tie to	U1335A-20H-3, 23	183.13	205.86
U1335A-20H-6, 107	188.47	211.19	Tie to	U1335B-21H-2, 84	186.14	211.19
U1335B-21H-6, 94	192.24	217.29	Tie to	U1335A-21H-3, 77	193.17	217.29
U1335A-21H-5, 118	196.58	220.70	Tie to	U1335B-22H-1, 143	194.73	220.70
U1335B-22H-6, 37	201.17	227.14	Tie to	U1335A-22H-2, 76	201.16	227.14
U1335A-22H-6, 57	206.97	232.95	Tie to	U1335B-23H-1, 123	204.03	232.95
U1335B-23H-5, 97	209.77	238.69	Tie to	U1335A-23H-2, 38	210.28	238.69
U1335A-23H-5, 105	215.45	243.86	Tie to	U1335B-24H-1, 47	212.77	243.86
U1335B-24H-6, 5	219.85	250.94	Tie to	U1335A-24H-1, 140	219.30	250.94
U1335A-24H-6, 52	225.92	257.56	Tie to	U1335B-25H-3, 22	225.02	257.56
U1335B-25H-5, 96	228.76	261.30	Tie to	U1335A-25H-1, 113	228.53	261.30
U1335A-25H-6, 16	235.06	267.84	Tie to	U1335B-26H-2, 82	233.62	267.84
U1335B-26H-5, 37	237.67	271.89	Tie to	U1335A-26H-1, 35	237.25	271.89
U1335A-26H-6, 30	244.70	279.34	Tie to	U1335B-27H-2, 103	243.33	279.34
U1335B-27H-6, 141	249.71	285.72	Tie to	U1335A-27H-2, 89	248.79	285.72
U1335A-27H-6, 13	254.03	290.96	Tie to	U1335B-28H-3, 28	253.58	290.96
U1335B-28H-6, 18	257.98	295.36	Tie to	U1335A-28H-2, 18	257.58	295.36
U1335A-28H-6, 11	263.51	301.29	Tie to	U1335B-29H-2, 63	261.93	301.29
U1335B-29H-5, 107	266.87	306.23	Tie to	U1335A-29H-1, 134	266.74	306.23
U1335A-29H-5, 120	272.60	312.09	Tie to	U1335B-30H-1, 84	270.14	312.09
U1335B-30H-5, 116	276.46	318.41	Tie to	U1335A-30H-2, 145	277.85	318.41
U1335A-30H-6, 122	283.62	324.18	Tie to	U1335B-31H-2, 55	280.85	324.18
U1335B-31H-6, 78	287.08	330.41	Tie to	U1335A-31H-3, 38	287.78	330.41
U1335A-31H-6, 21	292.11	334.74	Tie to	U1335B-32H-1, 138	289.68	334.74
U1335B-32H-5, 147	295.77	340.83	Tie to	U1335A-32H-2, 147	296.87	340.83
U1335A-32H-6, 106	302.46	346.42	Tie to	U1335B-33H-2, 68	299.98	346.42
U1335B-33H-6, 81	306.11	352.55	Tie to	U1335A-33H-3, 41	306.81	352.55
U1335A-33H-6, 44	311.34	357.08	Tie to	U1335B-34H-2, 46	309.26	357.08
U1335B-34H-6, 75	315.55	363.37	Tie to	U1335A-34H-3, 45	314.95	363.37
U1335A-34H-6, 61	319.61	368.03	Tie to	U1335B-35H-1, 135	318.15	368.03

Table T28 (continued).

Hole, core, section, interval (cm)	Depth (m) CSF	Depth (m) CCSF-A		Hole, core, section, interval (cm)	Depth (m) CSF	Depth (m) CCSF-A
U1335B-35H-6, 39	324.69	374.57	Tie to	U1335A-35H-1, 134	323.74	374.57
U1335A-35H-5, 89	329.29	380.12	Tie to	U1335B-36H-2, 37	328.27	380.12
U1335B-36H-7, 14	335.54	387.39	Tie to	U1335A-36H-3, 49	335.39	387.39
U1335A-36H-5, 45	338.35	390.35	Tie to	U1335B-37H-1, 30	336.10	390.35
U1335B-37H-6, 40	343.70	397.95	Append to	U1335B-38H-1, 8	343.88	398.12
U1335B-38H-6, 79	352.09	406.34	Append to	U1335B-39H-1, 5	352.85	407.10
U1335B-39H-7, 41	362.21	416.46	Append to	U1335B-40H-1, 8	362.38	416.62
U1335B-40H-6, 27	370.07	424.31	Append to	U1335B-41H-1, 8	370.18	424.42
U1335B-41H-6, 36	377.96	432.21	Append to	U1335B-42X-1, 23	378.43	432.67
U1335B-42X-6, 77	386.47	440.72	Append to	U1335B-43X-1, 19	386.39	440.64
U1335B-43X-6, 90	394.60	448.85	Append to	U1335B-44X-1, 19	395.99	450.24
U1335B-44X-6, 104	404.34	458.58	Append to	U1335B-45X-1, 24	405.64	459.89
U1335B-45X-4, 147	411.37	465.62	Append to	U1335B-46X-1, 9	415.09	469.34

Table T29. Magnetostratigraphic and biostratigraphic datums, Site U1335. (See table note.) (Continued on next page.)

Event	Age (Ma)	Depth CCSF-A (m)	Error (m)
C1n–C1r.1r	0.781	5.32	
C1r.1r–C1r.1n	0.988	6.55	
C1r.1n–C1r.2r	1.072	6.99	
C1r.2r–C1r.2n	1.173	7.63	
C1r.2n–C1r.2r	1.185	7.75	
C1r.2r–C2n	1.778	10.54	
C2n–C2r.1r	1.945	11.22	
C2r.1r–C2r.1n	2.128	11.97	
C2r.1n–C2r.2r	2.148	11.99	
C2r.2r–C2An.1n	2.581	14.58	
C2An.1n–C2An.1r	3.032	17.06	
C2An.1r–C2An.2n	3.116	17.29	
C2An.2n–C2An.2r	3.207	17.74	
C2An.2r–C2An.3n	3.330	18.21	
C2An.3n–C2Ar	3.596	19.36	
C2Ar–C3n.1n	4.187	21.72	
C3n.1n–C3n.1r	4.300	22.51	
C3n.1r–C3n.2n	4.493	23.88	
C3n.2n–C3n.2r	4.631	24.91	
C3n.2r–C3n.3n	4.799	26.33	
C3n.3n–C3n.3r	4.896	26.98	
C3n.3r–C3n.4n	4.997	27.56	
C3n.4n–C3r	5.235	29.83	
C3r–C3An.1n	6.033	34.13	
C3An.1n–C3An.1r	6.252	36.38	
C3An.1r–C3An.2n	6.436	37.77	
C3An.2n–C3Ar	6.733	40.04	
C3Ar–C3Bn	7.140	43.60	
C3Bn–C3Br.1r	7.212	43.77	
C3Br.1r–C3Br.1n	7.251	44.09	
C3Br.1n–C3Br.2r	7.285	44.90	
C3Br.2r–C3Br.2n	7.454	46.20	
C3Br.2n–C3Br.3r	7.489	46.35	
C3Br.3r–C4n.1n	7.528	46.45	
C4n.1n–C4n.1r	7.642	46.57	
C4n.1r–C4n.2n	7.695	47.07	
C4n.2n–C4r.1r	8.108	48.10	
C4r.1r–C4r.1n	8.254	49.70	
C4r.1n–C4r.2r	8.300	50.07	
C4r.2r–C4An	8.769	54.39	
C4An–C4Ar.1r	9.098	63.96	
C4Ar.1r–C4Ar.1n	9.312	64.82	
C4Ar.1n–C4Ar.2r	9.409	65.41	
C4Ar.2r–C4Ar.2n	9.656	66.40	
C4Ar.2n–C4Ar.3r	9.717	66.76	
C4Ar.3r–C5n.1n	9.779	67.01	
C5n.1n–C5n.1r	9.934	67.97	
C5n.1r–C5n.2n	9.987	68.11	
C5n.2n–C5r.1r	11.040	73.97	
C5r.1r–C5r.1n	11.118	74.66	
C5AAn–C5AAr	13.183	126.18	
C5AAr–C5ABn	13.369	128.71	
C5ABn–C5ABr	13.605	134.58	
C5ABr–C5ACn	13.734	136.41	
C5ACn–C5ACr	14.095	140.70	
C5ACr–C5ADn	14.194	141.60	
C5ADn–C5ADr	14.581	156.67	
C5ADr–C5Bn.1n	14.784	162.38	
C5Bn.1r–C5Bn.2n	15.032	168.55	
C5Bn.2n–C5Br	15.160	172.47	
C5Br–C5Cn.1n	15.974	184.04	
C5Cn.1n–C5Cn.1r	16.268	189.59	
C5Cn.1r–C5Cn.2n	16.303	191.03	
C5Cn.2n–C5Cn.2r	16.472	192.01	
C5Cn.2r–C5Cn.3n	16.543	193.06	
C5Cn.3n–C5Cr	16.721	194.32	
C5Cr–C5Dn	17.235	201.37	
C5Dn–C5Dr	17.533	207.10	
C5Dr–C5En	18.056	216.52	
C5En–C5Er	18.524	223.37	
C5Er–C6n	18.748	230.43	
Nannofossils			
T *Pseudoemiliania lacunosa*	0.44	2.34	1.80
T *Calcidiscus macintyrei*	1.61	8.00	0.96
T *Discoaster brouweri*	1.93	8.00	0.96
T *Discoaster pentaradiatus*	2.39	12.17	1.97
T *Discoaster surculus*	2.49	12.17	1.97
T *Discoaster tamalis*	2.80	15.56	1.42
T *Sphenolithus* spp.	3.54	20.93	1.07
T *Reticulofenestra pseudoumbilicus*	3.70	20.93	1.07
T *Ceratolithus acutus*	5.04	26.99	1.10
B *Ceratolithus rugosus*	5.05	26.99	1.10
T *Triquetrorhabdulus rugosus*	5.28	30.85	1.41
B *Ceratolithus acutus*	5.35	30.85	1.41
T *Discoaster quinqueramus*	5.58	32.84	0.57
Tc *Nicklithus amplificus*	5.98	38.21	0.90
B *Amaurolithus* spp.	7.36	47.37	1.70
B *Discoaster berggrenii*	8.29	52.56	0.93
T *Discoaster hamatus*	9.69	66.11	1.03
T *Catinaster coalitus*	9.69	66.11	1.03
B *Discoaster hamatus*	10.55	70.29	1.49
T *Coccolithus miopelagicus*	10.60	70.29	1.49
B *Catinaster coalitus*	10.89	70.29	1.49
Tc *Discoaster kugleri*	11.58	81.99	1.50
Bc *Discoaster kugleri*	11.86	87.69	1.50
T *Coronocyclus nitescens*	12.12	94.95	0.16
T *Calcidiscus premacintyrei*	12.45	96.78	1.67
Tc *Cyclicargolithus floridanus*	13.33	121.44	1.05
T *Sphenolithus heteromorphus*	13.53	124.89	1.50
Tc *Discoaster deflandrei*	15.66	180.64	0.55
B *Discoaster petaliformis*	15.70	170.71	2.88
Tc *Discoaster deflandrei*	15.66	180.64	0.55
Bc *Sphenolithus heteromorphus*	17.71	206.33	1.50
Tc *Sphenolithus belemnos*	17.95	217.32	1.50
T *Triqutrorhabdulus carinatus*	18.28	220.32	1.50
B *Sphenolithus belemnos*	19.03	236.92	2.29
Tac *Triqutrorhabdulus carinatus*	22.09	367.92	3.50
B *Sphenolithus disbelemnos*	22.8	394.80	1.00
T *Sphenolithus delphix*	23.1	401.70	0.30
B *Sphenolithus delphix*	23.2	403.75	1.75
T *Sphenolithus ciperoensis*	24.4	459.75	0.45
X *T. longus/T. carinatus*	24.7	450.70	2.40
Tc *Cyclicargolithus abisectus*	24.7	443.95	4.35
Radiolarians			
T *Anthocyrtidium angulare*	1.21	6.57	2.39
B *Theocorythium trachelium*	1.76	10.38	1.42
B *Anthocyrtidium angulare*	1.97	10.38	1.42
T *Pterocanium prismatium*	2.08	10.38	1.42
B *Cycladophora davisiana*	2.89	13.30	1.50
T *Stichocorys peregrina*	2.90	17.33	2.54
T *Spongaster pentas*	3.98	21.07	1.20
T *Phormostichoartus doliolum*	4.03	21.07	1.20
T *Didymocyrtis penultima*	4.26	21.07	1.20
B *Pterocanium prismatium*	4.73	27.36	2.09
B *Nephrospyris renilla*	5.02	27.36	2.09
T *Solenosphaera omnitubus*	5.32	27.36	2.09
T *Spongaster berminghami*	5.57	31.45	2.00
T *Stichocorys johnsoni*	6.53	38.65	2.20
T *Calocycletta caepa*	6.60	38.65	2.20
Trans *S. delmontensis* > *S. peregrina*	7.75	42.97	2.12
B *Stichocorys peregrina*	7.84	46.58	1.50
B *Solenosphaera omnitubus*	8.25	49.86	1.78
T *Diartus hughesi*	8.39	49.86	1.78

Table T29 (continued).

Event	Age (Ma)	Depth CCSF-A (m)	Error (m)
T *Botryostrobus miralestensis*	8.59	56.95	1.50
T *Diartus petterssoni*	8.63	56.95	1.50
Trans *D. petterssoni* > *D. hughesi*	8.76	60.45	2.00
B *Spongaster berminghami*	8.76	64.23	1.78
T *Stichocorys wolffii*	8.95	64.23	1.78
B *Diartus hughesi*	8.99	64.23	1.78
T *Cyrtocapsella japonica*	10.31	67.52	1.50
T *Carpocanopsis cristata*	10.88	71.18	2.16
T *Cyrtocapsella cornuta*	11.86	93.08	2.04
B *Diartus petterssoni*	12.11	100.01	1.50
B *Cyrtocapsella japonica*	12.41	107.90	1.91
B *Lithopera neotera*	12.95	107.90	1.91
T *Stichocorys armata*	13.50	125.74	2.20
T *Acrocubus octopyle*	13.88	125.74	2.20
T *Calocycletta costata*	14.23	134.42	2.22
T *Dorcadospyris dentata*	14.67	163.32	0.59
Trans *D. dentata* > *D. alata*	14.78	170.89	3.05
T *Liriospyris stauropora*	14.83	163.32	0.59
B *Liriospyris parkerae*	15.03	174.92	0.97
B *Dorcadospyris alata*	15.08	174.92	0.97
T *Carpocanopsis cingulata*	15.13	186.39	0.54
T *Lychnocanoma elongata*	15.15	186.39	0.54
B *Lithopera renzae*	16.77	192.23	2.03
B *Calocycletta costata*	17.49	199.50	2.23
B *Dorcadospyris dentata*	17.72	210.39	2.22
B *Liriospyris stauropora*	17.72	213.59	0.99
B *Stichocorys wolffii*	18.57	241.84	0.54
B *Dorcadospyris forcipata*	18.61	261.11	1.62
T *Dorcadospyris simplex* s.s.	18.69	261.11	1.62
T *Dorcadospyris praeforcipata*	19.77	283.64	2.21
B *Dorcadospyris simplex* s.s.	20.34	301.49	2.26
B *Stichocorys delmontensis*	20.68	303.20	2.26
T *Lophocyrtis pegetrum*	20.89	323.93	1.41
T *Theocyrtis annosa*	21.38	332.06	0.53
B *Calocycletta virginis*	21.39	332.06	0.53
T *Eucyrtidium mitodes*	21.95	356.97	2.27
B *Calocycletta serrata*	22.04	363.90	0.52
B *Cyrtocapsella cornuta*	22.26	394.88	1.07
B *Cyrtocapsella tetrapera*	22.35	394.88	1.07
T *Artophormis gracilis*	22.62	408.12	0.53
B *Eucyrtidium diaphanes*	22.95	419.28	2.09
T *Dorcadospyris cyclacantha*	22.98	408.12	0.53
B *Dorcadospyris cyclacantha*	23.29	419.28	2.09
T *Dorcadospyris papilio*	23.31	423.06	1.69
T *Liriospyris longicornuta*	24.12	438.43	1.19
T *Lychnocanoma apodora*	24.50	441.68	2.07
B *Lychnocanoma elongata*	25.05	447.52	0.77
B *Acrocubus octopylus*	25.09	447.52	0.77
B *Calocycletta robusta*	25.27	464.46	1.50
B *Liriospyris longicornuta*	25.29	464.46	1.50
B *Lychnocanoma apodora*	25.55	464.46	1.50
Foraminifers			
T *Globigerinoides fistulosus*	1.77	11.13	1.32
B *Globorotalia (Truncorotalia) truncatulinoides*	1.92	7.90	1.20
T *Globigerinoides extremus*	1.98	9.59	1.32
T *Globorotalia pseudomiocenica*	2.30	9.59	1.32
T *Globoturborotalita woodi*	2.30	13.95	1.50
T *Globorotalia (Menardella) multicamerata*	2.98	23.09	1.50
T *Dentoglobigerina altispira*	3.47	43.54	5.68
T *Sphaeroidinellopsis seminulina*	3.59	16.48	1.50
B *Globorotalia (Menardella) exilis*	4.45	17.65	2.21
B *Sphaeroidinella dehiscens* s.l.	5.54	23.01	2.43
B *Globorotalia tumida*	5.57	31.36	1.89
B *Globorotalia (Hirsutella) margaritae*	6.08	43.92	0.95
B *Globorotalia plesiotumida*	8.58	58.93	2.67
T *Globorotalia (Menardella) praemenardii*	10.09	74.08	4.55
T *Paragloborotalia mayeri*	10.46	73.36	0.69
B *Globoturborotalita decoraperta*	11.49	80.37	0.71
B *Globoturborotalita nepenthes*	11.63	86.66	0.71
T *Globorotalia (Fohsella) fohsi* s.l.	11.79	86.64	1.50
B *Globorotalia (Fohsella) fohsi robusta*	13.13	118.54	0.81
B *Globorotalia (Fohsella) fohsi* s.l.	13.41	120.96	4.03
T *Globorotalia praescitula*	13.73	127.37	4.79
B *Globorotalia (Fohsella) "praefohsi"*	13.77	128.69	2.03
T *Globorotalia (Fohsella) peripheroronda*	13.80	131.17	2.56
T *Clavatorella bermudezi*	13.82	131.33	0.20
B *Globorotalia (Fohsella) peripheroacuta*	14.24	141.58	1.50
B *Clavatorella bermudezi*	14.89	141.58	1.50
B *Globorotalia (Menardella) archeomenardii*	16.26	179.52	2.65
B. *Praeorbulilna sicana*	16.97	191.20	1.28
T *Catapsydrax dissimilis*	17.54	213.94	4.54
T *Globoquadrina binaiensis*	19.09	207.07	4.78
T *Paragloborotalia kugleri*	21.12	308.74	2.59
T *Paragloborotalia pseudokugleri*	21.31	308.74	2.59
B *Globoquadrina dehiscens*	22.44	361.54	1.94
B *Paragloborotalia kugleri*	23.0	401.67	1.38
B *Paragloborotalia pseudokugleri*	25.2	445.01	4.12

Note: T = top, B = bottom, Tc = Top common occurrence, Bc = Bottom common occurrence, Tac = top acme, X = abundance crossover, Trans = transition.

Table T30. Results from APCT-3 temperature profiles, Hole U1335B. (**See table notes.**)

Core	Temperature (°C)		Depth DSF (m)	In situ temperature (°C)	Thermal resistance (m^2K/m)
	Average at mudline	Minimum above mudline			
320-U1335B-					
3H	1.498	1.474	22.3	1.64	24.9
5H	1.500	1.468	41.3	1.83	47.3
7H	1.511	1.465	60.3	2.00	67.8
9H	1.493	1.463	79.3	2.00	87.1
11H	1.510	1.473	98.3	2.22	104.4
Average:	1.502	1.469			

Notes: In situ temperatures were determined using the TP-Fit software by Martin Heesemann. Thermal resistance was calculated from thermal conductivity data (see **"Physical properties"**) corrected for in situ conditions (see **"Downhole measurements"** in the "Methods" chapter).